

ELECTRON MICROPROBE INVESTIGATIONS
OF METAMORPHIC REACTIONS AND MINERAL GROWTH HISTORIES
KWOIEK AREA, BRITISH COLUMBIA

Thesis by
Lincoln Steffens Hollister

In Partial Fulfillment of the Requirements

For the Degree of
Doctor of Philosophy

California Institute of Technology

Pasadena, California

1966

(Submitted May 10, 1966)

ACKNOWLEDGEMENTS

I wish to thank Dr. Arden L. Albee for encouragement and guidance throughout the course of this research. Drs. L. T. Silver, H. P. Taylor, G. J. Wasserburg, and Mr. S. D. McDowell of the California Institute of Technology, Drs. J. Christie, W. G. Ernst, and J. Rosenfeld of the University of California at Los Angeles, and Dr. J. V. Smith of the University of Chicago were also helpful for their criticism and suggestions.

The analytical work on the electron microprobe was carried out under the direction of Mr. A. A. Chodos. Polished thin sections for microprobe samples were prepared by Mr. Rudolf Von Huene.

Analyzed minerals for microprobe standards were supplied by Drs. A. L. Albee, Fred Barker and R. G. Coleman of the U. S. Geological Survey, L. T. Silver, H. P. Taylor, J. Green of the University of Minnesota, and B. Evans of the University of California at Berkeley.

Without the help of a number of people in British Columbia, the field work for this thesis would have been impossible. Foremost amongst these people is Dr. K. C. McTaggart of the University of British Columbia, whose encouragement, warnings, and hints concerning entering the Kwoiek Area were invaluable. Dr. McTaggart also contributed to this work through discussions concerning problems of southwestern British Columbia regional geology.

Jim Gillen of Keefers is gratefully thanked for his help in a multitude of ways. His suggestions and aid greatly facilitated the

field work. Ray Washtock of North Bend, British Columbia, was also most helpful on logistical matters.

Without the cooperation of the Cattermole-Trethewey Logging Company, access to the Kwoiek Area would have been prohibitively difficult. The help of their employees in times of difficulty as well as general help in permission to use company roads and bridges is gratefully acknowledged.

The Department of Fish and Game of the Province of British Columbia allowed the author to take game for food, which made possible back-pack trips as long as three weeks in duration.

The Forestry Department of Canada allowed occasional use of a cabin and a fire lookout for shelter and made suggestions of access routes into the Kwoiek Area. The School Board of District Number 32 allowed the writer and field assistants to use the schoolhouse at Keefers, British Columbia, for a base camp.

Able field assistance was performed by David Hewitt (1963) and Tom Williams (1964). Mr. Hewitt is especially to be thanked as he worked without salary.

This work was carried out during the tenure of two Kennecott Copper Corporation Fellowships, two National Science Foundation Summer Fellowships, and a Woodrow Wilson Summer Fellowship. Research funds were supplied by the Geology Department, California Institute of Technology, and by a National Science Foundation grant (GP-2773).

The high quality of the drafted material is due to Miss Cathy Clancy. Mrs. Sarah Hollister patiently typed early drafts of the text.

ABSTRACT

The Kwoiek Area of British Columbia contains a pendant or screen of metamorphosed sedimentary and volcanic rocks almost entirely surrounded by a portion of the Coast Range Batholith, and intruded by several dozen stocks. The major metamorphic effects were produced by the quartz diorite batholithic rocks, with minor and later effects by the quartz diorite stocks. The sequence of important metamorphic reactions in the metasedimentary and metavolcanic rocks, ranging in grade from chlorite to sillimanite, is:

1. chlorite + carbonate + muscovite \longrightarrow epidote + biotite
2. chlorite + carbonate \longrightarrow actinolite + epidote
3. chlorite + muscovite \longrightarrow garnet + biotite
4. chlorite + epidote \longrightarrow garnet + hornblende
5. chlorite + muscovite \longrightarrow garnet + staurolite + biotite
6. chlorite + muscovite \longrightarrow aluminum silicate + biotite
7. muscovite + staurolite \longrightarrow garnet + aluminum silicate + biotite
8. staurolite \longrightarrow garnet + aluminum silicate

Continuous reactions, occurring between reactions 5 and 7, are:

- A. chlorite + (high Ti) biotite + Al_2O_3 (from plagioclase?) \longrightarrow
garnet + staurolite + (low Ti) biotite + O_2
- B. muscovite (phengitic) \longrightarrow garnet + staurolite + muscovite (less
phengitic) + O_2 (?)

Detailed electron microprobe work on garnet, staurolite, biotite,

and chlorite shows that:

(1) The garnet porphyroblasts are zoned according to a depletion model, called the Rayleigh depletion model, which assumes equilibrium between the edge of a growing garnet and the minerals which are unzoned, notably biotite, chlorite, and muscovite, but which assumes disequilibrium within the garnet.

(2) The staurolite porphyroblasts are also zoned, and from their zoning patterns reactions A, B, and 5 are documented. Progressive reduction of iron with increasing grade of metamorphism is also inferred from the staurolite zoning patterns.

(3) During a late period of falling temperature garnet continued to grow and the biotite and chlorite reequilibrated. The biotite, chlorite, and garnet edge compositions can vary from point to point in a given thin section, indicating that the volume of equilibrium at the final stage of metamorphism was only a few cubic microns.

(4) The horizon within the garnet that grew at maximum temperature can be identified. The Mg/Fe ratio of this horizon, if the garnet composition is a limiting composition in the $\text{Al}_2\text{O}_3 - \text{K}_2\text{O} - \text{FeO} - \text{MgO}$ tetrahedron, increases systematically with increasing metamorphic grade. Biotite and chlorite compositions also show a general increase in Mg/Fe ratio with increasing metamorphic grade, but staurolite appears to show the reverse effect.

(5) The Mg/Fe ratio at the maximum temperature horizon of the garnet porphyroblasts is a function of its Mn content as evidenced from the study of five garnet-bearing rocks, collected from one outcrop

area, with the same assemblage but with differing proportions of minerals.

An important implication of zoned minerals is that the effective composition of a system in a phase lies on the join between the homogeneous minerals (if there are two) and not within three- or four-phase fields when a zoned mineral, such as garnet or staurolite, is present in the assemblage.

Study of the three aluminum silicates found in the Kwoiek Area showed that a constant pressure change in polymorphs from andalusite to kyanite to sillimanite took place with increasing temperature. This transition series is best explained by the metastable formation of andalusite.

Photographic materials on pages 15, 121, 160, 162, and 164 are essential and will not reproduce clearly on Xerox copies. Photographic copies should be ordered.

	Page
Reaction (5) -- chlorite + muscovite \longrightarrow aluminum silicate + biotite . . .	53
Reaction (6) -- muscovite + staurolite \longrightarrow aluminum silicate + garnet + biotite	54
Reaction (7) -- staurolite \longrightarrow garnet + aluminum silicate	54
Origin of non-primary muscovite	55
Variables Affecting Metamorphic Reactions	59
IV ANALYTICAL RESULTS	62
Introduction	62
Garnet	65
General statement	65
Rayleigh fractionation in garnet	75
Application of Rayleigh depletion model to specimen 350B	79
Discussion of specimens 350A, 350B, 350C, 350D, and 350F	101
Two-history garnet	119
Origin of five-phase assemblages	122
Biotite and Chlorite	127
Staurolite	149
Aluminum Silicate	159
V CONDITIONS OF METAMORPHISM	174
Temperature and Total Pressure	174
Oxygen Pressure and its Influence on Staurolite Composition	177
VI SUMMARY OF CONCLUSIONS	186

	Page
APPENDIX	190
Mineral Abbreviations Used in Text	190
Assemblages of Metamorphic Samples Discussed in text	191
Analytical Technique	192
The microprobe and accessories	192
Polishing technique	192
Carbon coating	193
Experimental conditions	193
Standards	195
REFERENCES	207

LIST OF ILLUSTRATIONS

Figure		Page
1	Geographic Limits of the Kwoiek Area	5
2	Geologic Map	8
3	Structure Section	9
4	Map Showing Distribution of Quartz Diorite Intrusives and Mapped Isograds	28
5	ACKF Tetrahedra	33
6	Geometric Relations for Deriving AFM Diagram of Fig. 7	43
7	AFM Biotite and Muscovite Projection Diagrams .	44
8	Melting Relations in the System $KAlSi_3O_8 - H_2O$.	57
9	Mn, Fe, and Mg Profiles Across a Garnet of Sample 188C	66
10	Mn, Fe, and Mg Profiles Across a Garnet of Sample 314	67
11	Mn, Fe, and Mg Profiles Across a Garnet of Sample 382	68
12	Mn, Fe, and Mg Profiles Across a Garnet of Sample 222	69
13	Mn, Fe, and Mg Profiles Across a Garnet of Sample 370B	70
14	Mn, Fe, and Mg Profiles Across a Garnet of Sample 410	71
15	Mn, Fe, Mg, Ca, Al, Si, and Ti Profiles Across Garnet of Samples 350A, 350B, 350C, 350D, and 350F	73
16	Mn, Fe, and Mg Profiles Across a Garnet of Sample 350B	80
17	Comparison of Half of Mn Profile of Fig. 16 and Calculated Mn Profile	83

Figure		Page
18	Comparison of Measured and Calculated Profiles of Fig. 16 for Mg and Fe	84
19	Comparison of Measured and Calculated Mg/Fe Profiles of Fig. 16	87
20	Thompson Projection, Showing Effect of the Growth of Zoned Garnet on the Biotite/ Chlorite Ratio	91
21-23	Plot of Edge Content of Mn, Fe, and Mg in Garnet of 350 Series Rocks Against Average Mn, Fe, and Mg Content of Coexisting Chlorite and Biotite	95-97
24	AKFM Tetrahedron Indicating the Location of the Four-phase Volume Gar - Bio - Chl - Stl	103
25	Plot of Mn in Garnet 350B Against Mg/Fe Ratio	105
26-27	Plot of Mn vs. Mg/Fe for Several Garnet Grains of Samples 350A, B, C, D, and F.	107, 108
28	Figures 26 and 27 Superimposed with Envelopes Drawn Around Points of Each Sample	109
29	Atom Percent Mn/Mn+Mg+Fe Against Atom Percent Mg/Mg+Fe for Data Discussed by Albee (1965b) and the Present Work	113
30	Plot of Mn Content Against Mg/Fe Ratio in the Maximum Temperature Horizon of Garnet for all Garnet Analyzed in the Kwoiek Area	115
31	Plot of the Mn Fractionation Factor Between Garnet and Rest of Rock Against Mn ₀ and Mn Content of Total Rock	117
32a	Thompson Projection Showing Chl - Bio - Gar - Musc and Chl - Gar - Stl - Musc Assemblages	125
32b	Thompson Projection at a Higher Temperature Than That of Fig. 32a	125
33	Profiles for Indicated Elements Across Two Biotite and Two Chlorite Grains	129
34	Mn, Fe, and Mg Profiles Across a Biotite of Sample 350B	130

Figure		Page
35	Plots of Average Fe Against Average Mg of Several Biotite Grains from Each of Four Samples	133
36	Plot of Average Fe Against Average Mg for Seven Biotite Grains of Sample 222	135
37	Plot of Average Fe Against Average Mg for Several Biotite and Chlorite Grains from Each of Three Samples	136
38a	Plot of Average Fe Against Average Mg for 23 Biotite Grains From Sample 350B	139
38b	Locations of the Analyses of Fig. 38a Shown on a Sketch of the Thin Sections	139
39	Plot of Atom Percent Mn/Mn+Mg+Fe in Garnet Against Atom Percent Mg/Mg+Fe Garnet and Atom Percent Mg/Mg+Fe Biotite	142
40	Plot of Atom Percent Mn/Mn+Mg+Fe in Garnet Against the Mg-Fe Distribution Function Between Garnet and Biotite	143
41	Plot of the Mn Content of Garnet in the Maximum Temperature Horizon Against the Mg/Fe Ratio of Coexisting Chlorite and Biotite	146
42	Plot of Mg/Fe Ratio in Chlorite Against the Mg/Fe Ratio of Coexisting Biotite	148
43	Mn, Fe, Mg, Si, Al, and Ti Profiles Across a Staurolite of Sample 350F	150
44	Mn, Fe, Mg, Si, Al, and Ti Profiles Across a Staurolite of Sample 374	151
45	Plot of Maximum Temperature Mg/Fe Ratio of Garnet Against Average Mg/Fe Ratio of Coexisting Staurolite	157
46	Al ₂ SiO ₅ Phase Diagram After Bell (1963) Showing Possible Stable Paths of Observed Aluminum Silicate Transitions in the Kwoiek Area . . .	168

Figure		Page
47	Al ₂ SiO ₅ Phase Diagram After Bell (1963) Showing Inferred Metastable-Stable Transition Path of Observed Aluminum Silicate Transitions in the Kwoiek Area	168
48	Summary of Data on the Al ₂ SiO ₅ Phase Diagram to Date	175
49	Relation of P _{H₂O} to P _{CO₂} for Graphite-Bearing Rocks at P _{gas} = 1000 bars	178
50	Hypothetical Garnet and Staurolite Stability Fields in a P _{O₂} - T Plot	182
51	Figure 50b with the Inferred Relative Position of the Hematite-Magnetite Buffer Curve and a Graphite-Gas Buffer Curve	184
52-58	Calibration Curves for Translating Background-Corrected, Normalized Counting Rates to Weight Percent of the Element	197-202

LIST OF PLATES

Plate		Page
1	Thinly-bedded greywacke rock type	15
2	Photomicrograph of garnet in specimen 188C . . .	121
3	Polished rock surface showing andalusite cross sections, specimen 180	160
4	Photomicrograph of andalusite of plate 3	160
5	Polished rock surface showing andalusite cross sections, specimen 160A	162
6	Photomicrograph of an andalusite cross section of Plate 5 showing andalusite surrounded by kyanite	162
7	Photomicrograph of a square outlined area of specimen 40 showing kyanite pseudomorphous after andalusite	164
8	Photomicrograph of a square outlined area of specimen 370A showing kyanite pseudomorphous after andalusite and rimmed by sillimanite . .	164

LIST OF TABLES

Table		Page
1	Generalized succession of units	12
2	Modes of intrusive rocks	21
3	Coexisting assemblages with increasing metamorphic grade in high-Ca rocks	35
4	Assemblages in high-Ca rocks	36
5	Anorthite contents of plagioclase in some metasedimentary rocks	41
6	Assemblages in low-Ca rocks	46
7	Coexisting assemblages with increasing metamorphic grade in low-Ca rocks	47
8	Numbers used in calculations on Garnet 350B	82
9	Mode of specimen 272	92
10	Modes of five rocks collected from the same outcrop	102
11	Total analyses of garnet from the 350 series rocks	111
12	Total analyses of four horizons in staurolite 350F	153
13	Trace element analyses of aluminum silicate polymorphs	170
14	Samples used for microprobe standards	203
15	Interday factors and approximate backgrounds	204

INTRODUCTION

The purpose of this thesis is to establish a framework of knowledge of the processes by which a rock recrystallizes during metamorphism. In order to achieve this aim, a metamorphic area, the Kwoiek Area of southern British Columbia, was chosen which, on the basis of earlier reconnaissance work (Duffell and McTaggart, 1952), appeared to have had a simple history of metamorphism compared to many that have been studied in some detail. An area of contact metamorphism was chosen so that the effects of a wide range of temperatures of metamorphism could be studied in a relatively small area.

The rocks which were studied form a roof pendant or screen on the east flank of the Coast Range Batholith. The pendant is almost completely surrounded by hornblende-biotite or biotite quartz diorite, and several stocks intrude the interior of the pendant.

The batholith surrounding the pendant appears to have produced the main metamorphic effects; whereas the stocks, which intruded at, or shortly after, the peak of metamorphism, produced only slight effects on the rocks in their immediate vicinity. The metamorphic grade ranges from lower greenschist facies through upper almandine-amphibolite facies (Turner and Verhoogen, 1960), and rocks of both basaltic and pelitic compositions were affected by all grades of metamorphism. Carbonate rocks are absent from most of the Kwoiek Area.

Although seven months were spent in the field, the detailed sample collecting necessary for a petrochemical study precluded detailed

geologic mapping. The weight of samples collected determined the length of time spent in any part of the area, because the samples had to be backpacked out to the road for distances ranging between one and three days' hike. The geology of the Kwoiek Area, presented in the next chapter, is based both on the author's work and on the work of Duffell and McTaggart (1952).

The major contribution of this work was based on the petrologic study of about 300 thin sections and the analytic study, with an ARL microprobe, of the mineral phases in about 40 of the thin sections. About 100 thin sections, selected from about 600 hand specimens, were studied, which were representative of all grades of metamorphism and of the different rock types. Specific areas which appeared to be most favorably suited for the study of the processes by which a rock recrystallizes during metamorphism were then investigated in greater detail by cutting the additional thin sections. The 40 thin sections on which the analytic work was done were selected for their relevance in solving specific questions that arose during the petrologic phase of the investigation.

The outline of the analytic work was as follows:

- (1) A single metasedimentary rock whose assemblage contained the maximum number of coexisting minerals found in the Kwoiek Area, and which was common to the Kwoiek Area, was selected for a detailed analysis of the compositional variations of each mineral in the rock.
- (2) Four other rocks with the same assemblage and from the same outcrop as the rock studied above were similarly studied to confirm ideas

developed in the examination of the single rock.

(3) The analytic work was extended to higher and lower grade samples in order to test ideas developed and to answer questions which arose under (1) and (2), above.

GEOLOGIC DESCRIPTION

Introduction

The Kwoiek Area is defined by the outline of a roof pendant or screen located on the eastern flank of the Coast Range Batholith, British Columbia, Canada. Extending northwesterly from North Bend, B. C., the pendant is approximately 25 miles long and about six miles in width (Fig. 1). Except for the southeastern end, where it is cut by faults along the east side of the Frazier River (Duffell and McTaggart, 1952), the pendant is entirely surrounded by hornblende-biotite or biotite quartz diorite. At least twelve stocks of similar composition intrude the interior of the pendant. These stocks range in diameter from less than a quarter mile to about a mile and a half.

The Kwoiek Area is one of rugged relief, cut by several deep through-going valleys, which were modified by valley glaciers in Pleistocene time. The total relief is about 9000 feet, but locally it seldom exceeds 5000 feet. Vertical geologic control should be good, but the exposure below timberline (5000-6000 feet) is exceedingly poor and the full benefit of the 9000 feet of relief cannot be realized. Exposure above timberline is excellent. Only snowfields and talus slopes keep the exposure above timberline from being almost continuous.

The lack of bedrock outcrops below timberline makes the structural and stratigraphic aspects of this study exceedingly tenuous. The stratigraphic and structural interpretations given below are, therefore,

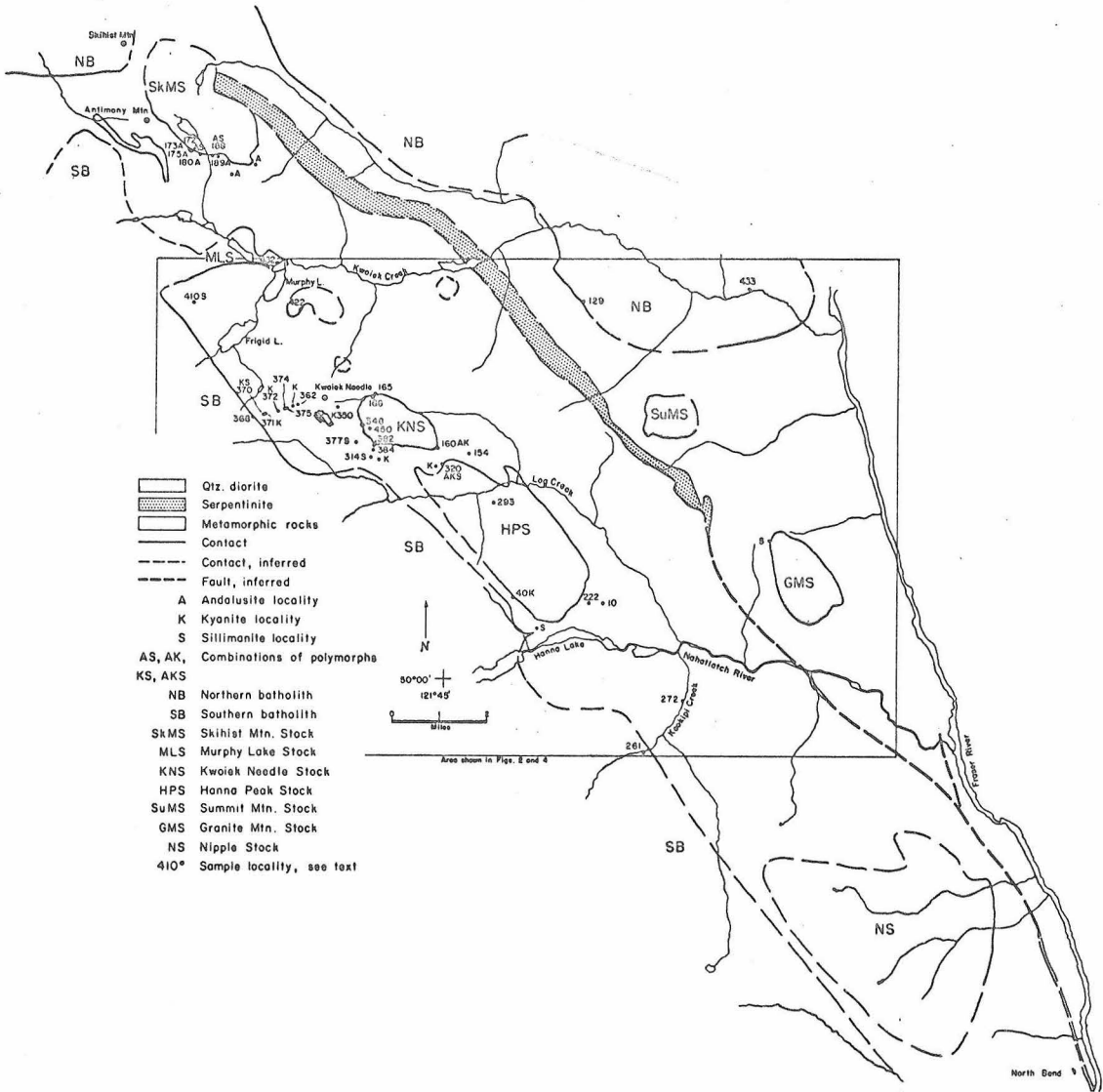


Fig. 1. Geographic limits of the Kwoiek Area, showing locations of stocks, batholiths, major serpentinite body, sample numbers mentioned in text, and locations of Al_2SiO_5 anhydrous polymorphs. Outlined area same as Figs. 2 and 4.

to be regarded as preliminary only and not the major contribution of this work.

Several major geologic features in the Kwoiek Area have a general northwesterly trend as shown on Fig. 1. These include the shape of the pendant itself, the general strike of the bedding and foliation (Fig. 2) and the general trend of the major stratigraphic units (Fig. 2). The major serpentinite belt also has a northwest trend, extending from Skihist Mountain Stock southeastward and continuing southeastward from North Bend another forty miles into the Hope Map Sheet (Cairns, 1942). The alignments of many of the stocks within the pendant also are in a northwesterly direction.

Stratigraphy

Age of rocks

No fossils have been found in the Kwoiek Area; and, as the general stratigraphic-structural knowledge of southwestern British Columbia is incomplete, age assignments are conjectural. Some lithologic units are similar in appearance to named units to the southeast and northeast and these similarities are discussed in the appropriate places below; however, the ages of the similar named units are also uncertain. The rocks southeast of the Kwoiek Area and on the same structural trend as the roof pendant have been assigned ages ranging from Permo-Carboniferous to (?) Lower Cretaceous. The sedimentary and volcanic units are definitely older than the quartz diorite intrusives of the Coast Range Batholith, which have yielded K-Ar ages

Fig. 2. Geologic map showing distribution of major mapped units.

A-A' is line of structure section of Fig. 3. See Fig. 1 for key to batholith and stock names.

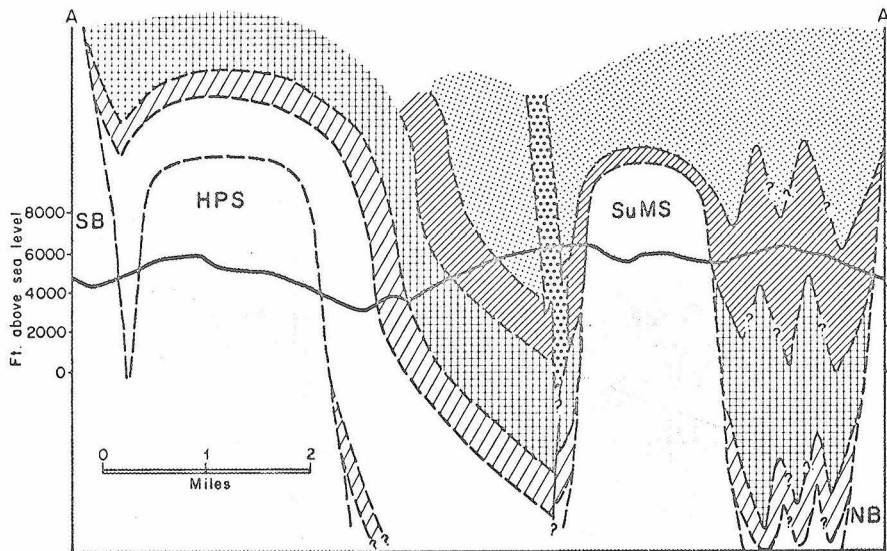


Fig. 3. Structure section along line A - A' of Fig. 2, showing inferred relations of stratified rocks to the quartz diorite intrusives. See Fig. 1 for key to batholith and stock names.

of about 100 million years at several localities (K. C. McTaggart, oral communication, 1964).

At two localities, graded beds indicate younger rocks are to the southwest. One of the localities is approximately two miles north of North Bend on the Frazer River and is in the unit mapped as the Ladner Group (Upper Jurassic or (?) Lower Cretaceous) on the Hope Map Sheet (Cairnes, 1942).

The other locality is $1\frac{1}{2}$ miles southeast of Kwoiek Needle and a quarter mile south of the southern contact of Kwoiek Needle Stock. In the field the rock in this area has a striking lithologic similarity to the Ladner Group (Cairnes, 1942) and the Brew Group (Duffell and McTaggart, 1952), except that the similar units of the Ladner Group contain 10-20 percent CaCO_3 whereas the graded beds south of Kwoiek Needle Stock do not contain a major calcium-bearing phase.

At a third locality, half a mile west of Kwoiek Needle, pillow structures indicate that younger rocks are to the east. The pillows are in the amphibolite unit that crosses Kwoiek Needle and, although relatively undeformed, have been metamorphosed to the almandine-amphibolite facies.

The abundant serpentinite in the Kwoiek Area can also be given a relative age assignment. The serpentinite apparently intrudes the metasedimentary rocks, but it has been cut and metamorphosed by the quartz diorite intrusives.

Stratigraphic succession.

Table 1 shows the inferred stratigraphic succession in the Kwoiek Area. This succession is based on the above evidence for the relative ages of several of the units, the distribution of the two amphibolite units which are the best marker units in the area, and the general spatial relations of the other rock types. The non-amphibolite units are difficult to distinguish in the field because they are all essentially greywacke. However, three criteria were found useful for subdividing the greywacke: graphite content, the presence of more than five percent of a major calcium bearing phase (plagioclase excluded) and, to a lesser extent, grain size of the matrix in the lower grade rocks. The greywacke units (Fig. 2) are composed primarily of the thinly-bedded greywacke described below. In Table 1 it has been divided into two units, the lower greater than 2000 feet thick and the upper about 3500 feet thick. The two units are separated by an amphibolite unit which contains pillow structures, indicative of an igneous origin. The upper greywacke unit is overlain by a second amphibolite, which also contains pillow structures. This upper amphibolite unit appears to pinch out toward the north, east of Kwoiek Needle Stock. Approximately in the same stratigraphic position as the upper amphibolite, but probably below, is a conglomeratic greywacke unit, which was not mappable southeast from Kwoiek Needle Stock but which thickens progressively northwest beyond the limits of Fig. 2. The greywacke units also contain continuous beds of feather amphibolite, 6 inches to 2 feet thick, which occur in the high country west of Kwoiek Needle

Table 1

Generalized Succession of Units in the Kwoiek Area

<u>Unit</u>	<u>Range of thickness (feet)</u>
Calcic greywacke (upper) (top not exposed)	> 2500
Graphitic argillite	1000 - 7000
Calcic greywacke (lower)	1500 - 2500
Amphibolite (upper)	0 - 1500
Greywacke (upper) (conglomeratic greywacke unit, 0 - 1000 feet, near top)	3500 - 4000
Amphibolite (lower)	1000 - 2000
Greywacke (lower) (bottom not exposed)	> 2000

Stock and west of Murphy Lake. These beds are thought to be metamorphosed pyroclastic deposits because they are of thin, uniform thickness over distances of at least half a mile and contain no primary evidence, such as pillow structure, of being a volcanic flow. Their mineralogy, however, is similar to that of the metavolcanic rocks. Below timberline, where outcrops are scarce and discontinuous, specimens of metamorphosed pyroclastic deposits cannot be distinguished from the metamorphosed volcanic flows.

The other rock types described below, such as the calcic greywacke and the graphitic argillite, occur rarely in the greywacke units and increase in abundance towards the top of the upper greywacke unit.

Two calcic greywacke units, separated by a graphitic argillite unit, are also distinguished on Fig. 2. The calcic greywacke units contain, in order of decreasing abundance, calcic greywacke, greywacke, calcic graphitic argillite, and graphitic argillite rock types. The graphitic argillite unit contains, in order of decreasing abundance, graphitic argillite, calcic graphitic argillite, calcic greywacke, and greywacke. The total thickness of the three units averages about 8000 feet.

Rock Descriptions

Metasedimentary rocks, low grade

The major rock type is a greywacke. As discussed above, the map units were arbitrarily defined according to the abundance of several variations of the greywacke. Thus, a description of the greywacke will

serve as a basis for describing the other rock types. In the Kwoiek Area most of the rock types occur in an almost unmetamorphosed state, although there are some metamorphic effects in even the lowest grade rocks. These effects are typically the development of chlorite porphyroblasts and some recrystallization of the quartz and feldspar.

The greywacke is typically thinly bedded, and this primary sedimentary feature can be identified in even the highest grades of metamorphism. It is only obliterated with the development of migmatite. The rock consists of dark-grey, fine-grained beds, typically less than 4 mm. thick, and rarely as much as 5 cm. thick, alternating with light-grey, coarser-grained beds of the same thickness range (plate 1). The light beds consist of 25-50 percent quartz and plagioclase clasts, ranging in diameter from .05 to .2 mm., in a matrix of finer-grained quartz and plagioclase as well as white mica and chlorite, typically .01 to .05 mm. in the long dimension. The white mica and the finer-grained chlorite invariably show preferred orientation parallel to the bedding. Where coarse, 0.2 to 1 mm. long chlorite porphyroblasts develop, they show no preferred orientation. Graphite constitutes less than 5 percent of the rock.

The calcic greywacke rock type is similar to the greywacke except that it contains 5 to 25 percent calcite in blebs of about the same size as the coarsest quartzo-feldspathic fraction. In somewhat higher grades of metamorphism clinozoisite (or epidote) and actinolite are developed. The clinozoisite or epidote has no preferred orientation and ranges in size up to .5 mm. The actinolite, in needles up to 1 mm.

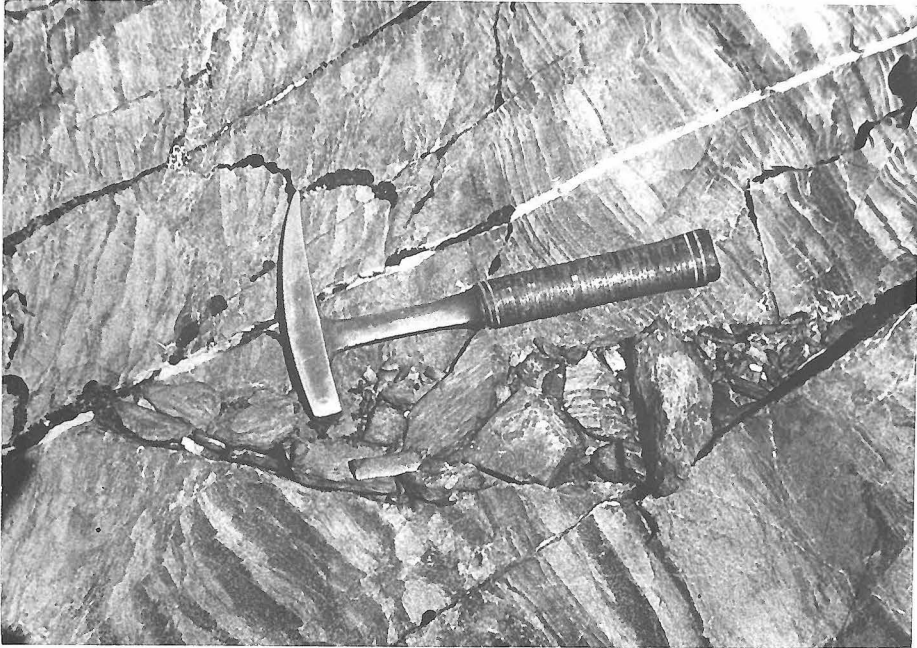


Plate 1. Thinly-bedded greywacke rock type found on ridge between Kwoiek Needle and Pyramid Mountain (Fig. 2).

long, occurs in sheafs parallel to schistosity but randomly oriented within the planes of schistosity.

The graphitic argillite is finer grained than the greywacke and appears to have the mineral content of the greywacke's matrix except that abundant graphite is present. Graphite-rich layers with 75 percent or more graphite are common. These layers, 2-4 mm. thick, alternate with quartzo-feldspathic layers of similar thickness and with an average grain size of about .2 mm. It is not clear if this is the original, clastic grain size or is a product of recrystallization. A rock was classified as "graphitic" if graphite could be identified in handspecimen.

The calcic-graphitic rock type is a variant of the graphitic argillite and the calcic greywacke. More than 5 percent of a major calcium-bearing phase is present as is more than 10 percent graphite. The grain sizes also range between the two types, the coarser-grained rocks being called calcic-graphitic greywacke, and the finer-grained rocks being called calcic-graphitic argillite.

The conglomeratic greywacke contains a matrix which could be classified as any of the above rock types but contains pebbles and cobbles, which in some places are two feet in diameter. In many cases the pebbles and cobbles are angular in shape and include volcanic, calcic greywacke, or greywacke rock types. Quartzite clasts are common.

Metasedimentary rocks, high grade

In the higher grades of metamorphism the sedimentary textures and general grain size of the greywacke are preserved (except in the gneissic and migmatitic rock described below) but aluminum-silicate porphyroblasts up to 2 cm. long, staurolite porphyroblasts up to 6 mm. long, and garnet porphyroblasts up to 1 mm. in diameter are easily recognized with the unaided eye. These porphyroblasts are scattered throughout the rock but tend to be more concentrated in the darker, less quartzo-feldspathic beds. On weathered surfaces the staurolite grains, being more resistant than the rest of the rock, project out distinctly, and it is easy to observe the twin habits of the staurolite. On one specimen 60° twins, 90° twins, untwinned grains, and "triplets," or doubly 60° twinned staurolite grains, were observed. The chlorite in the higher metamorphic grades maintains its non-preferred orientation, the biotite (.2 to .5 mm.) also is typically not oriented, the staurolite is not oriented, and the aluminum silicates are generally randomly oriented within planes of schistosity or bedding. Modes of several high-grade greywackes are given in Tables 9 and 10.

In the higher grades of metamorphism the calcic greywacke develops amphibole porphyroblasts up to 1 cm. long which, on a weathered surface, are seen to lie in the foliation planes but randomly oriented. The amphibole grains are generally in sheaf-like aggregates. Garnet porphyroblasts up to 2 mm. in diameter are also present in rocks of suitable grade. Calcic pyroxene occurs at two localities next to stocks.

The graphitic argillite in the higher grades of metamorphism preserves its lower-grade textural features except that porphyroblasts of andalusite up to an inch or more in length can be present. These porphyroblasts lie parallel to the bedding planes. The other metamorphic minerals that grow in this rock type, such as biotite, staurolite, and garnet, are generally too fine-grained to readily identify with the unaided eye.

Typical localities of the various rock types are as follows: The greywacke occurs in well-exposed outcrops west and east (Plate 1) of Kwoiek Needle. The calcic greywacke, which is similar in outcrop appearance to the greywacke, crops out along the Fraser River, two miles north of North Bend. Pitted, weathered surfaces on the calcic greywacke in the low grades are common and rocks of this type are exposed near the road two miles south of the main bridge crossing the Nahatlatch River. The graphitic argillite is well exposed near the mouth of the Nahatlatch River as well as on the ridge south of Pyramid Mountain.

Metavolcanic rocks.

The metavolcanic rocks, or amphibolites as they are mapped on Fig. 2, are typically dark green, fine-grained, hard, massive rocks. All occurrences of this rock type mapped are found above the garnet grade of metamorphism and contain essentially the same minerals wherever found. The minerals are, in approximate order of decreasing abundance, amphibole, plagioclase, biotite, epidote, quartz, and garnet.

Opaques, ilmenite where positively identified, and sphene can also be present. The garnet porphyroblasts, as much as 3 mm. in diameter, are generally larger than those in the associated metasedimentary rocks. The amphibole crystals rarely show orientation but are typically less than 1 mm. long.

In many places of good exposure, such as around Kwoiek Needle, pillow structure can be seen. The rims of the pillows contain more amphibole and less epidote than the centers. The proportion of minerals in the matrix is about the same as in the rims of the pillows. Below timberline, where exposure is poor, pillows could not be identified.

Serpentinite.

Serpentinite bodies are common in the Kwoiek Area and occur in all of the mapped units. Most of the bodies are less than a few hundred feet wide and consequently are too small to be mapped.

The largest serpentinite mass crops out almost continuously from Skihist Mountain Stock southeastward to North Bend. Duffell and McTaggart (1952) show its extension beyond Skihist Mountain Stock to the northwest. The serpentinite mass is composed primarily of the serpentine minerals with rare chromite and magnetite pods. At its boundaries, where visible, reaction with the country rock is apparent.

Intense shearing within the serpentinite is common at the serpentinite-country rock contacts. In the wider parts of the large serpentinite mass the serpentinite has the classic pod and swirl

texture. Relic olivine or pyroxene was not identified; however, olivine, possibly formed from serpentine by contact metamorphism, occurs in the major serpentinite body at the contact with Skihist Mountain Stock. Nephrite boulders have been found in the major drainages of the Kwoiek Area as well as along the Fraser River. These boulders undoubtedly were weathered from the serpentinite of the Kwoiek Area and other serpentinite bodies in the eastern edge of the Coast Range Batholith, but none have been reported as found in place.

In addition to the major northwest-trending serpentinite body shown in Figs. 1 and 2, other large serpentinite bodies were noted west of Antimony Mountain, east of Antimony Mountain, and west and north of Murphy Lake. Commonly associated with the serpentinite is a coarse-grained hornblende diorite, containing, where unmetamorphosed, only the two minerals hornblende and plagioclase.

The best exposure of the serpentinite, showing all the contact effects and internal structure as well as the diorite associated with the serpentinite, is where the main serpentinite crosses Pyramid Mountain.

Intrusive rocks.

All the intrusive rocks are medium-grained (1-5 mm.), massive, and contain about 10 percent dark minerals. The texture is allotriomorphic granular. There is no chilling at the margins; in fact, the border phase of the intrusives, a muscovite quartz-diorite, is coarser grained than the normal biotite or hornblende-biotite quartz

Table 2

Modes of Intrusive Rocks

Sample number	293	433	129B	450	368	261	432	166I	166C	348	422
Plagioclase	61.8	61.8	62.2	60.4	51.6	53.4	57.0	65.4	53.2	57.4	46.2
K feldspar	-	-	-	-	-	-	-	-	-	0.2	4.0
Quartz	27.0	21.4	23.0	31.8	28.0	34.0	25.2	27.4	42.0	36.0	39.2
Biotite	9.3	2.8	12.0	7.4	16.0	10.4	12.8	6.0	0.2	-	-
Muscovite	-	-	-	0.2	0.2	0.4	0.4	0.4	2.3	4.6	9.2
Hornblende	-	5.0	0.2	-	4.2	1.8	3.2	-	-	-	-
Epidote	0.7	3.0	2.0	0.2	-	-	-	-	0.2	-	-
Chlorite	-	5.4	-	-	-	-	0.8	0.8	-	1.4	-
Opaque	-	0.2	-	-	-	-	0.2	-	-	0.4	0.8
Sphene	1.1	0.4	0.8	-	-	-	-	-	-	-	-
Garnet	-	-	-	-	-	-	-	-	-	tr	0.6
Pyroxene	-	-	-	-	-	-	0.4	-	-	-	-
Plagioclase composition	An ₂₅₋₅₅	An ₂₅₋₅₂	n.d.	An ₁₇	An ₃₁₋₅₂	An ₁₉₋₃₀	n.d.	An ₃₀	An ₁₈	An ₁₇	An ₂₅

Numbers in volume percent. Samples 450, 293, and 166I are from stocks; 368, 261, 432, 129B, and 433 are from the batholiths; and 166C, 422, and 348 are from the border phase associated with the stocks. See Fig. 1 for sample locations. Combined carlsbad - albite twins were used for the plagioclase compositions of 368 and 433. The Michel-Levy technique was used on the other specimens.

diorite. The batholithic rocks typically contain hornblende as well as biotite, whereas the stocks contain biotite only. The plagioclase of the batholithic rocks is more strongly zoned and contains a higher anorthite content. Most of the strongly-zoned feldspar grains are oscillatory zoned with as many as four compositional reversals.

Eleven representative samples of the intrusive rocks were selected for modal analyses, stained for potassium feldspar, and point-counted; these modes, based on 500 points, are presented in Table 2. The presence of garnet in several of the border phase rocks suggests possible contamination.

Gneissic and migmatitic rocks.

The greywacke units become gneissic and migmatitic within a quarter mile of the Southern Batholith contact, between the junction of Murphy Lake Stock with the Southern Batholith and the area south of Kwoiek Needle Stock. Grain size increases abruptly, and bedding gives way to gneissosity as the migmatite zone is entered from the less metamorphosed rocks away from the batholith. The rock is a coarse-grained biotite schist containing abundant irregular layers and pods of coarse-grained (0.5-1 mm.) quartz-plagioclase rock. The quartzofeldspathic fractions can constitute 10-25 percent of a typical outcrop. Assemblages of three migmatite specimens, 314, 377c, and 410, are given in the Appendix. In addition, the migmatite zone contains numerous quartz diorite dikes, as much as 30 feet thick. Rotated xenoliths indicate an intrusive origin.

Thin sections of the gneissic rocks show carlsbad and multiple albite-twinned plagioclase (andesine) as well as oscillatory-zoned plagioclase in both biotite and quartzo-feldspathic layers. The occurrences of multiply-twinned and oscillatory-zoned plagioclase grains in metamorphic rocks only in a narrow zone along the Southern Batholith contact, where the metamorphic temperatures can be presumed to be very high, suggests these grains might have crystallized from a melt. As evidence of injection is lacking, it is probable that the melt was formed by partial melting essentially in place. The time spent in the migmatite zone did not permit detailed tracing of the dikes; therefore, it is not known whether the dikes originate from the batholith or are melted fractions that moved out of the metamorphic rocks.

Structure

The major structural features include northwest-trending folds, which are believed to be related to the intrusion of the batholith, an inferred northwest trending fault, which is believed to be related to the intrusion of the serpentinite, and northerly-trending faults along the east side of the Fraser River, which are later than the intrusion of the batholith. The latter feature, not shown on Figs. 1 and 2, was mapped by Duffell and McTaggart (1952).

The amphibolite units are the only good marker units in the Kwoiek Area. The lower amphibolite, containing pillow structure (Table 1), was followed across Kwoiek Needle (Fig. 2) and appears to wrap around Kwoiek Needle and head northwest. However, a glacier on the north side

of Kwoiek Needle and the general inaccessibility of the region around Frigid Lake makes its northwestward extension uncertain. The amphibolite, containing pillow structure, encountered on a traverse west of Murphy Lake, is inferred to be the same one which crosses Kwoiek Needle. Pillow structures in the vicinity of Kwoiek Needle indicate younger rocks to the east, making the fold around Kwoiek Needle an anticline.

The fold which involves the upper amphibolite, about three-quarters of a mile southeast of Kwoiek Needle (Fig. 2), is the best confirmed fold of the Kwoiek Area. Its entire configuration was traced out in the field; and graded beds in the greywacke unit at its east limb indicate younger rocks to the west, making the fold a syncline. This amphibolite is believed to be the same as that shown wrapping around Hanna Peak Stock. Amphibolite was found just north of Hanna Lake, at two places up Kookipi Creek, and at numerous places along the east side of Hanna Peak Stock. The distribution of the amphibolite is consistent with the interpretation of an anticline with its axis nearly parallel and coincident with the long axis of Hanna Peak Stock.

The generally low easterly dipping (15° - 50°) beds between the serpentinite and the upper amphibolite and the steeply dipping beds east of the serpentinite are consistent with the interpretation of a synclinal axis nearly paralleling the main serpentinite. This synclinal axis coincides with an inferred fault along which the major serpentinite mass is presumed to have been intruded. This fold

interpretation is conjectural and is difficult to prove or disprove because of the absence of marker units northeast of the upper amphibolite where it occurs on the east side of Hanna Peak Stock.

The lack of small scale folds in individual outcrops or of folds in the feather amphibolites which are traceable for as much as a half mile, as well as the relatively low plasticity indicated by the textures, suggests that extensive small scale isoclinal folding related to the major folds is absent.

The structure section (Fig. 3) is based on the interpretation that the folding of the units is the result of the intrusion of the batholith and the stocks. This interpretation is primarily the result of observations on the change of attitude of bedding and foliation as one approaches a stock or batholith contact. The attitudes tend to parallel the contact near it, whereas the attitudes away from the contact can be at any angle to the contact. Well-documented examples of this are at the southern end of Hanna Peak Stock, northern end of Granite Mountain Stock, and the western edge of Kwoiek Needle Stock (see Fig. 2). Attitudes more than a quarter of a mile away from the stocks tend to parallel the Southern and Northern Batholith contacts. In detail, however, the stocks do cross-cut bedding.

Although the structural evidence strongly suggests the intruding stocks made room for themselves by pushing aside the intruded rocks, some assimilation and stoping must also have taken place. This is evidenced by numerous xenoliths at the contacts as well as the megaxenoliths as much as half a mile long seen in Kwoiek Needle Stock.

METAMORPHIC REACTIONS

Introduction

The variation of metamorphic grade in the Kwoiek Area is indicated by the distribution of isograds on Fig. 4. The broadest areas of high metamorphic grade are along the Southern Batholith contact. The grade decreases away from the contact to the northeast but increases on approach to the Northern Batholith contact as well as around each of the stocks. However, even at the stock contacts and at the contacts of the Northern Batholith the metamorphic grade is well below that found as much as a mile from the Southern Batholith contact. The grade at the contacts of the stocks close to the Southern Batholith contact is higher than that around the stocks closer to the center of the pendant. For example, the grade on the northeastern side of the Kwoiek Needle and Hanna Peak Stocks (KNS and HPS on Fig. 4) is greater than around Granite Mountain (GMS) or Summit Mountain Stocks (SuMS). The grade at the Northern Batholith (NB) contact is greater than that around Summit Mountain or Granite Mountain Stocks but is close to that at the northeastern contact of Hanna Peak Stock.

The isograds mapped are not simply the lines enclosing all occurrences of a given index mineral but represent the surface traces of metamorphic reaction surfaces. Isograd 2 on Fig. 4 does enclose all occurrences of garnet as well as representing a specific reaction. The sillimanite isograd could be shown on Fig. 4 but is not because it is

Fig. 4. Map showing distribution of quartz diorite intrusives and mapped isograds. Number and letter symbols indicate locations of particular assemblages as tabulated in Tables 3, 4, 6, and 7. See Fig. 1 for key to batholith and stock names.

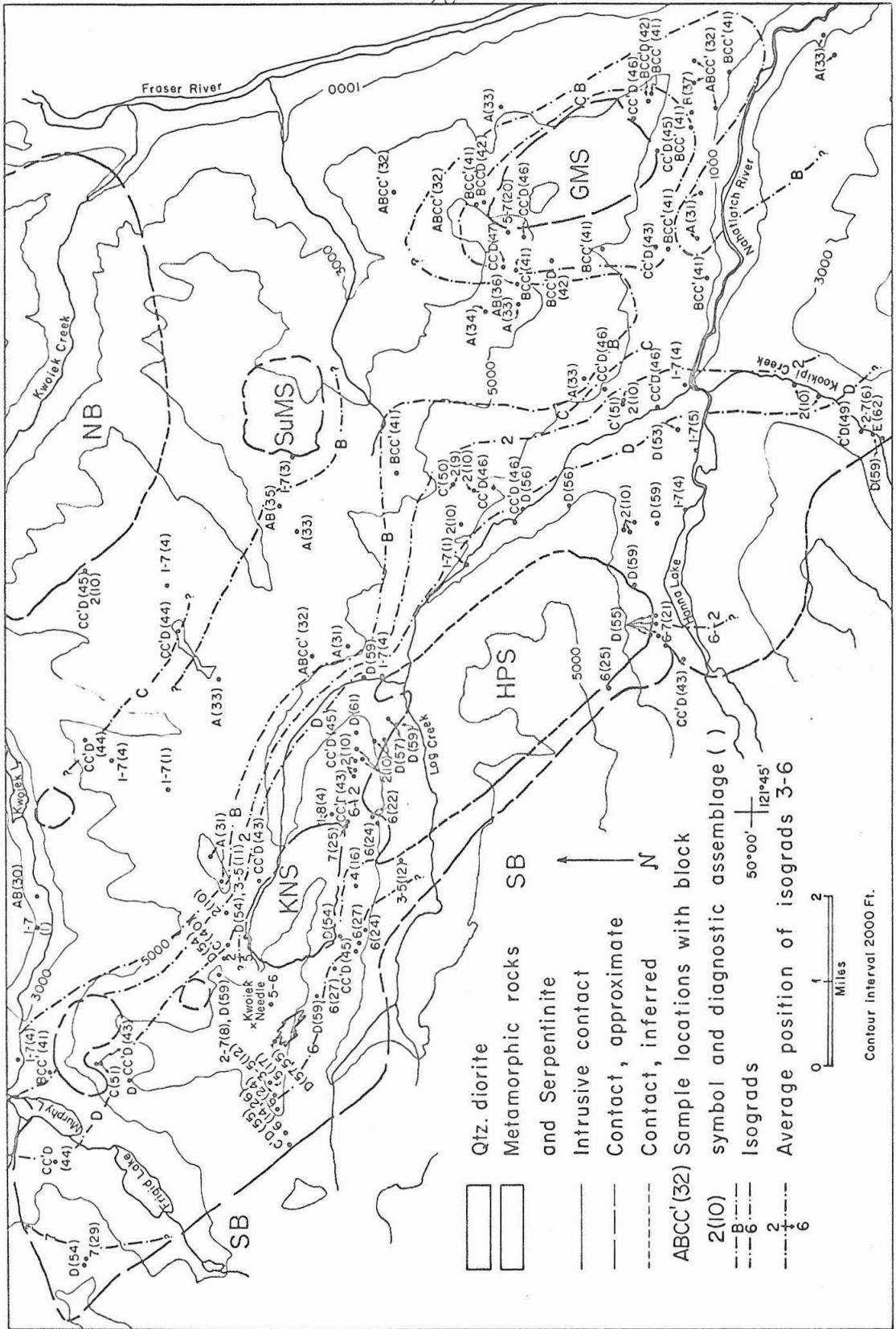


Fig. 4.

nearly coincident with isograd 6.

The isograds mapped in the Kwoiek Area are separated into two distinct types. One type consists of those reactions that have taken place in rocks with a moderate calcium content. By this is meant that in all metamorphic grades at least one major calcium-bearing mineral, such as diopside, an amphibole, epidote, or calcite, is present. The other type consists of rocks without a major calcium-bearing mineral, although significant amounts of calcium do occur in the plagioclase and garnet.

Most of the rocks in the Kwoiek Area give reactions in the first group and these reaction boundaries are the most instructive for giving an idea of relative temperature gradients in the lower grade rocks. However, in the higher grades, reaction boundaries for the high-calcium (high-Ca) rocks are not as closely spaced, relative to the inferred temperature gradient, as in the lower grade rocks. For example, assemblages including hornblende and garnet occur well before the appearance of staurolite in the low-calcium (low-Ca) rocks and persist into the area where sillimanite appears. Only at the igneous contacts does a calcic pyroxene appear. On the other hand, at least two isograds can be mapped in the low-Ca rocks in this interval, and two more must exist but are not mappable due to paucity of rocks with appropriate composition. Hence, isograds in high-Ca rocks are most useful in lower grade regions and isograds in low-Ca rocks are most useful in the higher grade regions.

The following sections give a detailed description of each of the isograds. However, all the analytical work was done on samples of the low-Ca rocks. The discussion of the isograds in the low-Ca rocks serves as the framework for the discussions on the analytical work.

The locations of the specimens mentioned in the text are shown in Fig. 1, and the assemblage for each specimen is listed in the Appendix. Also in the Appendix is a list of mineral names which are keyed to the abbreviations used in the text. The assemblages on which the location of the isograds was based are shown by number or letter symbols on Fig. 4 and are keyed to Tables 4 and 7.

Reactions in High-Ca Rocks

Eskola (1920) based his classic facies concept on the metamorphic minerals developed in rocks of basaltic composition. Little definitive work has been done since that time to establish a detailed sequence of reactions in basaltic or high-Ca rocks, although facies or subfacies have been defined and redefined by the occurrences of critical assemblages of minerals in metamorphosed basalts and high-Ca rocks (most recent review in Turner and Verhoogen, 1960). The Kwoiek Area presents an unusual opportunity to study reactions in high-Ca rocks because high-Ca rock compositions are found continuously from the quartz - albite - muscovite - chlorite subfacies of the greenschist facies to the sillimanite - almandine - muscovite subfacies of the almandine - amphibolite facies (Turner and Verhoogen, 1960). Thus it

should be possible to draw phase diagrams containing several coexisting assemblages for any given P and T in the Kwoiek Area. Changes in the topology of the phase diagrams with increasing grade of metamorphism will define an isograd for which a reaction can be written.

Graphical treatment of the high-Ca assemblages is difficult. Even in the presence of quartz and with $\mu_{\text{H}_2\text{O}}$ and μ_{CO_2} assumed externally controlled (Thompson, 1957), there are six components that are important: CaO, Na₂O, Al₂O₃, FeO, MgO, and K₂O. Therefore, several simplifying assumptions must be made. The first is that there is only one important Na₂O-bearing phase in the rocks, plagioclase, which occurs in all assemblages so that Na₂O is not a critical compositional variable. The second is that FeO and MgO can be treated as one component. This is true if the minerals dealt with have a complete solid solution with respect to MgO and FeO for the range of rock compositions observed in the field and do not have greatly different partition coefficient for FeO and MgO. This assumption is believed to be valid for chlorite, biotite, and calcic amphibole but breaks down with the appearance of garnet. These two assumptions reduce the total number of effective components to four, Al₂O₃, K₂O, FeO+MgO and CaO, which can form the corners of a tetrahedron. This tetrahedron is shown in Fig. 5. Figures 5a, 5b, and 5c represent the changes in topology of the diagram with increasing metamorphic grade prior to the first appearance of garnet. With the appearance of garnet, a mineral with limited Mg-Fe solid solution, a simple phase diagram cannot be drawn,

Fig. 5. ACKF tetrahedra showing four-phase assemblages of low-Ca rocks of blocks A, B, and C (Tables 3 and 4).

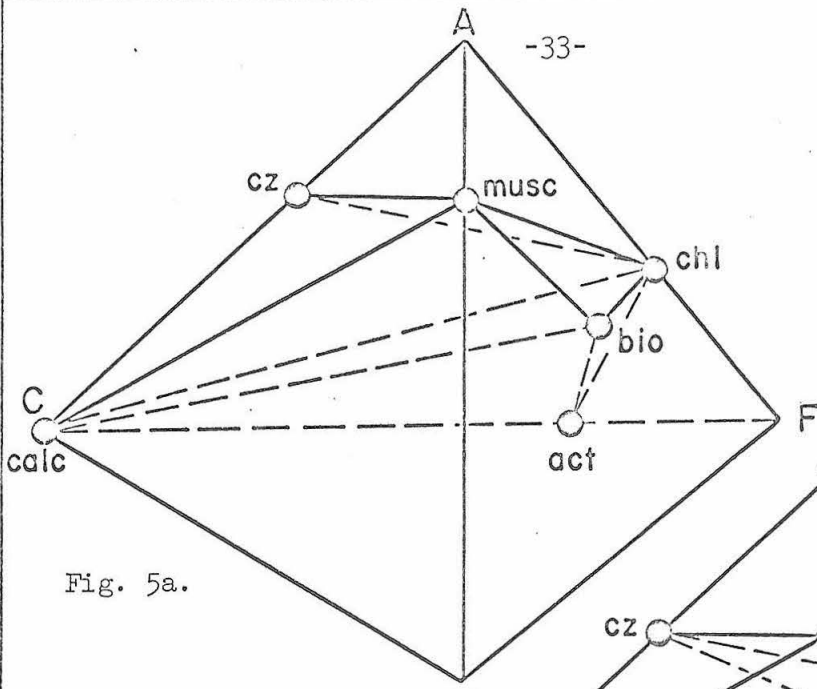


Fig. 5a.

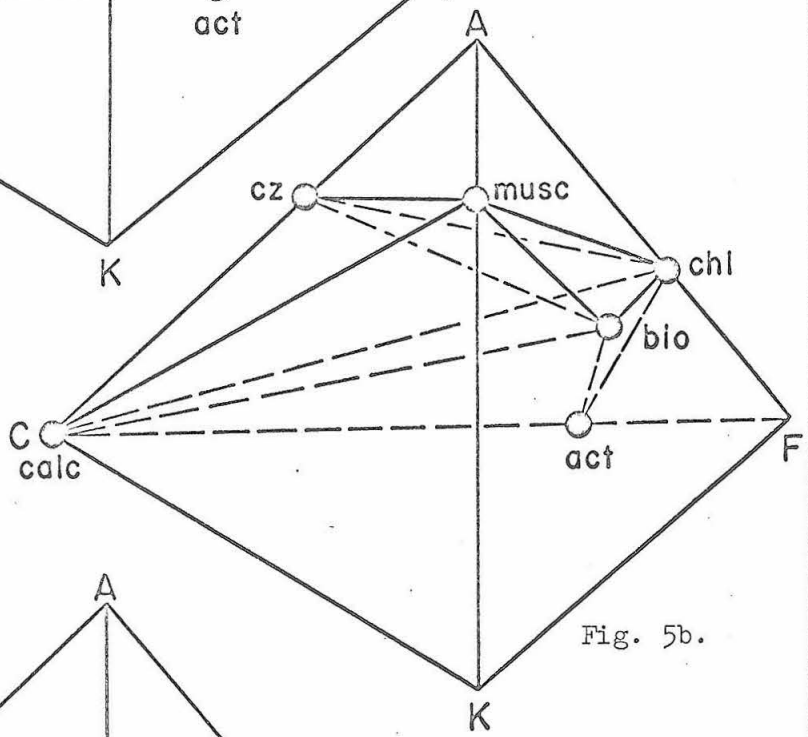


Fig. 5b.

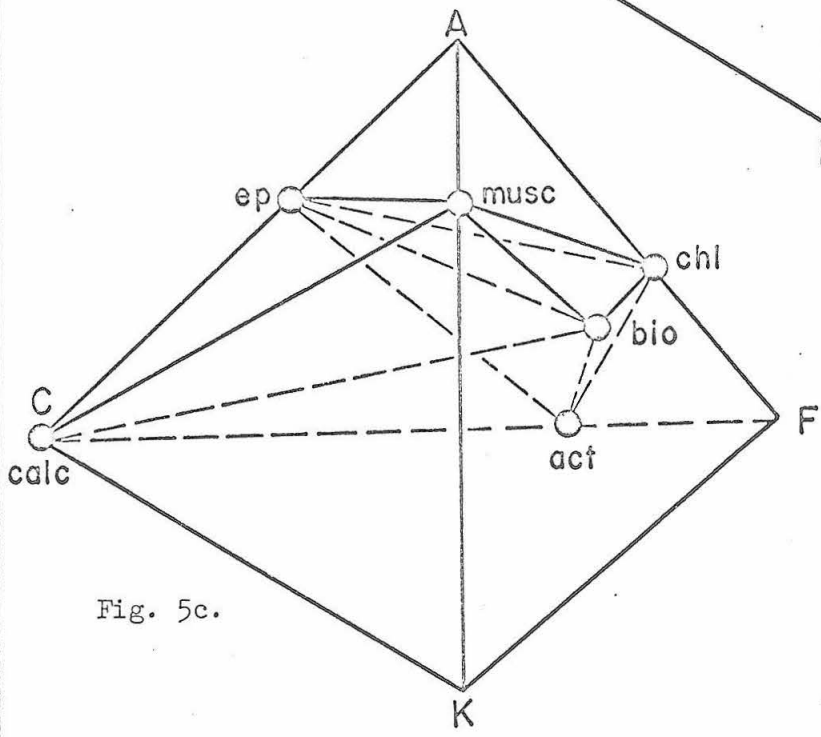


Fig. 5c.

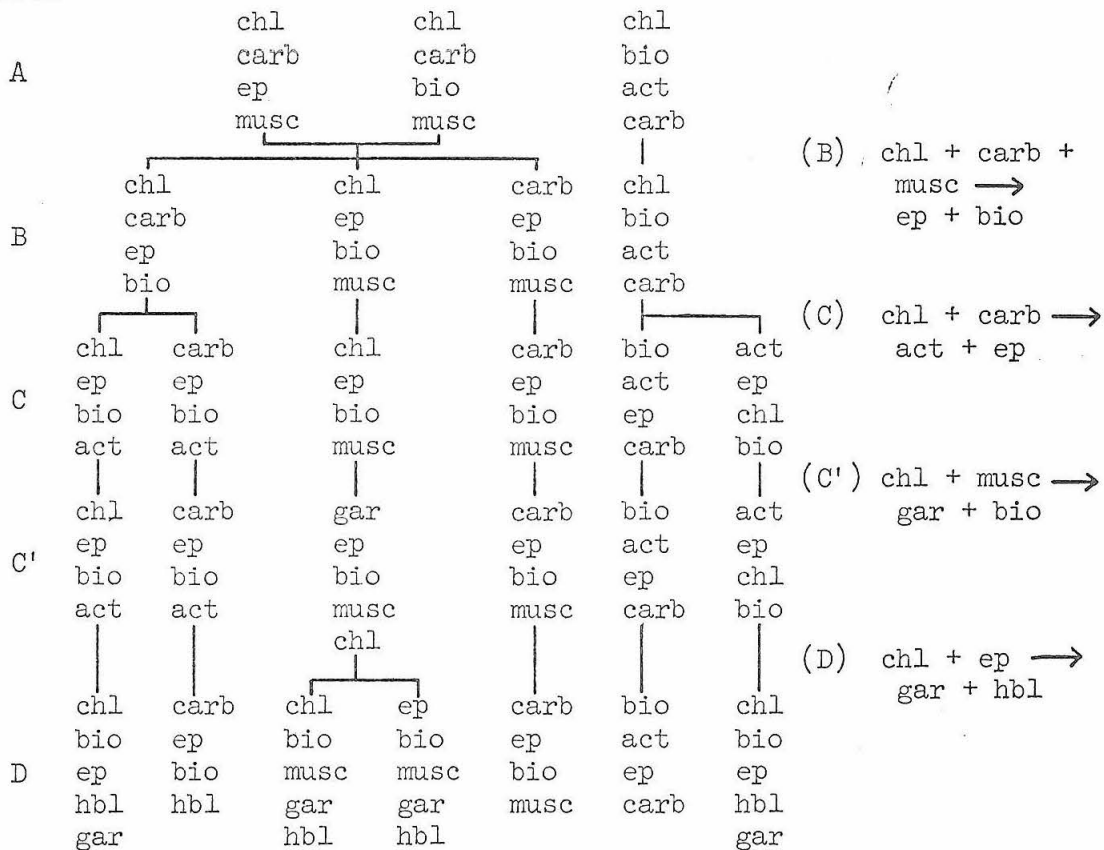
and it becomes convenient to represent the assemblage changes with metamorphic grade tabularly, as in Table 3.

The several groups of minerals listed from left to right on Table 3 are coexisting assemblages that can coexist over a range of temperature (solid pressure assumed constant in the Kwoiek Area). This range of temperature is called a block and is labeled A, B, C, C', or D. To go from one block to another in the direction of increasing temperatures (for example from block A to block B) a reaction must take place that involves the breaking of tie-lines on Fig. 5 or the appearance or disappearance of a phase. The lines connecting assemblages of different blocks show the new assemblages which must form when one of the reactions take place. Not all assemblages will change from one block to another, and assemblages in higher temperature blocks can be produced by more than one path, originating from initially different assemblages. For example, the chl - carb - ep - musc and the chl - bio - act - carb assemblages can both lead to the chl - ep - bio - act assemblage. The reactions between blocks are isograds and can be mapped. On Fig. 4 the isograds are labeled by the block symbol (letters for high-Ca rocks and numbers for low-Ca rocks) of the higher grade group of assemblages. Table 4 shows the list of all assemblages found, the number of rocks of each assemblage found, and a number keyed to sample localities on Fig. 4 (the numbers in parentheses on Fig. 4). Not all the observed assemblages contain all the minerals that could be found in the rock. This is because the compositional fields indicated by planes and lines on

Table 3

Coexisting Assemblages
with Increasing Metamorphic Grade in High-Ca Rocks

Block



The assemblages in each block can coexist at the same metamorphic grade, which increases by blocks from top to bottom. The reactions between blocks are indicated, and letters in parentheses refer to isograds mapped on Fig. 4. Lines connect assemblages related by the reactions.

Table 4

Assemblages in High-Ca Rocks Observed in the Kwoiek

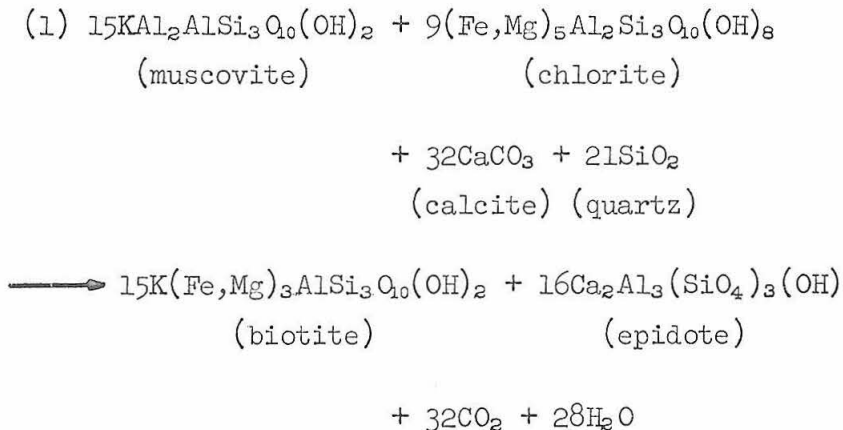
Area and Number of Specimens Observed with Each Assemblage

Block	Assem- blage number	Assemblage						Number specimens found
AB	30		chl	carb				1
A	31	musc	chl	carb				8
ABCC'	32	musc	chl		ep			7
A	33	musc	chl	carb	ep			7
A	34	musc	chl	carb		bio		1
AB	35		chl	carb		bio		1
AB	36		chl	carb			amph	1
B	37		chl	carb	ep	bio		1
BC?	38		chl	carb	ep	bio	amph	1
ABCC'D	39					bio	amph	5
ABCC'D	40		chl			bio	amph	7
BCC'	41	musc	chl		ep	bio		10
BCC'D	42		chl		ep	bio		4
CC'D	43				ep		amph	5
CC'D	44		chl		ep		amph	4
CC'D	45				ep	bio	amph	4
CC'D	46		chl		ep	bio	amph	7
CC'D	47			carb	ep	bio	amph	1
C'D	48		chl		ep	bio	gar	1
C'D	49	musc			ep	bio	gar	1
C'	50	musc	chl		ep		gar	2
C'	51	musc	chl		ep	bio	gar	3
D	52	musc	chl			bio	amph	1
D?	53	musc	chl		ep	bio	amph	1
D	54						amph gar	4
D	55					bio	amph gar	8
D	56	musc			ep	bio	amph gar	2
D	57				ep	bio	amph gar	2
D	58		chl		ep		amph gar	1
D	59		chl			bio	amph gar	7
D	60	musc	chl			bio	amph gar	1
D?	61	musc	chl		ep	bio	amph gar	1
E	62					bio	amph calcic pyroxene	1

Block letters refer to blocks of Table 3 which contain the assemblage. The assemblage number is keyed to the isograd map, Fig. 4. All assemblages contain quartz and plagioclase and most contain ilmenite and graphite as additional phases.

Fig. 5 are actually large volumes due to the variation of Fe and Mg. Thus a rock composition is almost as likely to fall in a three-phase volume as in a four-phase volume. Possible assemblages outside the volume calc - ep - musc - chl - bio - act of Fig. 5 are not considered in this section.

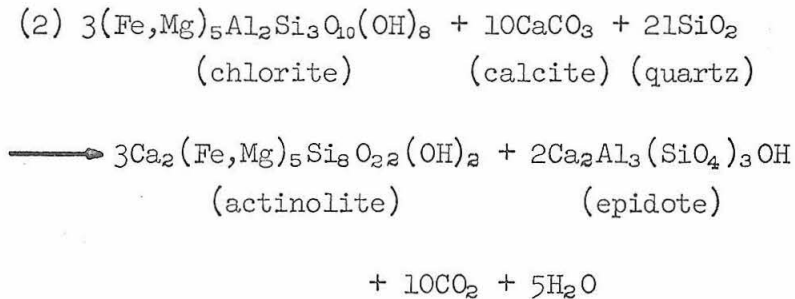
The first reaction identified is based on the observation that in the rocks furthest from any stock or batholith and which appear low grade texturally the assemblages designated in block A are common. In rocks closer to a heat source than those of block A, the three minerals chl - carb - musc were not found together, but combinations involving two of the three were found together. Thus a reaction involving all three of these minerals must have taken place. No new mineral is present in block B that is not present in block A, but biotite and epidote became more abundant. Therefore a reaction of the type



must have taken place.

Equation (1) has been mapped on Fig. 4 and labeled isograd B, indicating the passing from block A to block B of Table 3 and from Fig. 5a to Fig. 5b.

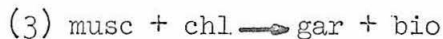
At higher grades it was noted that chlorite and carbonate are not found together, but a blue-green amphibole (probably close to actinolite in composition) becomes abundant. This indicates a reaction of the type



has taken place.

Equation (2) is represented in Fig. 4 as isograd C.

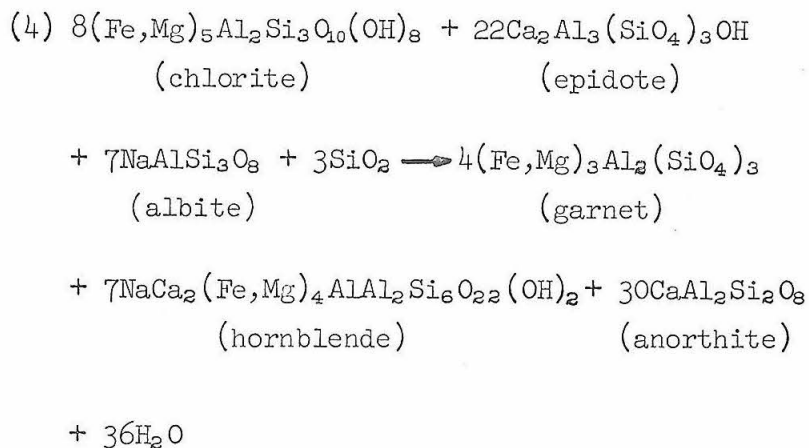
The next apparent change of mineralogy is the appearance of garnet by the reaction



This reaction will be discussed in the next section as it properly belongs to the low-Ca reaction series. It is important to mention here because it does occur at a lower grade than the next reaction which involves the appearance of hornblende with garnet.

With the appearance of hornblende and garnet together, epidote and chlorite do not appear stably together, thus suggesting a reaction

of the type



This reaction is represented as isograd D on Fig. 4 and is the last clearly recognizable reaction in the high-Ca rocks before the appearance of calcic pyroxene at two localities at igneous contacts.

The predicted consequences of reaction 4 are that the plagioclase will increase in anorthite content and the amphibole will be more like a true hornblende than the actinolite of the lower grade rocks. These predictions are supported by changes in optical properties of the phases. The plagioclase has a distinctly higher relief than that in block C assemblages, and the amphibole pleochroism in the \underline{z} direction becomes a darker green than in the lower grade amphiboles.

As can be seen in Table 4, not every assemblage is diagnostic of a particular block. Fewer phases than those listed for each assemblage may be present, thus increasing the ambiguities of determining by the assemblage which block a particular rock belonged to. It is possible,

however, to fix the isograds within general limits by comparing different assemblages from rocks collected close to one another. For example, the assemblage chl - bio - musc - ep can occur in block B or C and the bio - ep - amph assemblage can occur in block C or D. If the two assemblages are collected from adjacent outcrops, it is clear that they both belong to block C as they both overlap this block.

Reactions in Low-Ca Rocks.

In the lower metamorphic grades of the Kwoiek Area the low-Ca rocks might be classified as pelitic since they consist predominantly of quartz, muscovite, and chlorite. However, in the higher grade rocks, marked by the appearance of staurolite, primary muscovite is generally absent and the most common assemblage is chl - bio - stl - gar with quartz, plagioclase, ilmenite, and graphite. In the rare cases where primary muscovite is present with staurolite or an aluminum silicate, chlorite is absent.

The term "primary muscovite" was used above to distinguish the muscovite in rocks, in which it is abundant, is oriented along foliation planes, and has a grain size the same or smaller than the coexisting biotite, from two other types of muscovite not considered to be primary. One type consists of shimmer aggregates apparently replacing staurolite, aluminum silicate, or rarely garnet porphyroblasts at their margins. This type can occur anywhere in the Kwoiek Area. Several such aggregates were shown to be muscovite by x-ray

diffraction. The other type of non-primary muscovite consists of porphyroblasts several millimeters long which cross-cut the foliation as well as other minerals in the rock. A discussion of the significance of the non-primary muscovite types is given at the end of this section.

Plagioclase is abundant in the high grade pelitic rocks but the absolute amount present is difficult to determine due to its very small size (< .05 mm.). It probably makes up on the order of 25 percent of the quartzo-feldspathic fraction in most cases. The plagioclase compositions in Table 5 are based on microprobe analysis for CaO. Plagioclase was abundant in all but sample #10 which contained only a trace. Assemblages of the specimens are listed in the Appendix. It is not known why the compositions of individual grains, which are nearly homogeneous, vary so much from point to point in a thin section.

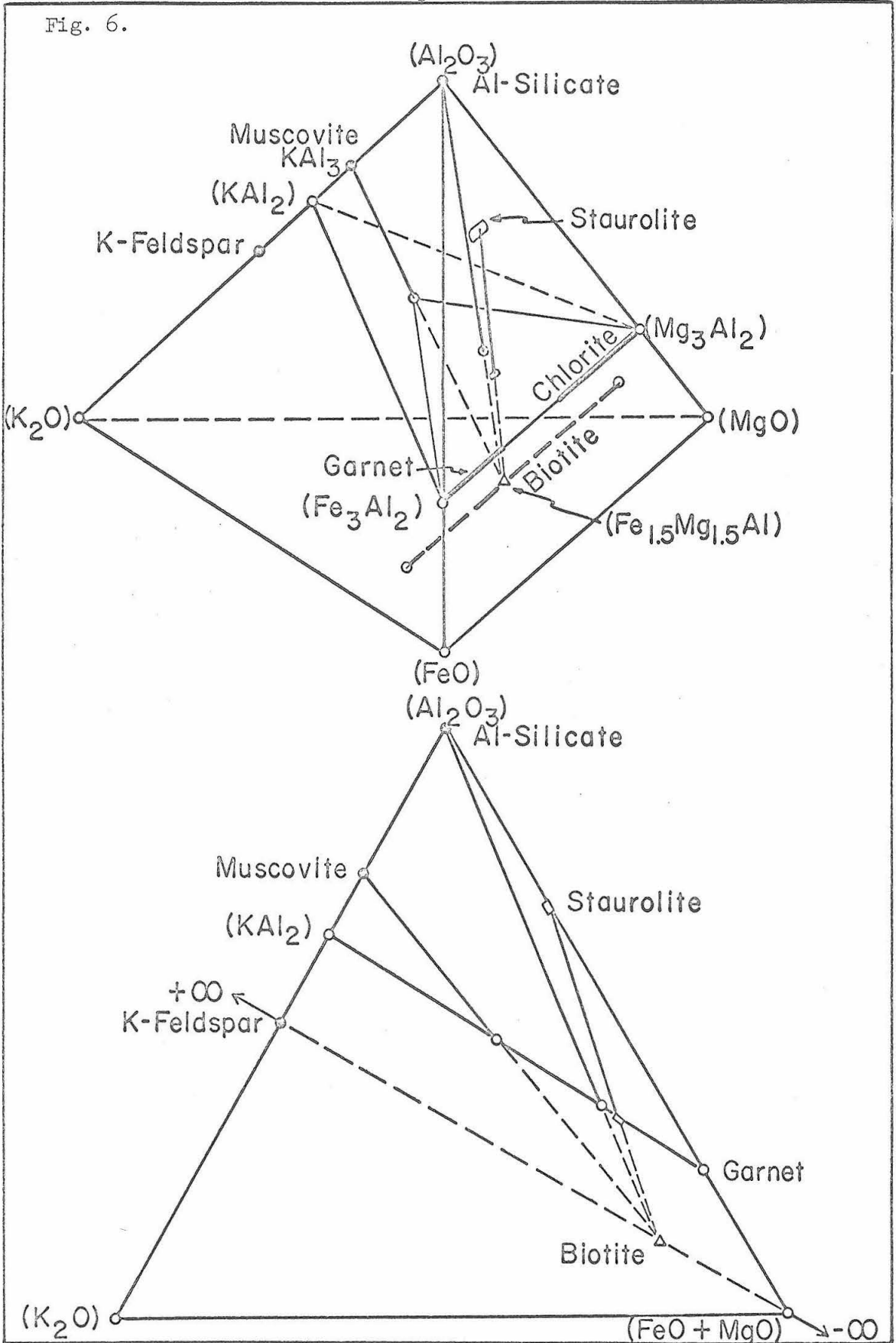
Table 5

<u>Sample Number</u>	<u>Anorthite Contents</u>
154a	28, 30, 31, 34, 35, 35, 46
10	8, 10, 17, 22, 23
350B	31, 28 (edge) - 31 (center)
371C	39

The observed mineral assemblages and the compositions of the coexisting phases are in the $K_2O - Al_2O_3 - FeO - MgO$ system; muscovite-bearing assemblages may be shown on a projection from muscovite

Fig. 6. Geometric relations for deriving AFM diagram of Fig. 7 using biotite ($K Fe_{1.5} Mg_{1.5} AlSi_3 O_{10} (OH)_2$) as a projection point. The three corners of the biotite projections of Fig. 7 are the muscovite composition projected onto the $KAl_2 - Fe_3Al_2 - Mg_3Al_2$ plane, Fe_3Al_2 , and Mg_3Al_2 .

Fig. 6.



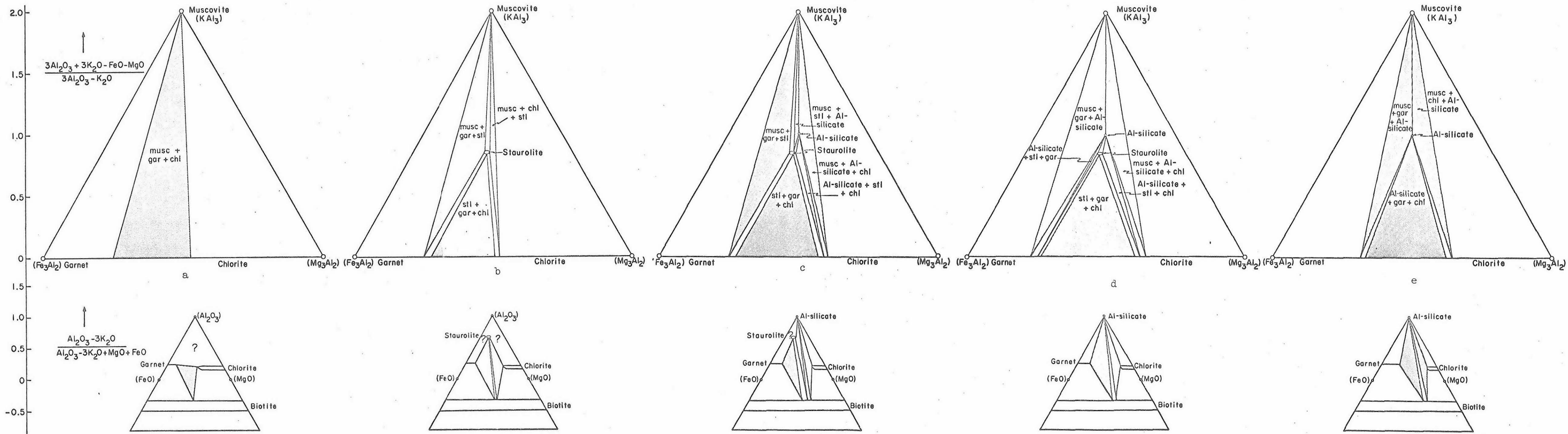


Fig. 7. AFM biotite (upper) and muscovite (lower) projection diagrams showing topologies of diagrams between reactions involving breaking of tie-lines or first appearance or loss of a phase.

(Thompson, 1957), and biotite-bearing assemblages may be shown on a projection from biotite as shown in Figs. 6 and 7. The projection of Figs. 6 and 7 is used because most of the assemblages above the staurolite grade do not contain muscovite, but all the low-Ca rocks of the Kwoiek Area, above the biotite grade, contain biotite.

A three-phase assemblage on either projection would contain the six components SiO_2 , Al_2O_3 , K_2O , MgO , FeO , and H_2O ; it would be tri-variant in P , T , and $a_{\text{H}_2\text{O}}$ so long as any additional phases introduce a new component, and as long as any additional component introduces a new phase. Plagioclase, epidote, graphite, tourmaline, apatite, pyrite, pyrrhotite, or zircon may or may not be present above the garnet grade in any assemblage, but in each case they introduce an additional component. The MnO and Fe_2O_3 content is low and is contained in other phases rather than introducing additional phases; hence, they may constitute additional variables affecting the composition of phases in the three-phase assemblage.

Table 6 shows the mineral assemblages observed in the low-Ca rocks of the Kwoiek Area. The locations of critical assemblages for the defining of isograds are shown in Fig. 4 in a similar manner as for the high-Ca rocks. However, numbers are used for the block symbols rather than letters. All the possible assemblages that could be found in a rock whose initial composition is within the gar - chl - musc - bio volume are shown in Table 7, which is analogous to Table 3 for the high-Ca rocks. The reactions between blocks listed in Table 7 correspond to the changes of topology between the phase diagrams of

Table 6

Assemblages in Low-Ca Rocks Observed in the Kwoiek

Area and Number of Specimens Observed with Each Assemblage

Block	Assemblage number	Assemblage							Number specimens found
1 - 7	1	musc	chl						8
1 - 7	2	musc		bio					3
1 - 7	3			bio					2
1 - 7	4	musc	chl	bio					16
1 - 7	5		chl	bio					1
2 - 7	6	musc(1)		bio	gar				10
2 - 7	7			bio	gar				4
2 - 7	8		chl	bio	gar				17
2	9	musc	chl		gar				1
2	10	musc(1)	chl	bio	gar				24
3 - 5	11	(musc)		bio		stl			1
3 - 5	12	musc(2)		bio	gar	stl			5
3 - 6	13			bio	gar	stl			4
3 - 7	14		chl	bio	gar	stl			21
3 - 7	15	(musc)	chl	bio	gar	stl			5
4	16	musc(1)	chl	bio		stl			3
5	17	(musc)		bio		stl	ky		1
5 - 6	18		chl	bio		stl		and	1
5 - 7	19	(musc)		bio				and	1
5 - 7	20			bio				silli	1
6 - 7	21	(musc)		bio	gar			silli	1
6	22	(musc)		bio	gar	stl	ky	and silli	1
6	23	(musc)		bio	gar	stl		and silli	1
6	24	(musc)		bio	gar	stl	ky		4
6	25			bio	gar	stl	ky		1
6	26			bio	gar	stl	ky	silli	1
6	27	(musc)		bio	gar	stl		silli	2
?	28			bio		stl		and cord	1
7	29		chl	bio	gar			silli	1

Block numbers refer to blocks of Table 7 which contain the assemblage. The assemblage number is keyed to the isograd map, Fig. 4. All assemblages contain quartz, plagioclase, ilmenite, and graphite as additional phases.

(musc): muscovite of all samples with this assemblage is coarse, cross cutting (see text).

musc (2): two samples of this assemblage contain coarse, cross cutting muscovite; the rest contain primary muscovite.

Fig. 7.

The actual composition of both muscovite and biotite differs slightly in the various assemblages and the projection is made from a pure muscovite ($KAl_2AlSi_3O_{10}(OH)_2$) for the muscovite projection and from a biotite composition that contains equal amounts of molar FeO and MgO ($KFe_{1.5}Mg_{1.5}AlSi_3O_{10}(OH)_2$) for the biotite projection. Thus the horizontal axis on the biotite projection is made linear in Fe/Fe+Mg. The composition of the projection phase will be fixed for a given three-phase assemblage, trivariant in P, T, and a_{H_2O} , and could be indicated on the diagram.

Figures 7a, b, c, d, and e show the changes of topology of the projections with increasing grade of metamorphism based on the observed assemblages. Two points of note that can be seen in the comparison of the two projections is that staurolite persists to higher temperatures in non-muscovite bearing assemblages than in muscovite-bearing assemblages, and garnet can exist stably with chlorite at least into the grade of metamorphism where staurolite is no longer stable.

Anticipating the analytical data of later sections, it was observed that garnet and staurolite are zoned whereas muscovite, chlorite, and biotite are unzoned. Therefore, no reaction can be written involving either garnet or staurolite as reactants unless the garnet or the staurolite show evidence of resorption. In the highest grade rocks of the Kwoiek Area, the staurolite does show evidence of resorption. The reactions given in Table 7 and to be discussed below are based on this premise as well as on the premise that pro-grade

recognize in the field.

Reaction (3) -- chlorite + muscovite \rightarrow staurolite + garnet + biotite

The detailed reaction can be broken into the two reactions:

(2) chlorite + muscovite \rightarrow garnet + biotite

(4) $155(\text{Fe,Mg})_5\text{Al}_2\text{Si}_3\text{O}_{10}(\text{OH})_8 + 246\text{KAl}_{1.67}(\text{Fe,Mg})_{0.5}\text{AlSi}_3\text{O}_{10}(\text{OH})_2$
(chlorite) (muscovite)

$\rightarrow 40(\text{Fe,Mg})_4\text{Al}_{18}\text{Si}_8\text{O}_{46}(\text{OH})_2 + 246\text{K}(\text{Fe,Mg})_3\text{AlSi}_3\text{O}_{10}(\text{OH})_2$
(staurolite) (biotite)
 $+ 145\text{SiO}_2 + 580\text{H}_2\text{O}$

If the rock were initially too magnesian to produce garnet before staurolite, reaction (4) could occur before reaction (3) in rocks of the composition being considered here.

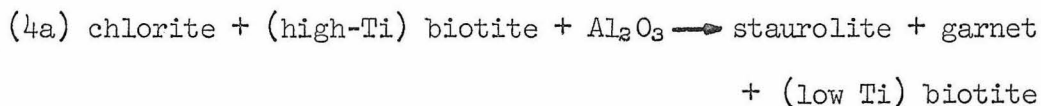
The important consequence of reaction (3) is that the garnet and staurolite which are growing by reaction (3) must be growing at constant temperature because according to the empirical evidence of most metamorphic terraines, including Kwoiek Area, the five phases involved in reaction (3) are not found stably together. Thus, the reaction will proceed under constant temperature until either muscovite or chlorite are used up. The implication of reaction (3) taking place under constant temperature is that the Fe/Fe+Mg ratios of the ferromagnesian minerals must remain constant. It cannot be proven whether chlorite or biotite obey this criterion but the analytical work on the staurolite shows that the criterion is met for that mineral. A discussion of the staurolite zoning and its bearing to this argument is given on page 149ff. The

garnet zoning pattern is not conclusive because of the complicating effects of the additional components MnO and CaO.

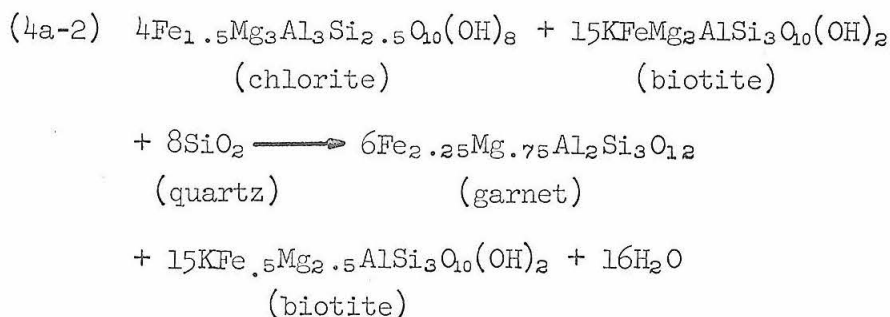
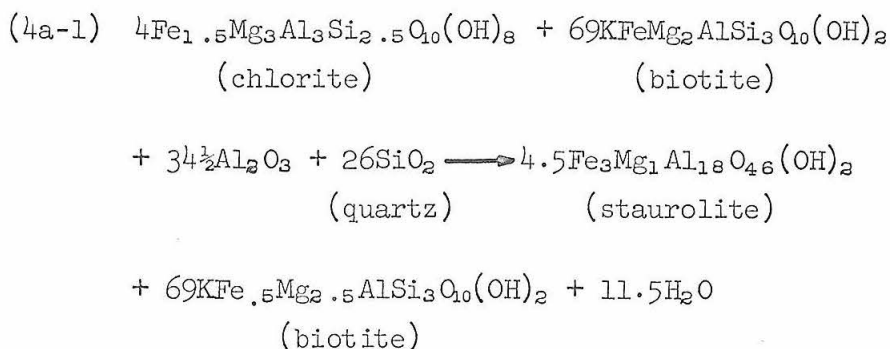
Reactions involving the growth of garnet and staurolite after the disappearance of chlorite or muscovite.

After the completion of reaction (3), the assemblage is either chl - bio - gar - stl or musc - bio - gar - stl, depending on whether muscovite or chlorite is used up. In both cases, there is analytical evidence that the staurolite and garnet continued to grow by some new reaction. The textural and analytical evidence of this reaction is discussed on page 149ff. The textural evidence consists of a discontinuous break in the growth history of the staurolite marked by differences in the concentration of inclusions (both graphite and quartz) between the outer and inner zones or by small grains of quartz located along the zone boundary. The analytical evidence consists of abrupt changes in Mg, Ti, Al, and Si contents across the staurolite textural boundary.

One reaction proposed here for the continuous growth of staurolite and garnet in the more common assemblage chl - bio - gar - stl is



Reaction (4a) can be split into the two reactions



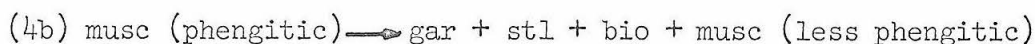
in order to illustrate the approximate relative amounts of the minerals using approximately correct mineral formulas. Extensive analytical work was done to determine what minerals and what approximate formulas of the minerals were involved in reaction (4a). The problem is to maintain growth of both garnet and staurolite in the assemblage gar - stl - bio - chl - ilm - plag - qtz - graph. Analyses showed that the excess Al needed on the reactant side of equation 4a does not come from a change in aluminum content of biotite or chlorite. A possible source for the Al_2O_3 could be a reaction between plagioclase and garnet as suggested by the increase of Ca in garnet shown on the garnet profiles (Fig. 15).

Analytic work on biotite did show, however, that the biotite on the reactant side of reaction (4a) had consistently 10 percent higher

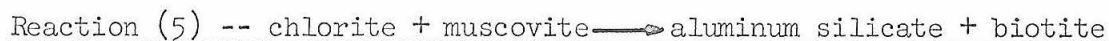
Ti content than that on the product side, corresponding to an increase in Ti in the staurolite, as shown in the staurolite zoning profile of Fig. 43.

Reaction (4a-1) may involve some reduction of Fe as it progresses since the total analyses of the staurolite (Table 12) suggest a decrease in Fe⁺³ content from the central zone to the outer zone. Reduction of Fe⁺³ during progressive metamorphism of rocks containing graphite is expectable and is discussed in Part V.

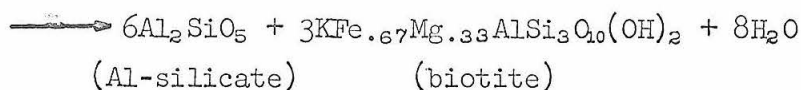
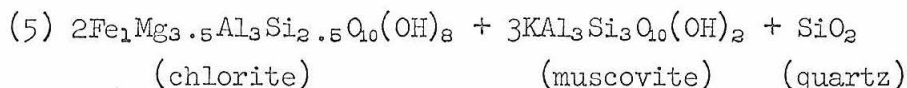
An alternative to reaction (4a), that for the growth of staurolite and garnet from the musc - gar - stl - bio assemblage is:



This reaction is difficult to prove analytically because the number of rocks of the Kwoiek Area with the musc - stl - gar - bio assemblage is small. Analyses of muscovites in the Kwoiek Area do show significant contents of Ti, Mg, and Fe which must be present to produce the ferro-magnesian minerals garnet, staurolite, and biotite. Reaction (4b) may also take place under conditions of increasing reduction of iron as many phengites contain ferric iron.



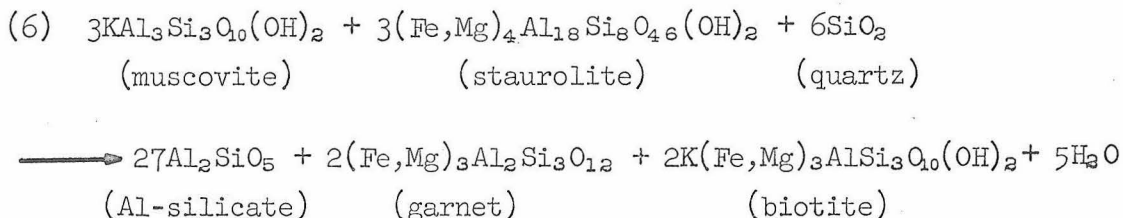
The detailed reaction is:



This reaction involves the first appearance in the Kwoiek Area rocks of an aluminum silicate, either kyanite or andalusite; but would be observed only in the relatively high-Mg rocks where chlorite and muscovite do not react to give garnet or staurolite until the aluminum silicate stability field is reached.

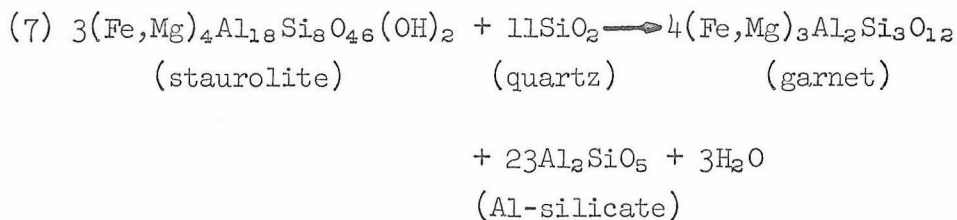
Reaction (6) -- muscovite + staurolite \rightarrow aluminum silicate + garnet + biotite

The detailed reaction is



This reaction involves the loss of staurolite (or preservation of unreacted but unstable staurolite) or muscovite from the assemblages, stl - Al-silicate - musc - bio or stl- gar - musc - bio.

Reaction (7) -- staurolite \rightarrow garnet + aluminum silicate



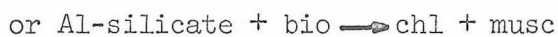
This reaction involves the resorption of staurolite and is inferred to have taken place in the highest grade rocks west of Murphy Lake Stock. For example, in rock 410, staurolite is present but has been partially

resorbed. Several grains of anhedral staurolite can be seen in a small area which, although made up predominantly of quartz and plagioclase, still preserves a euhedral staurolite outline. The grains of staurolite within this area make up only about one-fifth of the area of the staurolite outline and preserve optical continuity.

Origin of non-primary muscovite

The origin of the two types of non-primary muscovite is problematical. The fine-grained, shimmer-aggregate type occurs on the margins of staurolite grains, wherever staurolite is present. In some cases, where staurolite is completely or almost completely replaced, chlorite is also present at the former staurolite edge. Shimmer aggregates also occur at the margin of the aluminum silicate grains, especially andalusite, and in this case the shimmer aggregate is entirely muscovite, as verified by x-ray. The coarse, cross-cutting porphyroblasts, on the other hand, can occur in any assemblage but only within about 1000 feet of an intrusive contact.

The shimmer-aggregate muscovite is inferred to be the product of retrograde reactions of the type:



In the case of the former, the assemblage is changing from, for example, a gar - stl - chl - bio stable assemblage to a gar - chl - bio - musc assemblage. In the latter case the assemblage is changing from, for example, a stl - Al-silicate - chl - bio assemblage to a

musc - stl - chl - bio assemblage, or, if staurolite retrogrades also, to a musc - chl - bio assemblage.

The coarse, cross-cutting muscovite porphyroblasts could have formed also by a retrograde phase of metamorphism but with fluids from the nearby intrusive rocks inducing better crystallized muscovite. However, in some rocks containing the coarse muscovite, the staurolite and garnet are euhedral and appear unaltered, indicating they could not have been part of a retrograde reaction. The biotite also appears fresh and if this mineral retrograded to muscovite, one or two secondary iron bearing phases, such as chlorite and/or opaques, should be produced as well. Many of the coarse muscovite-bearing rocks do not contain any chlorite (Table 6), nor do they contain any clearly secondary minerals.

These observations suggest an unusual genesis for the coarse, cross-cutting muscovite porphyroblasts. One possibility is by metasomatism. In order to take an assemblage from the bio - stl - gar - Al-silicate field, the most common assemblage containing the coarse muscovite as an extra phase, to a field containing muscovite, K_2O must be added with a reaction relationship; or K_2O and Al_2O_3 , with the proportions of muscovite, must be added. A possible reaction relationship could be K_2O reacting with the aluminum silicate. The aluminum silicate minerals kyanite and sillimanite are generally not euhedral, and the kyanite typically appears partially resorbed.

In light of recent experimental work by Seki and Kennedy (1965) it seems reasonable to expect K_2O to be an introduced component.

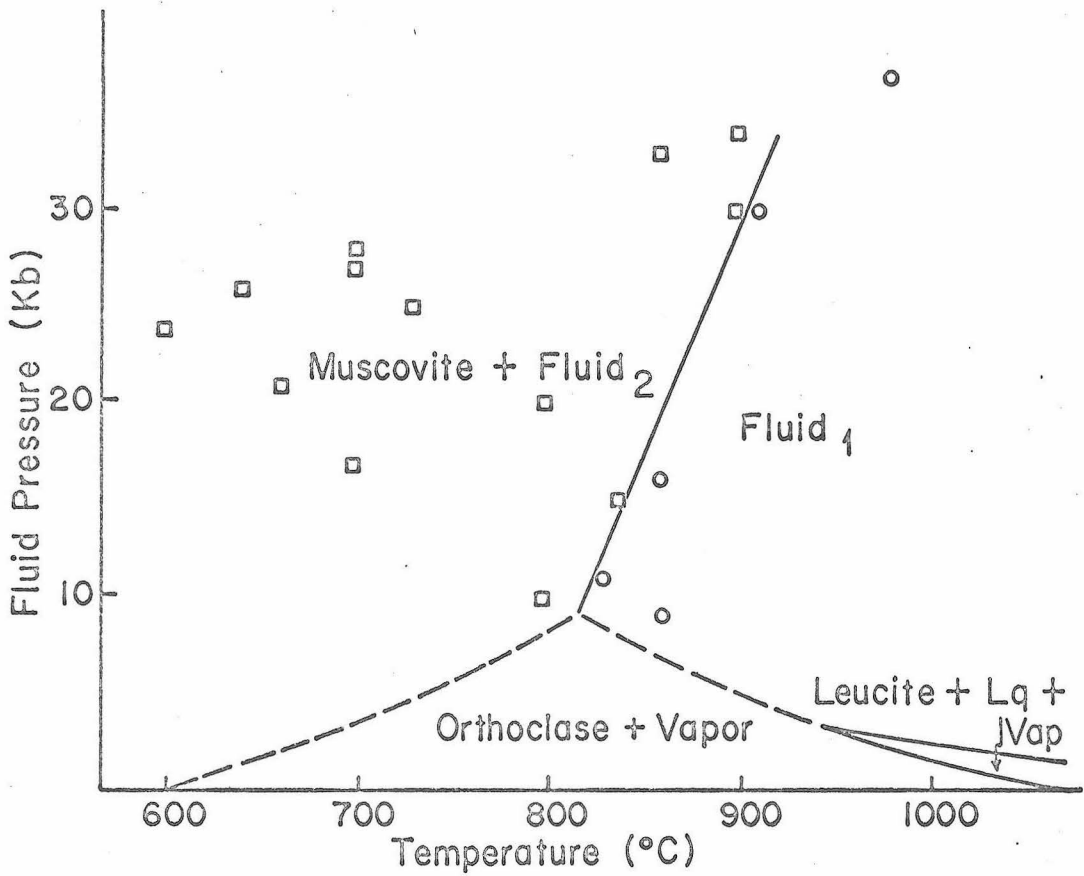


Fig. 8. Melting relations in the system $KAlSi_3O_8 - H_2O$ (after Seki and Kennedy, 1965). Fluid₁ has the composition $KAlSi_3O_8 + H_2O$; fluid₂ has the composition $K_2O \cdot 6SiO_2 + H_2O$.

Experiments on the melting relations in the system $\text{KAlSi}_3\text{O}_8 - \text{H}_2\text{O}$ indicate that late stage orthoclase, crystallizing from a cooling magma, can react with the vapor present to give muscovite + fluid rich in K_2O and SiO_2 (Fig. 8). These components are then free to move into the surrounding environs.

Supporting evidence for the possibility of this mechanism taking place is that there are several small bodies of plutonic rock, notably at the border of Kwoiek Needle Stock and at the border of Skihist Mountain Stock, which are muscovite quartz diorites (Table 1). The muscovite quartz diorite is similar to the biotite quartz diorite that is common in the Kwoiek Area except for the presence of muscovite. It might be concluded that these rocks originally contained potassium feldspar which reacted with water to give the muscovite and fluids rich in K_2O and SiO_2 . The SiO_2 given off in the reaction could well have gone to form the quartz veins found at several places in and near to the intrusive rocks.

The alternative metasomatic possibility, that of an introduction of the muscovite composition rather than just K_2O , is partially supported by one occurrence of a monomineralic veinlet containing muscovite in a border phase specimen. This indicates that the muscovite composition was at least locally mobile; but how it got into its mobile form is not known.

Variables Affecting Metamorphic Reactions

The variables affecting the temperatures of the reactions discussed above are P_{solid} , $P_{\text{H}_2\text{O}}$, P_{CO_2} (decarbonization reactions only), rock and/or mineral composition, and possibly P_{O_2} . Therefore, some of the isograds mapped on Fig. 4 may not be isotherms because of local variations of the above variables. The purpose of this section is to determine, for each isograd, how closely the isograds represent isotherms.

It is reasonable to assume P_{solid} was a constant in the Kwoiek Area during metamorphism as the area is a single pendant or screen in a batholith. The variables $P_{\text{H}_2\text{O}}$ and P_{CO_2} are difficult to evaluate within the scope of the present work, and, therefore, the following assumptions will be made: (1) $\mu_{\text{H}_2\text{O}}$ and μ_{CO_2} are externally controlled (Thompson, 1957), (2) μ_{CO_2} and $\mu_{\text{H}_2\text{O}}$ have some dependent relation on temperature. Assumption (2) assumes that to an approximation the composition of the initial pore fluid in the metasedimentary rocks was constant from outcrop to outcrop in the Kwoiek Area. This assumption is reasonable because the metasedimentary rocks of the Kwoiek Area are essentially one type, greywacke (Part II).

Granting these assumptions and that P_{solid} is everywhere the same, an evaluation can be made on the importance of rock and mineral composition. Clearly, rock composition is important. Without the appropriate rock composition a reaction could not be identified. This is certainly true for reaction (5) and other possible, but unknown reactions in the high-Ca group. However, the problem is how rock and mineral

composition affect the location of isograds that are mapped. In other words, if a reaction is mapped at two different localities, has it occurred at the same temperature at both localities?

In a four component system, if the reaction involves four phases, the phase rule restrains the reaction to take place at a fixed temperature because the compositions of the phases are fixed for a given temperature (given the above assumptions). However, if only three phases are involved as reactants or products, there is one more degree of freedom, and the temperature of the reaction, where the reaction is observed to take place, will vary depending on the composition of the individual minerals.

With this thought in mind, it is clear that the temperatures of isograds B and C are dependent on the composition of the phases as reactions involve only four phases in a five component system. The fact that isograds B and C on Fig. 4 make reasonable sense with respect to intrusive contact outlines is suggestive that the compositional dependence is not important; but the best evidence that the compositional dependence is not important is that only one rock was found with five phases (assemblage number 38, located off the map of Fig. 4) which overlapped two blocks (in this case blocks B and C). If reactions B and C took place over a wide range of temperature, more assemblages would be found overlapping blocks A and B or B and C. Therefore, although the temperatures of isograds B and C are dependent on composition, the dependence is not important so that isograds B and C on Fig. 4 are, to an approximation, isotherms.

Isograd D, representing the reaction between five phases in a five component system does, according to the phase rule, represent an isotherm. By the same argument isograds 3, 5, (in the presence of staurolite), 6, and 7 (in the presence of chlorite or muscovite) must also represent isotherms. Isograds 2 and 4 (not in the presence of garnet) are not isotherms because they involve the same components as isograds 3, 5, 6, and 7, but have one less phase. Arguments cannot be made as to how close isograd 2 approximates an isotherm because a distinctive intermediate assemblage, as could be expected between blocks A and B or B and C, would not be expected. Isograd 4 could not be mapped due to paucity of rocks with suitable composition.

ANALYTICAL RESULTS

Introduction

In the study of metamorphic rocks two important assumptions are usually made. The first is that equilibrium was reached or closely approached during the recrystallization of the rock; the second is that the phases present in any metamorphic rock, as well as their compositions, represent the maximum temperature that the rock reached. The latter assumption had to be made due to the difficulty of obtaining analytical data on grain homogeneity and compositional variations of a phase at different points in a rock. With the availability of the electron microprobe to petrologists it is now possible to test the second assumption. The first assumption is more difficult to test directly, especially in light of the data obtained in testing the second assumption; however, the consistency of certain types of data suggests equilibrium was attained or closely approached during the metamorphism of most rocks of the Kwoiek Area.

In this part, the following points will be made:

- (1) The garnets of the Kwoiek Area are zoned.
- (2) The zoning patterns of the garnets follow a model, called the Rayleigh depletion model, of removal of the material in the garnet from the system during growth of the garnet.
- (3) Comparison of the observed garnet zoning and Rayleigh model zoning leads to an interpretation of the garnet's thermal history.
- (4) Many of the rocks of the Kwoiek Area continued to recrystallize with continued growth of garnet during the decreasing

temperature stage of metamorphism.

(5) The recrystallization during decreasing temperatures makes the determination of meaningful distribution functions very difficult.

(6) The horizon within a garnet that grew at maximum temperature is preserved, can be identified, and its composition can be related to temperature.

(7) Total analyses of five garnets suggest little ferric iron is contained in the garnets of the Kwoiek Area.

(8) Biotite in a thin section tends to have nearly the same Mg/Fe ratio along planes parallel to foliation or microbedding, but can vary in a direction normal to the microlayering.

(9) Variation of the Mg/Fe ratio in biotite in single thin sections probably means there were smaller areas of equilibrium at the end of the retrograde phase of metamorphism than at the maximum temperature of metamorphism.

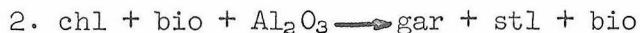
(10) Individual biotite and chlorite grains are homogeneous except for the occurrence of chlorite as interlayers in the biotite.

(11) The biotite-chlorite Mg/Fe distribution function is nearly constant, 0.85, for all grades of metamorphism.

(12) The Mg/Fe ratio in biotite and chlorite generally increases with metamorphic grade.

(13) The staurolite of the Kwoiek Area is zoned.

(14) Study of the zoning and present assemblages leads to the conclusion that the staurolite grew by either of two groups of reactions:



or



(15) Several total analyses in different parts of a staurolite grain, coupled with the Al zoning pattern of the garnet, suggest a net reduction of Fe between reactions 1 and 2 and between 1 and 3.

(16) Profiles of individual staurolite grains indicate that the Mg/Fe ratio decreases with increasing temperature rather than increasing as it does for garnet, biotite, and chlorite.

(17) Andalusite formed in the Kwoiek Area as a metastable phase.

The data in this chapter are given in terms of counts per second unless otherwise indicated. The counting rates have been corrected for background only where indicated. For comparative purposes, background-corrected counting rates have been normalized to a given day of work, May 31, 1965. These data are so noted; otherwise, only the date on which the data was obtained is indicated. Conversion factors to May 31, as well as some background readings, are given in the Appendix. Also given in the Appendix are the analytical techniques and standard curves for converting the counting rate of an element into weight percent. A list of the assemblages of the rocks discussed is also given in the Appendix, and the locations of these samples are shown in Fig. 1.

Garnet

General statement.

Garnet is the best understood and, excluding biotite, is the most abundant metamorphic mineral in the Kwoiek Area. Because of its abundance, marked zoning patterns, and presence over a wide temperature range in several apparently invariant assemblages, garnet was subjected to the most intense study in this work.

Two to five garnets were analyzed for Mn, Fe, and Mg in each of twenty-six thin sections containing garnet in several assemblages and from several grades of metamorphism. Seven of the twenty-six samples were analyzed for Ca and Ti, and five were analyzed for Si and Al. Eleven profiles with analyses at 10 micron intervals are shown in Figs. 9-15. These profiles will be referred to throughout the remainder of the text to illustrate various points. The profiles of Figs. 9, 10, and 15c are special cases; all the other profiles from the Kwoiek Area are similar to Figs. 11-14, 15a, 15b, 15d, and 15f.

In most cases the shape of the Mn curve across a garnet resembles a bell. Mg and Fe behave in a reciprocal fashion to the Mn curve. Where the change of Mn with respect to radius is the greatest, the change of Fe and Mg (with opposite sign) is also the greatest.

At the very edge of the garnet Mg, Fe, and Mn do very interesting things. Mn in most garnet grains has a very slight upturn (Figs. 6, 15a-15c), but this upturn can be apparently absent (Fig. 15d) or merely suggestive (Fig. 15f). As the interval between measurements was 10 microns, the apparent absence of an upturn does not necessarily mean

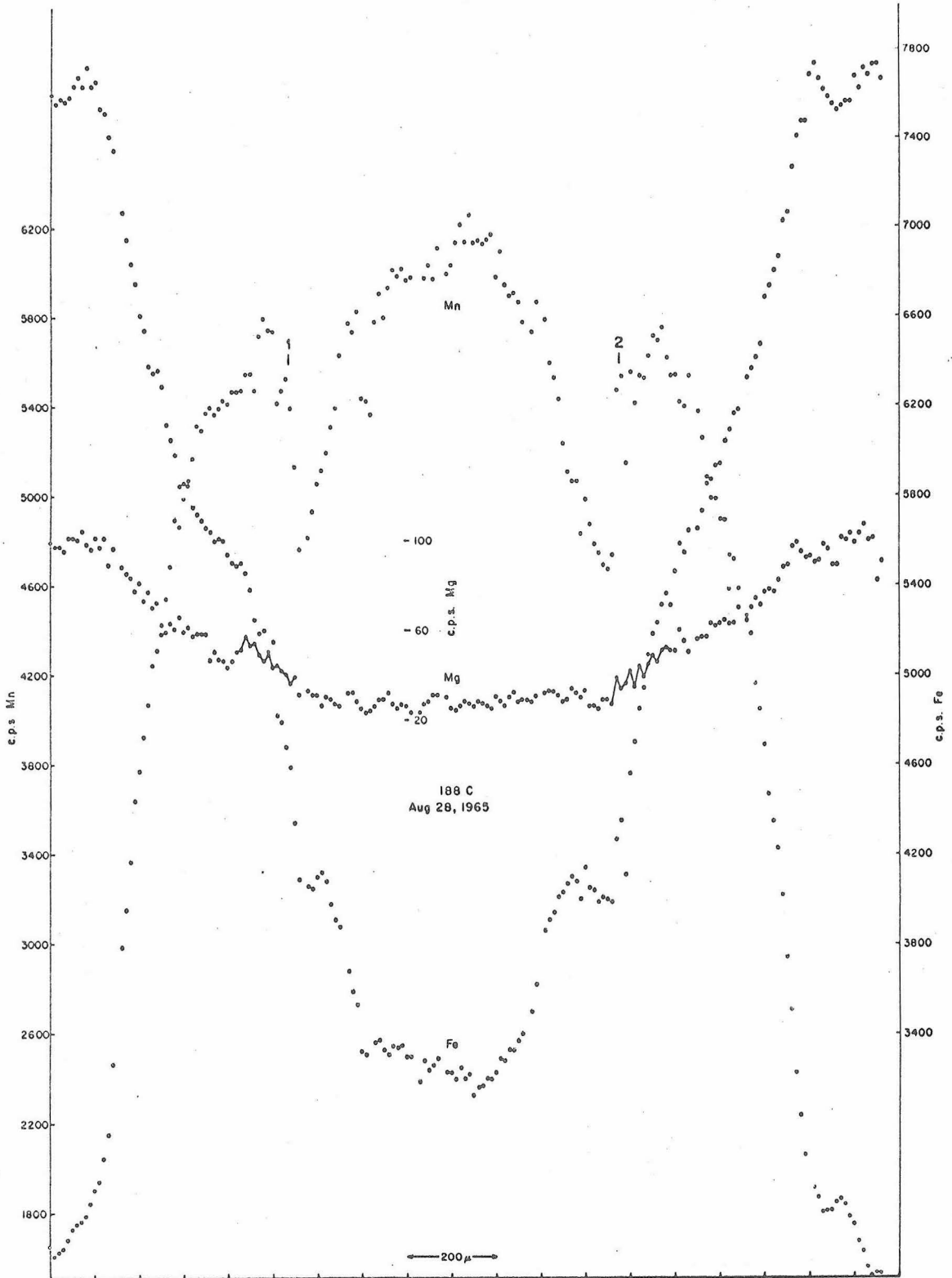


Fig. 9. Mn, Fe, and Mg profiles across a garnet of sample 188C (see Plate 2).

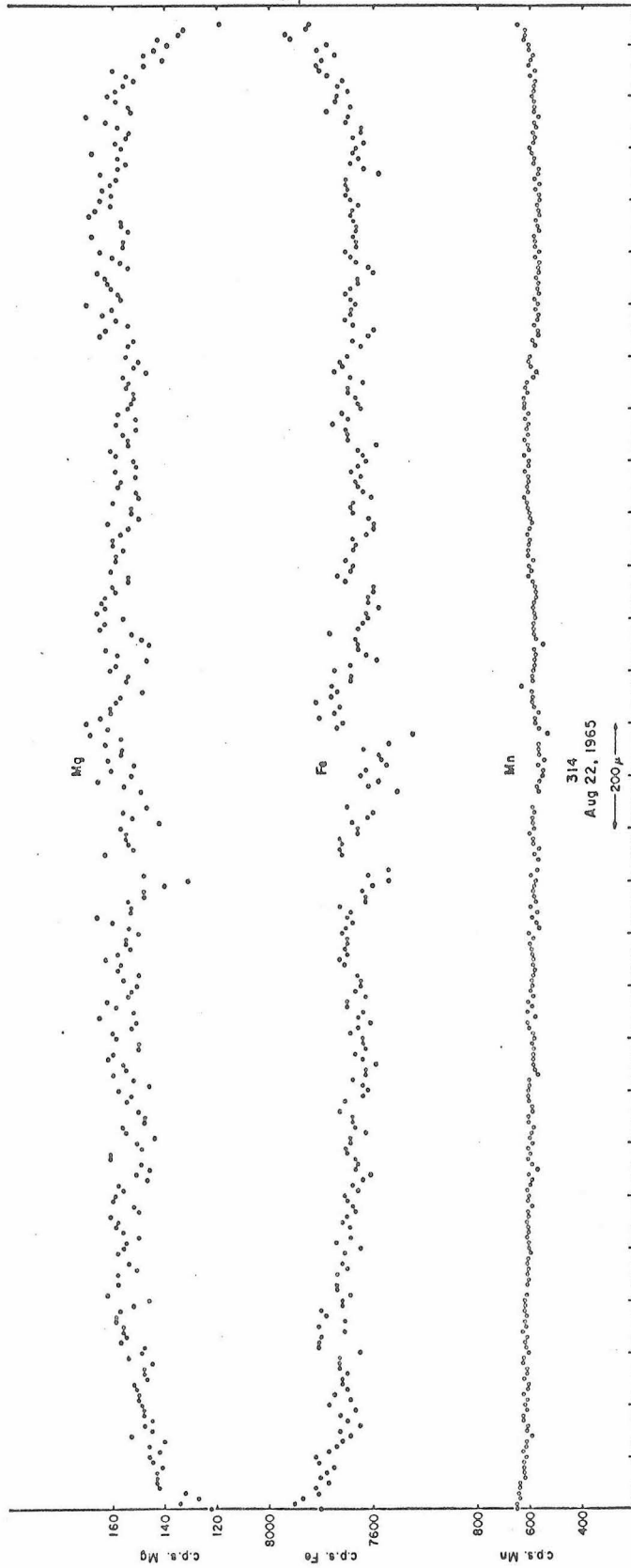


Fig. 10. Mn, Fe, and Mg profiles across a garnet of sample 314.

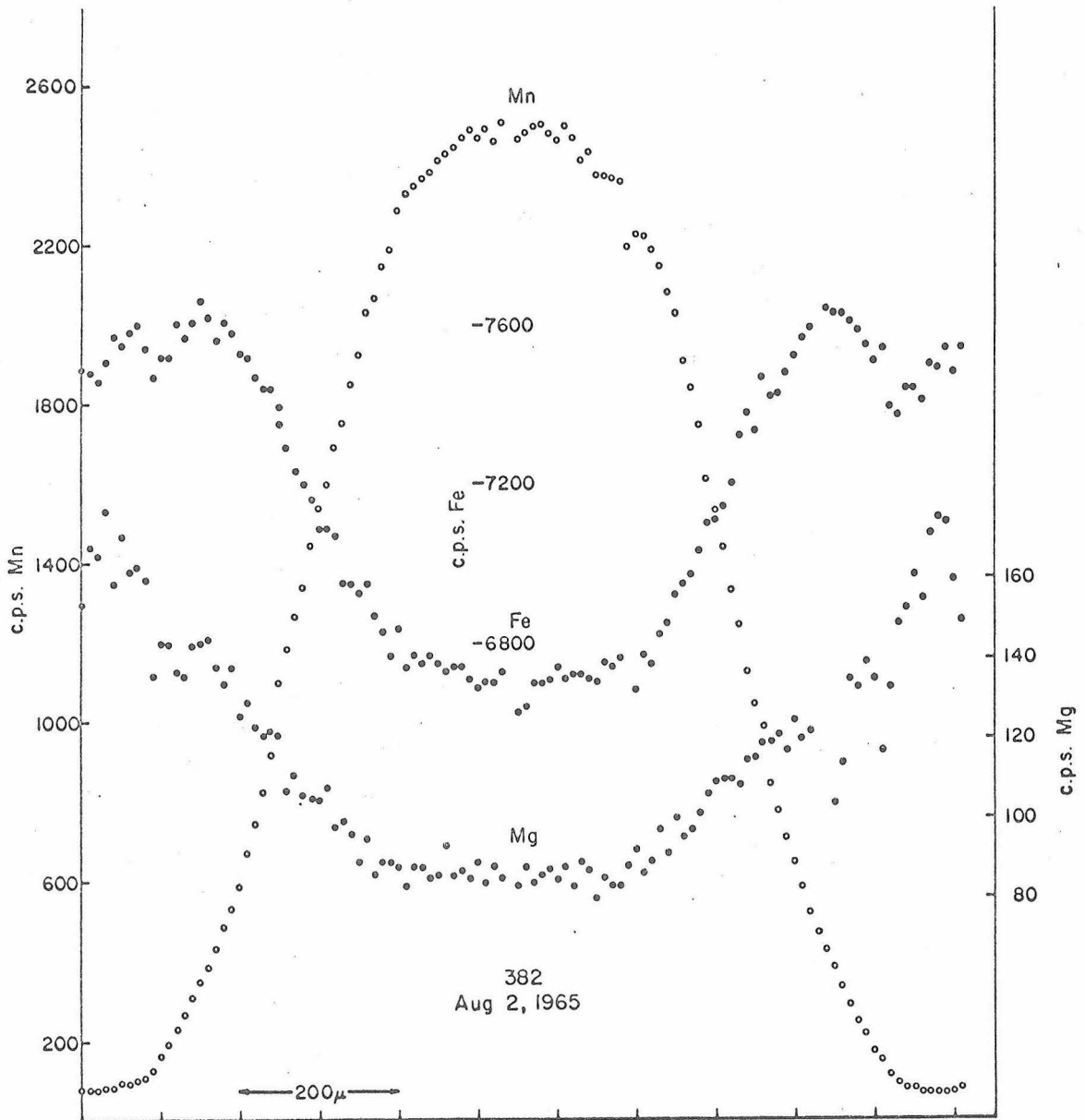


Fig. 11. Mn, Fe, and Mg profiles across a garnet of sample 382.

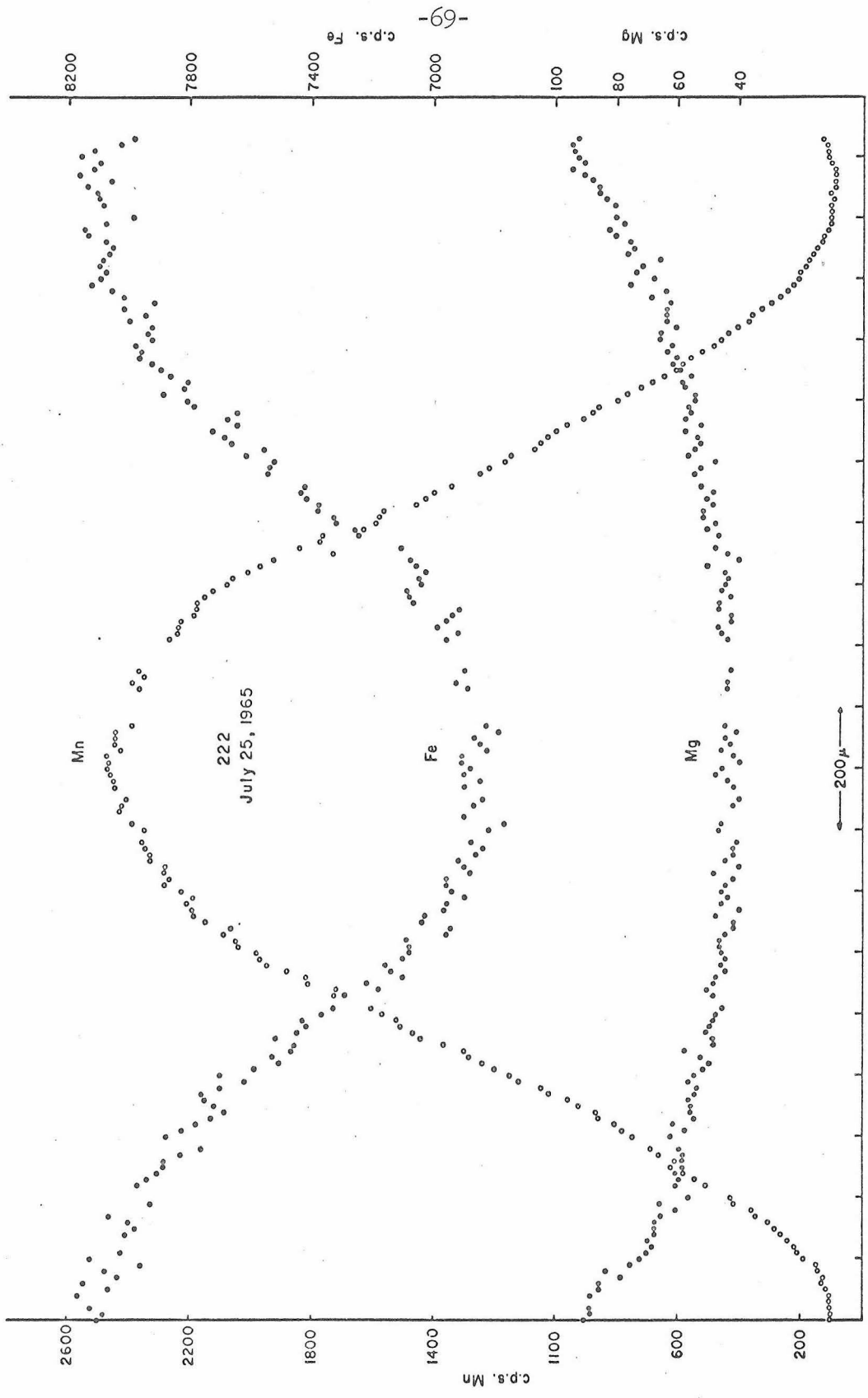


Fig. 12. Mn, Fe, and Mg profiles across a garnet of sample 222.

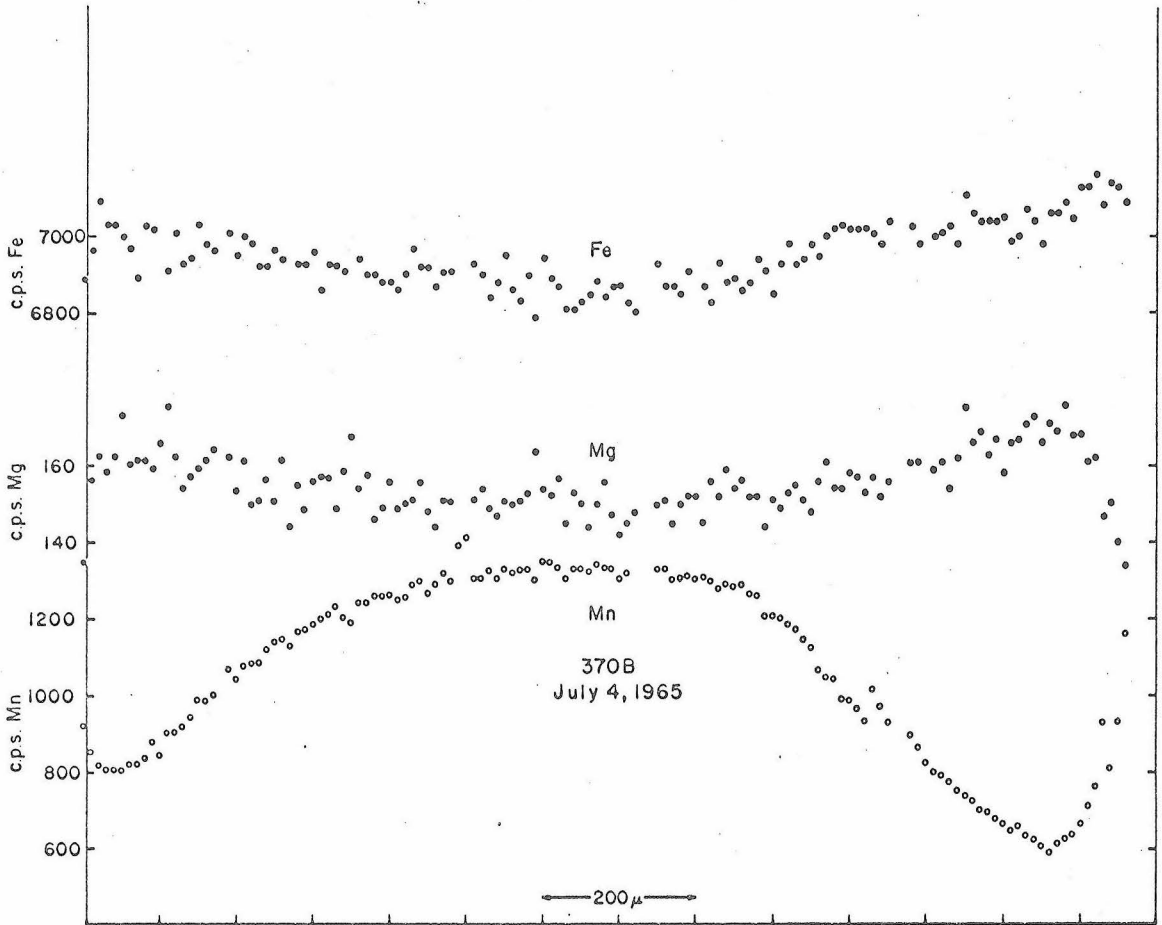


Fig. 13. Mn, Fe, and Mg profiles across a garnet of sample 370B.

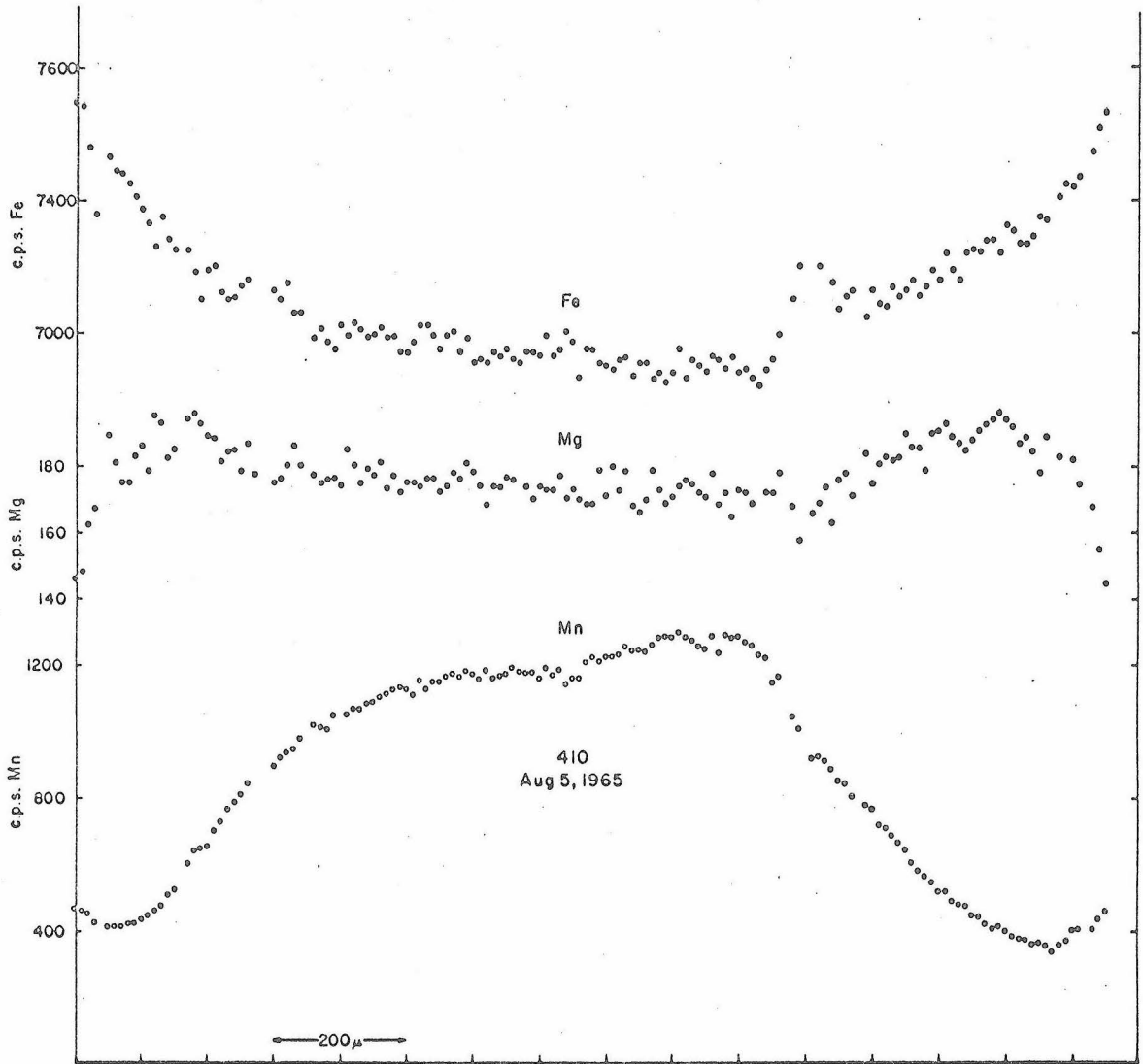
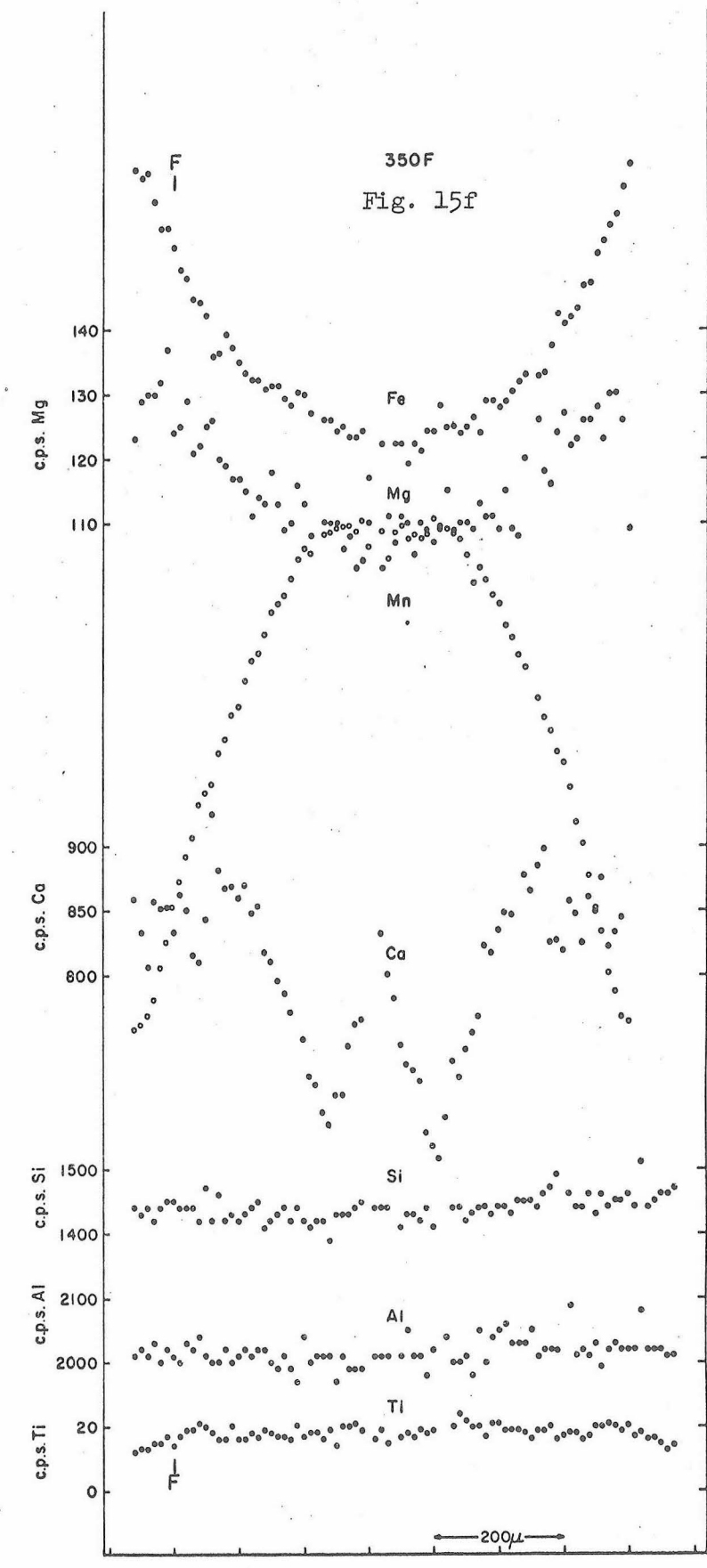
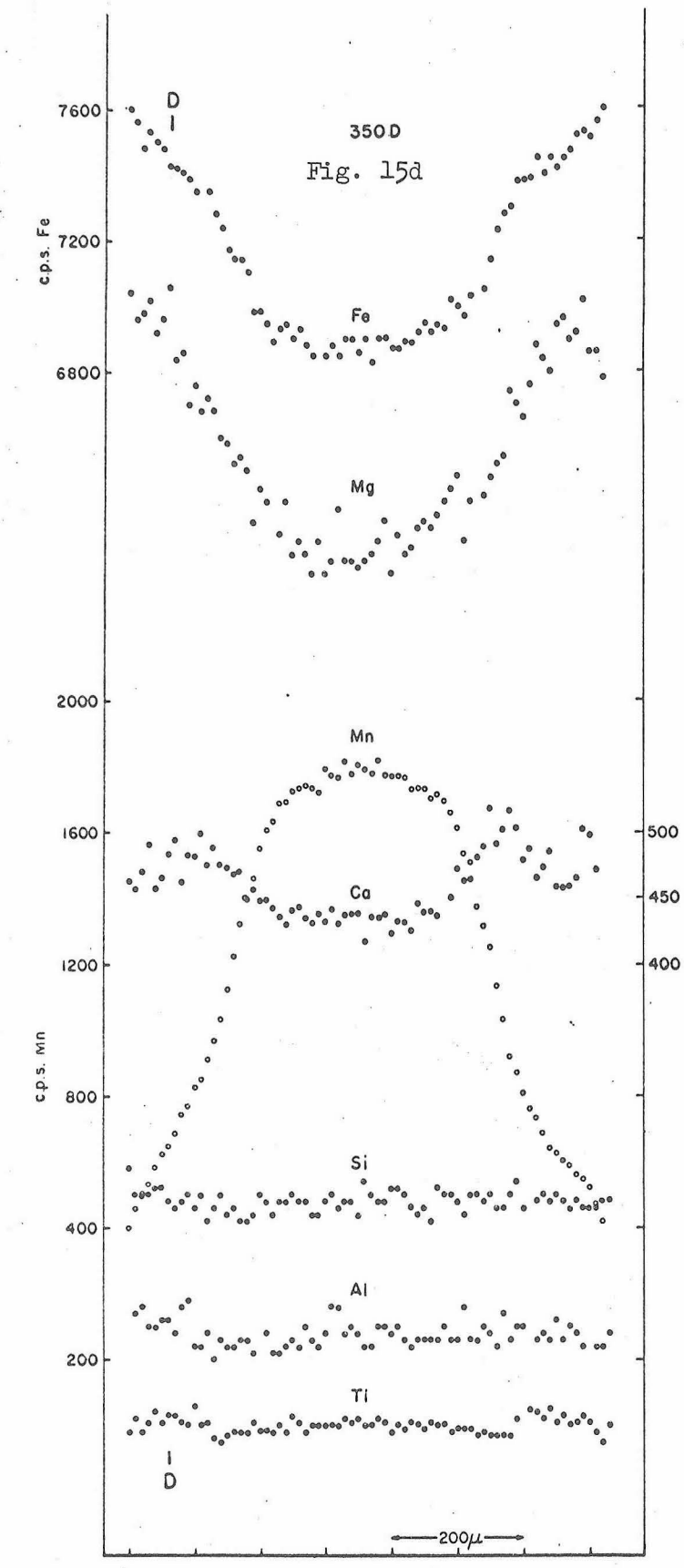
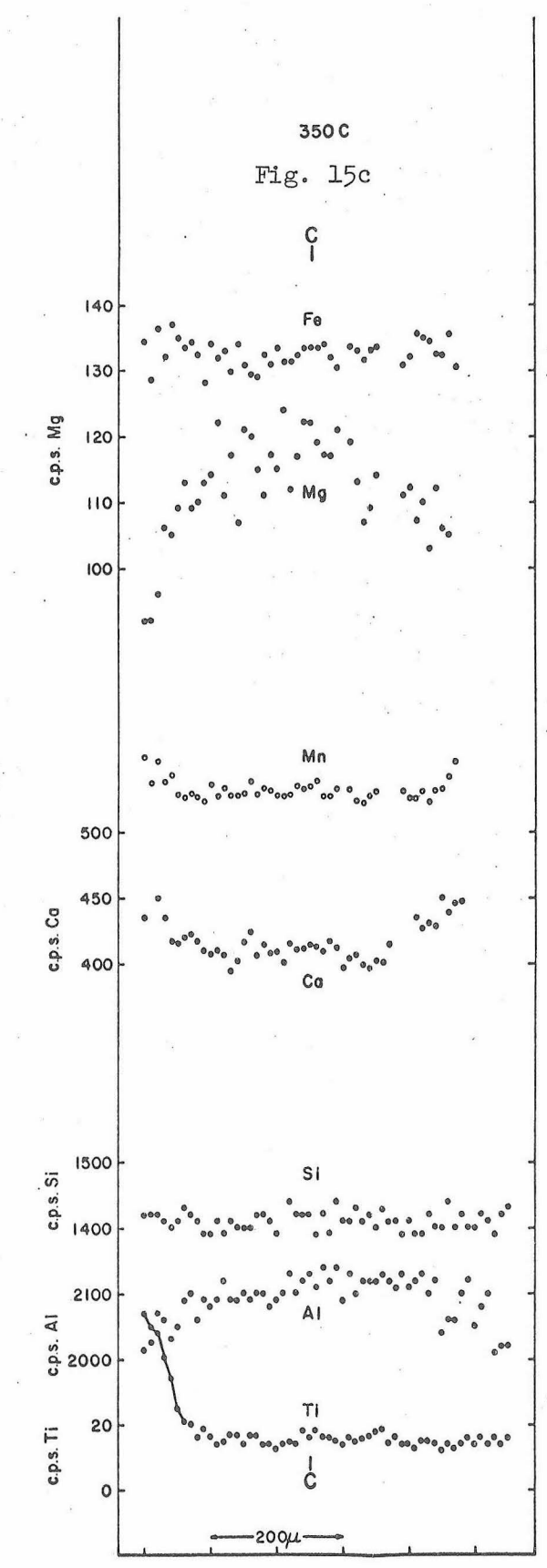
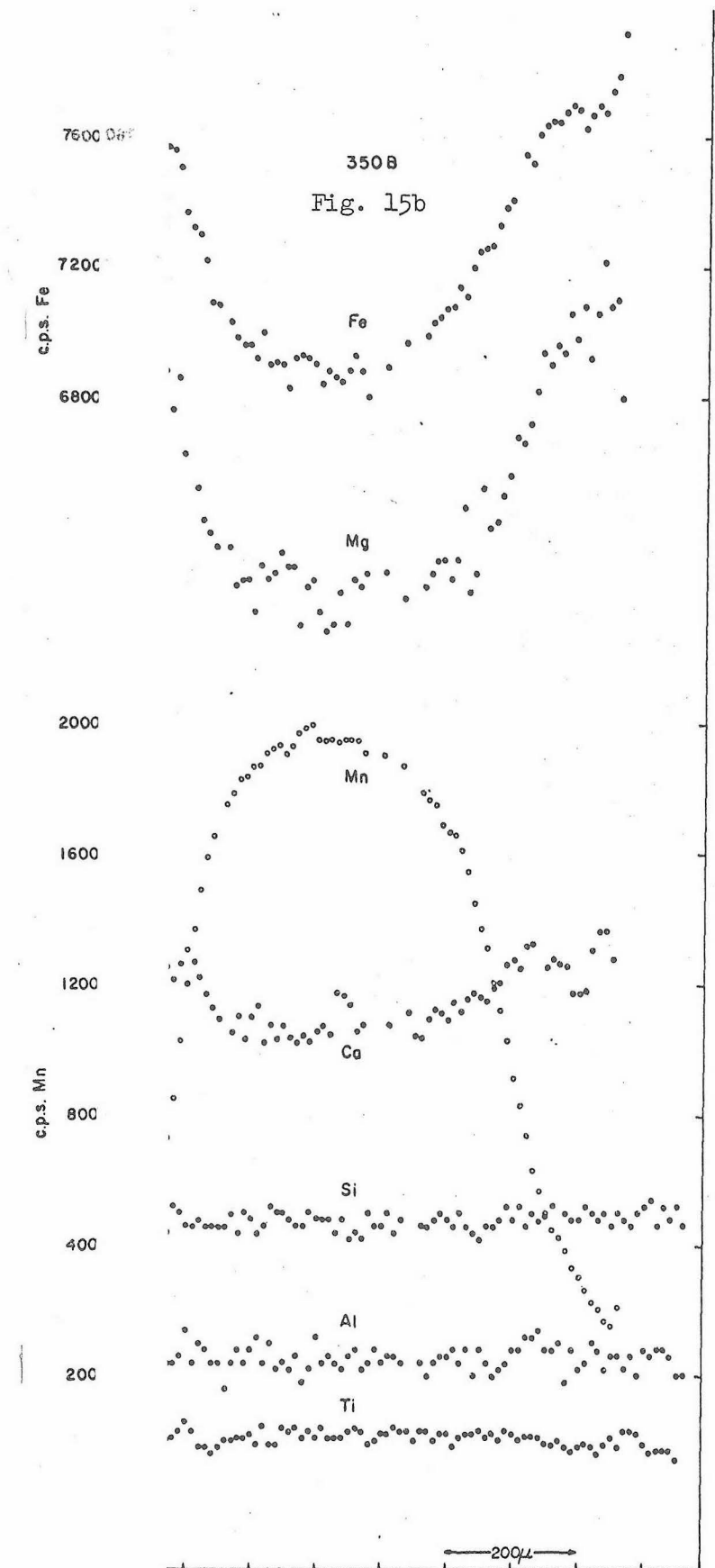
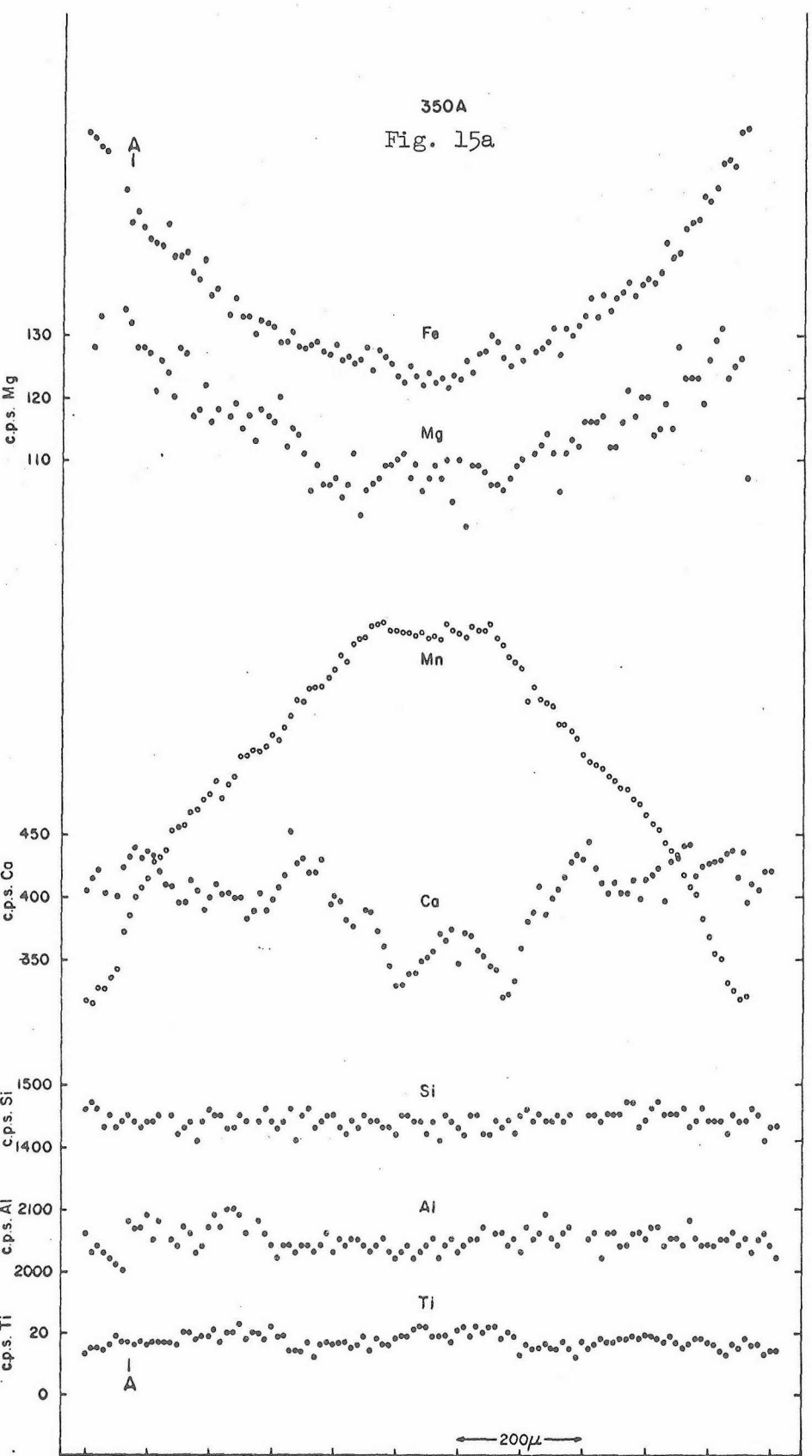


Fig. 14. Mn, Fe, and Mg profiles across a garnet of sample 410.

Fig. 15. Mn, Fe, Mg, Ca, Al, Si, and Ti profiles across garnet of samples 350A (Fig. 15a), 350B (Fig. 15b), 350C (Fig. 15c), 350D (Fig. 15d), and 350F (Fig. 15f).

Dates of data: 350A, B, C, and D, May 31, 1965 for Mn, Fe, Mg, and Ca, and Jan. 21, 1966 for Ti, Si, and Al; 350F, Aug. 27, 1965 for Mn, Fe, and Mg, Sept. 6, 1965 for Ca, and Jan. 21, 1966 for Ti, Si, and Al.

See Appendix for backgrounds, normalization factors, and calibration curves. Letters refer to location of analyses in Table 11.



there is no upturn as the upturn might take place in the outer few microns. This is probably the case in Fig. 15f. The garnet of Fig. 15d was not as euhedral as the others so that the absence of the upturn might be due to partial resorption of the garnet. It should be noted that most of the garnets of the Kwoiek Area show good crystal faces, but some are nearly spherical and others are anhedral. The garnet of Fig. 9 was anhedral and that of Fig. 10 was subhedral.

Fe also shows an edge effect. Although Fe generally increases steadily towards the garnet edge, its rate of increase with respect to garnet radius goes up very sharply, in many cases, in the outer 10 microns. This effect is seen in Figs. 10 and 15b.

The change in slope of the Mg curve in the outer 10 to 100 microns of all examples except Fig. 12 is striking, and, as will be shown subsequently, is the most significant. In most cases Mg reaches a maximum near, but not at, the garnet edge and then drops off steeply towards the edge with the slope increasing sharply in the outer 10 microns. This pattern of Mg zoning is present in most of the garnets of the Kwoiek Area.

The Ca zoning of the 350 rocks is not monotonic with respect to radius. In Fig. 15a, Ca has a high value at the garnet center, decreases for about 100 microns, reverses and increases the next 100 microns, reaches a maximum, drops, reaches another maximum, and drops slightly at the edge. Figure 15f shows a similar Ca profile. The other Ca profiles of Fig. 15 appear simpler, but this may be because the profiles did not pass as near the garnet centers as those of

Figs. 15a and 15f. The Ca profile of a garnet from a garnet-hornblende rock (sample 350E) was similar to that of Fig. 15f. On the other hand, a profile from a gar - bio - chl - musc assemblage (sample 10) showed a bell-like pattern, high at the center and a factor of 15 lower at the edge.

Si is constant in the five Si profiles; but Al and Ti, although nearly constant, show significant variation. In Fig. 15a, about 300 microns from the left edge, there is an outward increase in Ti at about the same place as a small outward increase in Al. There is no symmetrical effect on the right side. In Fig. 15d, there is a definite, symmetric change of Ti. The Al change is not as clear although the average Al content is higher in the outer zone than in the central zone. Figure 15f shows a small change in Al content about 200 microns from the left side and about 250 microns from the right side. The small changes in Ti and Al might not be noticed except that they correspond to features observed in profiles of coexistent staurolite. An interpretation of these features is given on page 149ff.

Rayleigh fractionation in garnet.

The almost ubiquitous shape of the Mn, Fe, and Mg curves in different assemblages in different grades of metamorphism in the Kwoiek Area suggests there must be a single explanation for the shape of the curves. The existence of any zoning is somewhat unexpected in metamorphic rocks. The garnets are not in equilibrium with themselves, as complete chemical equilibrium requires that a phase be homogeneous.

Since the internal layers of the garnet are not in equilibrium with themselves, they cannot be in equilibrium with the rock external to the garnets. In fact, only the infinitesimally thin outer layer of the garnet can possibly be in equilibrium with the rest of the rock. In the calculations that follow, equilibrium of the outermost layer of the garnet with the rest of the rock will be assumed. The results of the calculations will lend credence to this assumption. A consequence of the lack of internal equilibrium in a growing garnet is that the effective composition of the equilibrium system is constantly changing away from the garnet composition. This fact is useful for the determination of which of several possible metamorphic reactions can occur.

The removal of a phase from a system as it forms was treated by Rayleigh (1902) for the case of a liquid condensing from a multi-component vapor, with the liquid being completely removed from the system as it condensed. Neumann, et al. (1954) and McIntire (1963) used the Rayleigh depletion model in considering the theoretical distribution of trace elements in crystals crystallizing from a magma as well as the concentration of trace elements in the magma during crystallization. Taylor and Epstein (1962) used the Rayleigh approach in considering the change of oxygen isotope ratios in crystals and melt during fractional crystallization of a magma. Mazor and Wasserburg (1965) used the Rayleigh approach in describing inert gas contents in thermal springs.

Using the basic method of Rayleigh (1902), the following is a derivation of the formula used for the present work, which gives the weight percent of an element at the garnet edge as a function of the weight of garnet crystallized from the rock.

The terms used are:

M_G = weight fraction of element in garnet edge

W_M^R = weight of element in rock external to crystallized garnet.

W_R = weight of rock external to garnet

M_R = weight fraction of element in rock excluding that in garnet.

λ = fractionation factor, M_G/M_R

W^0 = initial weight of rock, prior to garnet crystallization

W_M^0 = initial weight of element in rock, prior to garnet crystallization

M^0 = initial weight fraction of element in rock, prior to garnet crystallization

W^G = total weight of crystallized garnet

$$(1) M_G = \frac{-dW_M^R}{-dW_R}$$

Equation (1) is a statement of the assumption of removal of garnet from the rock as the garnet crystallizes.

$$(2) M_G = \lambda M_R = \lambda \frac{W_M^R}{W_R}$$

Equation (2) is an expression of chemical equilibrium, which is assumed.

Combining (1) and (2) and rearranging gives

$$(3) \quad \lambda \frac{dW_R}{W_R} = \frac{dW_M^R}{W_M^R}$$

Integration, assuming λ a constant, gives

$$(4) \quad \lambda \ln \frac{W_R}{W^O} = \ln \frac{W_M^R}{W_M^O}$$

and

$$(5) \quad \lambda \ln \frac{W_R}{W^O} = \ln \frac{M_R W_R}{M_O W^O}$$

$$(6) \quad \lambda \ln \frac{W_R}{W^O} = \ln \frac{M_R}{M_O} + \ln \frac{W_R}{W^O}$$

$$(7) \quad \ln \frac{M_R}{M_O} = (\lambda - 1) \ln \frac{W_R}{W^O}$$

$$(8) \quad \frac{M_R}{M_O} = \left(\frac{W_R}{W^O} \right)^{\lambda-1}$$

Using (2) and

$$(9) \quad W_R = W^O - W^G$$

The final equation is

$$(10) \quad M_G = \lambda M_O \left(1 - \frac{W^G}{W^O} \right)^{\lambda-1}$$

Equation (10) gives the weight fraction of an element at the edge of a garnet in terms of M_O , the weight fraction of that element in the rock as a whole (including all that is in the crystallized garnet); W^G , the weight of the crystallized garnet; W^O , the weight of the original system; and λ , the fractionation factor.

Equation (10) says nothing about where in the structure of garnet the element goes, nor does it say anything about the effects of other elements on that element. In fact, equation (10) assumes that the garnet could fill its eight-fold or R^{+2} position entirely with one element, such as Mn, even if Mg, Ca, and Fe are available. This is obviously erroneous because, if Mg, Ca, and Fe are available in the rock, some will always go into the R^{+2} position of the garnet.

Application of Rayleigh depletion model to specimen 350B

A first test of equation (10) was made on a garnet from specimen 350B (Fig. 16) collected about 0.34 miles east of Kwoiek Needle. Before dealing further with Fig. 16, the similarity of Fig. 16 and Fig. 15b should be noted. The two profiles are from across different garnets but from the same rock. The positions of the two garnets on a sketch of the thin section is shown in Fig. 38.

The mode of 350B, based on 1000 point counts, is as follows:

garnet	4.1	
biotite	29.6	
chlorite	4.3	40.5
staurolite	2.5	
ilmenite	1.0	
graphite	2.8	59.5
quartz and plagioclase	55.7	
total	100.0	

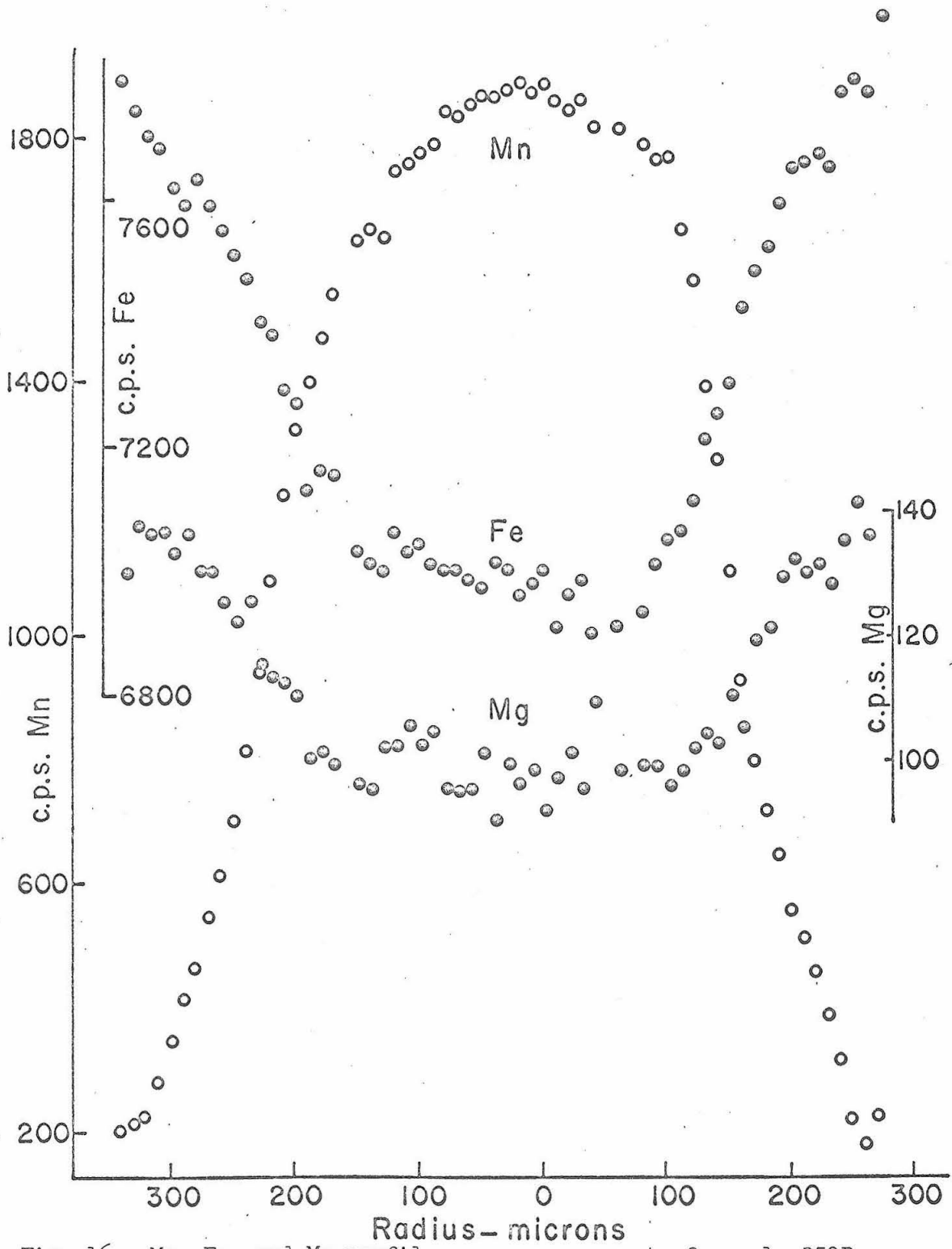


Fig. 16. Mn, Fe, and Mg profiles across a garnet of sample 350B (different garnet than Fig. 15b); May 12, 1965 data.

Since the mode is in volume percent and the calculations are based on weight percent, a small error is introduced in the calculations. The fact that all the calculations are based on counting rates without matrix correction compensates in part for this error since the difference in counting rates between two minerals with the same weight percent of an element is roughly inversely proportional to the difference in density.

We shall assume in the calculations that W^0 , the weight of the system, is the sum of the volume percentages of the minerals that exchange Fe and Mg with the garnet. M_0 is, then, the weight fraction of the element in the ferromagnesian minerals and not the rock as a whole. The ferromagnesian minerals are taken as biotite, chlorite, garnet, and staurolite. Ilmenite is neglected because of its small amount in all the rocks and because its small grain size makes its analysis difficult.

In solving equation (10), λ , M_0 , and W^0 must be evaluated. M_0 , which is the average weight percent of an element in all the ferromagnesian minerals, was evaluated by determining the average content of each element in each mineral and weighting these numbers by the relative proportions of the minerals in the rock. The average content of the elements in garnet had to be determined by graphical integration over the garnet as a sphere. These numbers are probably in error more than those of biotite and chlorite because the integration was performed on only one garnet of specimen 350B whose composition was assumed to be the average of all the garnets. This assumption is not entirely

correct because the garnets vary in size and, although the edge compositions are similar, the center compositions are different indicating either (1) the garnets began to grow at different stages in the metamorphism or (2) not all garnets equilibrated with the same size and composition rock system at the initiation of crystallization.

The "constant" λ was evaluated by solving equation (10) for both the center of the garnet and near the edge of the garnet where the Mg counts are the highest. In the center $W^G/W^O = 0$ so $\lambda = M_G/M_O$, where M_G is the counts of element measured in the center and M_O as indicated above. At the garnet edge λ was evaluated by taking $W^G/W^O = 4.1/40.5$ (the garnet/sum of ferromagnesian minerals volume ratio) and M_G the counts at the edge. The numbers used for each element and the evaluated λ 's are given in Table 8.

Table 8

Numbers Used in Calculations on Garnet 350B

May 12 Data, Background Corrected

	Center			Edge		
	Mn	Fe	Mg	Mn	Fe	Mg
M_O	83.6	398	416	83.6	398	416
M_G	1885	697	97	226	772	137
λ	22.6	1.75	.233	23.8	2.1	.299

Figures 17 and 18 show the solution of equation (10) for Mn and Fe and Mg, using the center λ 's, compared with the measured values for

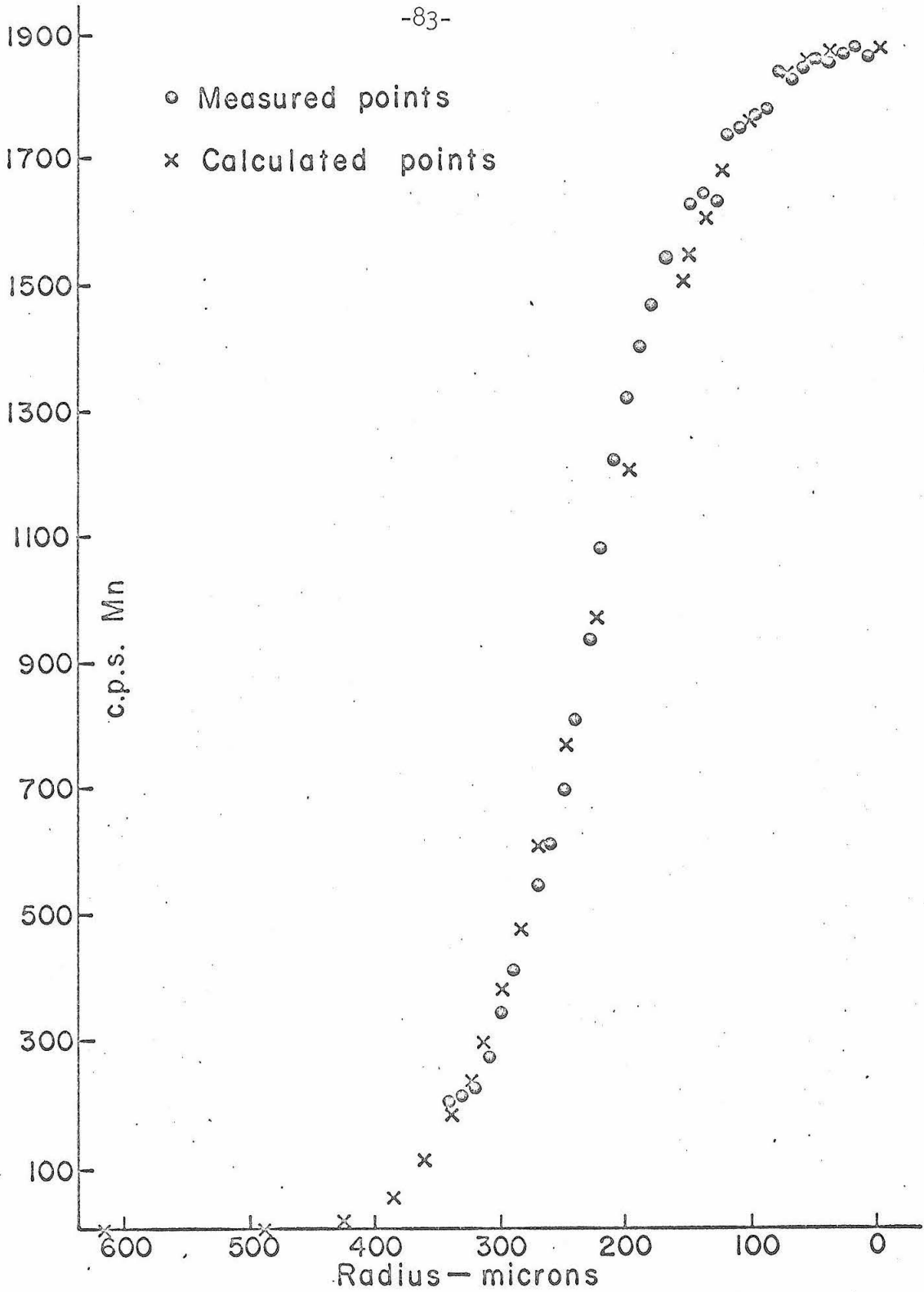


Fig. 17. Comparison of half of Mn profile of Fig. 16 and calculated Mn profile, using Rayleigh depletion model.

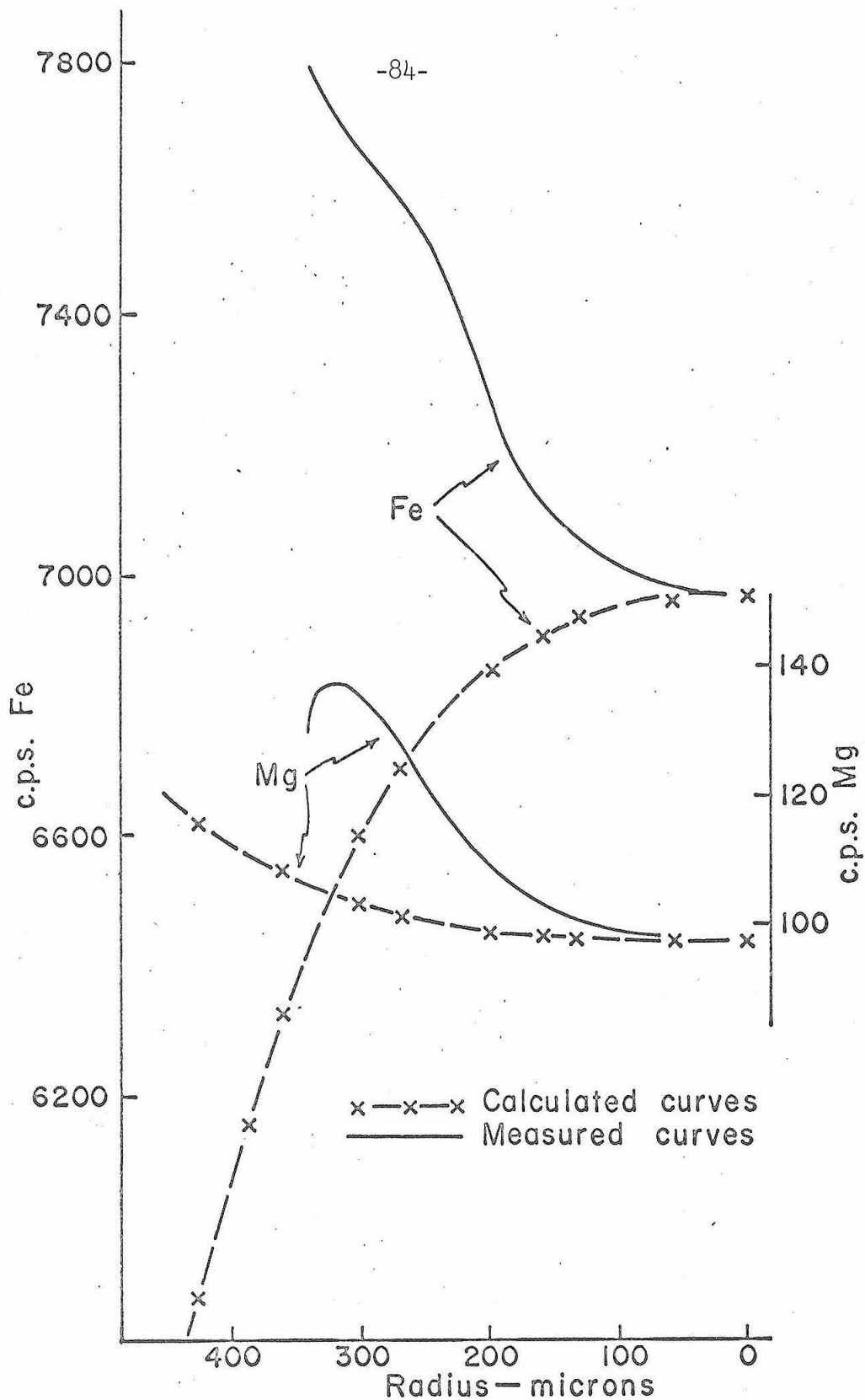


Fig. 18. Comparison of measured and calculated profiles of Fig. 16 for Mg and Fe.

the left half of the garnet traverse of Fig. 16.

The similarity of the two Mn curves is remarkable and is indicative that the assumptions made above, at least for Mn, are probably valid. The most important of these assumptions included in the basic Rayleigh equation is that as the garnet crystallized its composition was removed from the system. Rayleigh's depletion model must then be the major reason for the fact that the garnet in specimen 350B and, by inference, the reason most garnet of the Kwoiek Area is strongly zoned.

The slight divergence of the calculated and measured curves in the vicinity of 150 microns from the garnet center can be explained by the probability that the microprobe traverse did not pass through the center of the garnet because the measurement was made on a garnet in a thin section. A profile which does not pass through the garnet center is broader near the center of the profile than one through the garnet's center. This is to be expected as each spherical zone is approximated more and more by a tangent as the traverse is made further from the garnet center.

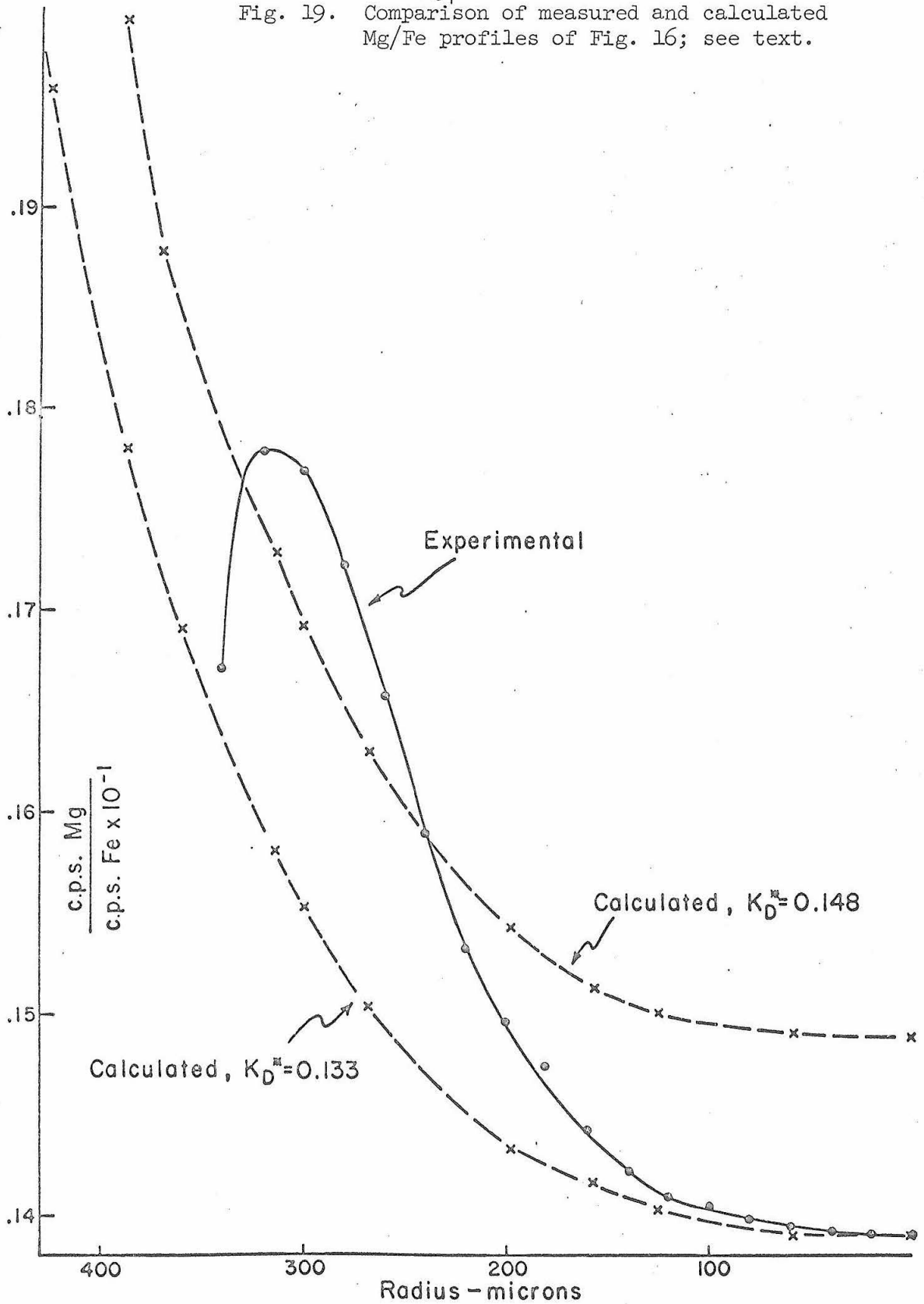
If the garnet had continued to grow, the Mn content would be expected to follow the calculated curve where it has been calculated beyond the existing garnet's edge. Garnets have been found, with very small edge contents of Mn, which show Mn profiles similar to the calculated curve of Fig. 17. Figures 11 and 12 are two such examples. (Note: Background for Figs. 11 and 12 is about 40 c.p.s., bringing the Mn content very near zero.)

The fact that the Mg and Fe calculated curves diverge from the measured curves (Fig. 18) is not surprising when we consider that Mg, Fe, and Mn enter the same site in the garnet, and that λ_{Mn} is much greater than λ_{Fe} or λ_{Mg} . Although there are Rayleigh effects on Mg and Fe, they are small relative to that on Mn. Thus, to a first approximation, Mn in the garnet is dependent on the Rayleigh effect; and, as Mn decreases, Mg and Fe must increase to maintain atomic balance in the garnet structure.

The calculated Mg/Fe ratio more closely approximates the observed Mg/Fe ratio. Figure 19 shows the measured Mg/Fe ratio curve as a function of radius compared with two calculated Mg/Fe ratio curves. One, labeled $K_{\text{D}}^* = 0.138$, was calculated using λ_{Mg} and λ_{Fe} evaluated at the garnet center, and the other, $K_{\text{D}}^* = 0.148$, was evaluated near the garnet edge. Although the calculated and measured curves are similar in shape and magnitude, the differences are sufficient to call for an explanation. We shall deal first with those parts of the curves from the garnet center to about 40 microns from the edge.

As the distribution function, K_{D} , can be defined as $(\text{Mg}/\text{Fe})_{\text{A}}/(\text{Mg}/\text{Fe})_{\text{B}}$, where A and B are two coexisting mineral phases, and will generally approach one with increasing temperature (Albee, 1965a, page 276), one might surmise that the differences between calculated and experimental curves from the garnet center to 40 microns from the garnet edge are due to rising temperature during garnet growth. However, K_{D}^* is not the distribution function between garnet and some other coexisting phase but rather between garnet and all the other

Fig. 19. Comparison of measured and calculated Mg/Fe profiles of Fig. 16; see text.



ferromagnesian minerals in the rock (K_D^* is calculated using counting rate ratios which are a function of the atomic ratios). Therefore, K_D^* will vary with changing proportions of minerals during garnet growth.

The magnitude and direction of the mineral proportion dependence on K_D^* is indicated in the following equation:

$$(11) \quad K_D^* = \frac{\lambda_{Mg}^R}{\lambda_{Fe}^R} = \frac{\lambda_{Mg}^B X_B + \lambda_{Mg}^C X_C + \lambda_{Mg}^S X_S}{\lambda_{Fe}^B X_B + \lambda_{Fe}^C X_C + \lambda_{Fe}^S X_S}$$

where λ^R is the fractionation factor between garnet and rest of rock; λ^B , λ^C , λ^S are the fractionation factors between garnet and biotite, chlorite, and staurolite, respectively; and X_B , X_C , X_S are the weight fractions of biotite, chlorite, and staurolite, respectively, in the rock exclusive of garnet. The mineral fractionation factors are equilibrium fractionation factors at any stage of garnet growth and are assumed at this stage of the calculations to be constant during garnet growth.

Equation (11) can be simplified by the observation that staurolite of the Kwoiek Area is zoned but biotite and chlorite are not zoned. Thus, the fraction of staurolite, X_S , in equilibrium with the assemblage at any stage of garnet growth is infinitesimally small, and equation (11) reduces to:

$$(12) \quad K_D^* = \frac{\lambda_{Mg}^R}{\lambda_{Fe}^R} = \frac{\lambda_{Mg}^B X_B + \lambda_{Mg}^C X_C}{\lambda_{Fe}^B X_B + \lambda_{Fe}^C X_C}$$

The present rock has $X_B = .873$ and $X_C = .127$. As we want to avoid for now the outer 40 microns, we shall pick $X_B = .8$ and $X_C = .2$ as values not too far from what would be expected at a stage 40 microns from the edge of the garnet.

The mineral fractionation factors are more difficult to evaluate.

The fractionation factors at the outer edge of the garnet are:

$$\lambda_{Mg}^B = 0.30$$

$$\lambda_{Fe}^B = 2.16$$

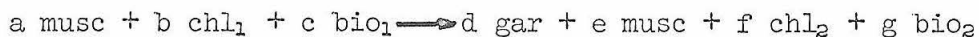
$$\lambda_{Mg}^C = 0.21$$

$$\lambda_{Fe}^C = 1.83$$

Using λ_{Mg}^B as .32, λ_{Mg}^C as .22, λ_{Fe}^B as 2.1, λ_{Fe}^C as 1.8, X_B as .8, and X_C as .2 in equation (12), K_D^* equals 0.147, close to the calculated value of 0.148. The increase of the Mg mineral fractionation factor and the decrease of the Fe fractionation factor was made because, as will be discussed later, the edge of the garnet probably grew at a lower temperature than that part 40 microns from the edge; hence, the fractionation factors in from the edge should be closer to one than at the edge. The numbers were picked in such a way as to get a K_D^* close to 0.148 in order to see what change of mineral proportions, keeping the mineral fractionation factors constant, is necessary to get a K_D^* close to 0.133 for the garnet center. A value of $X_B = .3$

and $X_C = .7$ will give a K_D^* of 0.132, close to 0.133. Hence, by increasing X_B from 0.3 to 0.8, the differences between the K_D^* calculated and K_D^* measured curves can be accounted for, keeping the mineral fractionation factors constant. Therefore, either a change in proportions of minerals in the matrix or a temperature change could account for the difference in Fig. 19.

It is not unreasonable to expect the biotite/chlorite ratio to increase during garnet growth. In Fig. 20 the three-phase field bio - chl - gar is plotted on the Thompson Projection. Since the garnet is zoned, only the outermost rim of the garnet is in equilibrium with the biotite and chlorite; but the biotite and chlorite are homogeneous. Therefore, the composition of the effective system will lie on the chlorite-biotite join. As the garnet continues to grow, it will continue to be zoned, and the effective composition of the system will move along line a - a' as the garnet composition is removed from the system. At some later stage of garnet growth the three-phase field gar - chl - bio will have moved to g' - c' - b' and the biotite/chlorite ratio will have increased. The equation for this reaction must be of the form:



where $a > e$, $b > f$, $c < g$, and $c/b < g/f$. Also, Mg/Fe of bio_2 and chl_2 will be greater than the Mg/Fe ratio of bio_1 and chl_1 , respectively.

The above calculation would be further complicated in assemblages

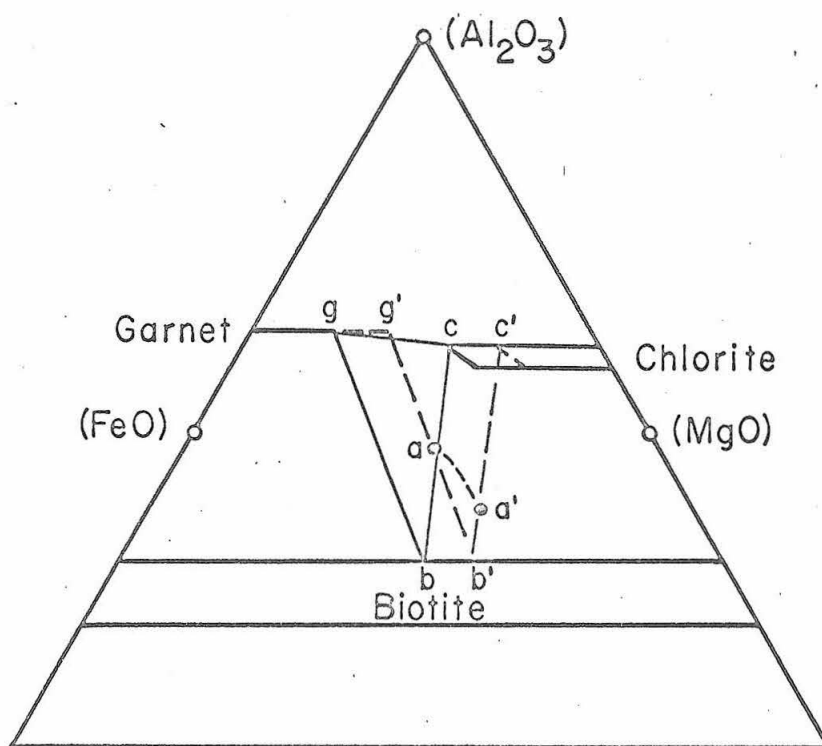


Fig. 20. Thompson projection, showing effect of the growth of zoned garnet on the biotite/chlorite ratio in the assemblage musc - gar - bio - chl; see text.

containing muscovite. Table 9 shows the mode of a rock collected very close to isograd 2 (Fig. 4) with a lower biotite/chlorite ratio than that of 350B and a large amount of muscovite. Since the

Table 9

Mode of Specimen 272, 500 Counts

garnet	26.4
biotite	12.6
chlorite	16.2
white mica	23.2
ilmenite	3.0
epidote	0.2
graphite	0.8
quartz and plagioclase	37.6

inferred reaction at garnet nucleation involves muscovite as a reactant (see reaction (2), Part III, low-Ca rocks) and the muscovite is homogeneous and contains significant amounts of Mg and Fe, the K_D^* at garnet nucleation must be affected by the presence of muscovite. The effect of the earlier chlorite + muscovite reaction on the garnet zoning pattern must be listed as one of the uncertainties in the analysis of the garnet zoning.

The assumption that λ_{Mg}^R , λ_{Fe}^R , and λ_{Mn}^R are constants must also be evaluated. This assumption is obviously not completely correct because λ_{Mg}^R and λ_{Fe}^R are individually dependent on the biotite/chlorite ratio as is λ_{Mn}^R . Another, possibly independent,

compositional factor is the effect of variation of Mn on λ_{Mg}^R and λ_{Fe}^R , Mg on λ_{Mn}^R and λ_{Fe}^R , and Fe on λ_{Mg}^R and λ_{Mn}^R . Figures 21, 22, and 23 show biotite and chlorite compositions plotted against the composition of the garnet edge for five rocks of the same assemblage, including 350B, collected within 100 feet of one another. Although there is deviation in the data due to the variation of biotite composition from point to point in a rock and the difficulty of accurate analysis of the garnet edges, several distinct trends appear. A straight line can be drawn through the Mn data and the origin indicating that λ_{Mn}^{bio} and λ_{Mn}^{chl} are not affected by relative amounts of Mg and Fe. However, the Mg and Fe data do not lie on a line through the origin, indicating that λ_{Mg} and λ_{Fe} are dependent on Mn content in the rock. Reference lines for constant λ_{Mg} and λ_{Fe} are shown on Figs. 22 and 23.

Figures 22 and 23 show that both λ_{Fe} and λ_{Mg} for biotite and chlorite increase with decreasing Mn in the garnet; therefore, λ_{Fe}^R and λ_{Mg}^R increase with decreasing Mn in garnet. However, the lower the Mn content at the garnet edge, the lower the biotite/chlorite ratio in the rock and the lower λ_{Fe}^R , so that the two effects, biotite/chlorite ratio and Mn content, work against one another.

It can be concluded from the Mg/Fe ratio data that the zoning from the garnet center to the 40 micron horizon could have taken place at nearly constant temperature. The crossing of constant K_D^* lines, although in the direction expected for increasing temperature from garnet center outwards, can be best explained in terms of changing biotite/chlorite ratio. Although the zoning can be explained for the

Fig. 21. Plot of edge content of Mn in garnet of 350 series rocks against average Mn content of coexisting chlorite (top scale) and biotite (bottom scale).

Fig. 22. Plot of edge content of Fe in garnet of 350 series rocks against average Fe content of coexisting chlorite and biotite. Lines of constant $\text{Fe}_{\text{gar}}/\text{Fe}_{\text{chl}}$ and $\text{Fe}_{\text{gar}}/\text{Fe}_{\text{bio}}$ ratios are indicated.

Fig. 23. Plot of edge content of Mg in garnet of 350 series rocks against average Mg content of coexisting chlorite and biotite. Lines of constant $\text{Mg}_{\text{gar}}/\text{Mg}_{\text{chl}}$ and $\text{Mg}_{\text{gar}}/\text{Mg}_{\text{bio}}$ ratios are indicated.

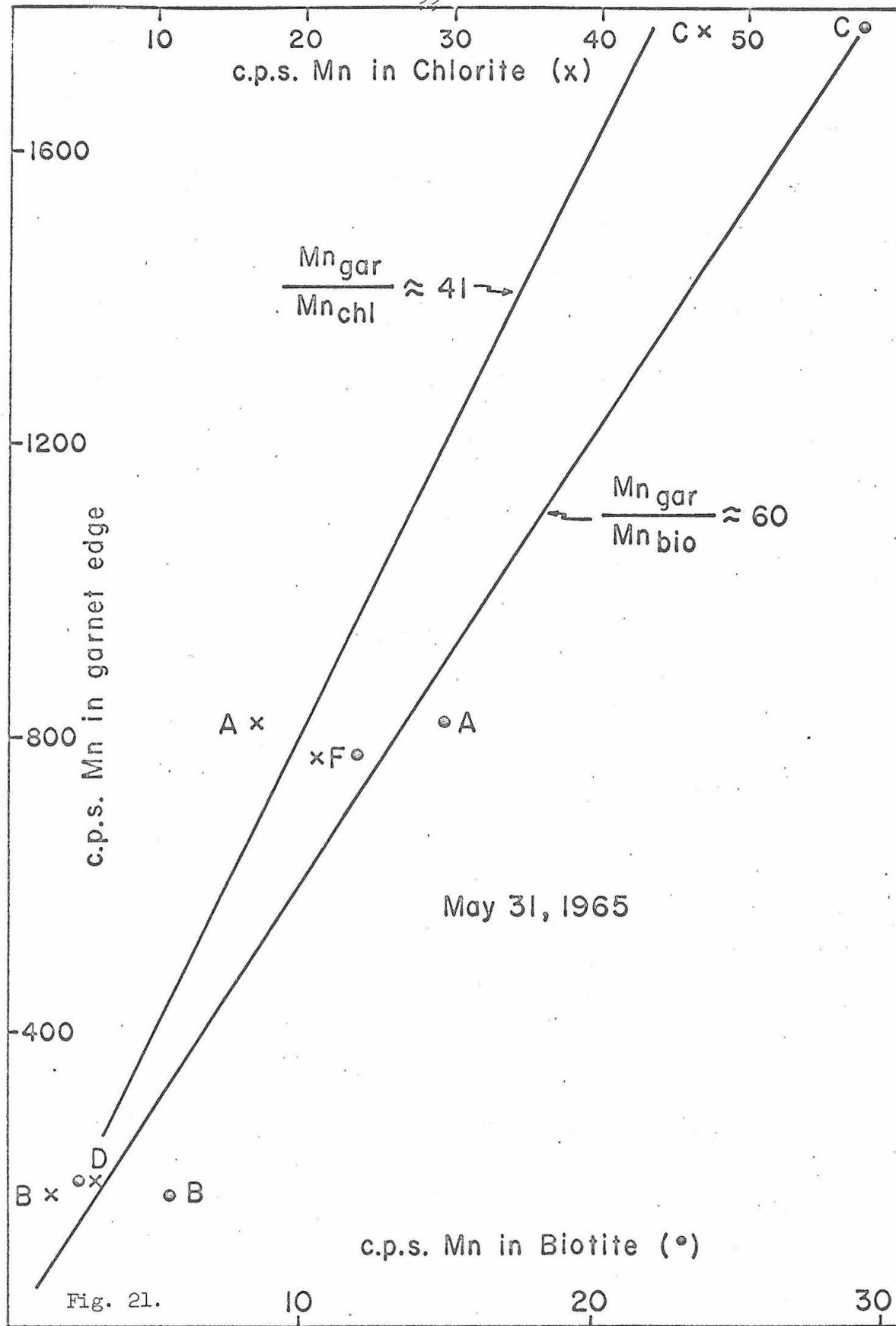


Fig. 21.

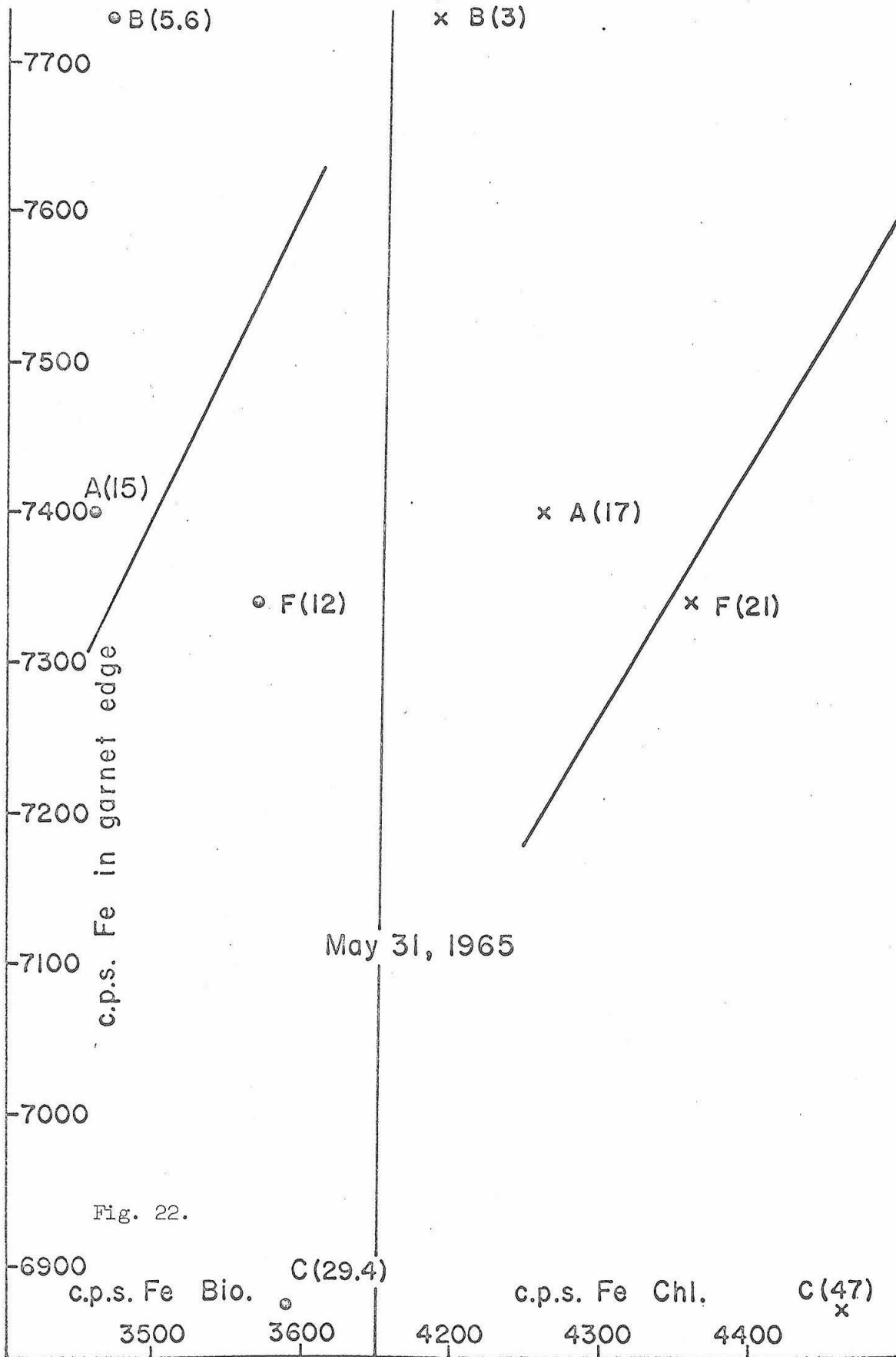


Fig. 22.

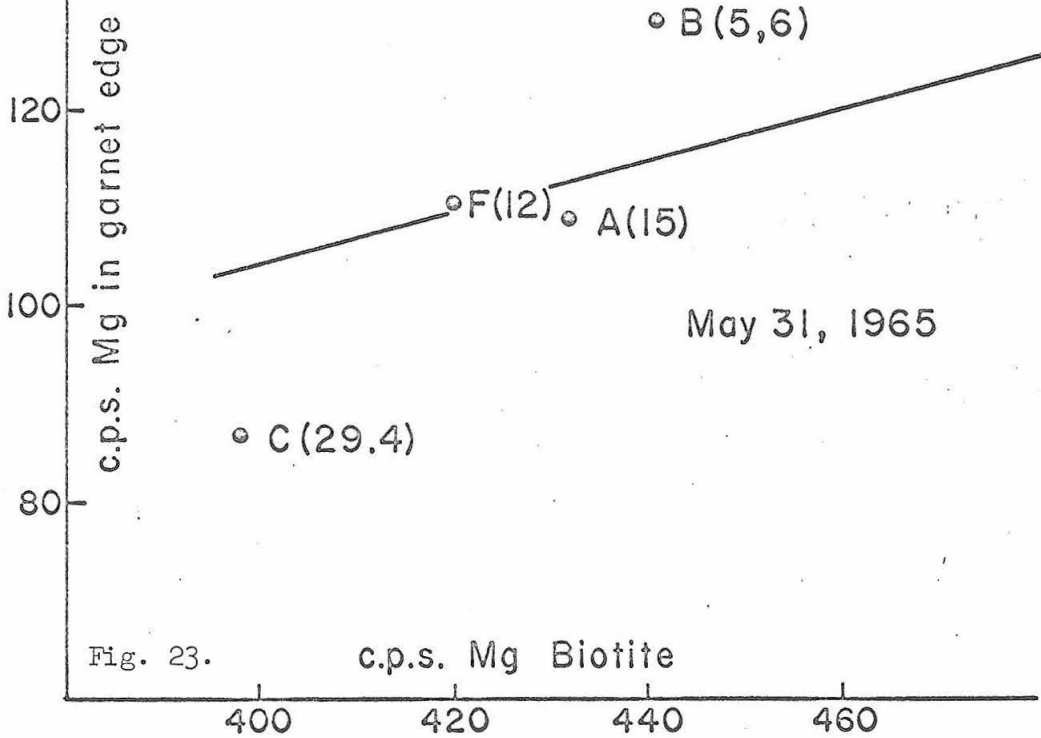
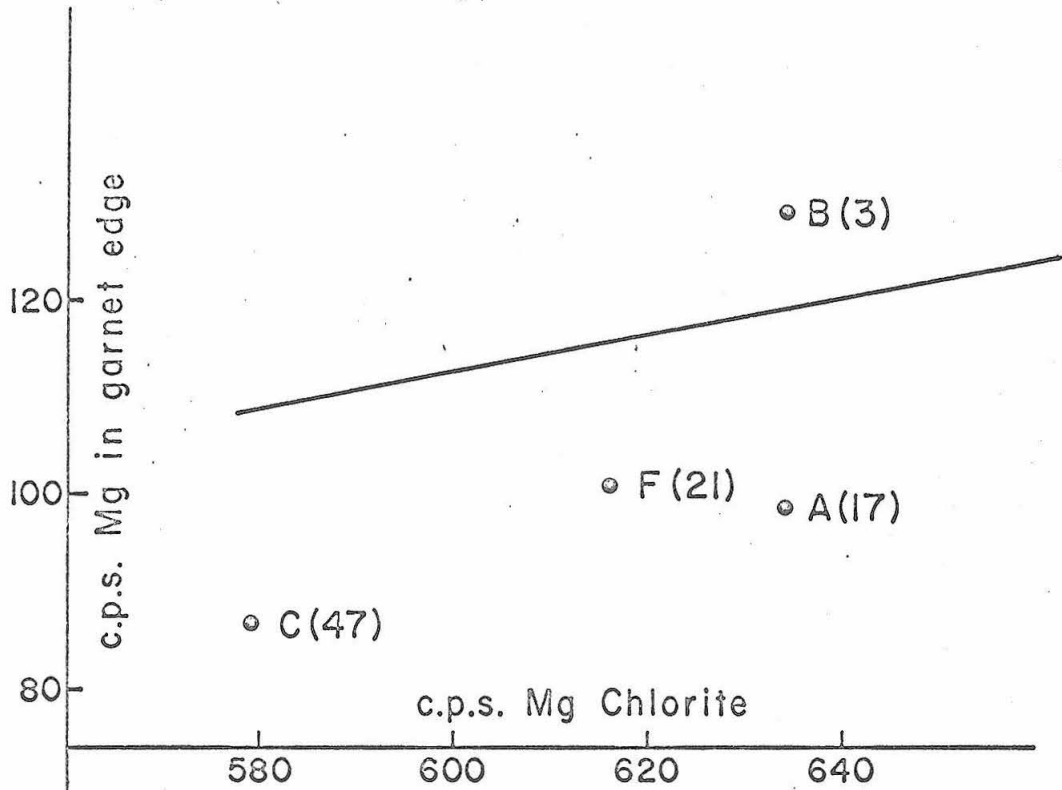


Fig. 23.

case of constant temperature, it is, however, unreasonable to think that temperature did not increase because there must have been a driving force, quite likely rising temperature, which kept the garnet-making reaction going.

The evidence from the Mn experimental and calculated profiles indicates slightly increasing temperatures to about 40 microns from the edge. This is based on the fact that the calculated λ_{Mn}^R for the center and for 40 microns from the edge are nearly the same. Since λ_{Mn}^{bio} is $>$ λ_{Mn}^{chl} at the edge, the same relation must hold for within the garnet, and, therefore, λ_{Mn}^R must increase with increasing biotite/chlorite ratio. The fact that λ_{Mn}^R at the center and 40 microns from the edge is nearly the same indicates that an increase of temperature, which would drive λ_{Mn}^R towards one, must have counterbalanced the effect of changing biotite/chlorite ratio.

The zoning in the outer 40 microns of garnet 350B is striking since both the Mg/Fe ratio curves (Fig. 19) and Mn curves (Fig. 16) show a reversal in sign of slope about 40 microns from the edge. If it is assumed the outer zoning effects were incorporated during garnet growth and are not the result of inward diffusion during a late stage of reequilibration of the garnet with its surroundings, it must be concluded that the garnet grew under conditions of decreasing temperature. A growing garnet, even during decreasing temperature, requires an increase of the biotite/chlorite ratio and, therefore, as pointed out above, an increase of K_D^* . However, the Mg/Fe zoning pattern crosses decreasing K_D^* curves outward from the garnet center (Fig. 19).

This, then, implies that another variable besides the biotite/chlorite ratio is working to decrease K_D^* in such a way as to overcompensate for the biotite/chlorite ratio effect on K_D^* . Temperature is probably the other variable as decreasing temperature would drive K_D^* away from one which in this case means a smaller number.

On the other hand, the upturn of Mn at the garnet edge implies an increase of λ_{Mn}^R from about 23 to about 55 which is in the direction of lower temperature, away from one. This is also the same direction expected for an increase of biotite/chlorite ratio, and the two effects must be added together to give the large increase in λ_{Mn}^R .

The incorporation of the zoning effects in the outer 40 microns is believed to have occurred during growth of the garnet. The zoning effects could conceivably be due to the reequilibration of the outer garnet layer with the rest of the rock during decreasing temperature but without garnet growth. This mechanism implies diffusion of Mn into the garnet and Mg out of the garnet. If Mn diffused, a discontinuous intersection of the diffusion profile and the original Rayleigh profile might be expected. The intersection should be discontinuous because abrupt changes of slope of Mn profiles are seen in many garnets indicating that self diffusion of Mn in the garnets, a mechanism which would tend to homogenize the garnet, is negligible (Fig. 9). In garnet 350B one could argue that there is a discontinuous intersection of profiles; however, in Figs. 13 and 14 are shown garnet profiles in which the Mn upturn takes place over 100 microns rather than 10 microns

and shows no evidence of a discontinuous intersection of two types of profiles.

A plausibility argument suggesting growth of garnet, rather than just reequilibration of garnet edge, during decreasing temperature is that when the temperature begins to decline a garnet is already nucleated; and, because the reaction making garnet is still a dehydration reaction, the garnet would be expected to continue to grow. The driving force of the reaction may be a decrease in $\mu_{\text{H}_2\text{O}}$ with falling temperature.

Regardless of whether garnet grew during decreasing temperature or simply had its edge reequilibrated with its surroundings during decreasing temperature, an important point is that there was reequilibration and exchange of elements between minerals during decreasing temperature. This fact indicates that in the Kwoiek Area the compositions of the mineral phases representing the last temperature of equilibrium do not represent the maximum temperature of metamorphism.

The probable model for the thermal history of garnet 350B is as follows. The garnet grew under conditions of either constant or slightly increasing temperature to a point about 40 microns from the edge. At this point temperature began to drop rapidly with respect to rate of garnet growth and the garnet stopped growing at some indeterminate point during the temperature decline. The horizon in the garnet representing the stage of growth during the maximum temperature of metamorphism is probably very near, but somewhat to the garnet center, from the point where the experimental curve just begins to cross

decreasing K_D^* curves, near radius = 280 microns, Fig. 19.

Discussion of specimens 350A, 350B, 350C, 350D, and 350F

The validity of the interpretation of the maximum temperature horizon of the garnet in sample 350B can be tested by the study of other garnets formed under identical conditions. Four other samples, which contain the same assemblage but different mineral proportions and which were collected within 100 feet of sample 350B, have been studied. The modes of these four rocks are shown in Table 10 together with the mode of 350B. The assemblage is gar - bio - stl - chl - ilm - qtz - plag - graph except that 350C contains as additional phases a white mica shimmer-aggregate surrounding the staurolite (this texture has been discussed in Part III) and one large grain of kyanite. The kyanite occurs as partially resorbed grains within an area with a square outline interpreted below as indicating the former presence of andalusite. The kyanite grains are surrounded by a plagioclase-biotite aggregate, which effectively armors the kyanite from the rest of the thin section. Hence, it is interpreted that the garnet belongs to a gar - bio - chl - stl assemblage and not a kyanite assemblage.

The four-phase assemblage, gar - bio - chl - stl, is shown on the $Al_2O_3 - K_2O - FeO - MgO$ tetrahedron (Fig. 24). In terms of the diagram the assemblage is trivariant in P, T, and a_{H_2O} ; but since the Fe/Mg ratio in the phases is also dependent on Mn content (to be shown below for garnet), the Mn content of some phase must also be taken as a variable. Thus, the Fe/Mg ratio in the maximum temperature

Table 10

Modes of Five Rocks Collected from
the Same Outcrop .34 Miles East of Kwoiek Needle

	350A	350B	350C	350D	350F
Garnet	1.0	4.1	0.1	2.8	1.4
Biotite	26.8	29.6	34.1	27.1	23.8
Staurolite	6.3	2.5	4.5	5.0	8.2
Chlorite	0.8	4.3	0.3	4.4	0.6
Ilmenite	0.6	1.0	1.2	1.0	0.8
Kyanite	-	-	0.8	-	-
White mica	-	-	1.3	-	-
Subtotal	35.5	41.5	42.3	40.3	34.8

Numbers in volume percent. Plagioclase, quartz, and graphite, in undetermined relative amounts, make up the rest of each rock.

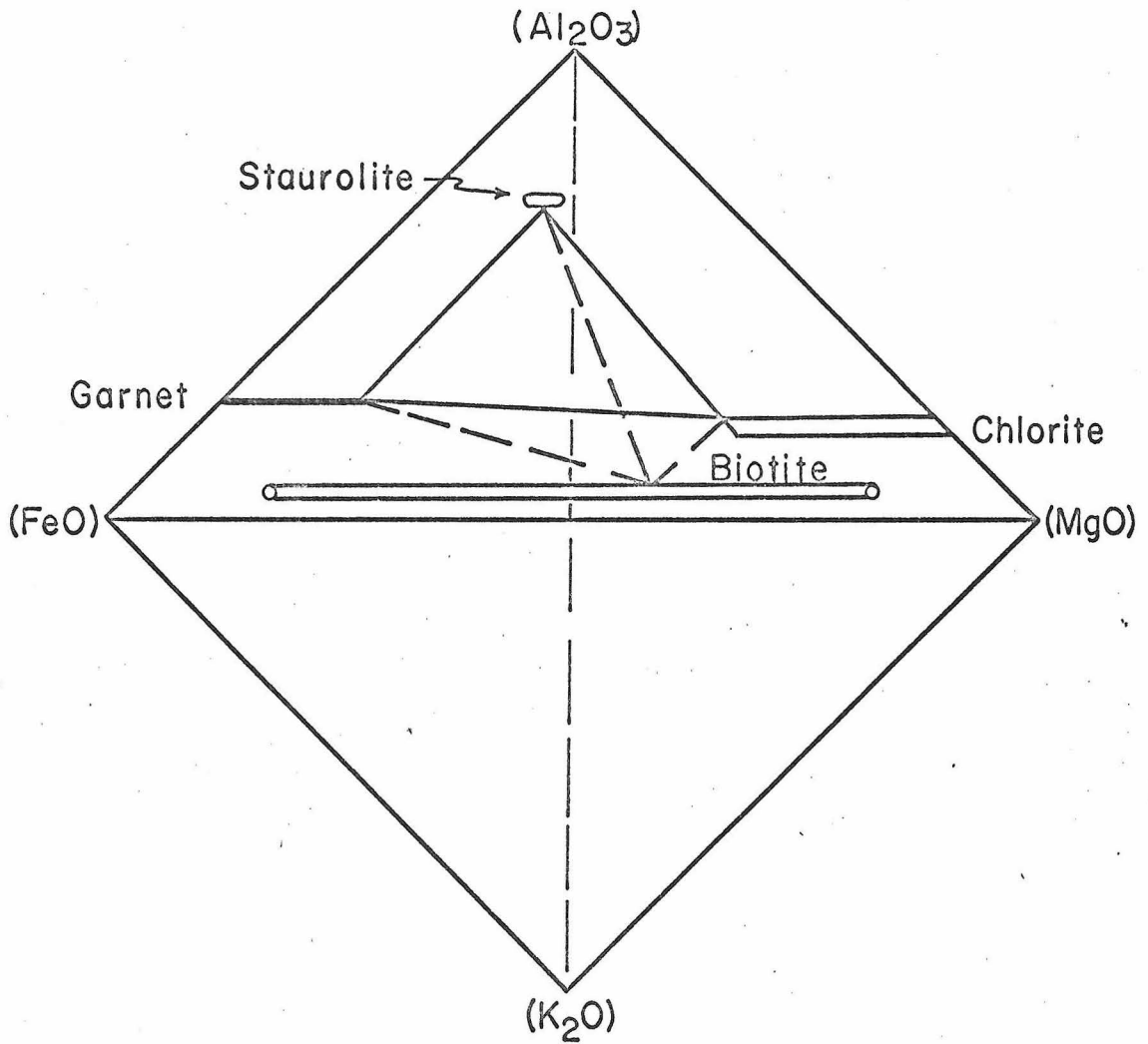


Fig. 24. AKFM tetrahedron indicating the location of the four-phase volume gar - bio - chl - stl and showing that the garnet composition in this assemblage is a limiting composition.

horizons of the garnet should be nearly the same for all rocks of this same assemblage from a single outcrop if they have identical Mn contents. The garnet composition at maximum temperature is a limiting composition for a given Mn content and in the discussion below will be referred to as the maximum temperature, limiting Mg/Fe ratio.

The garnet profiles for all five rocks are shown in Figs. 15a-15f. The maximum temperature horizon for garnet 350B was determined by use of a plot of Mg/Fe garnet against radius (see Fig. 19). It could as well have been determined by use of a plot of Mg/Fe garnet against Mn content (Fig. 25) as Mn content is a function of radius. This type of plot was used to determine the maximum temperature horizon of the garnet from samples 350A, C, D, and F.

Analyses of spots averaging about 50 microns apart for all garnet of the 350 series rocks, background corrected, and normalized to the May 31, 1965 date, are plotted in Figs. 26 and 27. The edge compositions are labeled e. Envelopes have been drawn around the garnet data of each of the five samples, and these envelopes are shown superimposed in Fig. 28 with the inferred limiting composition, maximum temperature compositions indicated by large circles. Visually fitted curves are drawn through these points as well as through the edge compositions. Although there is some uncertainty for the location of the edge and maximum temperature compositions (especially for 350D), there is clearly an inverse relation of Mn to the Mg/Fe ratio for both the compositions at the edge and at the maximum temperature horizon.

Fig. 25. Plot of Mn in garnet 350B (Fig. 16) against Mg/Fe ratio, compared with calculated curves for $K_D^* = 0.133$ and 0.148 .

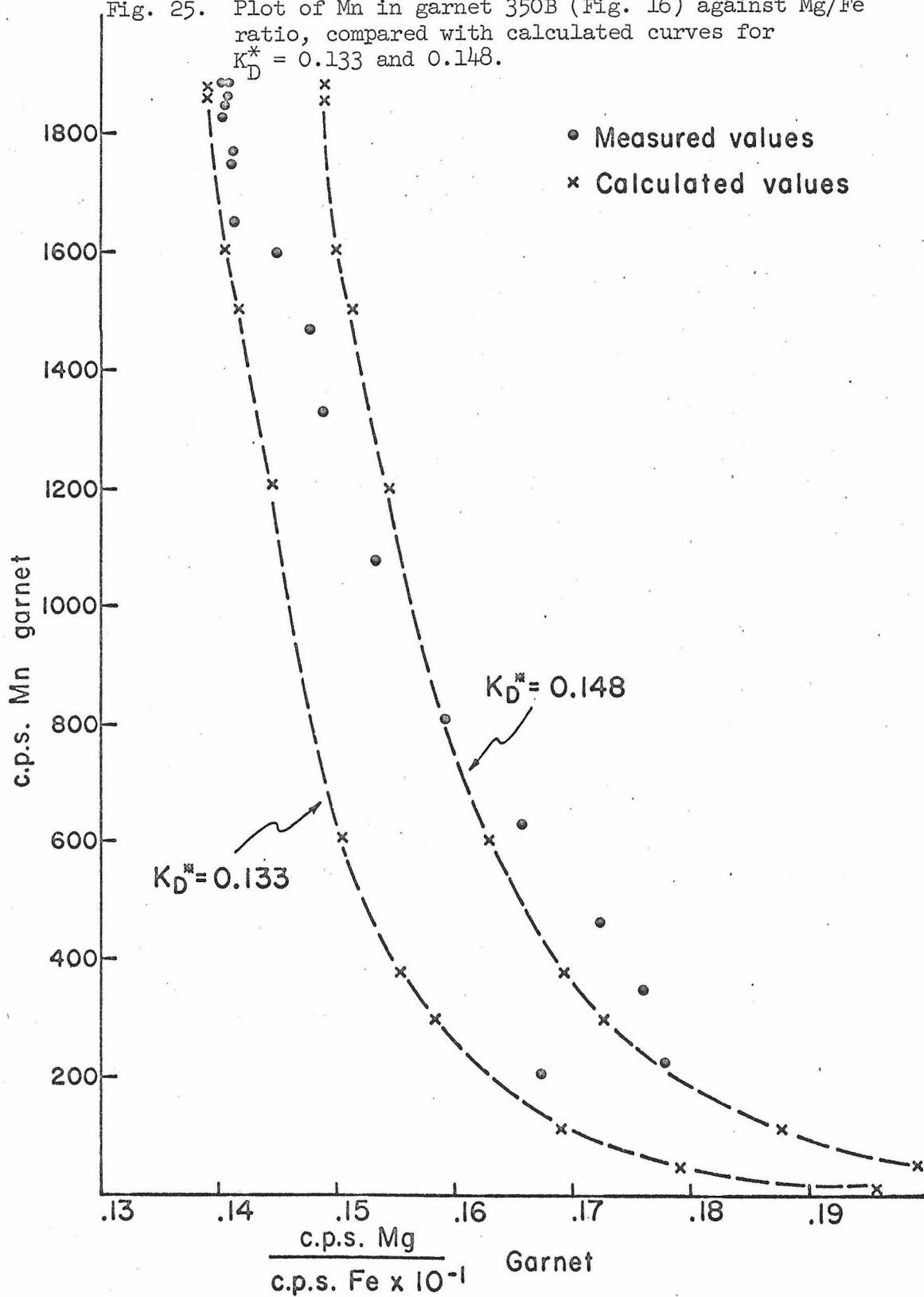


Fig. 26. Plot of Mn vs. Mg/Fe for several garnet grains of samples 350B and 350D. Edge compositions marked by e.

Fig. 27. Plot of Mn vs. Mg/Fe for several garnet grains of samples 350A, 350C, and 350F. Edge compositions marked by e.

Fig. 28. Figs. 26 and 27 superimposed with envelopes drawn around points of each sample. Large circles represent compositions inferred to represent the maximum temperature. Solid line, visually fitted to large circles, shows dependence of Mg/Fe ratio on Mn content. Dashed line shows dependence of Mg/Fe ratio on Mn content for the edge compositions.

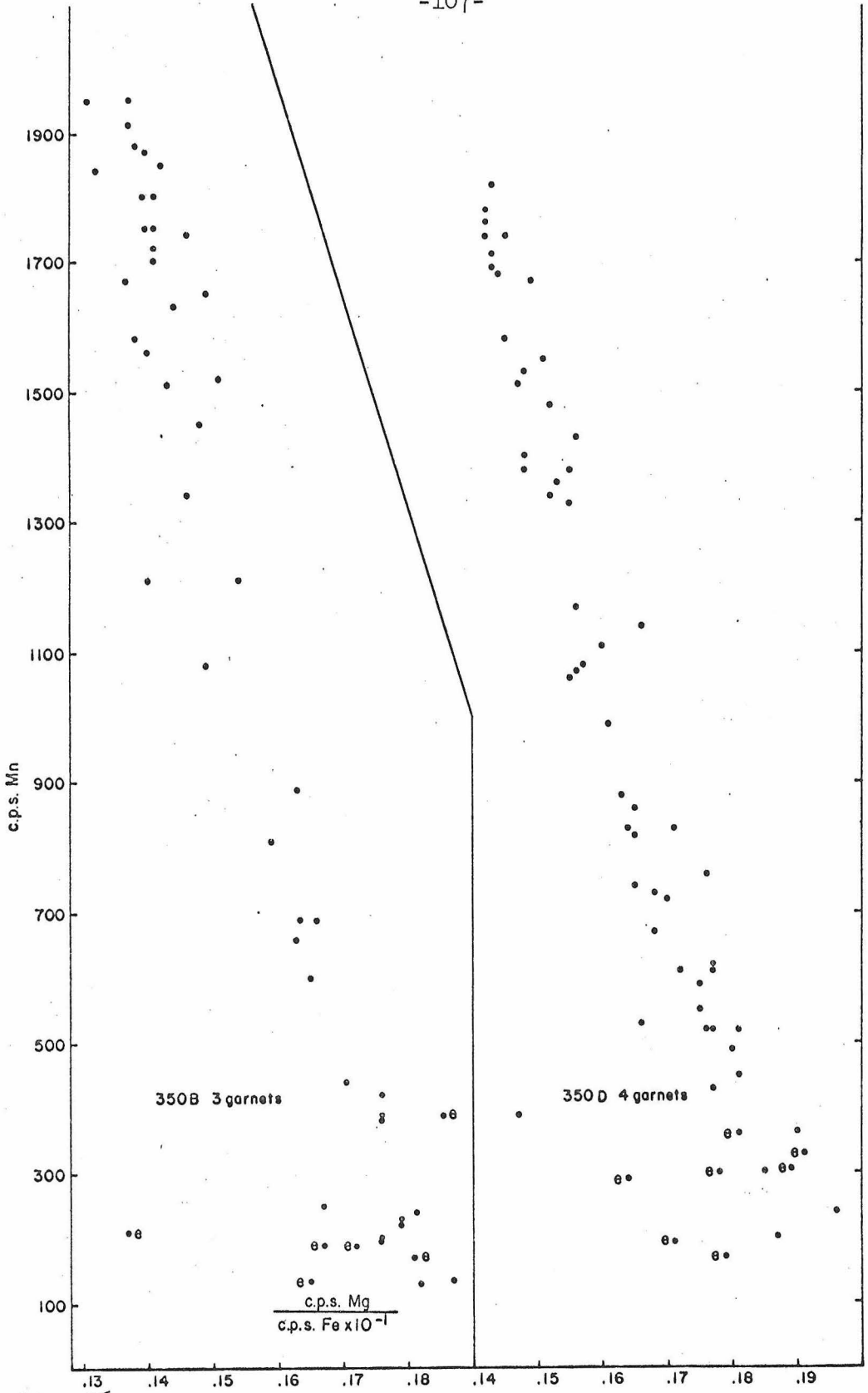


Fig. 26.

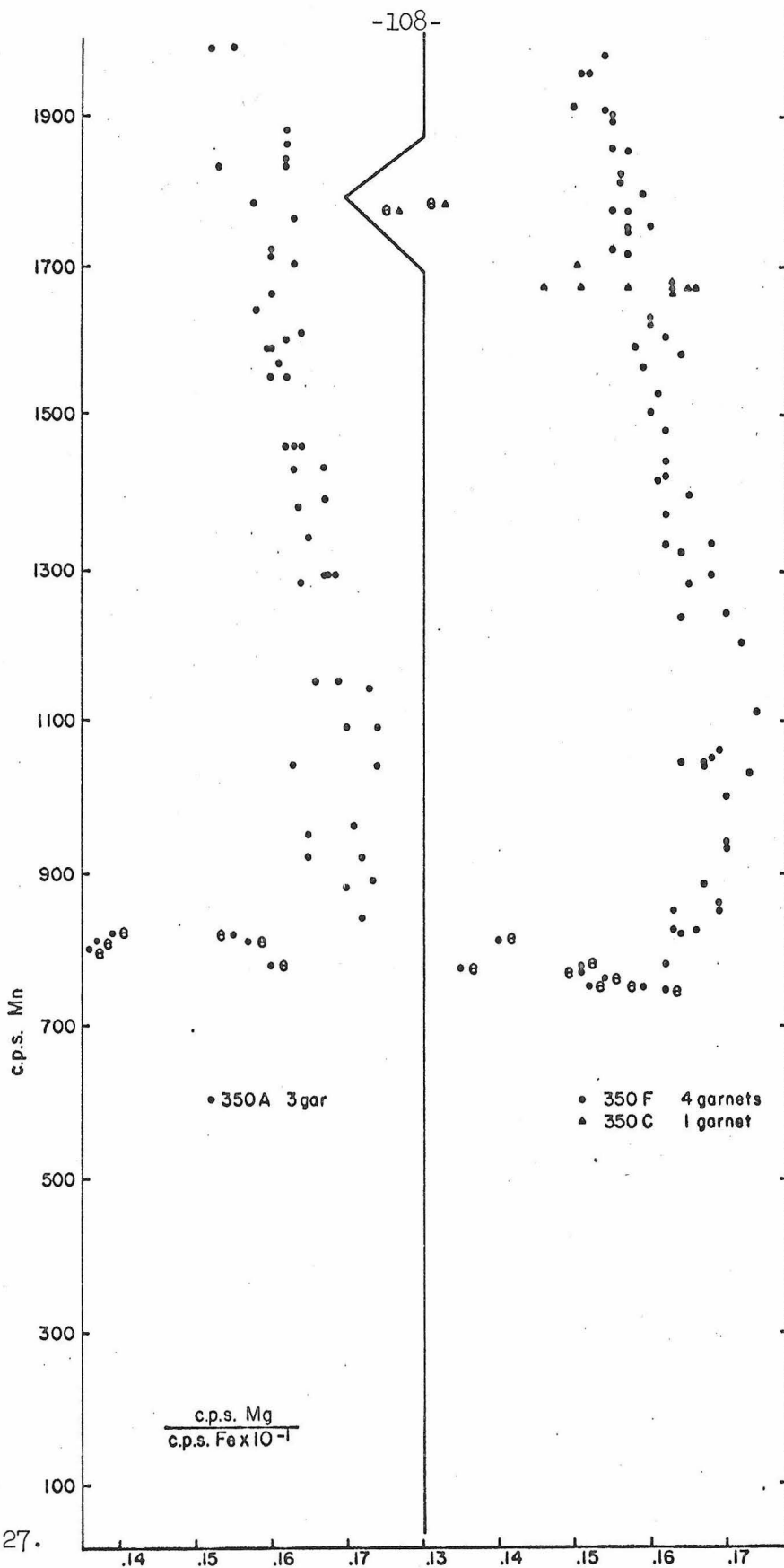


Fig. 27.

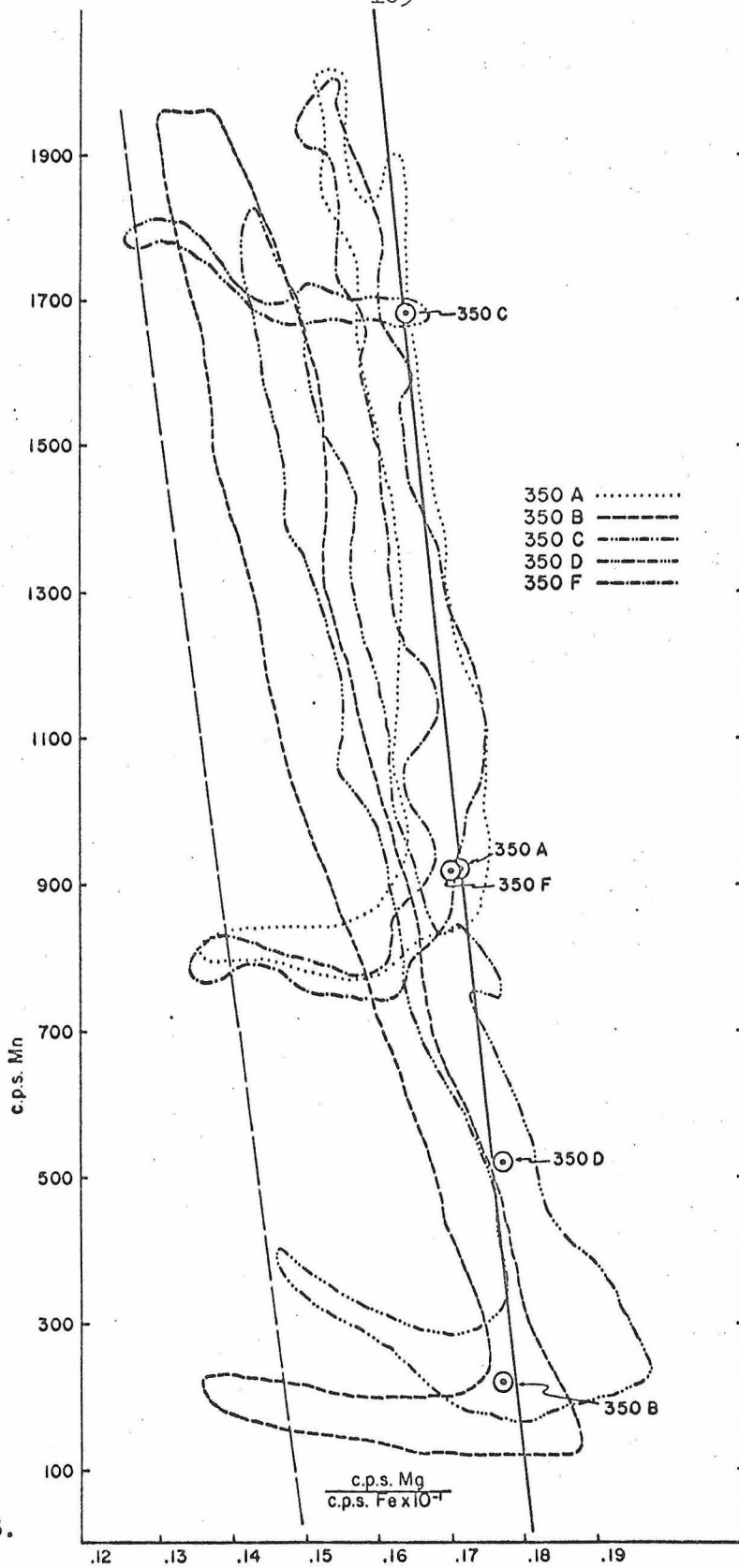


Fig. 28.

Albee (1965b) also pointed out this relation based on atom percent $Mn/(Mn+Mg+Fe)$ and atom percent $Mg/(Mg+Fe)$ in the chemically analyzed garnets from muscovite assemblages studied by Phinney (1963).

In order to more directly compare the study of Albee (1965b) with the results of the present study, total chemical analyses were made near the maximum temperature horizons of the 350 series rocks at the points marked A, B, C, D, and F on Fig. 15. The results are shown in Table 11 and are plotted with Phinney's data in Fig. 29. The slope is similar, and it is interesting that the best fit line of the present data passes very near the garnet data of Frost (1962) for a muscovite-free, gar - bio - stl assemblage. The lines through the present data and Phinney's data are at different locations because the assemblages are different. It would be most important to determine if the dependence of the Mg/Fe garnet ratio on Mn content has the same or different slope at much higher or lower grades than that of Fig. 29. It is encouraging, however, that the published data from chemical analyses of probably zoned garnets gives the same slope as the microprobe analyses on correlated horizons.

The fact that the five points do lie on a reasonable line is evidence that the limiting composition, maximum temperature horizon has been identified from one outcrop area. It is also clear that Mn is a variable affecting the Mg/Fe ratio and that in comparing limiting composition, maximum temperature Mg/Fe ratios from point to point in a metamorphic terrane, these ratios must be corrected for the Mn content.

Table 11

Total Analyses of Garnet from the .350 Series Rocks

	A	B	C	D	F
SiO ₂	36.2	35.3	35.6	36.42	36.2
TiO ₂	.06	.08	.06	.09	.06
Al ₂ O ₃	22.8	22.5	23.3	22.7	22.2
FeO	30.18	31.78	28.99	31.02	30.18
MnO	4.12	1.28	6.24	2.25	3.89
MgO	4.16	4.55	3.85	4.42	4.05
CaO	2.22	2.17	2.18	2.40	2.16
Total	99.74	97.66	100.22	99.30	98.74

Formulas

A	(Fe _{2.019} Mg _{.496} Mn _{.279} Ca _{.190}) _{2.98} Al _{2.05} (Si _{2.9} Al _{.1}) ₃ O ₁₂
B	(Fe _{2.137} Mg _{.544} Mn _{.087} Ca _{.187}) _{2.955} Al _{2.03} (Si _{2.9} Al _{.1}) ₃ O ₁₂
C	(Fe _{1.939} Mg _{.435} Mn _{.423} Ca _{.187}) _{2.984} Al _{2.05} (Si _{2.85} Al _{.15}) ₃ O ₁₂
D	(Fe _{2.078} Mg _{.526} Mn _{.152} Ca _{.206}) _{2.96} Al _{2.05} (Si _{2.91} Al _{.09}) ₃ O ₁₂
F	(Fe _{2.04} Mg _{.488} Mn _{.266} Ca _{.187}) _{2.98} Al _{2.04} (Si _{2.92} Al _{.08}) ₃ O ₁₂

The analyses are in weight percent and were made at the points marked A, B, C, D, and F on Fig. 15, near the inferred maximum temperature horizon. Formulas calculated on the basis of 12 oxygen atoms to a formula unit.

Fig. 29. Atom percent Mn/Mn+Mg+Fe against atom percent Mg/Mg+Fe for data discussed by Albee (1965b) and the present work. The open circles represent analyses by Phinney (1963) for the musc - gar - bio - stl assemblage, the cross represents data of Frost (1962) for a gar - bio - stl assemblage, and the solid circles are the data of the present work for the chl - gar - bio - stl assemblage.

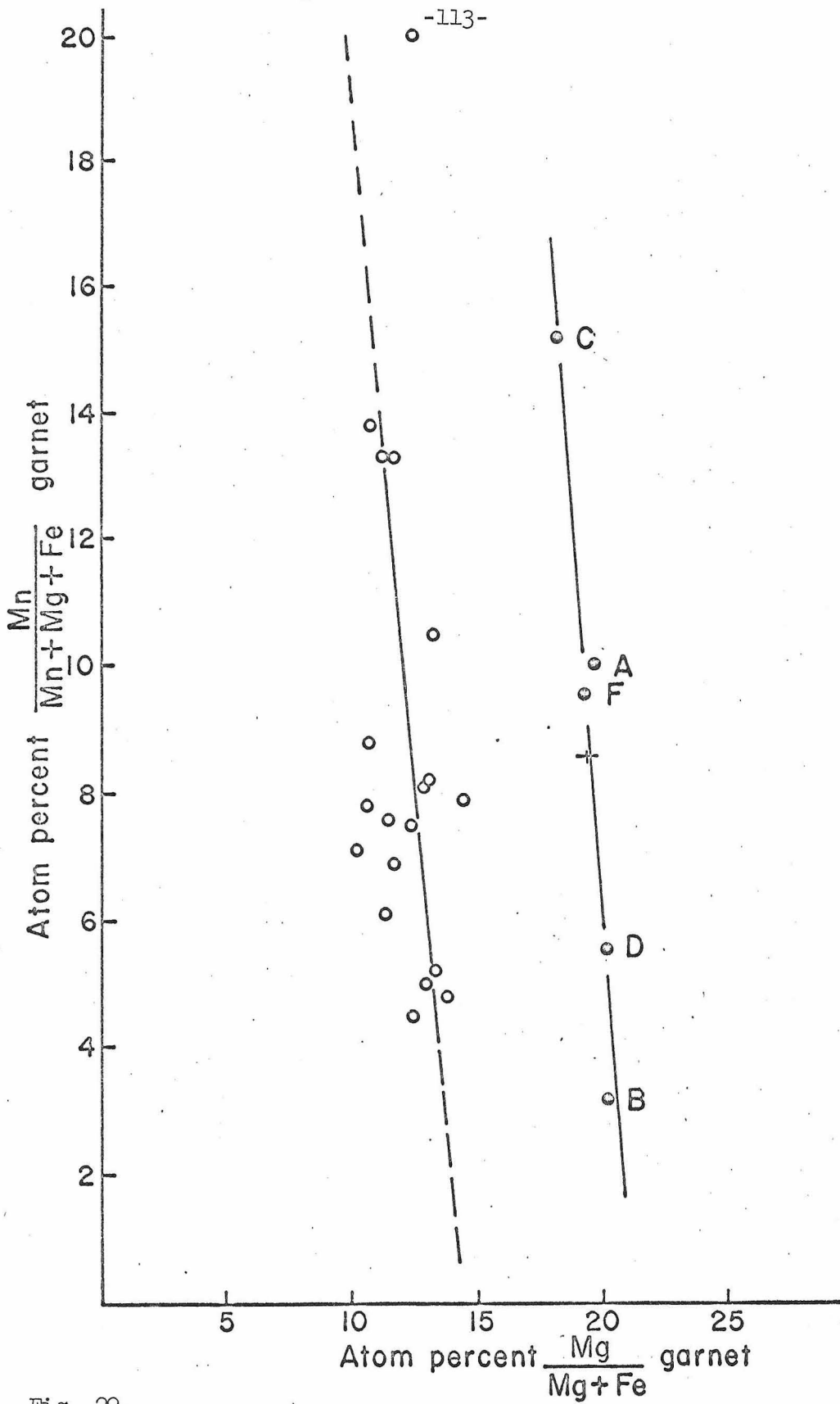


Fig. 29.

The approximate relative range of temperature over which the 350 rocks grew can be determined by comparing the data of Fig. 28 with those of Fig. 30. On Fig. 30, maximum temperature Mg/Fe ratios for garnet at all grades of metamorphism above the garnet grade are plotted against the Mn content of the maximum temperature horizon. The data of the 350 series rocks, both edge compositions and maximum temperature compositions, are also shown. The arrows indicate direction of increasing metamorphic grade (sample locations on Fig. 1 and assemblages in the Appendix) between samples containing a limiting garnet composition in the $Al_2O_3 - K_2O - FeO - MgO$ tetrahedron. The garnets which do have limiting compositions show a progression of increasing Mg/Fe ratios with metamorphic grade and demonstrate that the limiting composition is sensitive to temperature changes. Figure 30 also shows that the range of temperature in which the 350 rocks grew was small relative to the range of temperature between the beginning of garnet grade (lower temperature than that represented by sample 154a) and the maximum temperature the 350 rocks grew in.

The temperature at which the 350 series garnet stopped growing (represented by the dashed line on Fig. 30) is interpreted as being lower than the temperature at nucleation. Returning to Fig. 28, it is seen that the garnet of samples 350 A, B, D, and F nucleated at a composition between the best-fit edge line and the maximum temperature line. These positions between the two lines are not proportional to differences in temperatures of nucleation but probably reflect different biotite/chlorite ratios at nucleation. For example, the center

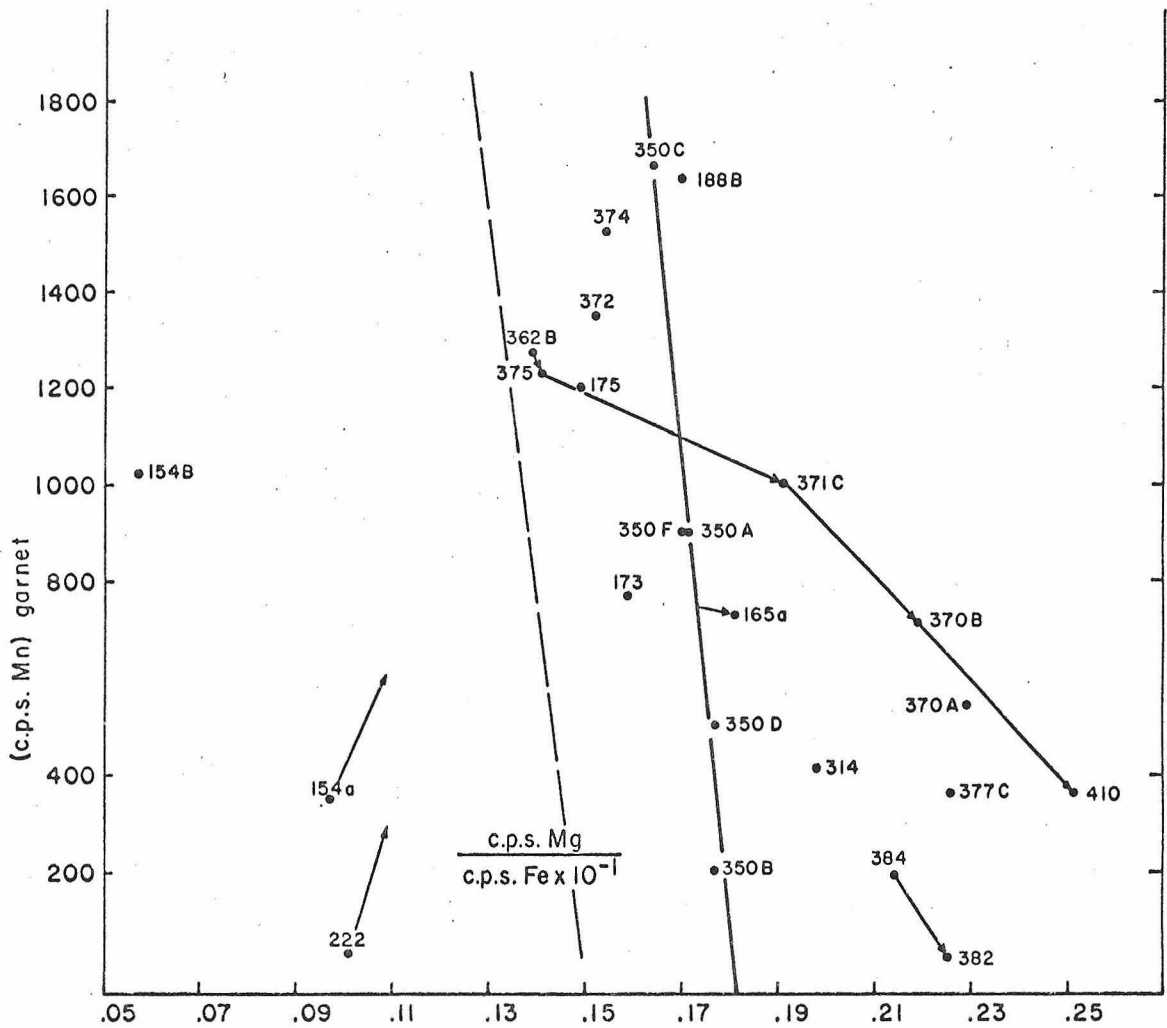


Fig. 30. Plot of Mn content against Mg/Fe ratio in the maximum temperature horizon of garnet for all garnet analyzed in the Kwoiek Area. Arrows indicate direction of increasing grade of metamorphism between garnet samples with limiting compositions. Solid and dashed lines same as in Fig. 28. Assemblages of samples in Appendix.

composition of garnet 350C plots on the maximum temperature point (Fig. 27). All the points around which the envelope of 350C is drawn (Fig. 28) are actually decreasing temperature compositions. As the biotite/chlorite ratio was very large at the nucleation of garnet 350C, shown below, it is probable that garnet 350C nucleated very close to the maximum temperature.

Figure 31 shows graphically the basis for the interpretation that specimen 350C had a very high biotite/chlorite ratio at garnet nucleation. It also shows that the compositions at garnet nucleation of the garnet of samples 350 A, B, D, and F reflect differing biotite/chlorite ratios at nucleation. Shown on Fig. 31 is λ_{Mn}^R determined at the garnet centers plotted against Mn_0 , the initial Mn content of the ferromagnesian minerals, and Mn of the total rock, which includes quartz and plagioclase with the ferromagnesian minerals. Both sets of points show the same thing. High λ_{Mn}^R values correspond to low Mn rock contents and also low garnet contents (numbers in parentheses are the percentage contents of garnet in the rocks). In other words, the more Mn in the rock, the more garnet. More important, however, is the value of λ_{Mn}^R in each of the rocks. As shown in a preceding discussion, λ_{Mn}^R is greater for larger biotite/chlorite ratios. The sequence of higher values of λ_{Mn}^R , B to D to F to A to C, corresponds in a general way to increasing Mg/Fe ratio of garnet nucleation in Fig. 28. The conclusion, then, is that all points of the garnet from each rock sample grew from center to maximum temperature horizon in a temperature range much smaller than

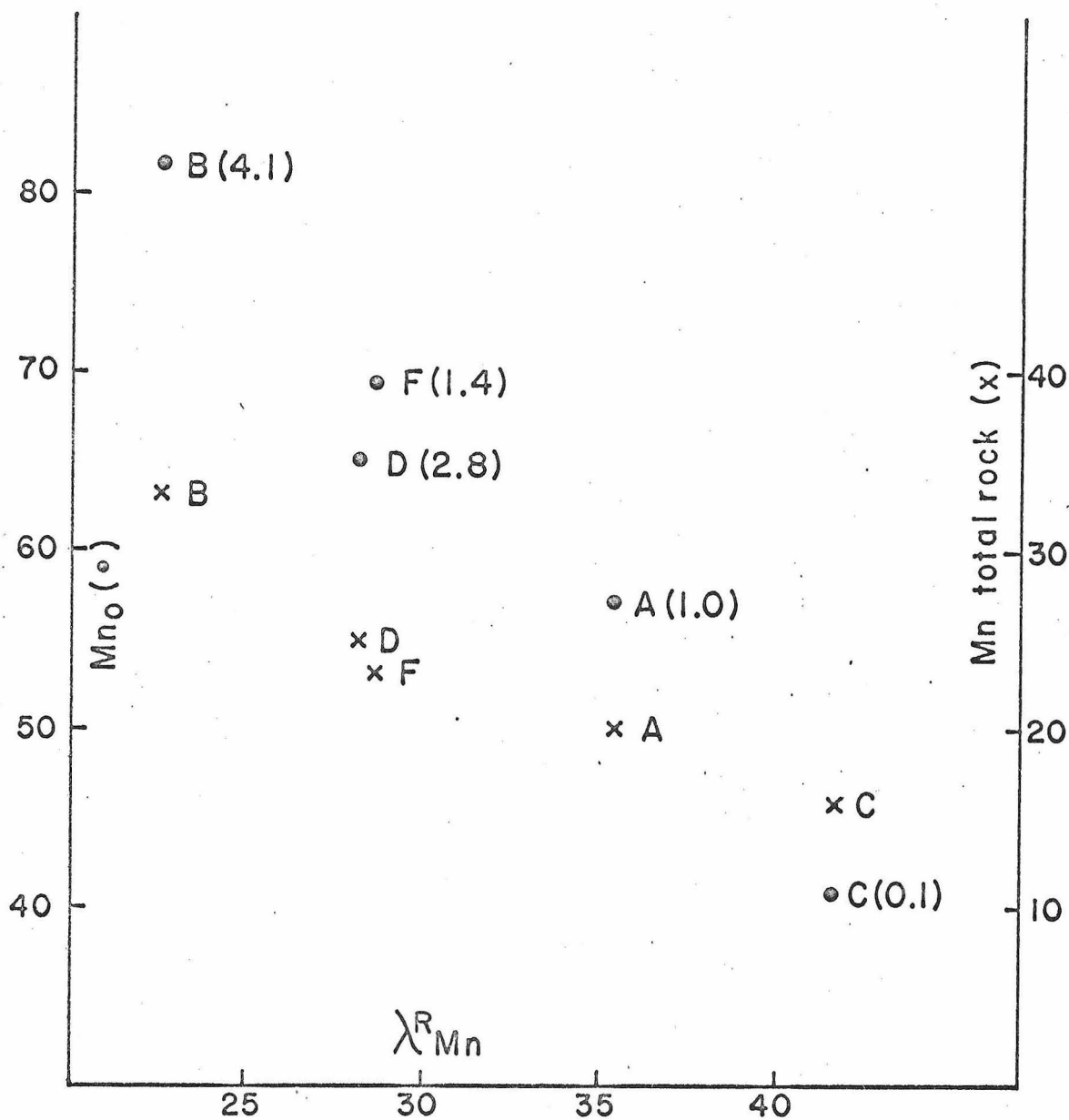


Fig. 31. Plot of the Mn fractionation factor between garnet and rest of rock (λ_{Mn}^R) against MnO (left axis and circles) and Mn content of total rock, including quartz and plagioclase (right axis and crosses) for the 350 series rocks. Numbers in parenthesis are modal garnet contents.

that between the maximum temperature and the temperature at which the garnet stopped growing. It is remarkable that the edge compositions do define a reasonable line (Fig. 28) because this implies that the garnet stopped growing at the same temperature.

The lack of zoning in garnet 350C, except at the edge, where Mn increases, can be understood by reference to equation (10). If the term W^G/W^O is small throughout the garnet growth history, i.e., if the relative proportion of garnet to the total of all the ferromagnesian minerals of the system is small even when the garnet has ceased to crystallize, then the term $(1 - W^G/W^O)^{\lambda-1}$ is close to one even when the garnet has finished growing and $M_G = \lambda^R M_O$ for both garnet center and garnet edge. The only variable affecting the zoning will be λ_{Mn}^R which, for only a small amount of garnet growth, will be constant as the biotite/chlorite ratio will not have changed appreciably. The increase of Mn at the edge is, of course, due to the increase of λ_{Mn}^R during the temperature decrease.

Another mechanism could lead to an apparently unzoned garnet. If Mn_O is extremely small in a rock, the initial Mn content in the garnet might be so small that even extreme zoning would not be analytically detectable. For example, the Mn in the garnet may change by the same proportion of the initial value as it did for garnet 350B, but an initial value of 20 c.p.s. going to 2 c.p.s. at the edge would be less striking than an initial value of 2000 c.p.s. going to 200 c.p.s., if only because of analytical problems. Moreover, a change from 20 c.p.s. to 2 c.p.s. will not produce detectable zoning in Fe

and Mg.

The microprobe garnet analyses in Table 11, except for 350B, give very good totals assuming that all iron is present as ferrous iron. The formulas, calculated on the basis of 12 oxygen atoms, are also reasonable and indicate little ferric iron can be present. This is in conformity with the concept of very low oxygen pressures during metamorphism (Part V). The aluminum content shown in the silica site of the formulas (Table 11) probably indicates errors in some of the calibration curves (Appendix).

Two-history garnet

All the garnets discussed so far have been interpreted to have had a single stage metamorphic history: The rocks were heated rapidly to their maximum temperature and then slowly cooled with no subsequent heating history. This simple history apparently did not hold for all the garnets of the Kwoiek Area. The field evidence, discussed in Part III, suggests that the major heat source for the metamorphism was the intrusion of the Southern Batholith. The thermal effects of the stocks were minor compared to that of the Southern Batholith; however, the effects of the stocks are evidenced, for example, by the relations of the high-Ca isograds to Granite Mountain Stock (Fig. 4). The effects of the stocks are also noticed in garnet collected close to stock contacts, but within the realm of influence of the Southern Batholith, notably around Skihist Mountain Stock and Kwoiek Needle Stock.

A photomicrograph of specimen 188C, from near Skihist Mountain Stock, is shown in Plate 2. The photomicrograph shows overgrowths of anhedral garnet (G_2) on euhedral garnet (G_1). The composition profiles of a garnet from this rock are shown in Fig. 9. The striking feature of the profile is the double peak of Mn. The points where the profile crosses the euhedral garnet outline are marked on Fig. 9 as points 1 and 2, near the top of the outer Mn peak.

It is inferred that the garnet grew euhedrally under the influence of the Southern Batholith and not the adjacent stock. This part of the profile is analogous to the whole profile of Fig. 13, with a large Mn edge upturn due to the period of decreasing temperature. The stock is then inferred to have intruded later than the batholith and reheated specimen 188C so that the garnet continued to grow to its anhedral form at a new high temperature level, and the Mn content again decreased toward the garnet edge. If the profile, left of point 1 and right of point 2, were combined, the resulting one-peak profile would be like other typical Rayleigh profiles.

Specimen 188C is the best example of a two-history garnet found in the Kwoiek Area but is not the only one. All the garnet collected from near stock contacts showed a ring of tiny inclusions, paralleling the present garnet outline, located some tens of microns in from the garnet edge. Specimen 382 (Fig. 11) is such a garnet. Here the Mn profile does not show the same effects as that of 188C but the Fe profile does show effects different from the single-history garnets. Instead of Fe monotonically increasing to the garnet edge, it increases

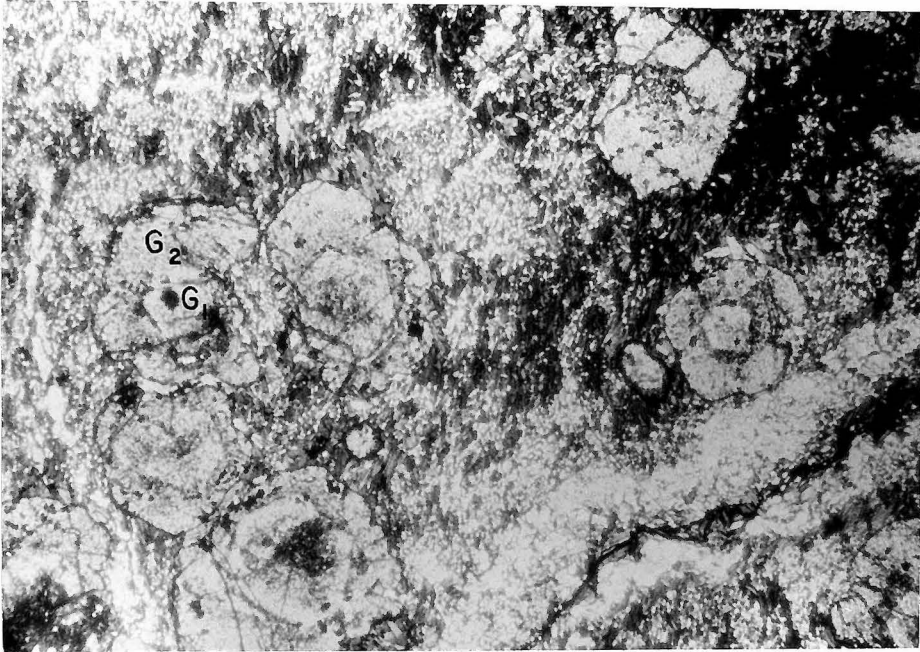


Plate 2. Photomicrograph of garnet in specimen 188C showing euhedral garnet (G_1) surrounded by anhedral garnet (G_2). The profiles of Fig. 9 were made across one of these grains. Total garnet diameter about 1 1/2 mm.

to the zone of tiny inclusions and then drops off. This type of Fe profile was noted in other garnet adjacent to stock contacts but was not noted in garnet outside of the heating influence of the stocks.

It is probable that zoning profiles such as those of Fig. 9 and Fig. 11 could be used to detect two or more stages of metamorphic history in areas where the geologic evidence of two stages of metamorphic history is not as clear as it is adjacent to the stocks of the Kwoiek Area.

Origin of five-phase assemblages

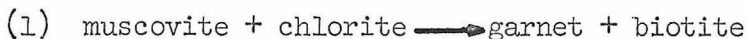
There have been numerous reports in the literature (e.g., Hietanen, 1961, Woodland, 1963, Green, 1963) of pelitic rocks containing an extra phase in the $Al_2O_3 - K_2O - FeO - MgO$ tetrahedron. For example, instead of having the apparent equilibrium four-phase assemblages gar - bio - stl - musc or stl - bio - chl - musc, there might be the five-phase assemblage gar - bio - stl - chl - musc. A very common five phase assemblage is bio - gar - stl - Al-silicate - musc.

Most authors have attempted to explain the five-phase assemblage by one or more of the following ways. (1) The assumption of μ_{H_2O} being externally controlled does not hold, (2) there is another component, such as Mn or Ca, stabilizing the garnet, (3) the chlorite in the assemblage is of retrograde origin, (4) the assemblage is a disequilibrium assemblage, or (5) there are two assemblages side by side on the scale of a thin section. The model given below to explain the five-phase assemblage phenomenon could best be included in the fourth

alternative.

The garnet of the Kwoiek Area as well as those of many other areas (Albee, et al., 1966, Evans, 1965; Banno, 1965) are now known to be zoned. This fact indicates that only the infinitesimally-thin outer layer of the garnet can be in equilibrium with the rest of the rock in many areas. Since garnet zones as it grows rather than reequilibrating with itself, one could ask how readily garnet will react and disappear slightly outside its field of stability. It is presumed here that garnet is so unreactive that it would not easily be destroyed if it were taken out of equilibrium with the assemblage.

For a bulk composition of the system below the garnet-chlorite join of Fig. 32a, prior to the replacement of the garnet-chlorite join by the staurolite-biotite join, garnet will grow by the reaction



as discussed in Fig. 20. However, due to the zoning and effective removal from the system of garnet, the effective composition of the system is along the biotite-chlorite join of the gar - bio - chl field (Fig. 32a). Hence, after the replacement of the garnet-chlorite join by the staurolite-biotite join, the effective composition of the system is in the stl - bio - chl field. If the garnet were able to react, the assemblage would be either gar - bio - stl - musc or stl - bio - chl - musc, depending on the initial rock composition; however, if garnet is unreactive the reaction:

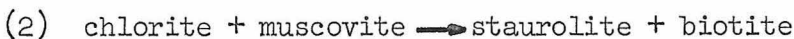


Fig. 32a. Thompson projection showing chl - bio - gar - musc and chl - gar - stl - musc assemblages.

Fig. 32b. Thompson projection at a higher temperature than that of Fig. 32a, showing relations at temperature of breaking of garnet - chlorite tie-line to biotite - staurolite tie-line.

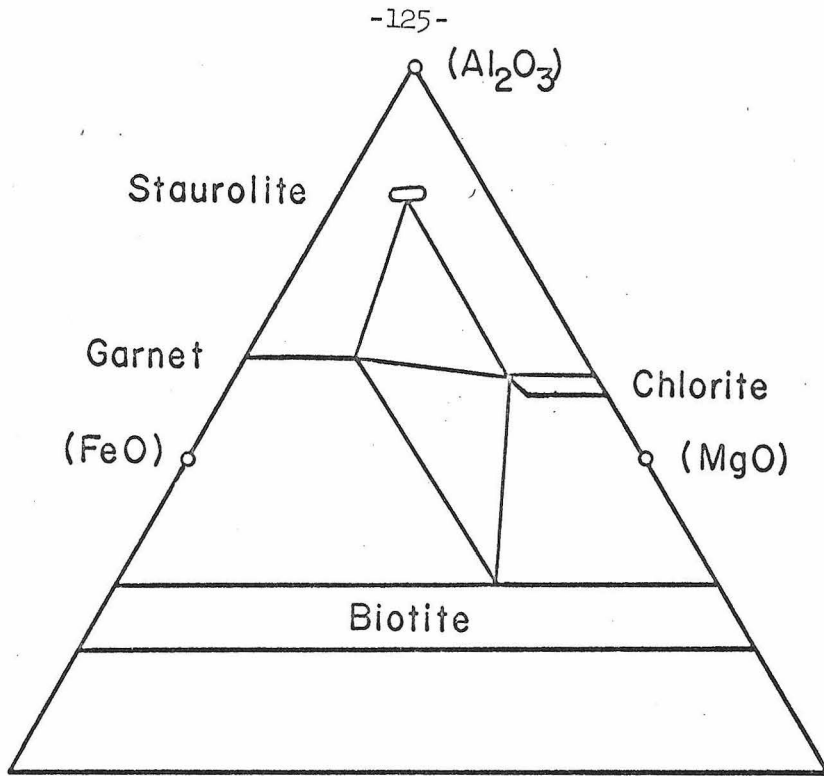


Fig. 32a.

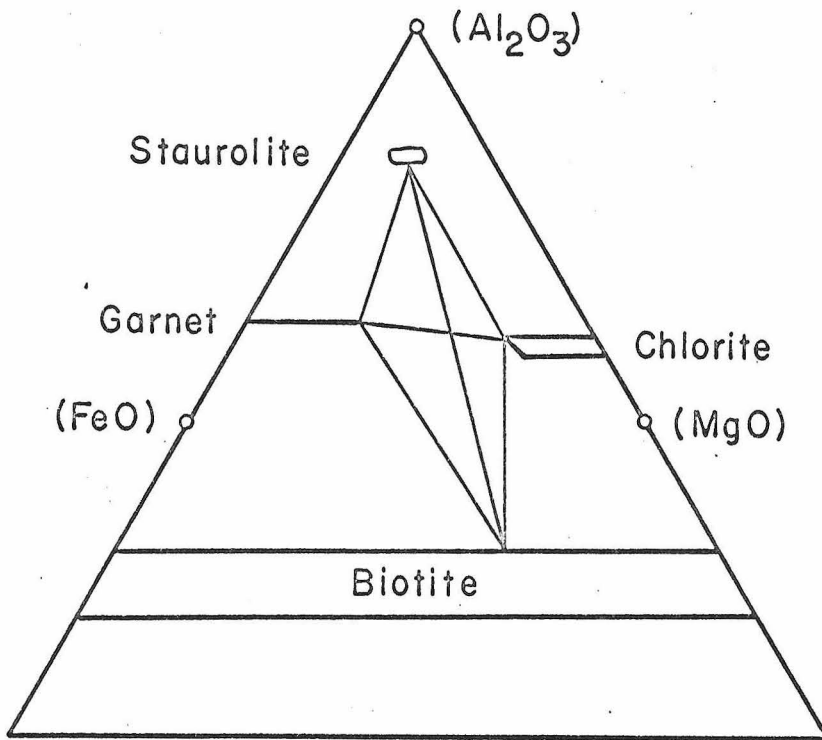


Fig. 32b.

would take the place of reaction (1), with garnet remaining in the assemblage as an inert phase. In this manner the five phases, gar - bio - stl - chl - musc would appear to be in an equilibrium assemblage but with one too many phases (Fig. 32b).

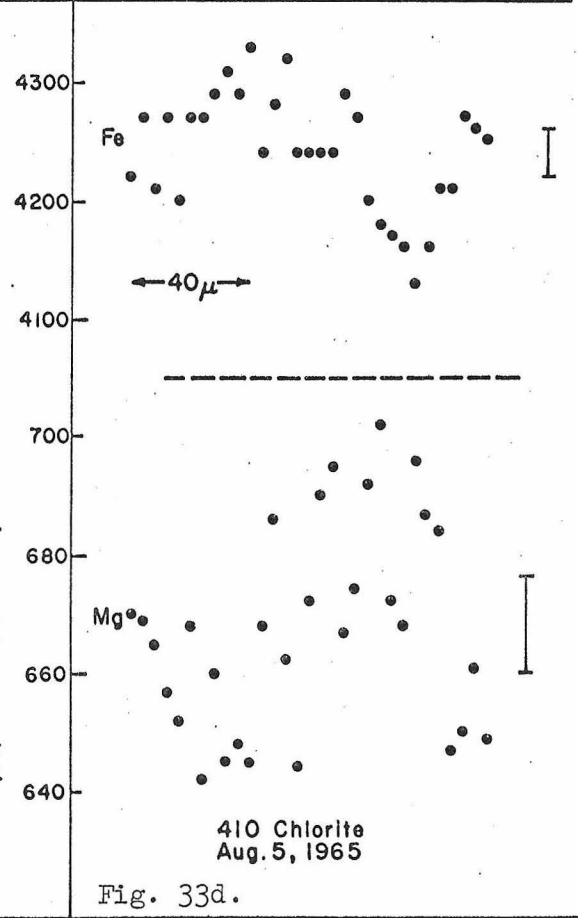
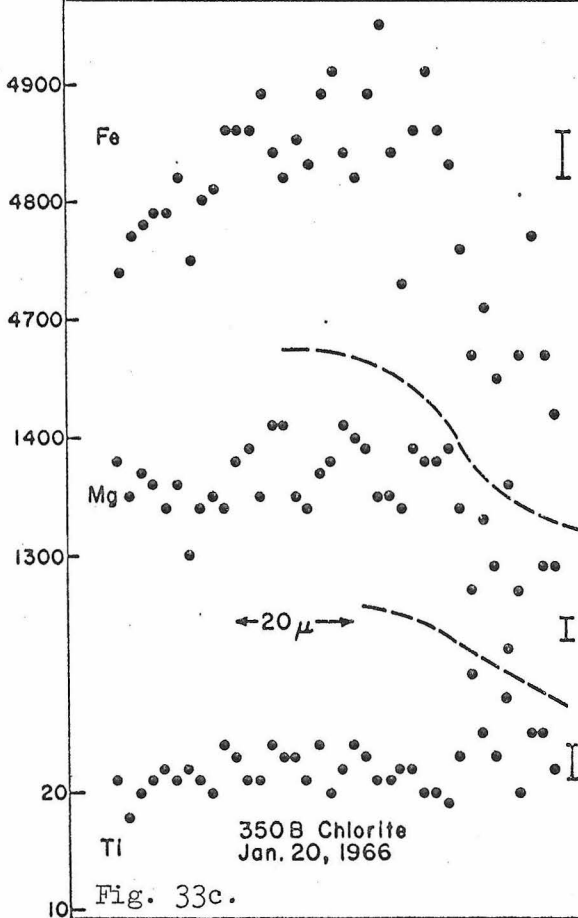
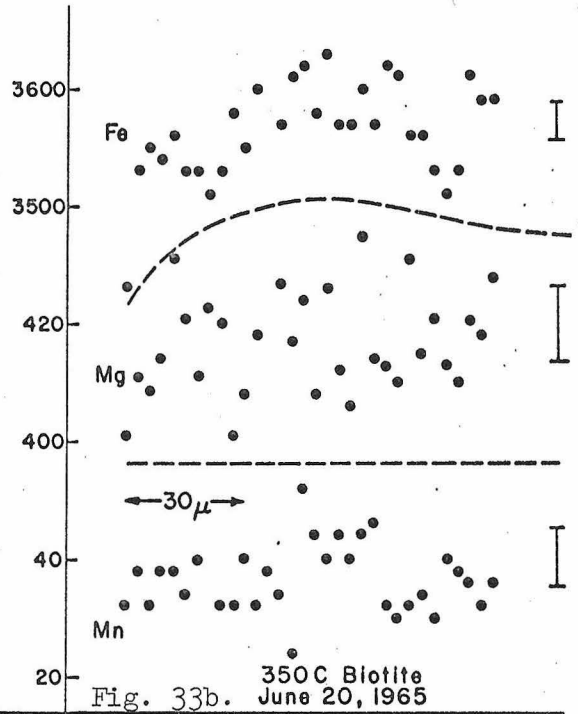
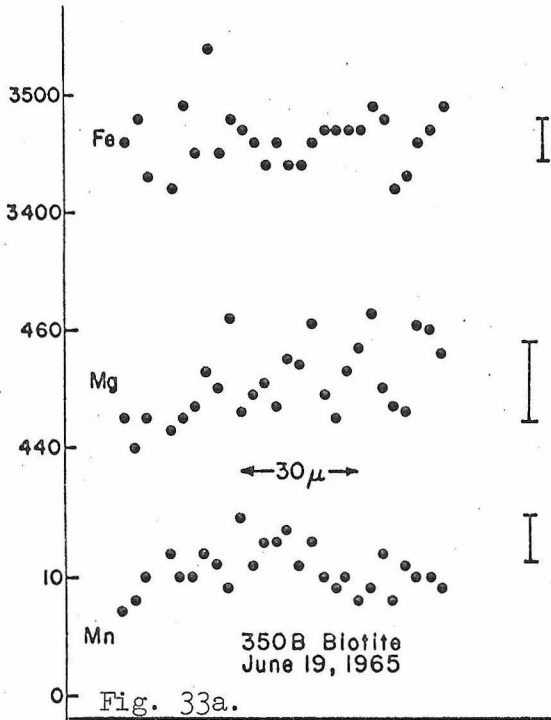
A consequence of this model is that in a region of prograde metamorphism, the garnet-biotite distribution functions would appear to diverge from, rather than approach, one. This would be because the biotite would continue to become more magnesian as reaction (2) progressed, but the garnet composition would remain the same. Also, one should exercise care in the choice of garnet for determining the limiting composition, maximum temperature Mg/Fe ratio. If the garnet were a part of a five-phase assemblage, the limiting composition, maximum temperature Mg/Fe ratio might not be systematic with respect to metamorphic grade.

Biotite and Chlorite

Both biotite and chlorite of the Kwoiek Area exhibit similar characteristics in their compositional variations and can therefore be considered together. The data on biotite are, however, more complete than on chlorite because biotite is much more plentiful in the Kwoiek Area.

Individual grains of biotite and chlorite from the Kwoiek Area are relatively homogeneous. Although traverses across single grains show variations greater than expected from counting rate statistics, the variations are not regular. Figs. 33, 34, 35, 36, and 37 exemplify the variation found in biotite and chlorite. Fig. 33 shows traverses across individual grains and indicates the lack of dramatic zoning like that seen in the garnet. The comparison of the Mn profiles of Figs. 33b and 34 indicates that although the Mn is different in both grains, it is constant across each grain. The biotite of Fig. 33b (350C) coexists with garnet 350C which is homogeneous and has an Mn counting rate of about 1800 c.p.s. The biotite of Fig. 34 coexists with garnet 350B, which has an edge counting rate of about 200 c.p.s. and a center counting rate of about 1800 c.p.s. Both rocks, 350B and 350C, come from the same outcrop. If the center of biotite 350B (Fig. 34) had grown in equilibrium with the associated garnet, it should have an Mn counting rate at its center comparable to that of 350C (Fig. 33b), since biotite 350C coexists with a garnet with a composition similar to the center composition of garnet 350B. As similar

Fig. 33. Profiles for indicated elements across two biotite (Figs. 33a, b) and two chlorite grains (Figs. 33c, d). Mn for biotite is corrected for background. Fifty percent of the points plotted are expected to fall within the ranges indicated by vertical bars by statistical counting rate theory. Scales indicated.



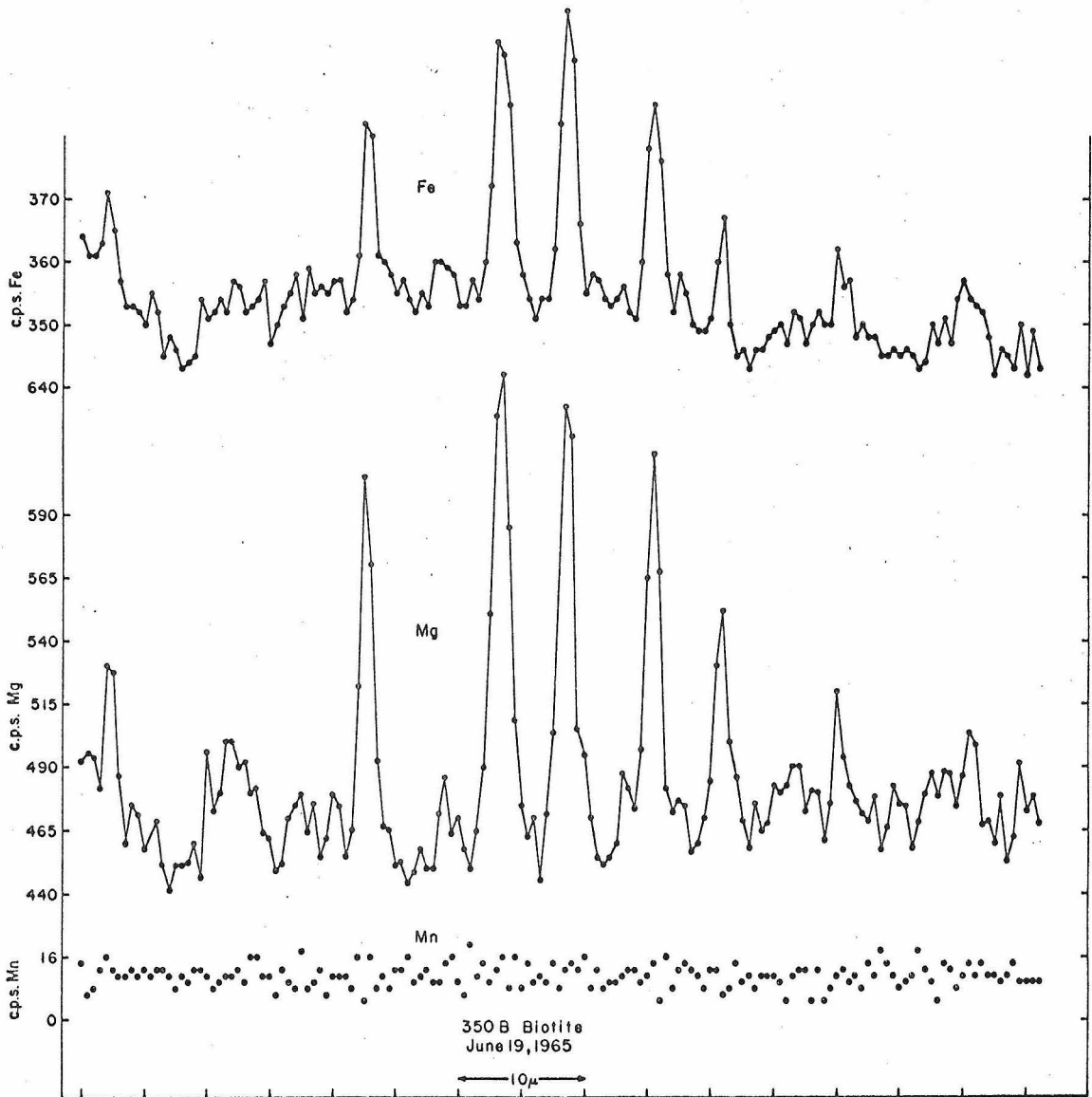


Fig. 34. Mn, Fe, and Mg profiles across a biotite of sample 350B showing effects of chlorite interlayering. Points are at 1 micron intervals. Mn profile is corrected for background.

relationships exist for biotite and chlorite coexisting with garnet in other rocks of the Kwoiek Area, it is concluded that biotite and chlorite continued to reequilibrate in response to changing conditions, in marked contrast to the garnet.

Chlorite interlayers in biotite are common, but the reverse is not true. Figure 34 shows Fe and Mg, as well as Mn, profiles across a large biotite grain of sample 350B, perpendicular to the cleavage. The analyzed spots are 1 micron apart, and the analyzed spot diameter is 2 microns. It is apparent that there is a mineral interlayered with biotite with a much higher Fe and Mg content than biotite. Chlorite must be the mineral as the Mg and Fe counting rates are similar to those of discreet chlorite grains in sample 350B. The chlorite interlayers in the sample shown in Fig. 34 are about 3 to 4 microns wide. These layers are only resolvable with the high powered objective. In most cases of chlorite interlayering, the layers are thinner than 3 to 4 microns so that the counting rate approaches but seldom reaches the true chlorite counting rate.

Figure 35 shows several typical biotite analyses, represented as plots of Fe against Mg. Each point represents an average of 10 to 15 separate analyses on a single grain. Effects of chlorite interlayering have been accounted for. The reason for the spread of points for each sample is puzzling. In order to better understand the scatter of data, adjacent biotites, but one with the cleavage parallel to the microscope stage (point p on Fig. 35c) and one with cleavage perpendicular to the stage (point c) were analyzed to see if orientation affected the

Fig. 35. Plots of average Fe against average Mg of several biotite grains from each of four samples. Each point represents an average of more than 15 analyses of the type shown in Fig. 33. See text.

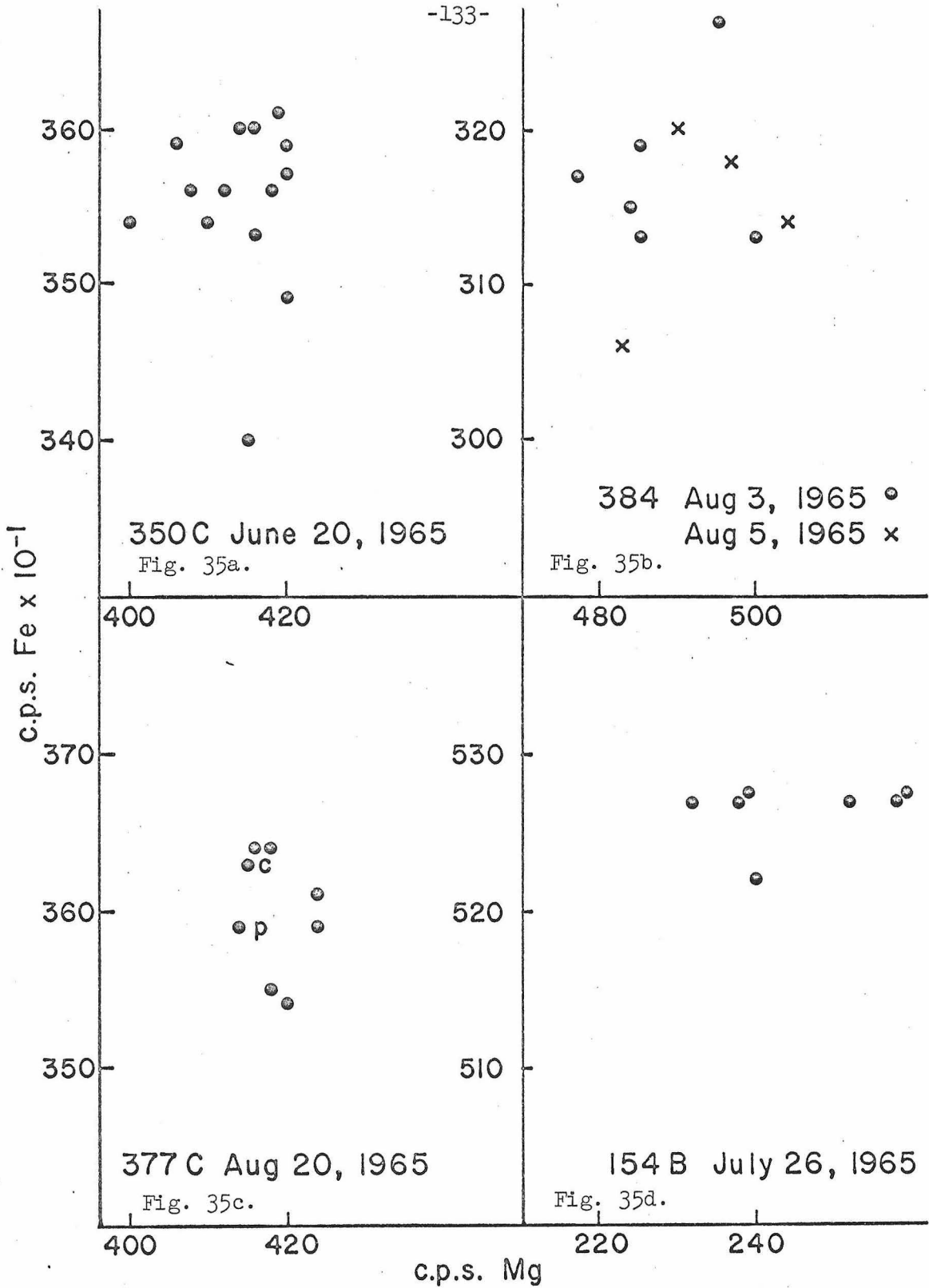


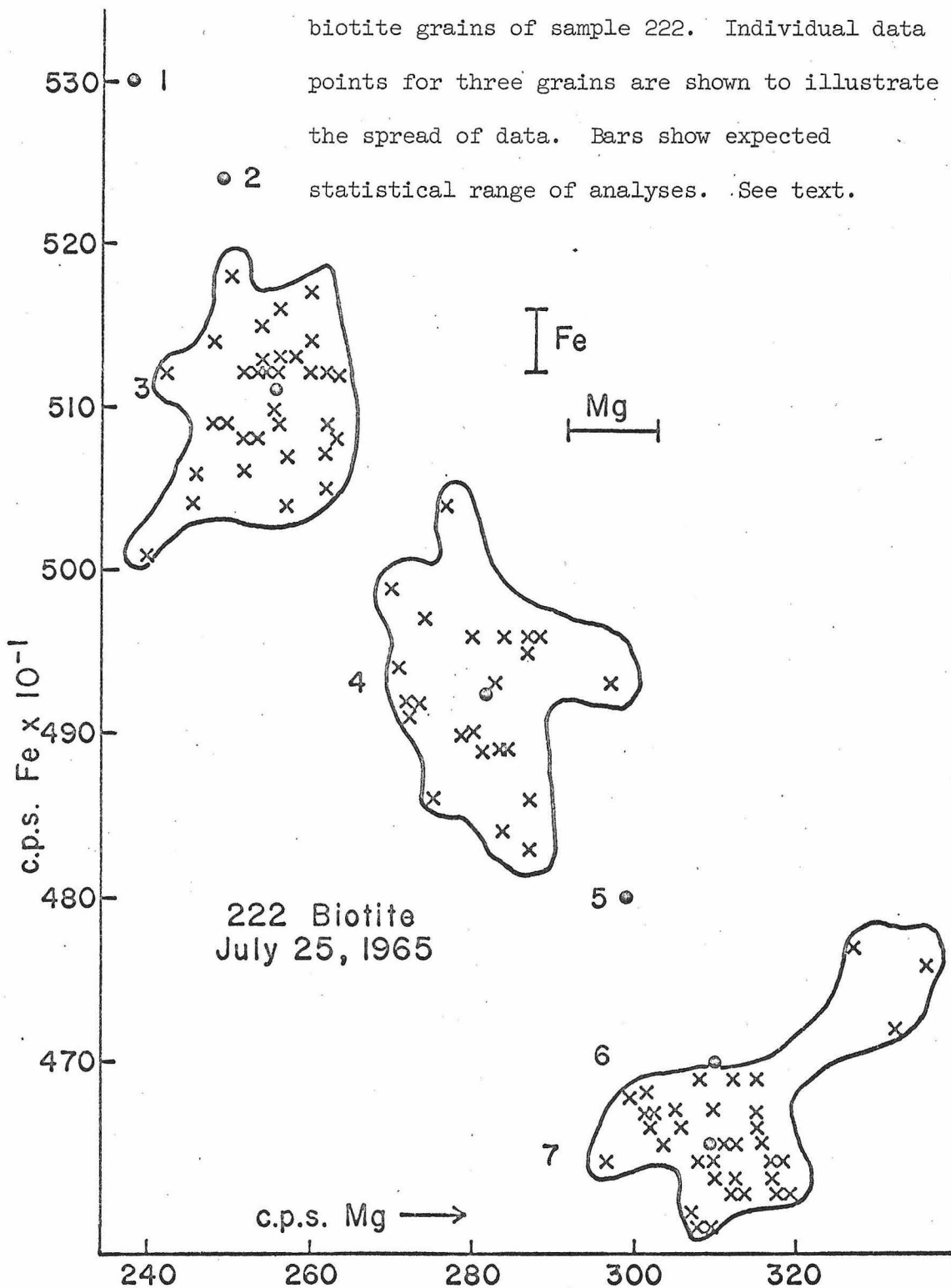
Fig. 35.

counting rates. Point c has about 3 percent higher Fe counting rate than point p. It is concluded that this represents the magnitude of counting rate differences that might be expected for biotite grains of differing orientation. This difference could be explained by a deeper electron penetration in grain c than grain p.

The biotite grain compositions of the samples shown in Fig. 35 are considered to be relatively homogeneous. That is, the average composition of each of the biotite grains does not vary significantly from point to point in a thin section. Figure 35 is to be contrasted with Figs. 36 and 37. Note that the horizontal and vertical scales are the same as for Fig. 35. There is clearly a systematic variation of Mg/Fe ratio from grain to grain; even the individual analyses for each point on a grain, shown for three grains in Fig. 36, do not overlap. The variations are in the direction expected for maintaining atomic balance: The lower the Fe content, the higher the Mg content. The analyses of Fig. 36 were taken from within an area less than 1 millimeter in diameter. Those of the biotites of Fig. 37a (two specimens) and the chlorite of Fig. 35b were taken from within an area 1 inch in diameter. These areas are no greater than those of Fig. 35. The data of Figs. 36 and 37 demonstrate that equilibration of a rock as it is now seen must be on an extremely small scale.

In order to understand these variations of Mg/Fe ratio, carefully located grains of biotite were analyzed from rock 350B. The results of this study are shown in Fig. 38. Analyses 6-13 were made on biotite flakes parallel to bedding foliation, very nearly along the same thin

Fig. 36. Plot of average Fe against average Mg for seven biotite grains of sample 222. Individual data points for three grains are shown to illustrate the spread of data. Bars show expected statistical range of analyses. See text.



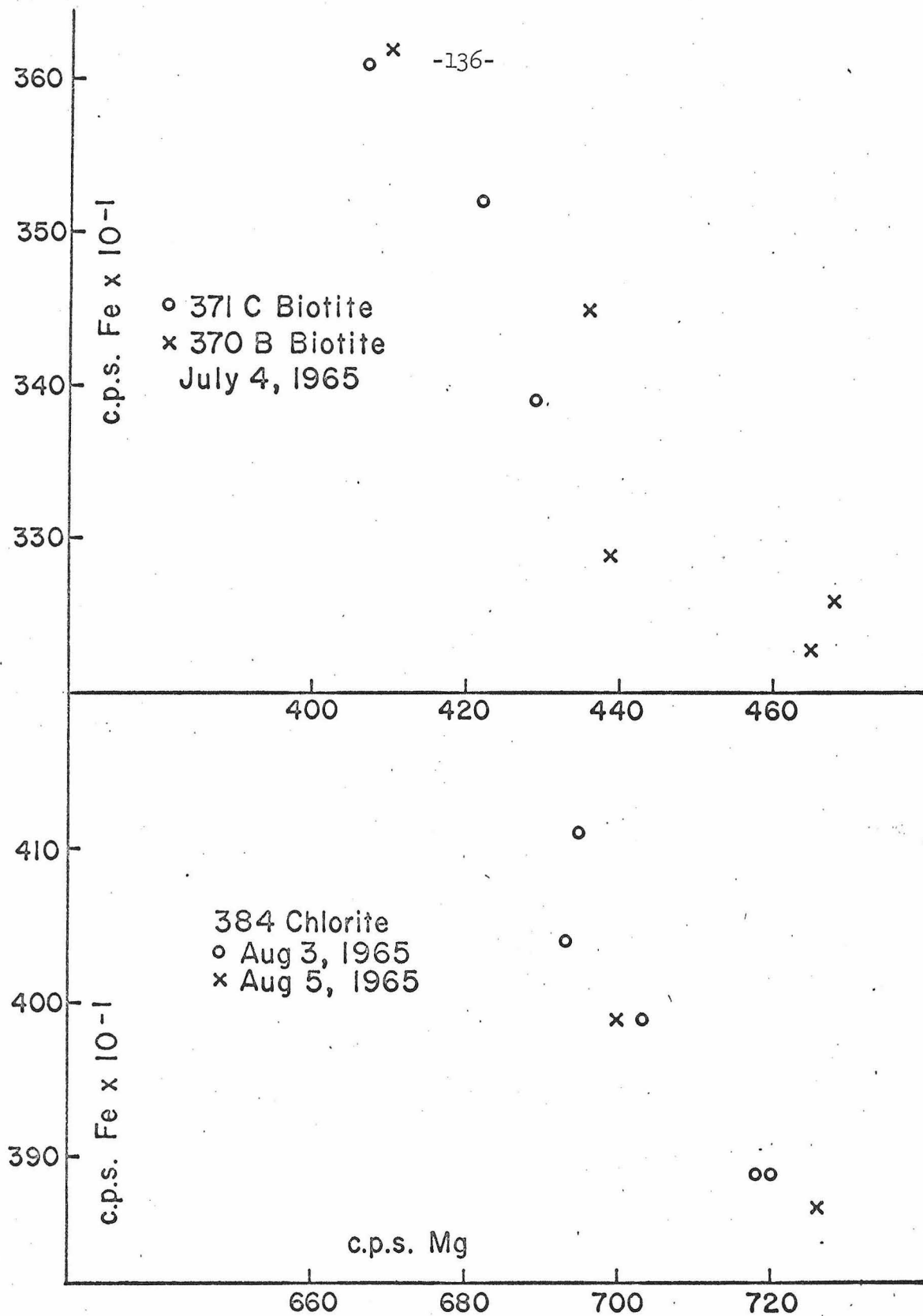


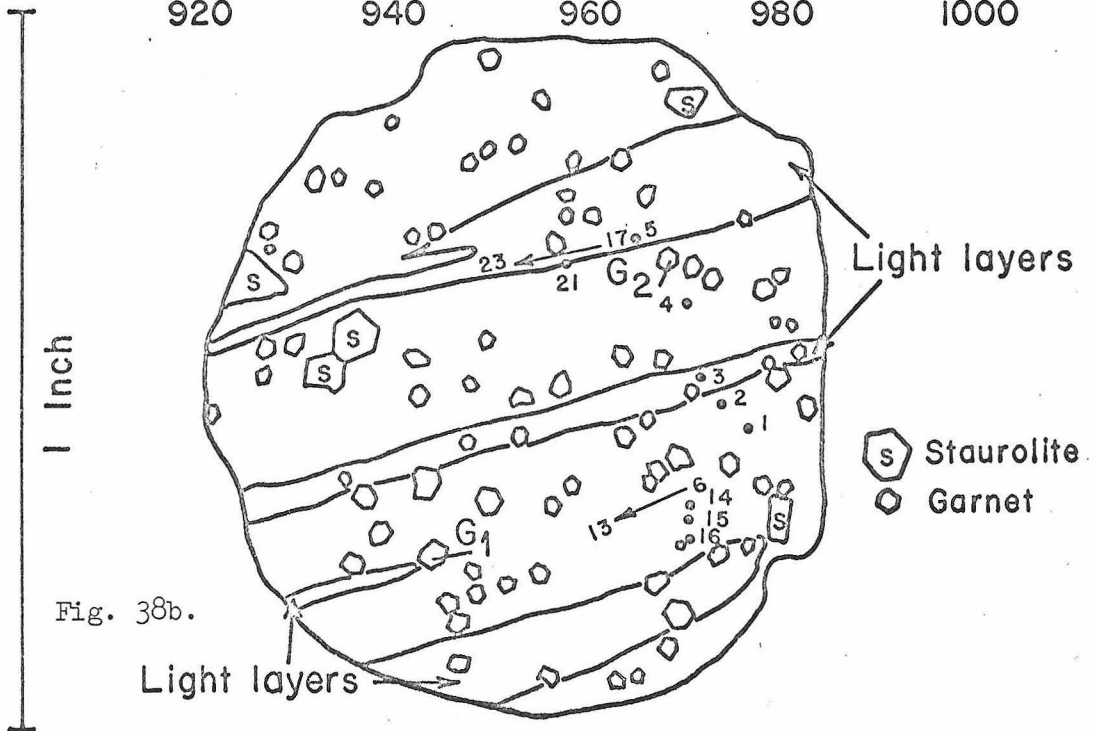
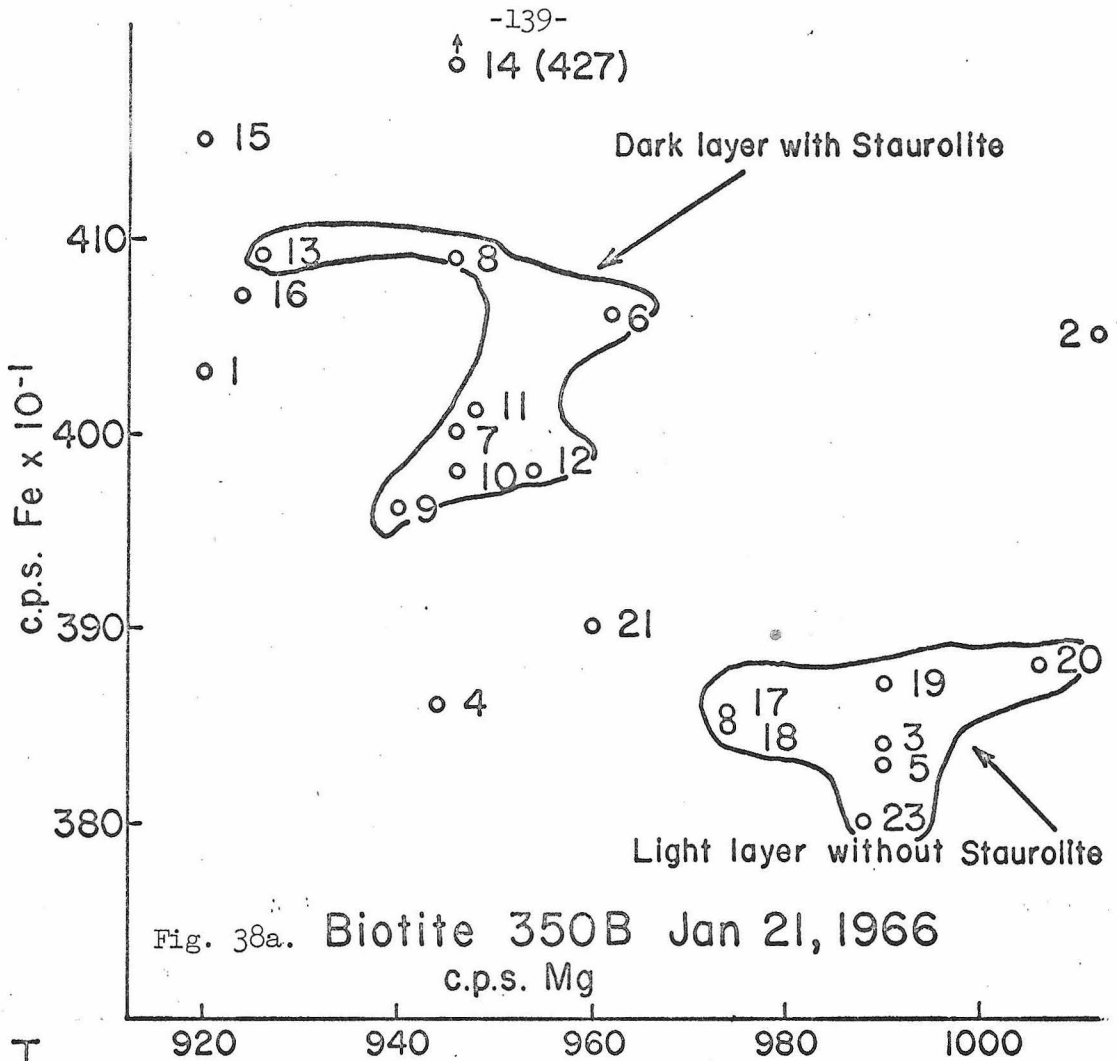
Fig. 37. Plot of average Fe against average Mg for several biotite and chlorite grains from each of three samples.

plane, of a dark bed of the thinly bedded greywacke. Analyses 5, 17-20, and 23 were made along a thin region within a light layer. The analyses from the dark layer, which contains staurolite as well as garnet and chlorite, plot in one "homogeneous" group with a lower Mg/Fe ratio than the "homogeneous" group from the light layer. Analysis 3, in a different light layer, also plots with the light layer analyses. Analysis 21, on the edge between a light and dark layer, plots between the dark layer and light layer analyses. The other analyses, 1, 2, 4, 14, 15, and 16, taken from scattered points around the thin section, but in dark layers, are irregular with respect to the other data.

The variations of biotite composition may or may not be significant for purposes of understanding the scale of equilibrium at the maximum temperature of metamorphism. The garnet data already suggest a tendency for the minerals of an assemblage to reequilibrate with decreasing temperatures. If the garnet grew during decreasing temperature, the biotite and chlorite must have reequilibrated with the edge composition of the garnet because they are involved in the reaction making the garnet. It does not seem unreasonable, then, to expect the volume over which equilibrium is attained to decrease with decreasing temperature until the scale of equilibrium is only a few microns. At the end of metamorphic recrystallization, a biotite or chlorite adjacent to a garnet might be in equilibrium with that garnet but not with a staurolite, or other minerals, 20 microns or so away. However, a biotite next to that staurolite might have been in equilibrium with it

Fig. 38a. Plot of average Fe against average Mg for 23 biotite grains from sample 350B. The two groups of points are from the dark and light thin beds of the greywacke.

Fig. 38b. Locations of the analyses of Fig. 38a are shown on a sketch of the thin section. The light layers are indicated as are the locations of staurolite and garnet porphyroblasts. G_1 is the garnet of Fig. 15b; G_2 is the garnet of Fig. 16.



when recrystallization ceased but would have a different composition than the biotite next to the garnet.

Biotite compositions may be closer to one another along individual thin laminae due to similar permeability, porosity, and local composition along all points within each lamina.

The narrow spread of data of maximum temperature composition of garnet from different points in a thin section (see Fig. 28) is strong support for the idea that the area of equilibration at maximum temperature was at least the size of a thin section with the same assemblage throughout. The spread of the limiting composition, maximum temperature Mg/Fe ratios of the garnet is only about 5 percent in spite of the difficulties of picking the maximum temperature horizon and in spite of the low Mg counting rate of garnet; whereas the spread of biotite compositions in Fig. 38 is about 10 percent.

The tentative conclusion, then, is that the rock as it is presently seen has smaller regions of equilibrium, representing the last stages of recrystallization during declining temperature, than it had at the thermal maximum. This assumes that the biotite of Figs. 36, 37, and 38 once had a more homogeneous composition at the peak of metamorphism than they do now, to be consistent with the concept of an invariant assemblage at constant P, T, $a_{\text{H}_2\text{O}}$, and Mn content.

Regardless of the variation of the biotite composition within single thin sections, it is instructive to compare biotite data and garnet data with the relations between biotite and garnet discussed by Albee (1965b). In this paper Albee plotted Mn content in the garnet against the Mg/Fe

Fig. 39. Plot of atom percent $Mn/Mn+Mg+Fe$ in garnet against atom percent $Mg/Mg+Fe$ garnet (open circles) and atom percent $Mg/Mg+Fe$ biotite (closed circles), after Albee (1965b) for the musc - bio - gar - stl assemblage of Phinney (1963).

Fig. 40. Plot of atom percent $Mn/Mn+Mg+Fe$ in garnet against the Mg-Fe distribution function between garnet and biotite. Open circles are the data of Phinney (1963) after Albee (1965b). Closed circles are for the data of the 350 series rocks. See text.

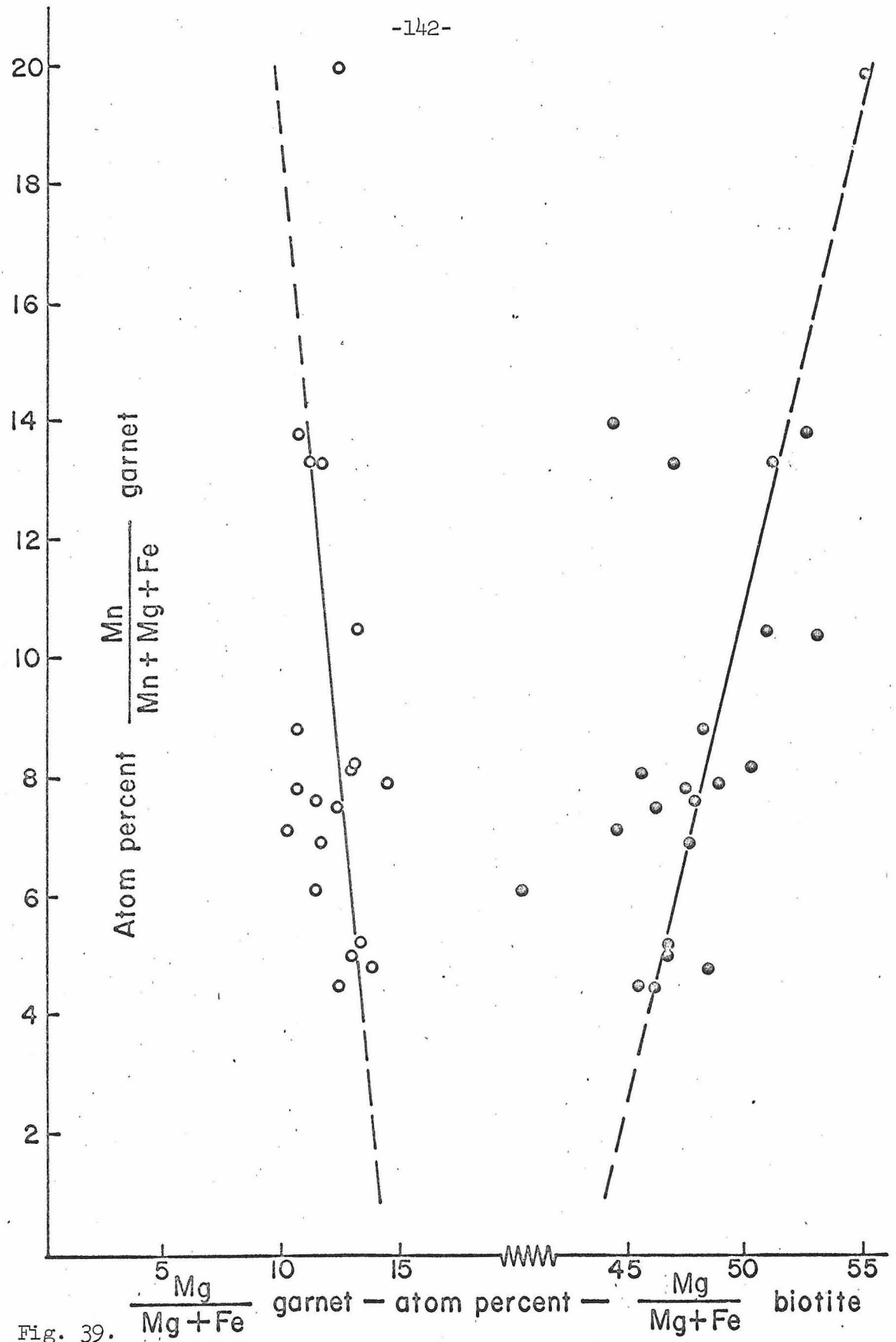


Fig. 39.

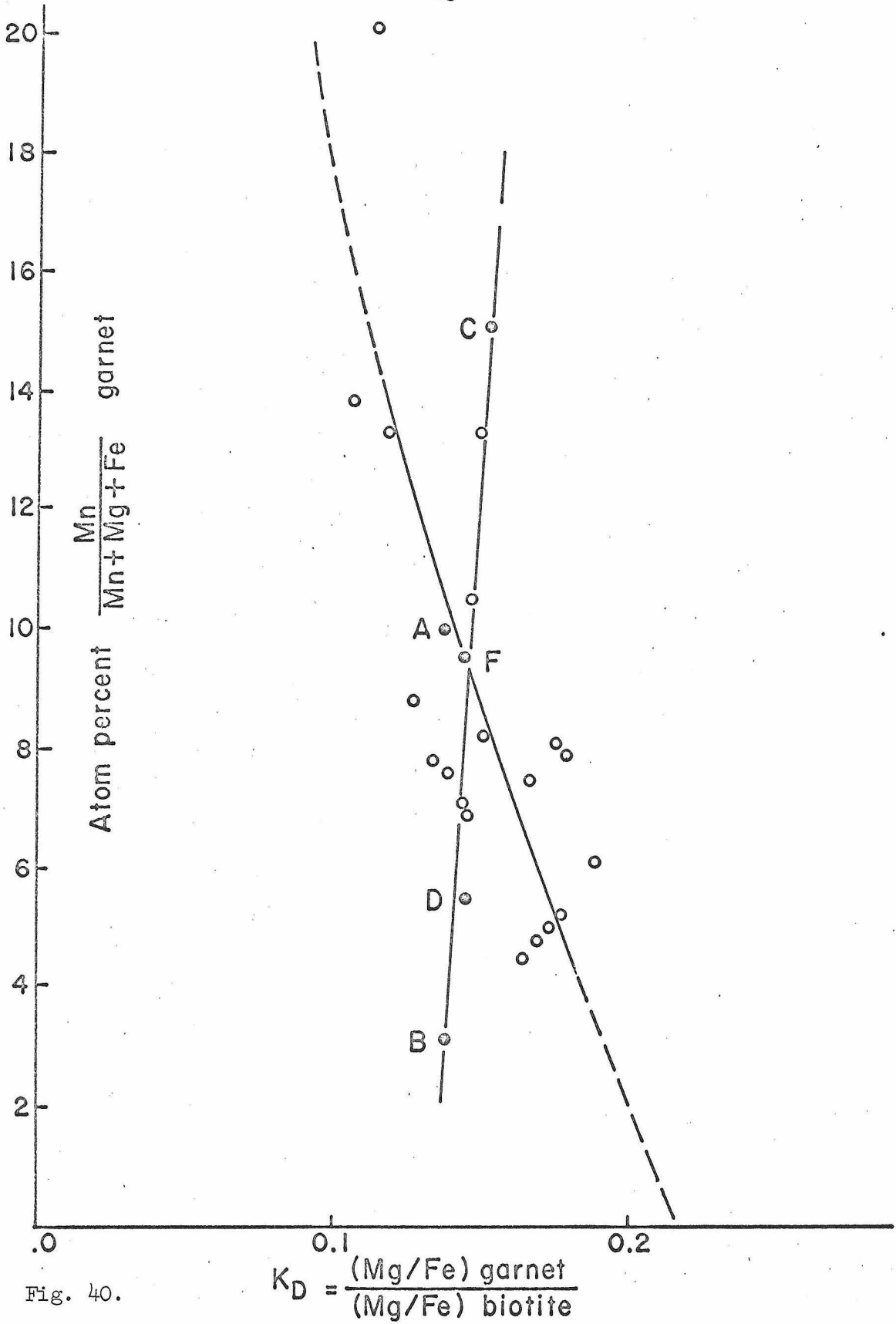


Fig. 40.

ratio in both garnet and biotite (Fig. 1, page 156, reproduced as here as Fig. 39). The Mn, Mg, and Fe were based on bulk chemical analyses from several localities (Phinney, 1963, Green, 1963, Frost, 1962; only the data of Phinney are shown in Fig. 39). Albee showed an inverse relation of Mn in garnet vs. Mg/Fe in garnet and a proportional relation of Mn in garnet vs. Mg/Fe in biotite. The Kwoiek Area garnets are consistent with the garnet data of Fig. 39 as discussed in Fig. 29.

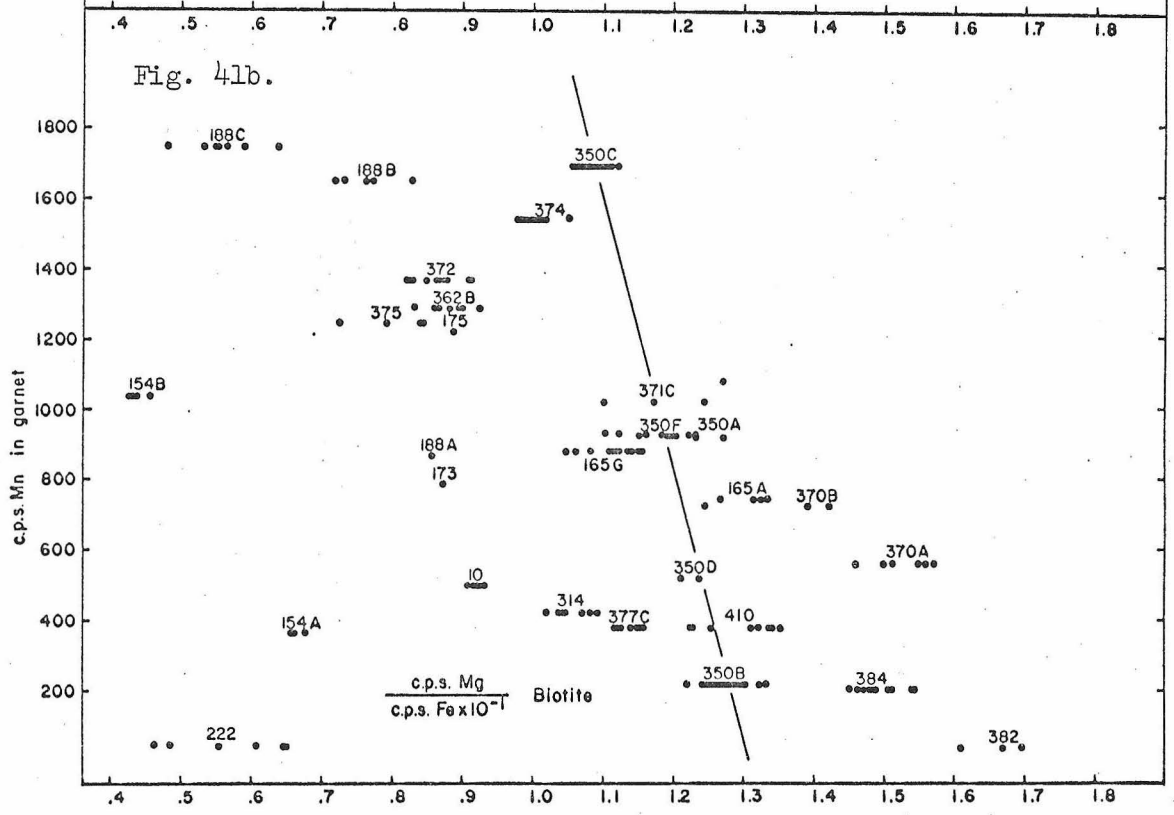
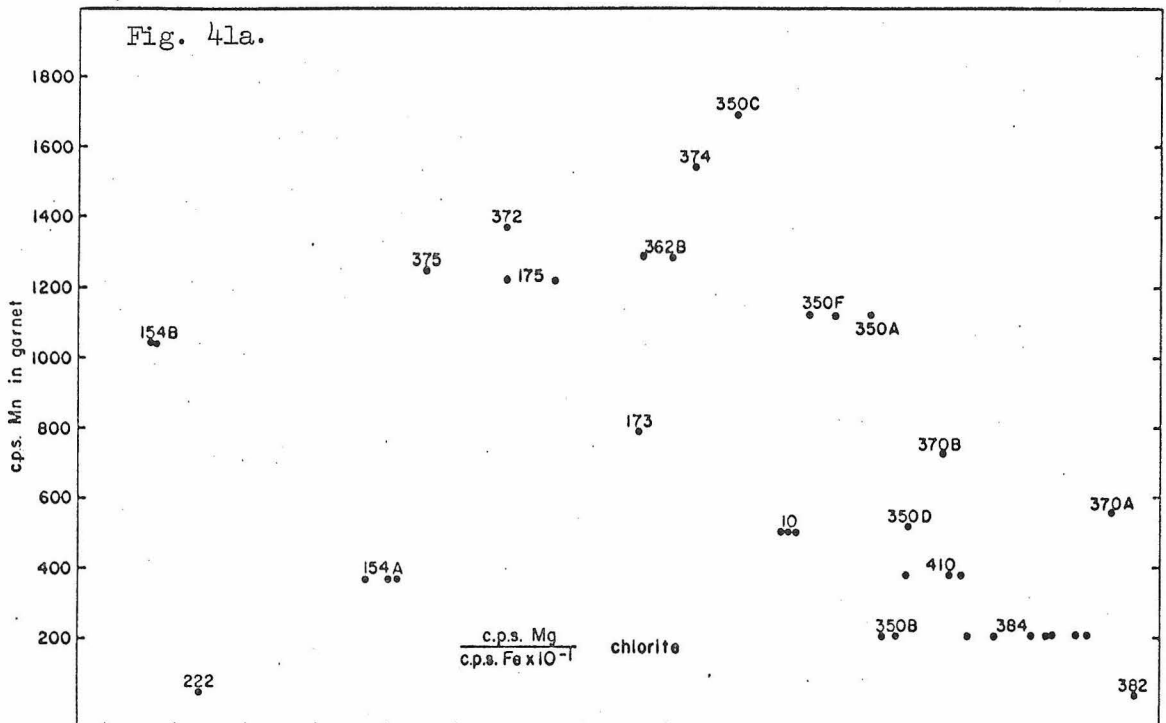
However, Albee shows the Mn_{gar} vs. Mg/Fe_{bio} curve with a different slope than the garnet curve and from this deduces that K_D gar - bio

($K_D \equiv (Mg/Fe)_{gar} / (Mg/Fe_{bio})$) is dependent on Mn content in the garnet.

This relation is partially reproduced here in Fig. 40.

Albee's biotite curve is not consistent with the data from the Kwoiek Area. Analyses of the biotites from the 350 series samples suggest an inverse relation of Mn_{gar} to Mg/Fe biotite (Fig. 41b), though complicated by the local variations of biotite composition within the thin section. Even though the biotite is presumed to have reequilibrated during retrogression, the fact that the biotite and the chlorite cannot "recover" elements lost to the garnet and staurolite indicates that the biotite and chlorite compositions could not have changed drastically. Therefore, the trend shown by the line through the 350 series biotite in Fig. 41b is very likely close to the real trend at the time of maximum temperature. The data of the 350 series samples, in terms of the counting rate distribution function and atomic percent (Mg/Mg+Fe+Mn) garnet, are also shown on Fig. 40 to emphasize the different trends. The counting rate K_D and atomic K_D differ by a small, nearly constant

Fig. 41. Plot of the Mn content of garnet in the maximum temperature horizon against the Mg/Fe ratio of coexisting chlorite (Fig. 41a) and biotite (Fig. 41b) for the rocks of the Kwoiek Area. Line on Fig. 41b is visually fitted to biotite data of the 350 series rocks.



amount. It is noteworthy that using Kretz's data for hornblende assemblages (Albee, 1965b, Fig. 4), one could draw a best fit curve through the biotite data with an inverse slope. It is probable that the dependence of K_D gar - bio upon Mn_{gar} is less than suggested by Albee (1965b), but the evidence does not yet rule out a smaller dependency.

Although the biotite and chlorite probably reequilibrated at lower than the maximum temperature reached by the rock, biotite and chlorite compositions vary systematically with metamorphic grade. The averages of the biotite and chlorite are plotted against garnet maximum temperature horizon Mn content in Fig. 41. The distribution functions between biotite and chlorite, on the other hand, are plotted graphically in Fig. 42, showing there is little systematic relation of K_D bio - chl with metamorphic grade. In fact, all the points cluster along a single value of $K_D = 0.85$, indicating either that the biotite and chlorite reequilibrated with one another to the same temperature during retrogression or that K_D bio - chl is very insensitive to temperature changes. Comparison of Fig. 41 with Fig. 31 shows that the higher values of Mg/Fe in both biotite and chlorite are generally found in the higher grade rocks, but the relation is not as systematic as for the garnet, probably due to reequilibration during decreasing temperature.

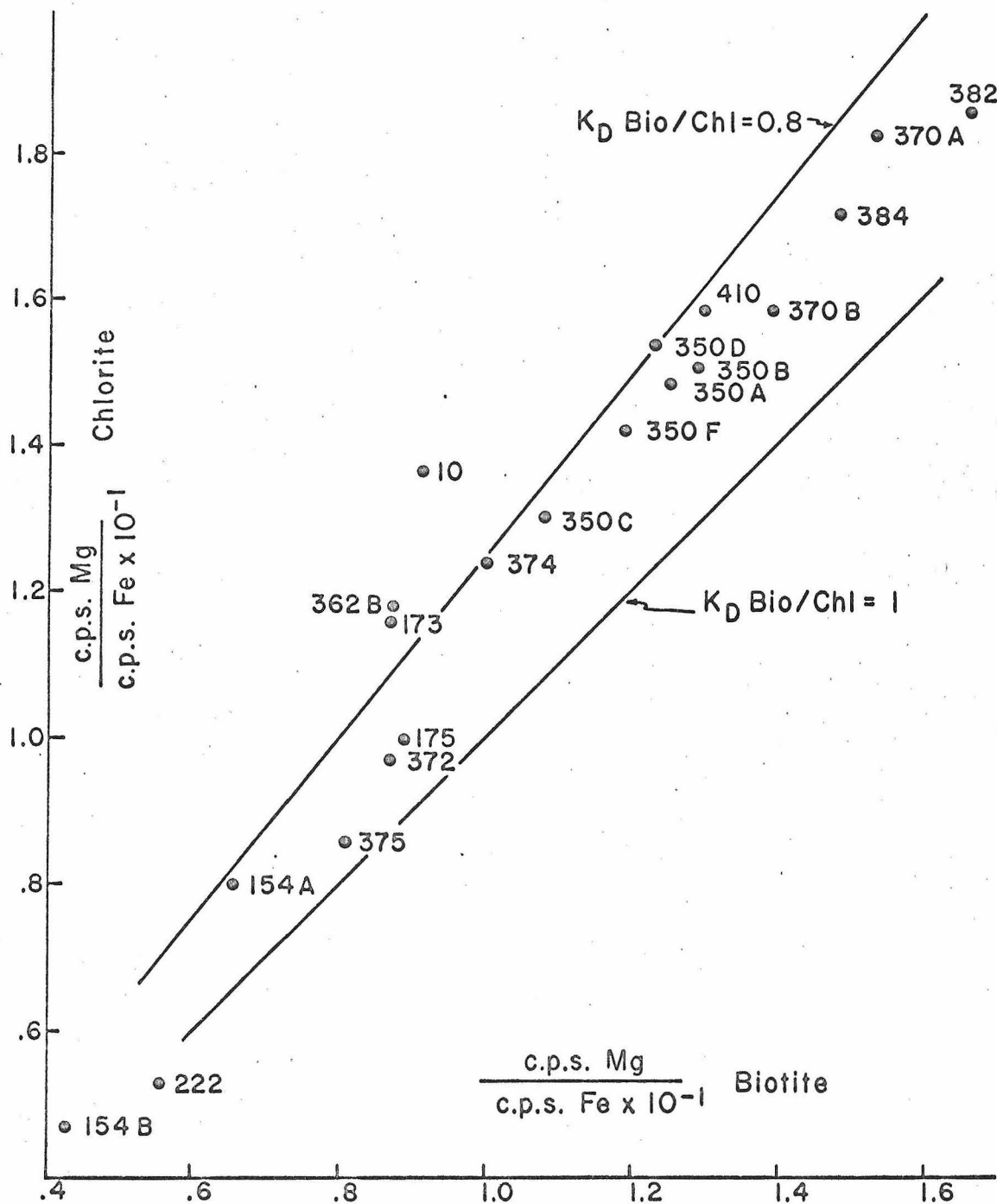


Fig. 42. Plot of Mg/Fe ratio in chlorite against the Mg/Fe ratio of coexisting biotite for the rocks of the Kwoiek Area. Two lines of constant Mg-Fe distribution between chlorite and biotite are shown for reference. High Mg/Fe values of both chlorite and biotite represent generally higher grade than low Mg/Fe values.

Staurolite

The staurolite in the Kwoiek Area is zoned, but most porphyroblasts of staurolite do not show the continuous zoning curves like garnet. The staurolite zoning profiles clearly fall into two types (Figs. 43 and 44). These two types can be correlated with two different assemblages and two different reaction sequences during growth. The type shown in Fig. 43, which shows discontinuous zoning in most elements, occurs in the assemblage stl - chl - gar - bio - ilm - graph. That shown in Fig. 44, although showing the same general features, does not have a discontinuous Ti zoning profile; it occurs in the assemblage stl - musc - gar - bio - ilm - graph.

The discontinuous zoning shown in Fig. 43 has both mineralogic and petrologic significance. It offers a clue as to the type of coupled substitutions that take place in the staurolite formula, a phenomenon not well understood; and it suggests the possibility of an abrupt change in the metamorphic reaction which is producing the staurolite. The contrast between the homogeneity of the central region and the zoned outer region of the staurolite may offer clues as to the thermal history of the staurolite.

The zoning pattern of Fig. 43 indicates that the substitutions involved are not Ti for Al and Al for Si. In fact, an increase of Ti marks a decrease of Al and an increase of Si rather than the expected constant Al and decrease of Si. In order to clarify this problem, four total analyses were made on one staurolite grain for all elements except

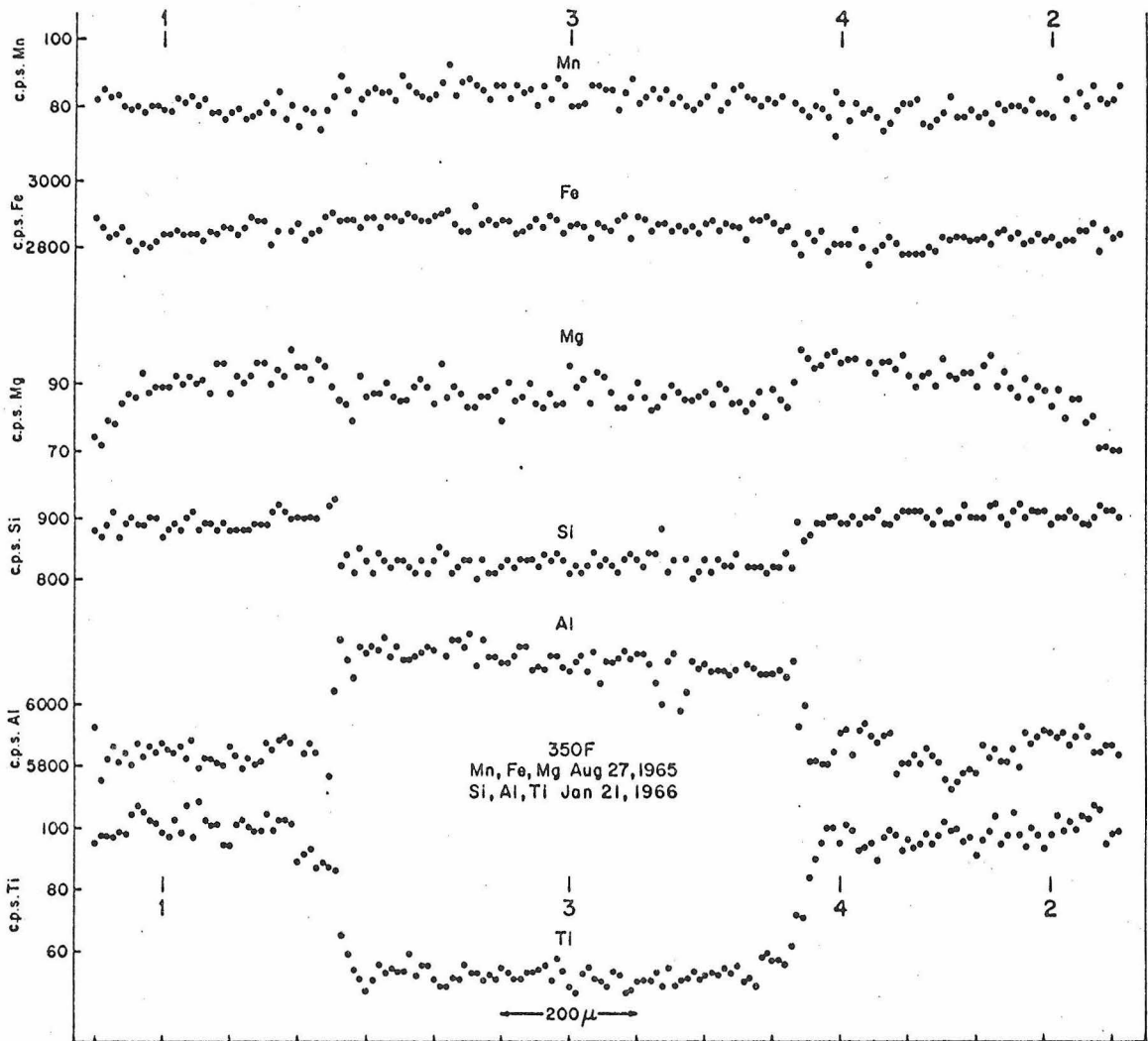


Fig. 43. Mn, Fe, Mg, Si, Al, and Ti profiles across a staurolite of sample 350F (chl - gar - bio - stl assemblage).

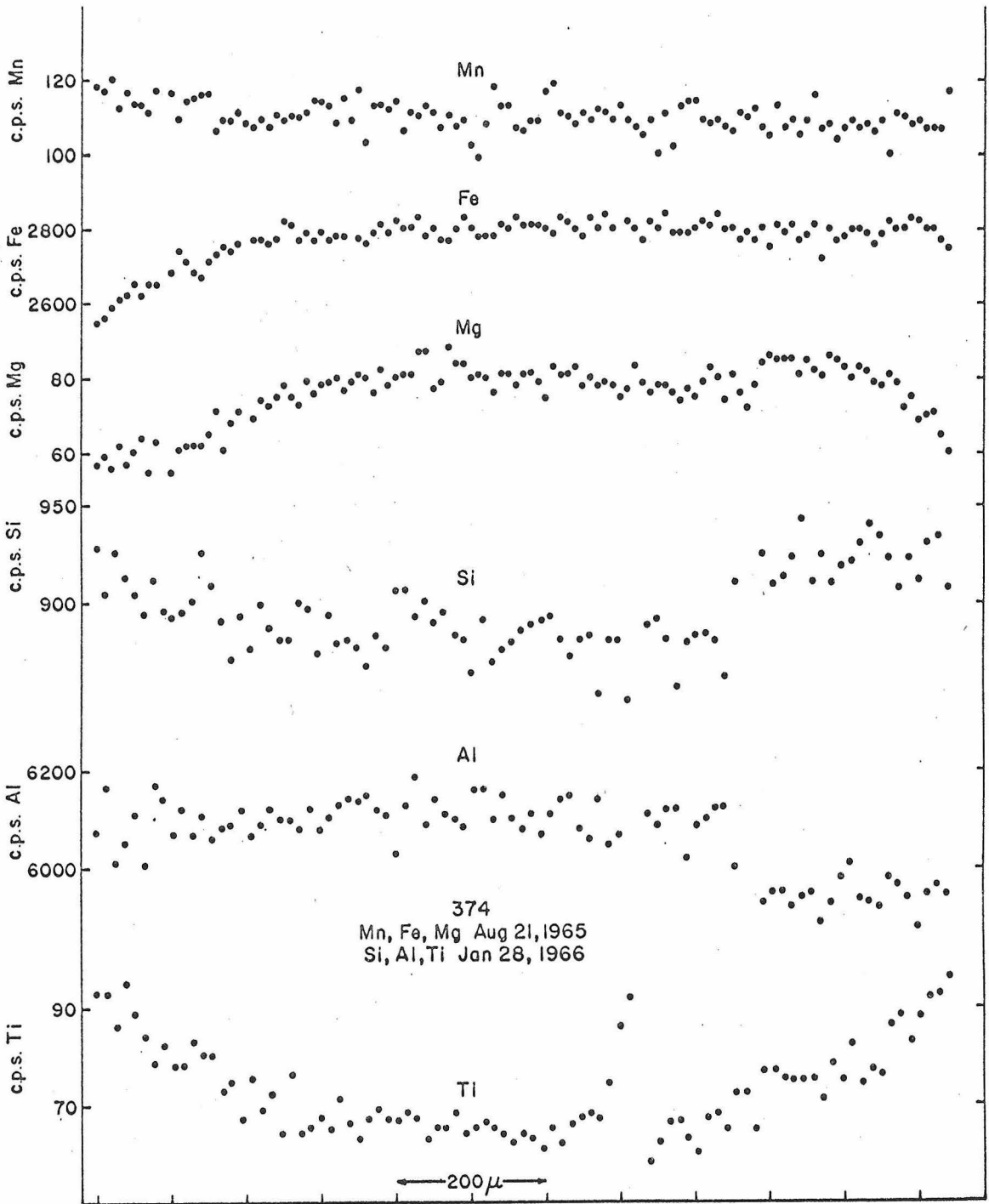


Fig. 44. Mn, Fe, Mg, Si, Al, and Ti profiles across a staurolite of sample 374 (musc - gar - bio - stl assemblage).

hydrogen (indicated as 1, 2, 3, and 4 on Fig. 43). These analyses and formulas, based on a normalization to 30 cations, are tabulated in Table 12. The formulas indicate that no substitution takes place in the Al position and that all substitution is in the (Fe,Mg) and Si positions. In the outer zone of the staurolite grain the 48 oxygens of the unit cell with a negative charge of 96 can be nearly balanced by two protons which, according to Naray-Szabo and Sasvari (1958), is the likely number of protons in the staurolite unit cell. In the central zone, 2.6 protons are necessary to balance the charge. Alternatively, assuming that the number of protons is constant in the staurolite formula, the charge would be balanced by changing 0.6 Fe⁺² atoms to Fe⁺³.

Although the analyses are not precise due to uncertainties in the calibration curves (Appendix) and due to the impossibility of determining H₂O and Fe⁺³ with the microprobe, they should be accurate relative to one another. Hence, the coupled substitution from the central to the outer zone can be described as either Ti⁺⁴ for (Fe,Mg)⁺², Si⁺⁴ for Al⁺³, and H⁺ leaving the structure, or Ti⁺⁴ for (Fe,Mg)⁺², Si⁺⁴ for Al⁺³, and Fe⁺³ → Fe⁺².

Independent evidence supports the Fe⁺³ → Fe⁺² hypothesis. If the staurolite shows a discontinuous zonation due to the reduction of iron, then the total assemblage must show a corresponding effect. Such an effect is suggested by the Al and Ti profiles of the garnet from outcrop 350 (Fig. 15). A discussion of the Al and Ti garnet zoning profiles has been given. The small, sharp increase in Al and Ti content

Table 12

Total Analyses of Four Horizons in Staurolite 350F

	1	2	3	4
SiO ₂	27.1	27.5	25.2	27.3
TiO ₂	.7	.69	.34	.65
Al ₂ O ₃	53.2	54.0	56.0	53.5
FeO	11.9	11.9	12.1	11.7
MnO	.15	.15	.15	.15
MgO	2.32	2.20	2.22	2.50
Total	95.37	96.44	96.01	95.80

	Formulas	(+) charge (excluding proton)
1.	$(\text{Mg}_{1.00}\text{Fe}^{+2}_{2.87}\text{Mn}_{.04}\text{Ti}_{.15})_{4.06}\text{Al}_{18}(\text{Si}_{7.83}\text{Al}_{.11})_{7.94}\text{O}_{48}\text{H}_2$	94.1
2.	$(\text{Mg}_{.94}\text{Fe}^{+2}_{2.84}\text{Mn}_{.04}\text{Ti}_{.15})_{3.97}\text{Al}_{18}(\text{Si}_{7.86}\text{Al}_{.19})_{8.05}\text{O}_{48}\text{H}_2$	94.3
3.	$(\text{Mg}_{.95}\text{Fe}^{+2}_{2.28}\text{Mn}_{.04}\text{Ti}_{.07}\text{Fe}^{+3}_{.6})_{3.94}\text{Al}_{18}(\text{Si}_{7.20}\text{Al}_{.86})_{8.06}\text{O}_{48}\text{H}_2$	94.0
4.	$(\text{Mg}_{1.07}\text{Fe}^{+2}_{2.81}\text{Mn}_{.04}\text{Ti}_{.14})_{4.06}\text{Al}_{18}(\text{Si}_{7.84}\text{Al}_{.11})_{7.96}\text{O}_{48}\text{H}_2$	94.1

The analyses are in weight percent and were made at the points marked 1, 2, 3, and 4 on Fig. 43. Formulas calculated on the basis of 30 cations to the unit cell.

outward from the center in some of the garnet of Fig. 15 is interpreted as having occurred at the same time that the discontinuous zoning changes of the staurolite took place. The Al increase would be expected if the rock were reduced during growth of the garnet because Fe^{+3} substitutes in the Al position. Since the result predicted in the garnet from the $\text{Fe}^{+3} \longrightarrow \text{Fe}^{+2}$ transition in the staurolite is seen, this transition is taken as more likely than the alternate method of maintaining atomic charge balance in the staurolite, that of moving protons out of the structure.

The lack of zoning in the central region of the staurolite (Figs. 43 and 44) can be interpreted by the Rayleigh depletion model using the following observations: (1) λ_{Fe} between staurolite and biotite is close to 1, (2) W^S/W^0 for the central zone is generally small (W^S = total weight of staurolite), (3) By analogy to Fig. 18 zoning due to Mg would not be pronounced until the staurolite was quite large since λ_{Mg} between staurolite and biotite is nearly the same as λ_{Mg} between garnet and biotite, and (4) there is no major element for which staurolite has a large affinity, such as garnet has for Mn. Therefore, according to the Rayleigh depletion model, zoning would not be expected in a staurolite if the λ 's were constant. If temperature changed, the λ 's would also change, producing zoning in the staurolite.

The interpretation of the growth history of the central region of the staurolite of Figs. 43 and 44 is consistent with the reaction which makes this portion of the staurolite being an invariant reaction

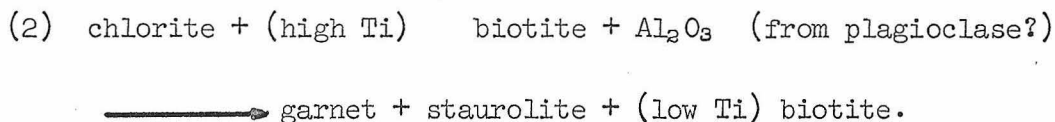
(Part III). The reaction takes place at constant temperature, if other variables are fixed. The reaction discussed in Part III was



Since empirically the maximum number of phases one can have in the $\text{Al}_2\text{O}_3 - \text{K}_2\text{O} - \text{FeO} - \text{MgO}$ tetrahedron is four, reaction (1) must take place at constant temperature until either chlorite or muscovite disappears, because reaction (1) involves five phases.

Since the Rayleigh depletion model does not predict zoning in the staurolite unless the fractionation factors change, the zoning in the outer parts of the staurolite must be due to changing fractionation factors, probably influenced by changing temperature. The temperature must be rising since the discontinuous change in the staurolite zoning profile of Fig. 43 is correlated with Al and Ti zoning changes in the coexistent garnet which are located well to the garnet center from the horizon where the temperature began decreasing.

The reaction making the staurolite of the outer zone of Fig. 43 was discussed in Part III and is inferred to be



Analytical work on the biotite shows 10 percent lower Ti on the right side of equation (2) than on the left, but the Al content of the chlorite and biotite does not drop. Therefore, an external source of Al_2O_3 was

needed which may have come from coexistent plagioclase. The calcium would go into the garnet.

The Mg/Fe ratio in the zoned part of the staurolite decreases outward indicating that in a single grain the Mg/Fe ratio decreases with increasing temperature. This is contrary to garnet, biotite, and chlorite, where the Mg/Fe ratio increases with metamorphic grade.

The average Mg/Fe ratio of individual staurolite grains from a range of metamorphic grade is plotted against the maximum temperature Mg/Fe ratio of coexistent garnet in Fig. 45. The vertical, or garnet, axis is a function of metamorphic grade as discussed in Fig. 30. The average Mg/Fe staurolite ratio does not show a consistent relation with metamorphic grade as shown by the arrows. The arrows are in the direction of increasing metamorphic grade between staurolite-garnet pairs. The long sequence of arrows, from 362B to 371C to 370B and to 410 shows increasing average Mg/Fe in staurolite to 370B, and then decreasing Mg/Fe to 410. The other two, shorter arrows show decreasing Mg/Fe in staurolite with increasing metamorphic grade. For all arrows, the trend is in the direction of K_D stl - gar approaching one, as indicated by two reference lines of constant K_D .

There is too much scatter of data and too few specimens to establish conclusive trends. For example, the four staurolite averages of 370A cover about 50 percent of the total staurolite variation. The staurolite from the five rocks of outcrop 350, with the same assemblage, also have a staurolite variation of nearly 50 percent of the total staurolite variation. If it were not for the

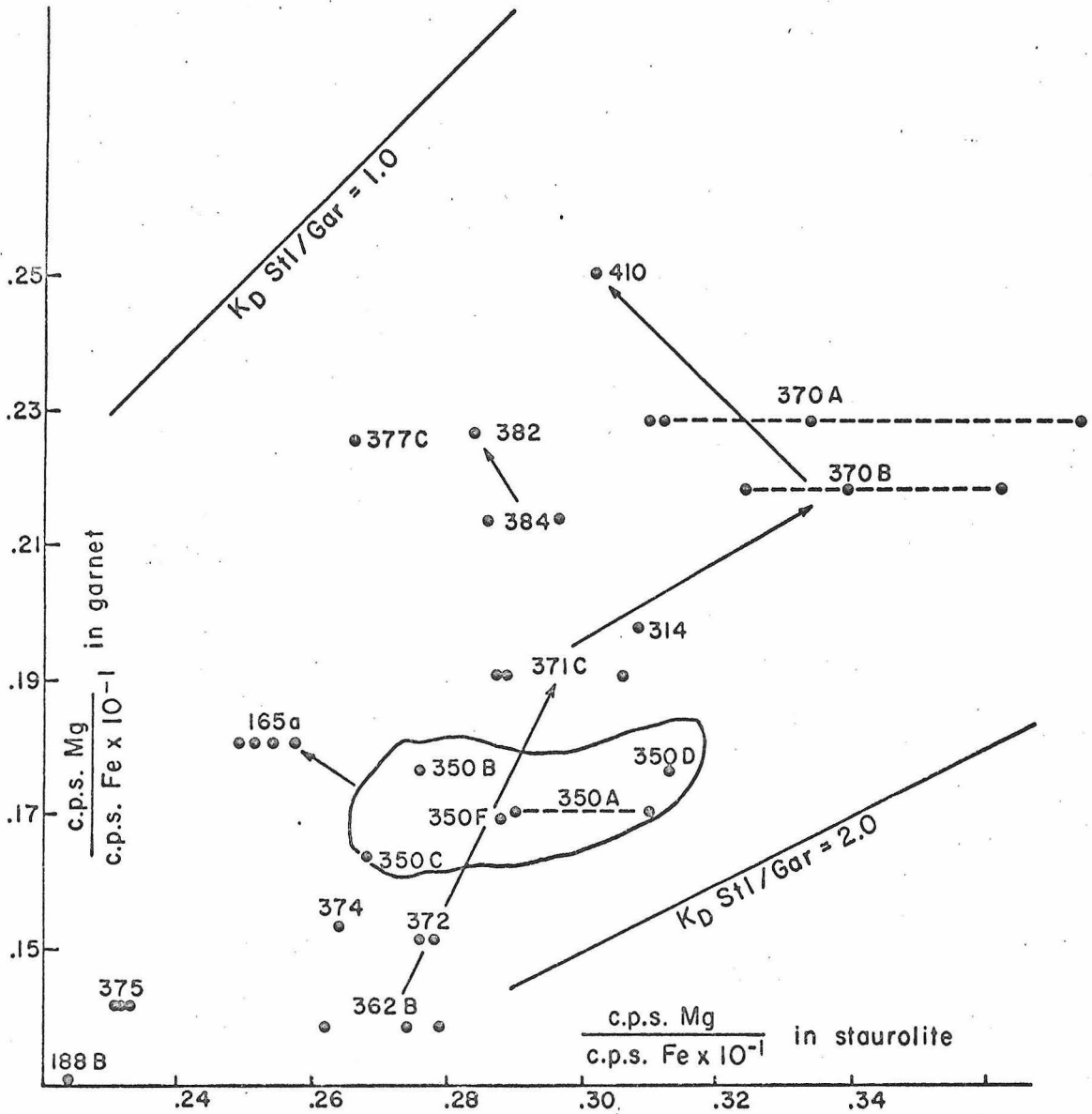


Fig. 45. Plot of maximum temperature Mg/Fe ratio of garnet against average Mg/Fe ratio of coexisting staurolite for all staurolite analyzed in the Kwoiek Area. Arrows show direction of increasing grade of metamorphism between assemblages containing a limiting garnet composition.

fact that each individual staurolite clearly shows a decreasing Mg/Fe ratio with radius, as seen in Figs. 43 and 44, the variations of Fig. 45 would not be considered significant. In Part V, a possible model to explain the variations of Mg/Fe in single staurolite, as well as the variations in average staurolite Mg/Fe ratio in rock 350, is discussed. The model might serve to explain the variations throughout the Kwoiek Area.

The zoning pattern of Fig. 44 has a similar explanation as that of Fig. 43 except that the reaction making the outer staurolite layer is of the type



which is discussed in Part III. The zoning is discontinuous in the elements Mg, Al, and Si, but not in Ti. Instead, Ti appears to rise continuously to the staurolite edge. This is reasonable since biotite is not a necessary reactant in reaction (3) and hence the Ti content in the staurolite is sensitive only to the continuous and increasing preference staurolite must have for Ti as the temperature rises and Fe^{+3} content decreases.

Aluminum Silicate

All three anhydrous aluminum-silicate polymorphs, andalusite, kyanite, and sillimanite, are present in the Kwoiek Area, and this fact alone makes the Kwoiek Area an unusual one. In only a few areas of the world have the three aluminum silicates been reported in the same area (i.e., Hietanen, 1956; Pitcher and Read, 1960; Woodland, 1963). Since the aluminum silicates are polymorphs with supposedly the same composition, the presence of all three in the Kwoiek Area should give an estimate of the pressure-temperature conditions which prevailed in the Kwoiek Area during its metamorphism. The experimentally determined triple point has been placed at 300° and 8 Kb by Bell (1963) and at 400° and 2.4 Kb by Weill (1966). The textural and geographic relations of the aluminum silicates in the Kwoiek Area, however, suggest one should exercise extreme caution in making deductions of pressure-temperature conditions based on the presence of the three polymorphs.

Plates 3 and 5 are photographs of smooth rock surfaces of aluminum silicate-bearing rocks. In both rocks there are nearly square cross sections of a mineral which has a chiastolite-type pattern of inclusions. However, for these two occurrences, as well as many others, not all occurrences of square-outline areas are andalusite as is illustrated by Plates, 4, 6-8. In specimen 180 (Plates 3 and 4), the square outline is andalusite, but in 160A (Plates 5 and 6) there is andalusite in the center but kyanite grains around the andalusite. Plate 7 is a photomicrograph of a square-outlined area that is now all kyanite. Plate 8 shows



Plate 3. Polished rock surface showing andalusite cross sections (A).

Largest andalusite about 2 mm. square. Specimen 180.

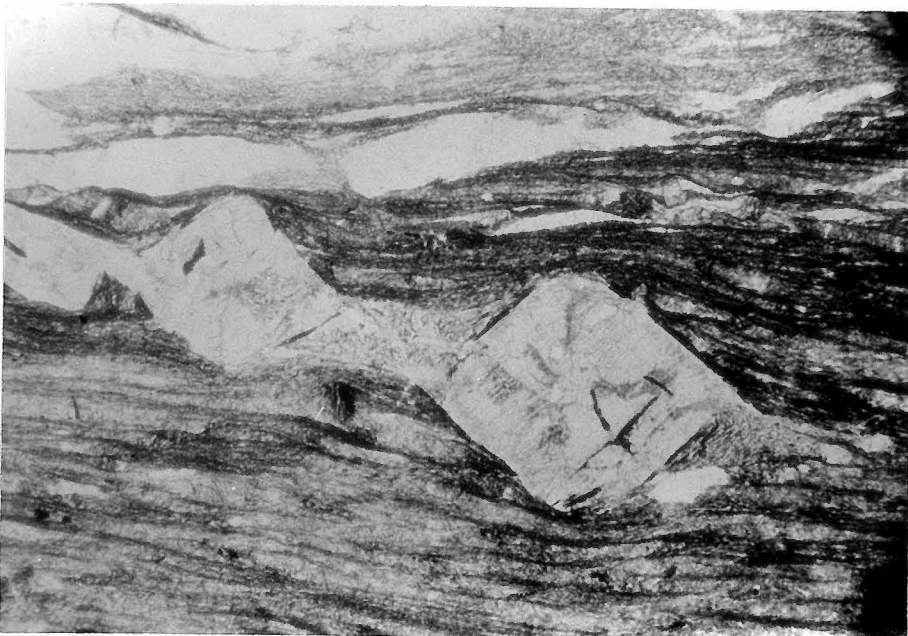


Plate 4. Photomicrograph (plane polarized light) of andalusite of

plate 3. Large andalusite about 2 mm. square.

Plate 5. Polished rock surface showing andalusite cross sections (A). Largest grain about 2 1/2 mm. square. Specimen 160A.

Plate 6. Photomicrograph (plane polarized light) of an andalusite cross section of Plate 5 showing andalusite (A) surrounded by smaller grains of kyanite (K). Outlines of two sides of former andalusite boundary are indicated. Andalusite and kyanite area 2 1/2 mm. square.

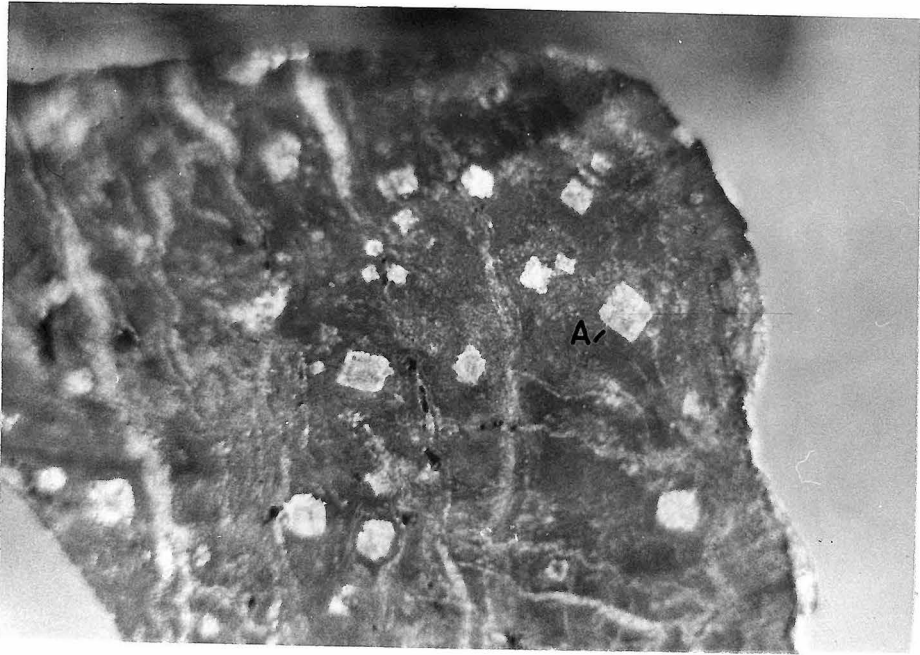


Plate 5.

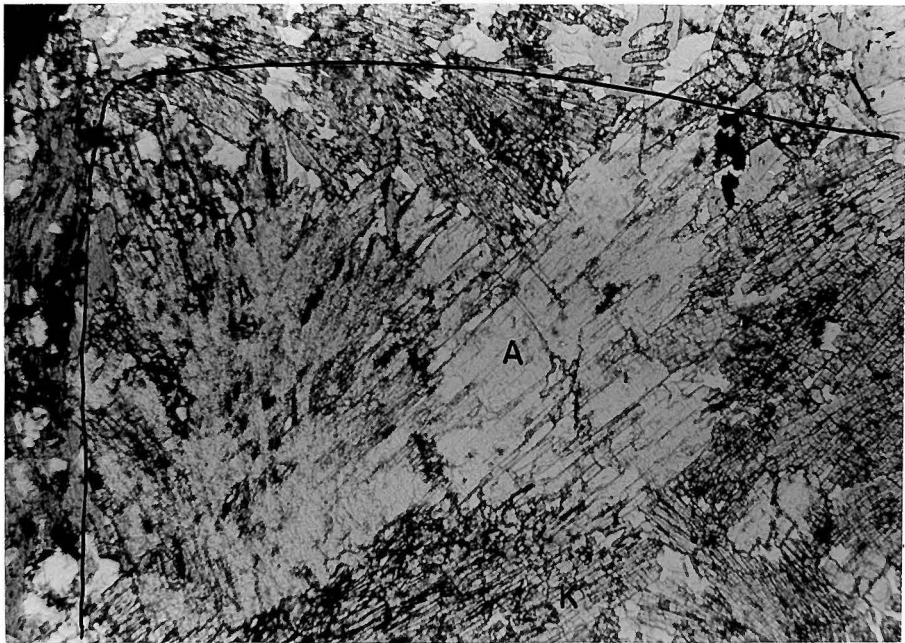


Plate 6.

Plate 7. Photomicrograph (plane polarized light) of a square outlined area of specimen 40. Andalusite has been completely transferred to kyanite. The kyanite pseudomorph is about 2 mm. square.

Plate 8. Photomicrograph (plane polarized light) of a square outlined area of specimen 370A. Former andalusite area now occupied by kyanite (K), staurolite (S), biotite (B), and quartz and plagioclase. Fibrolitic sillimanite (F) is developed at one corner. Pseudomorphic area is about 2 mm. square. Outlines of former andalusite boundary are indicated. Coarse sillimanite prisms occur elsewhere in thin section.

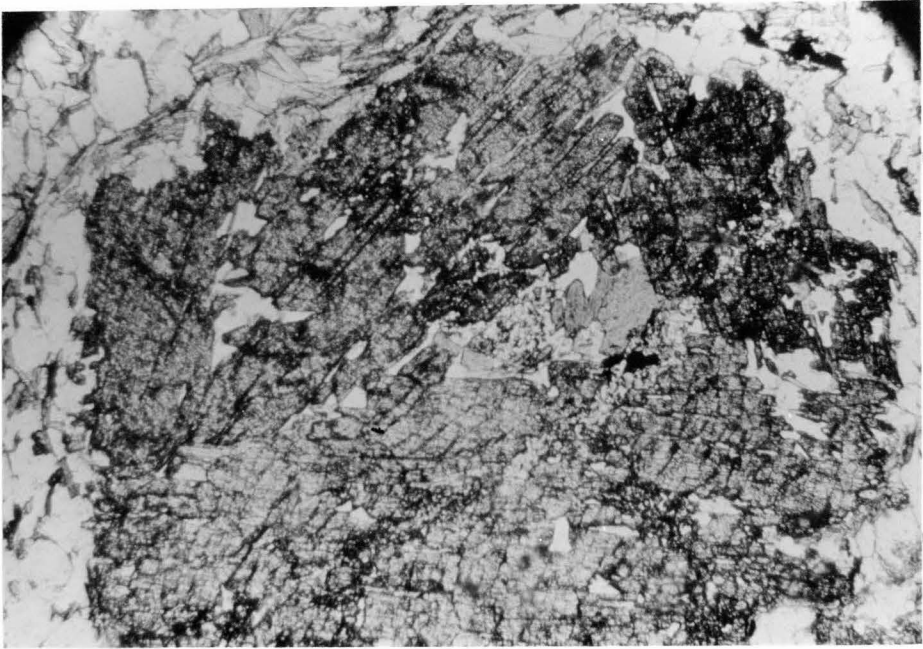


Plate 7.

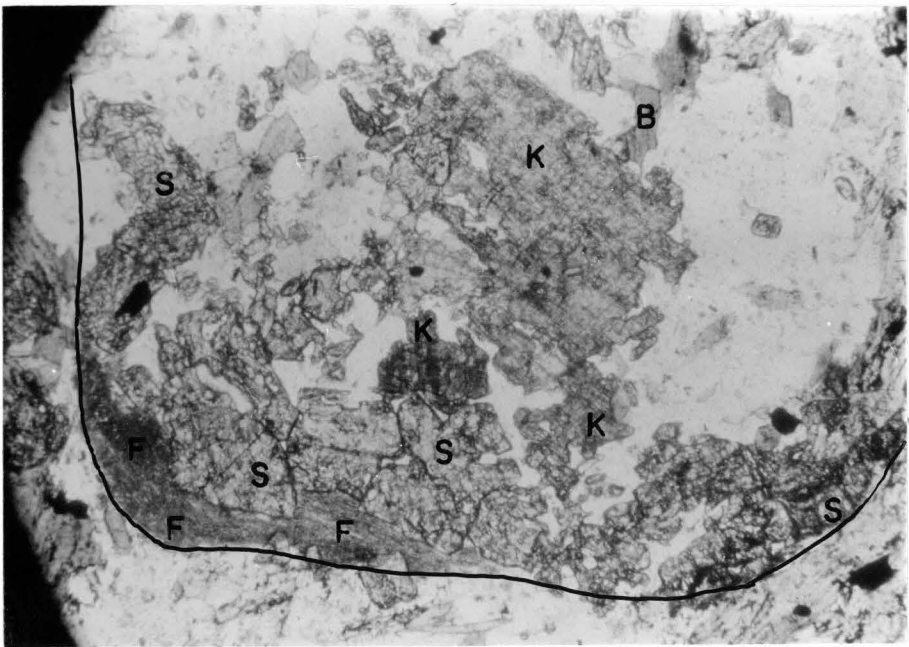


Plate 8.

a square-outlined area containing staurolite and kyanite rimmed by fibrolitic sillimanite. It is clear from Plates 3-8 that a sequence of polymorphic transitions has taken place with the sequence

andalusite → kyanite → sillimanite

The andalusite-to-kyanite part of the sequence has been reported in four other areas in the world (Tilley, 1935; Dike, 1951; Workman, 1963; Shams, 1965). Also identified around Skihist Mountain Stock, but not reproduced photographically, is fibrolitic sillimanite around andalusite within 20 feet of the stock contact. This textural relation indicates the polymorphic transition

andalusite → sillimanite.

The distribution of the aluminum silicate polymorphs in the Kwoiek Area is shown on the map in Fig. 1. Andalusite is common around Skihist Mountain Stock; and the only other andalusite occurrences are at the eastern edge of Kwoiek Needle Stock, where it is surrounded by kyanite (160A) and between Kwoiek Needle Stock and Hanna Peak Stock where it occurs with sillimanite and kyanite (320B). Kyanite pseudomorphous after andalusite is common along the ridge including Kwoiek Needle Stock and Kwoiek Needle up to the Southern Batholith contact west of Kwoiek Needle. Kyanite and sillimanite pseudomorphs after andalusite also occur in the narrow septum between Hanna Peak Stock and the Southern Batholith. Sillimanite occurs as the only aluminum silicate polymorph in the migmatite between Hanna Peak Stock and Murphy Lake Stock, and also at the western contact of Granite Mountain Stock. Kyanite and sillimanite

occur together (370A) on the ridge west of Kwoiek Needle near the Southern Batholith contact.

The two aluminum silicate polymorphic transition paths,

A, andalusite → sillimanite

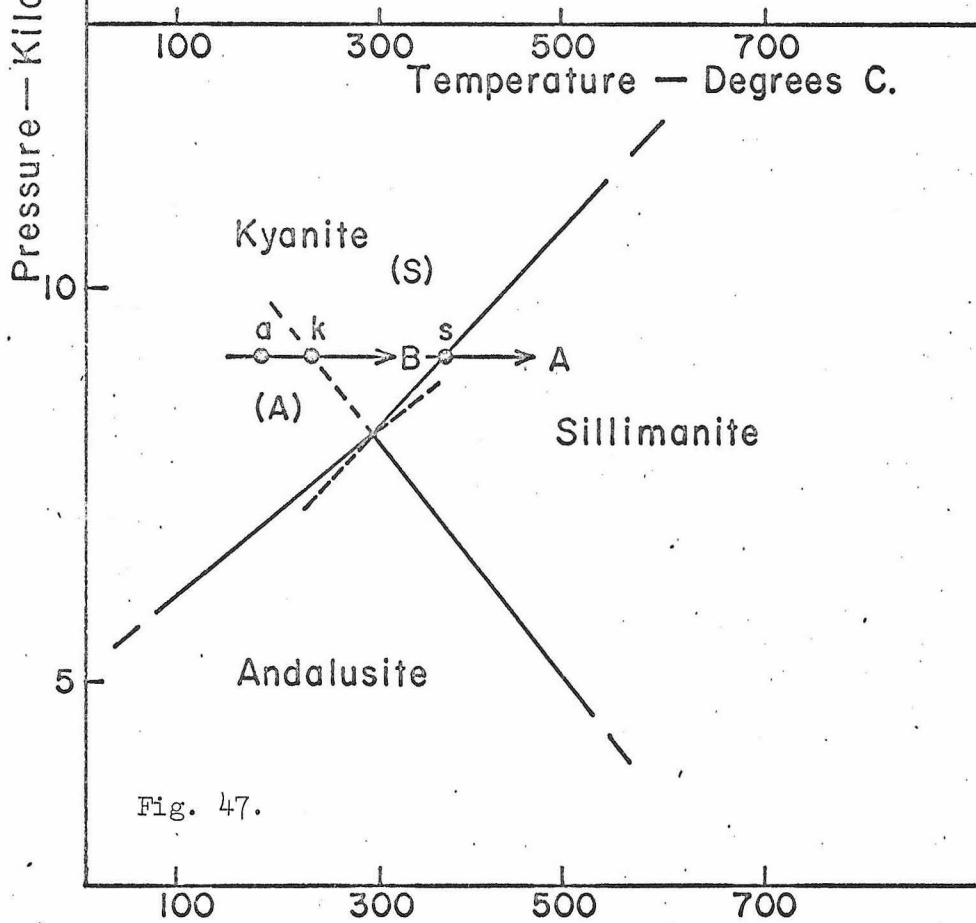
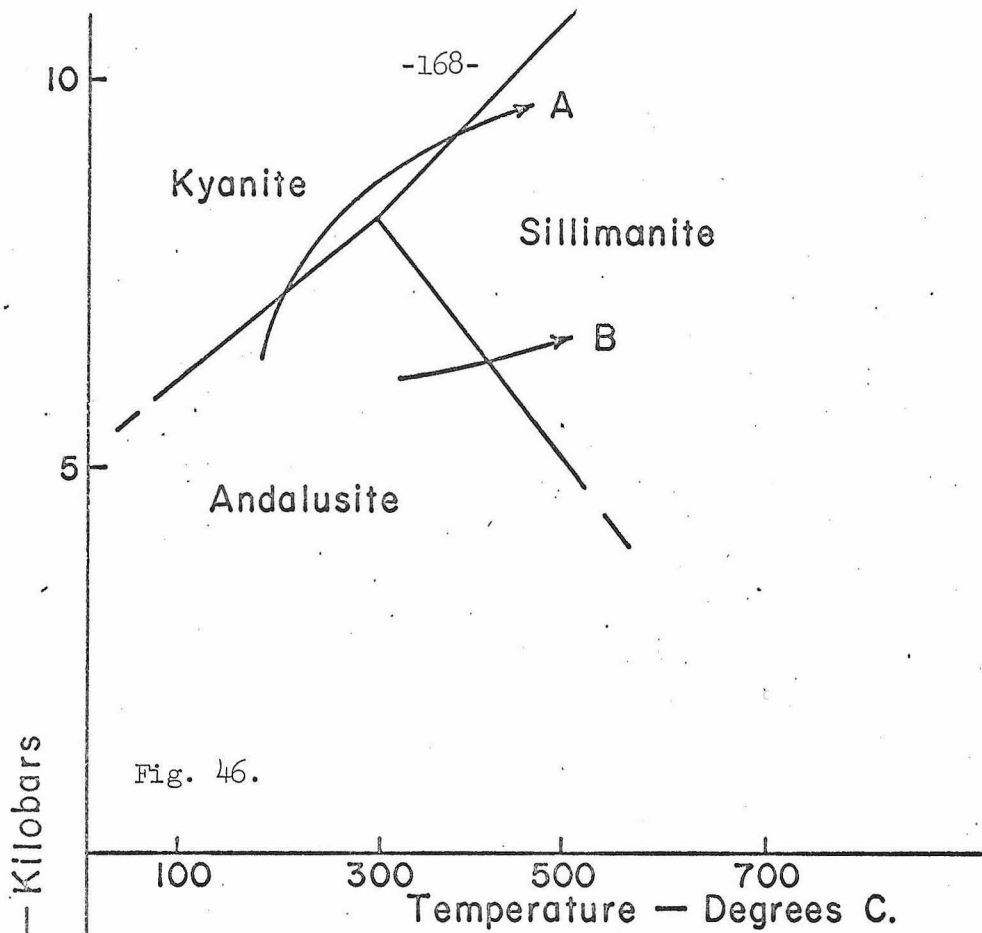
and, B, andalusite → kyanite → sillimanite

are shown on an experimental phase diagram for the aluminum silicates (Bell, 1963) as two separate trajectories (Fig. 46). The positions of each of the paths on Fig. 46 is arbitrary but it is clear that the two paths have to be different if they are both stable paths. To go stably from andalusite to kyanite to sillimanite involves not only a temperature increase but also a pressure increase. The transition of andalusite to sillimanite can be made at constant pressure, increasing temperature; increasing pressure, increasing temperature; or decreasing pressure, increasing temperature. However, the increasing temperature path for the andalusite to sillimanite transition cannot be the same as the andalusite to kyanite to sillimanite transition series.

The two areas, near Skihist Mountain Stock and along the ridge that includes Kwoiek Needle, are only five miles apart; they are at about the same elevation: 6000-7000 feet; the Kwoiek Area has not undergone extensive tilting since the metamorphism because contacts dip between 80 and 90° away from igneous bodies; the andalusite to sillimanite transition is seen in single handspecimens from near an intrusive contact and the andalusite to kyanite to sillimanite transition can be documented from less than one-eighth mile horizontally from the

Fig. 46. Al_2SiO_5 phase diagram after Bell (1963) showing possible stable paths of observed aluminum silicate transitions in the Kwoiek Area. See text.

Fig. 47. Al_2SiO_5 phase diagram after Bell (1963) showing inferred metastable - stable transition path of observed aluminum silicate transitions in the Kwoiek Area. See text.



Southern Batholith contact west of Kwoiek Needle. These relations taken together lead to the conclusion that both aluminum silicate transition paths occurred not only at constant pressure but also at about the same pressure. This is clearly contradictory, at least for the andalusite to kyanite to sillimanite path, to the relations shown in Fig. 46, which show the only path possible for andalusite to go stably to kyanite and kyanite to sillimanite.

Possible explanations are that andalusite formed metastably in the kyanite field or that impurities in the andalusite stabilized andalusite in the kyanite field.

If impurities stabilized andalusite, Fig. 47 can be taken as a stable phase diagram for a specified concentration of impurity in andalusite. Small amounts of impurities can be expected to change the stability curves by significant amounts because of the low free energy of transition of one aluminum silicate to another (Corlett and Smith, 1964). For the case of the Kwoiek Area, impurities in andalusite might be expected to stabilize it in part of the kyanite field. With increasing temperature, the transition of andalusite to kyanite (possibly with release of the impurities) could take place.

Wave length scans between 12Å and 1Å were made on selected aluminum silicate minerals with the microprobe. Conditions were 0.4 microamps sample current and 25 kilovolts accelerating voltage. Spot size was 5-10 microns. Table 13 shows the results of this study. The numbers given for each element found are in scale units above background (100 units full scale). As they are not calibrated against standards,

Table 13

Trace Element Analyses of Aluminum Silicate Polymorphs

Element Line	K K α	Ti K α	V K α	Cr K α	Fe K α	Cu K α	Sn L β	Ca K α	Mg K α
180 and	1.5	1.5	1.5	1.0	30	-	-	-	-
189 and	-	6	1.5	-	>69	-	-	-	3
314 silli	.5	-	2.5	5	22	-	-	-	-
314 silli	.5	-	3	6	24	6	.2?	-	-
370A silli	1.5	-	2	2	15	-	1	.5	-
370A ky	-	1	1.5	.5?	24	-	-	-	-
371C ky	.5?	-	1	2	16	-	2	-	-
160A and	-	2	1	-	28	-	-	-	-
160A ky	-	2	-	-	20	-	-	-	-
160A and	-	2	1	-	29	-	-	-	.5
160A ky	-	2	1	-	22	-	-	-	-
160A and	-	3	-	-	76	-	-	2	.5
160A ky	-	-	-	-	35	-	-	-	1.5

Analyses are given in units above background (100 units full scale). Coexisting aluminum silicate polymorphs and analyses on different grains of a sample are shown by identical sample numbers. See text.

absolute values of concentration cannot be determined for each element. Na_2O , which could be present in the aluminum silicates (Pearson and Shaw, 1960) was not analyzed for but it is probably present in only very small amounts, if at all, because the K_2O content is very low.

Little can be concluded from observed differences in trace element concentrations, even when two aluminum silicates are co-existing. One andalusite (189) has a markedly higher Fe content than the other andalusites, but the others, 180 and 160, have essentially the same elements and range of each element as kyanite and sillimanite. There does appear to be a slightly higher Fe content in the andalusite coexisting with the kyanite in sample 160. However, the difference is very small as an Fe peak height of 20 corresponds to about 0.2 weight percent Fe_2O_3 . It is hard to conceive that this small difference in Fe content would shift the andalusite-kyanite equilibrium boundary any significant amount. Therefore, the concept developed below, is probably the most likely.

A possible aluminum silicate sequence beginning with metastable formation of andalusite is shown diagrammatically in Fig. 47 where the metastable extensions of the experimentally determined transition curves are plotted, and the fields of the next most stable polymorphs, andalusite and sillimanite, are shown in the kyanite field. The observed aluminum silicate transitions in the Kwoiek Needle ridge area could have formed along the constant pressure line a, k, s with metastable andalusite forming in the metastable andalusite field a,

inverting to stable kyanite where the a, k, s path leaves field (A), and inverting to sillimanite at s where the hypothetical a, k, s path enters the stable sillimanite field.

The observed aluminum silicate transitions around Skihist Mountain Stock could be inferred to have taken place along the same path as those on Kwoiek Needle ridge except that instead of stable kyanite forming at k, metastable sillimanite formed. The differences in the two observed sequences might be due to the fact that the temperature gradient around Skihist Mountain Stock was steeper than that along Kwoiek Needle ridge away from the Southern Batholith contact. The much wider contact aureole in rocks of similar composition near the Southern Batholith than near Skihist Mountain Stock is evidence of this fact. Steeper temperature gradients of shorter time duration would be expected to be more favorable for the formation and preservation of metastable phases than a shallower gradient of longer time duration.

An alternate explanation to the differences in the two aluminum silicate transition series, that of different pressures in the two areas, is a possibility; but it is unlikely that the pressure differed significantly between the two areas.

The two transition series are shown to cease at different temperatures in Fig. 47, in spite of the fact that both stop at quartz diorite contacts, because evidence indicates that the temperatures were not the same adjacent to both contacts. First, there is a 600 foot migmatite zone adjacent to the main batholith where the andalusite to kyanite to

sillimanite sequence was documented, but no migmatite occurs around Skihist Mountain Stock. The origin of the migmatite is assumed to be partial melting rather than injection (discussed in Part II); and, hence, its presence may be indicative of higher temperatures since greywacke in the two areas is not grossly different. Second, the garnet data presented in Fig. 31 show that the limiting composition, maximum temperature Mg/Fe ratio of the garnet (Fig. 30) at Skihist Mountain Stock contact (173, 175) has a lower Mg/Fe ratio (i.e., lower temperature) than the garnet in the migmatite belt (371C, 370C, 370B, 410).

The complete picture of the formation of the aluminum silicates can now be summarized. The two observed sequences, andalusite to kyanite to sillimanite and andalusite to sillimanite, probably took place at nearly the same constant pressure. The one involving kyanite involved higher temperatures at the end of the sequence that were held for a longer period of time so that the kyanite to sillimanite part of the transition is presumed to be a stable sequence after initial metastable formation of andalusite. The andalusite to sillimanite sequence, if it is accepted that the two sequences took place at the same pressure, must involve metastable sillimanite as the andalusite to sillimanite transition ceased at a lower temperature than the kyanite to sillimanite transition. The transition presumably took place across the metastable extension of the andalusite-sillimanite boundary as shown in Fig. 47. The pressure of both transition series must be at the high pressure side of the aluminum silicate triple point.

CONDITIONS OF METAMORPHISM

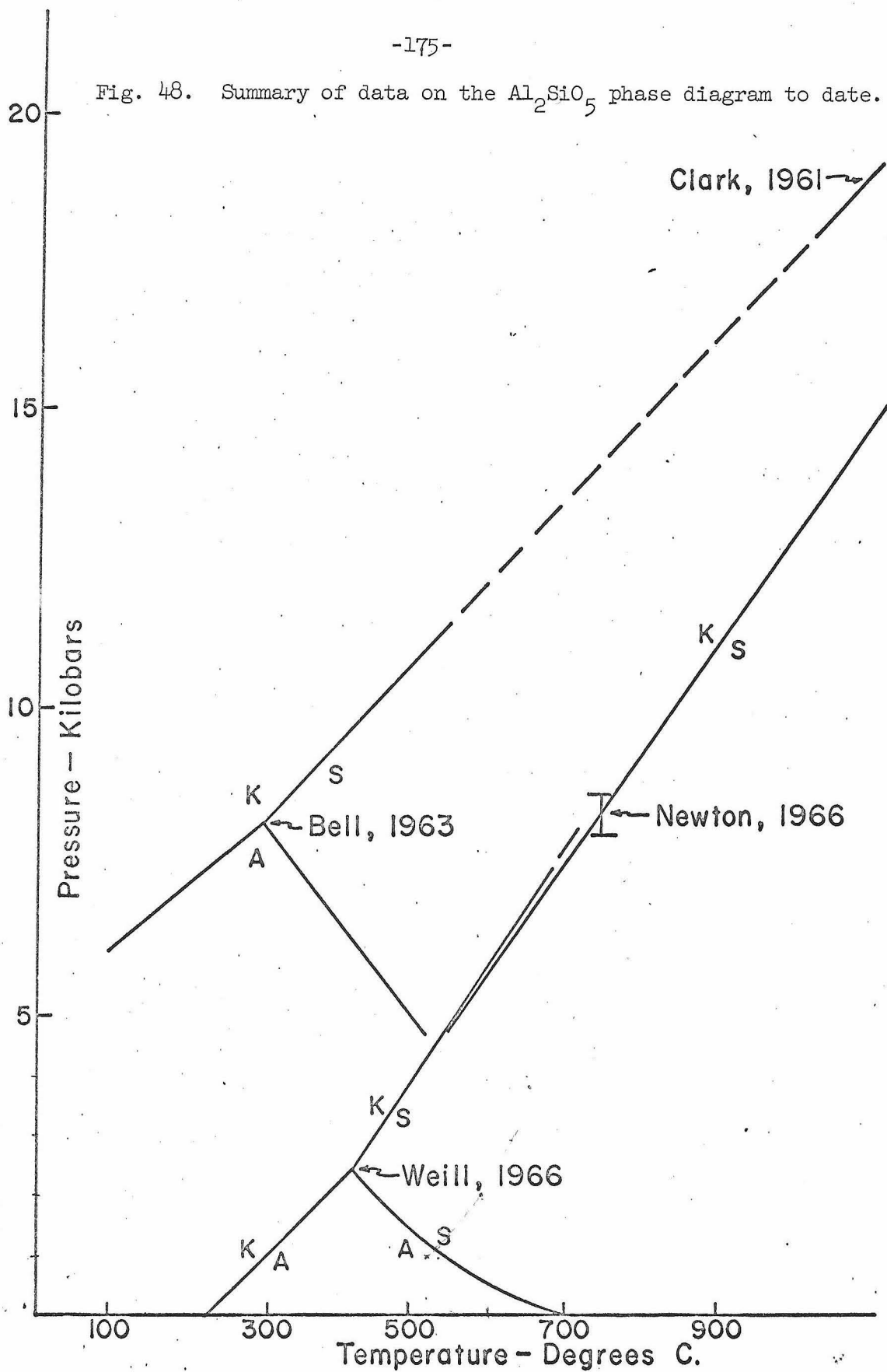
In most studies of metamorphic terranes attempts have been made to define the intensive variables of metamorphism such as P_{total} , P_{fluid} , $P_{\text{H}_2\text{O}}$, P_{O_2} , P_{CO_2} , and T . These attempts have primarily been speculative and this study can do little more; however, some limits on the variables involved can be made.

Temperature and Total Pressure

The temperatures in the Kwoiek Area clearly had a wide range, from those representative of the greenschist facies to those of the upper almandine-amphibolite facies. The upper limit is marked by the crystallization temperatures, at the pressures involved, of biotite quartz diorite; the lowest temperatures would be below the formation of epidote. Most workers would suggest a temperature range in the Kwoiek Area of between 300°C and 700°C , for these facies and limits.

The best independent evidence relating to the maximum temperatures reached at a few locations in the Kwoiek Area and the total pressure (total pressure is taken to be the same throughout the Kwoiek Area) is from the aluminum silicate polymorphs. Figure 48 summarizes some of the recent experimental work on the Al_2SiO_5 system. According to the arguments used in the preceding section, the observed transition of andalusite to kyanite to sillimanite took place at a pressure somewhat higher than that of the triple point; how much higher is not known, but presumably it was not more than half a kilobar. According to Fig. 48, the total pressure in the Kwoiek Area was, therefore,

Fig. 48. Summary of data on the Al_2SiO_5 phase diagram to date.



either slightly above 8 kilobars (Bell, 1963) or slightly above 2½ kilobars (Weill, 1966).

A piezobirifringent analysis (see Rosenfeld and Chase, 1961) was performed on one specimen from the Kwoiek Area (Rosenfeld, oral communication, 1966), and this analysis puts a definite restriction on which of the above two pressures was the closest to the true total pressure in the Kwoiek Area. The analysis was on quartz inclusions in a garnet of sample 410, which was collected near the kyanite to sillimanite transition but within the field of stability of sillimanite (Fig. 1). Rosenfeld found that quartz inclusions with the c-axis perpendicular to the microscope stage did not stress the garnet but quartz inclusions with the c-axis parallel to the microscope stage did. This observation, coupled with knowledge of quartz and almandine coefficients of thermal expansion and compressibility, gives a univariant curve along which the analyzed rock must have crystallized. This univariant curve intersects the kyanite-sillimanite boundary of Weill (1966) as well as that of Newton (1966) at 2.5 Kb and 450°C, which is not an unreasonable temperature and pressure for conditions one-eighth of a mile from the contact of a deep-seated batholith. The univariant curve defined by Rosenfeld does not intersect Bell's kyanite-sillimanite curve at any pressure or temperature. Hence, it is concluded that the triple point of Weill (1966) is more correct than that of Bell (1963) and that sample 410 crystallized at a temperature near 450°C and at a pressure of about 2.5 kilobars.

The above pressure estimate is supported by geologic evidence. The

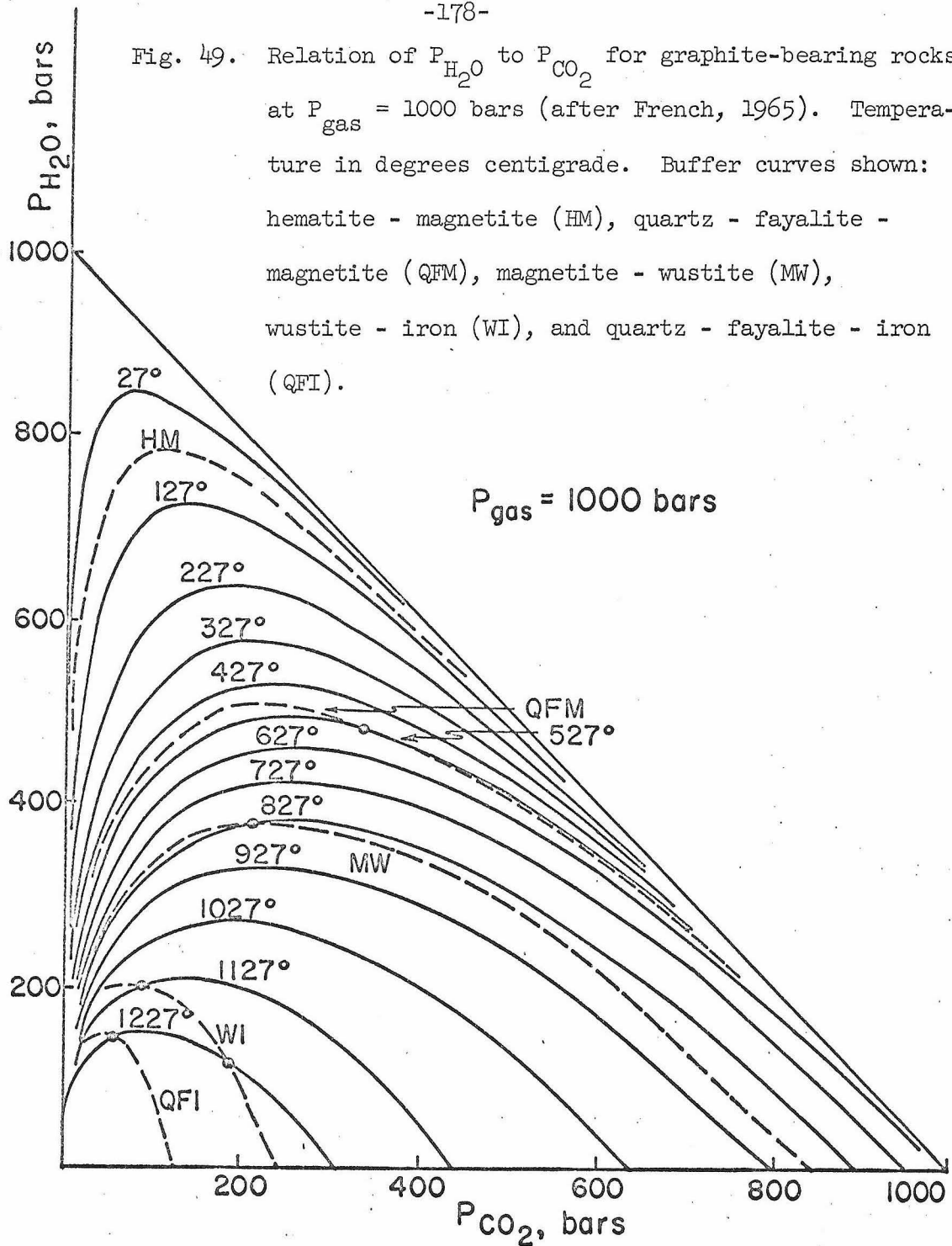
quartz diorite intrusives are believed to be about 100 million years old (K. C. McTaggart, oral communication, 1964), a lower Cretaceous age, and to have intruded sedimentary rocks of Upper Jurassic or (?) Lower Cretaceous age (Cairnes, 1942). According to Kummel (1961, page 16), the maximum known thickness of Jurassic age in North America is 22,000 feet. Even with the uncertainties of the above age assignments as well as thickness amplifying effects such as recumbent folds or thrust faulting, it is difficult to conceive of a load pressure greater than 2-3 kilobars.

Oxygen Pressure and Its Influence on Staurolite Composition

Graphite is present in the metamorphosed sedimentary rocks of the Kwoiek Area in all grades of metamorphism. The most common accessory opaque mineral is ilmenite; pyrite or pyrrhotite are also present in some rocks. Magnetite was looked for but not found in any metasedimentary rock. These observations alone suggest "low" values of P_{O_2} in the range of 10^{-20} to 10^{-25} atmospheres ($P_{fluid} = 2 \text{ Kb}$).

Recent data and discussion (French, 1965) offer further insight into the behavior of the partial pressures of the various gaseous species in the Kwoiek Area. Figure 13 of French (1965) is reproduced here as Fig. 49. This figure, for $P_{gas} = 1000 \text{ bars}$ (French argues that the qualitative relations of this diagram should not change for higher pressures) shows the relative compositions of CO_2 and H_2O in the gas phase for a rock in which graphite is available for reaction. Figure 49 indicates that graphite cannot be in equilibrium with a pure H_2O phase at the temperatures found in the Kwoiek Area.

Fig. 49. Relation of P_{H_2O} to P_{CO_2} for graphite-bearing rocks at $P_{gas} = 1000$ bars (after French, 1965). Temperature in degrees centigrade. Buffer curves shown: hematite - magnetite (HM), quartz - fayalite - magnetite (QFM), magnetite - wustite (MW), wustite - iron (WI), and quartz - fayalite - iron (QFI).

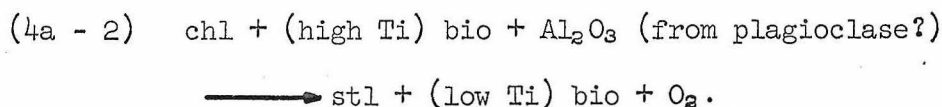
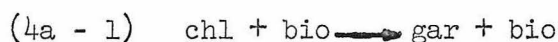


Although the exact temperature path in Fig. 49 is indeterminate for an open system, increasing temperature will lead to a lower concentration of H₂O in the gas phase and, according to French (1965), an increasing content of H₂ and CO. CH₄ will be abundant.

Common buffering systems are also shown in Fig. 49 and indicate that, in the presence of graphite, increasing temperatures lead to a net reduction of Fe in the solid phases present. This agrees with observations that the Fe₂O₃/FeO ratio decreases as metamorphic grade increases in the presence of graphite (Shaw, 1956, Zen, 1963, Miyashiro, 1964). In the Kwoiek Area, no total rock Fe₂O₃/FeO values were obtained, but arguments were made (page 154) for a reduction in Fe⁺³ content in the staurolite grade rocks with temperature increase.

The concept of increasing Fe reduction with increasing temperature suggests a reason for the observation that Mg/Fe in individual staurolite grains decreases with increasing temperature and that the staurolite analyses of the 350 series rocks show nearly 50 percent of the total staurolite variation found throughout the Kwoiek Area. These speculations, in turn, lead to a better understanding of the total gas pressure (P_{gas}) and partial pressures of the various components of the gas (P_i).

As in Part III, reaction 4a of Part III (low-Ca reactions) can be broken into the two reactions

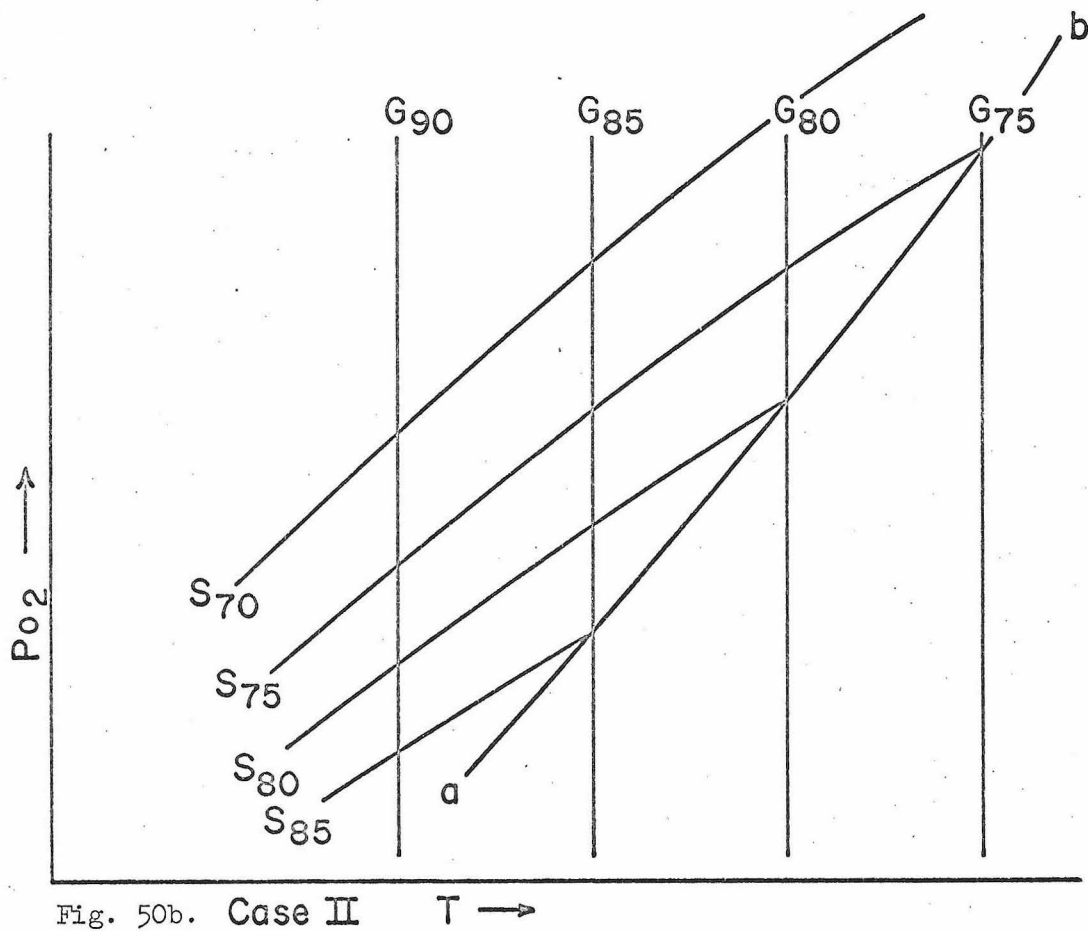
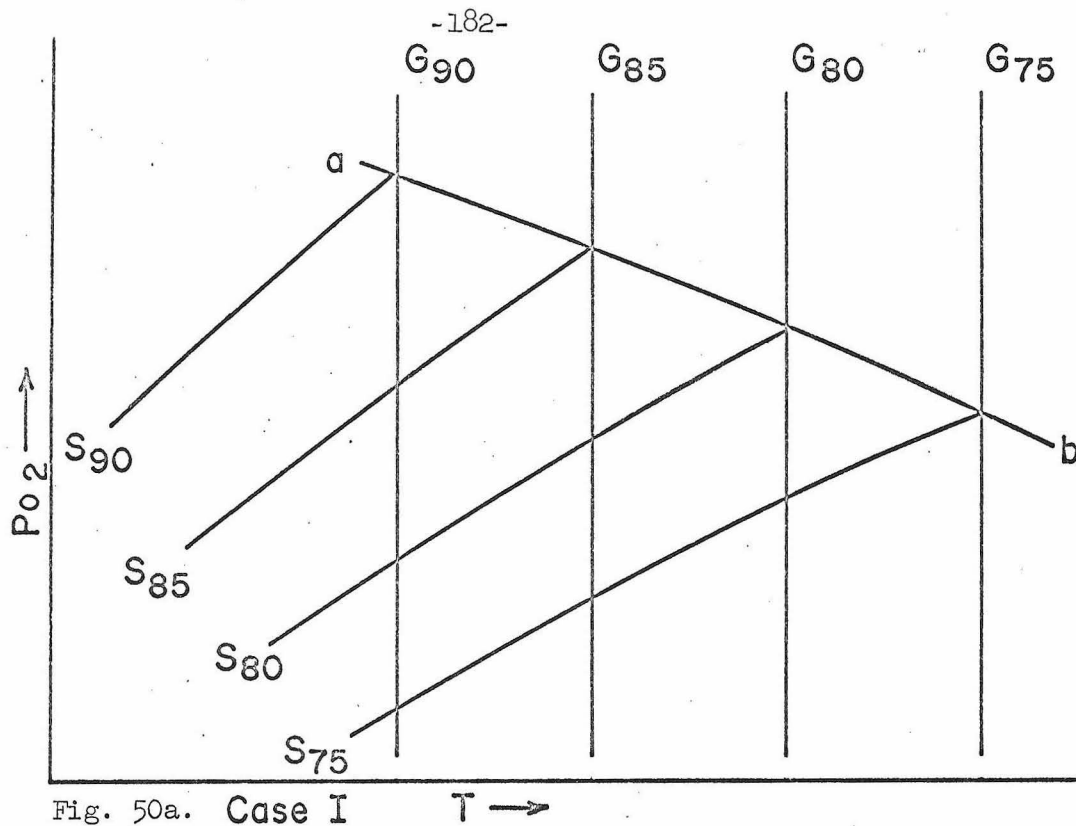


Oxygen is placed on the reactant side of equation (4a - 2) in conformity with the observation of progressively reduced iron in the staurolite with increasing temperature.

Since reaction (4a - 1), as it is written, does not involve oxidation or reduction, it can be represented by a family of curves, each for a specified garnet composition, nearly parallel to the P_{O_2} axis of a P_{O_2} - T plot (Fig. 50). This conforms with the observation that the Mg/Fe ratios of the five garnets of outcrop 350 appear dependent only on Mn content. However, the fact that the staurolite Mg/Fe ratios are not regular with respect to any other element, such as Ti or Mn, nor with respect to metamorphic grade, suggests that another variable or variables is responsible for the Mg/Fe variations. It is suggested here that P_{O_2} be used as the other variable; and, therefore, equation (4a - 2) is plotted in Fig. 50 as a function of P_{O_2} . The question then becomes how to orient the family of staurolite lines, representing different compositions of staurolite in equation (4a - 2), with respect to the garnet lines and, more importantly, with respect to reasonable P_{O_2} - T paths.

The analysis of the staurolite zoning gives us one piece of information which constrains the position of the lines for equation (4a - 2). At the discontinuous change in zoning in Fig. 43, there is a discontinuous change in the ratio Fe/Mg+Fe. The temperature change across the zone boundary is considered negligible. However, the change in Fe/Mg+Fe ratio is either positive or negative going from center outwards, depending on whether we consider

Fig. 50. Hypothetical garnet and staurolite stability fields in a P_{O_2} - T plot for the assemblage chl - gar - bio - stl - qtz - plag - ilm - graph. Line a - b is inferred high temperature stability limit of staurolite. Subscripts for staurolite (S) and garnet (G) give the atom percent Fe/Fe+Mg in staurolite and garnet at the indicated reaction boundaries. Fig. 50a, Case I; Fig. 50b, Case II. See text.



$$\text{Fe}^{+2}/(\text{Mg}+\text{Fe}^{+2}) \quad \text{or} \quad (\text{Fe}^{+2}+\text{Fe}^{+3})/(\text{Mg}+\text{Fe}^{+2}+\text{Fe}^{+3}) .$$

In the latter case, $\text{Fe}/(\text{Mg}+\text{Fe})$ decreases (Case I) in the outer zone, and in the former case (Case II) it increases. A further restriction is that the ratio $\text{Fe}/\text{Fe}+\text{Mg}$ in the staurolite cannot exceed that of the coexisting garnet. This arises from the fact that no staurolite has been observed, either in the Kwoiek Area or in any other area, in which $\text{Fe}/\text{Fe}+\text{Mg}$ in staurolite is greater than $\text{Fe}/\text{Fe}+\text{Mg}$ in coexisting garnet.

In Fig. 50a equations like equation (4a - 2) are plotted relative to the garnet equations for Case I. It is noted that for Case I the staurolite Mg/Fe ratio increases with temperature, which is contradictory to observation (see Figs. 43, 44, and 45). Case II (Fig. 50b), on the other hand, is consistent with observation and is also analogous to olivine stability curves (Wones and Eugster, 1965). It is concluded that Case II is the most reasonable.

Accepting Case II as the most reasonable, we must then infer a reasonable P_{O_2} - T path which, for increasing temperature, will give both increasing Mg/Fe in the garnet and decreasing Mg/Fe in the staurolite. In Fig. 51, the relative positions of the magnetite-hematite buffer curve and a graphite-gas buffer curve are drawn with respect to the staurolite and garnet curves of Case II.

The graphite-gas buffer curve is a buffer curve only under certain specified conditions. According to French (1965), the curve is a buffer curve in the presence of graphite if there are two restrictions

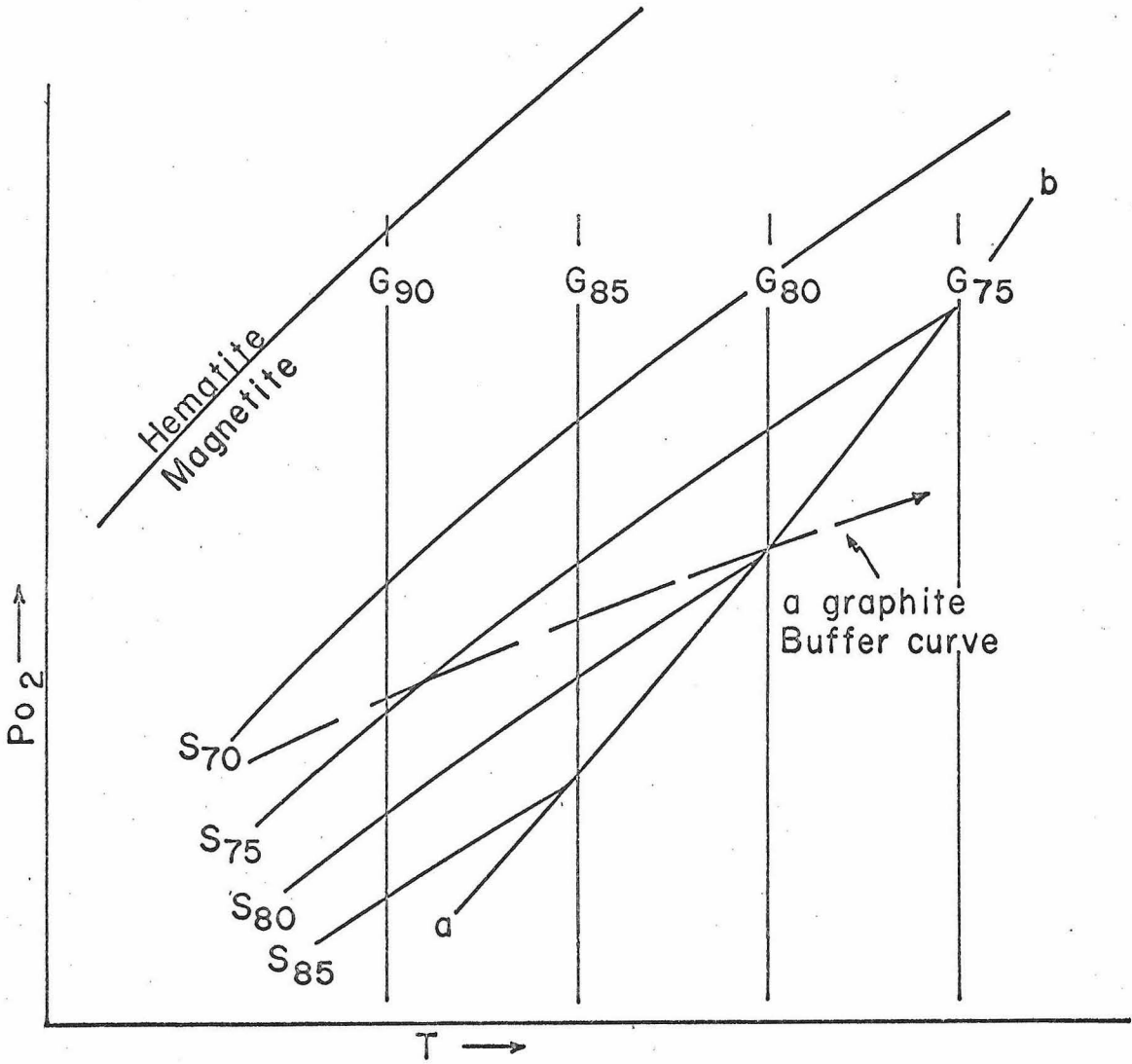


Fig. 51. Fig. 50b with the inferred relative position of the hematite - magnetite buffer curve and a graphite - gas buffer curve.

on the equation

$$(1) P_{\text{gas}} = P_{\text{H}_2\text{O}} + P_{\text{H}_2} + P_{\text{O}_2} + P_{\text{CO}_2} + P_{\text{CO}} + P_{\text{CH}_4} .$$

Even if it is assumed that $P_{\text{H}_2\text{O}}$ (or alternatively $\mu_{\text{H}_2\text{O}}$) is constant between the rocks of a single outcrop (e.g., the 350 series samples) and that $P_{\text{H}_2\text{O}}$ (or alternatively $\mu_{\text{H}_2\text{O}}$) has a systematic relation to temperature (discussed in Part III), equation (1) is still univariant at constant temperature. Accepting this model, it is possible to explain the non-systematic variations of staurolite composition in the five rocks of outcrop 350. The graphite-gas buffer curve of Fig. 51 will not be a true buffer curve as its position will be different in different rocks if any variable in equation (1), such as P_i or P_{gas} , varies from rock to rock in a given outcrop.

The model proposed above is speculative but it does explain the limited data available and does not contradict any data. If this model is accepted, local differences of P_{gas} or P_i "explain" the scatter of data of Fig. 45.

SUMMARY OF CONCLUSIONS

The most important contributions of this study are the conclusions based on the study of zoned garnet porphyroblasts. The interpretation of their zoning has come from a variety of sources, both geological and petrological, as well as analytical. The study of the biotite and chlorite indicates that these minerals continuously reequilibrated during the metamorphic history and acted as a reservoir of elements for the growth of the relatively unreactive minerals -- garnet, staurolite, and aluminum silicates. The biotite and chlorite continued to reequilibrate at lower temperatures subsequent to the peak temperature of metamorphism. The zoning patterns of the staurolite indicate that the metamorphism took place under increasingly reducing conditions as the temperature rose. The discontinuous zoning patterns in the staurolite show that early staurolite crystallization took place at constant temperature and that in most cases the garnet and staurolite grew by at least two different reactions. The reactions that produced the garnet and staurolite were inferred from the study of assemblages in rocks of different composition collected from grades of metamorphism ranging from low biotite and chlorite to sillimanite and into the temperature range of partial melting. The method of graphical projection used to illustrate the reactions differs from that used by Thompson (1957) in that a biotite composition is used as the projection point instead of muscovite.

The garnet porphyroblasts themselves grew according to a depletion model, called the Rayleigh depletion model. The assumptions in this model are that equilibrium existed between garnet rim and "reservoir" of biotite and chlorite and/or muscovite, but that disequilibrium existed within the garnet itself. Calculated curves for Mn and Mg/Fe ratio as a function of radius closely approximate the analytical curves. Although the temperature history for most of the garnet cannot be proven by the comparisons of calculated and analytical zoning patterns, it can be stated that the outer zones grew under conditions of decreasing temperature.

The fact that the garnet continued to grow with decreasing temperature and that the biotite and chlorite compositions vary from point to point in a given thin section indicates that distribution functions between garnet edge and biotite and chlorite simply reflect the temperature at which the rock stopped reequilibrating during the decreasing temperature period rather than the maximum temperature.

Assuming the bulk of the garnet grew under conditions of increasing temperature, a zone in each garnet is identified as having grown at the maximum temperature of metamorphism. Where this composition represents the limiting garnet composition in a four-phase field in the $Al_2O_3 - K_2O - FeO - MgO$ tetrahedron, it can be shown that the maximum temperature composition changed systematically to higher Mg/Fe values with metamorphic grade. Chlorite and biotite in rocks with limiting composition garnets increase in Mg

content, whereas staurolite shows the reverse effect.

The limiting composition, maximum temperature Mg/Fe ratio of garnet is dependent on the Mn content, if other variables are constant. Albee (1965b) showed a similar relationship; however, it appears that the distribution function of Fe and Mg between biotite and garnet is independent, or less dependent on Mn content than reported by Albee (1965b). In addition the Mg/Fe ratio of the garnet is dependent on the biotite/chlorite ratio.

In spite of uncertainties in the precise location of the maximum temperature zone in the garnet, the range of composition for the maximum temperature zone is smaller, in a given thin section, than for the edge. This indicates that the area of total equilibrium in a given rock was greater at the maximum temperature than in the rock as presently seen.

Although most of the garnet porphyroblasts grew under the influence of a single metamorphic event, garnet collected from near stocks, which were intruded after the main batholith, show the influence of the second metamorphic event in their zoning pattern. Such patterns could be applied to other metamorphic areas, where clear-cut evidence of two metamorphic histories is lacking, to determine how many metamorphic events were involved.

The fact that garnet porphyroblasts are zoned indicates that they may remain unreactive if a sequence of reactions takes them out of equilibrium with the rest of the minerals in the rock. Thus it is possible for a garnet to remain as an inert phase in an assemblage

with which it is not in equilibrium. The same is probably true for staurolite and the aluminum silicates. This concept may explain occurrences of rocks with more phases than would be predicted by the phase rule.

The Kwoiek Area is not the only one in the world with zoned garnets. Many of the garnet standards used for this work, collected from several different localities, were zoned; and zoned garnets have been reported from other areas (Banno, 1965; Evans, 1965; Albee, et al., 1966). Unzoned garnet porphyroblasts do not necessarily mean the Rayleigh depletion model is not important as they can be explained by either a low Mn content in the rock or by a small proportion of garnet relative to the other ferromagnesian minerals.

A constant pressure sequence of polymorphic changes from andalusite to kyanite to sillimanite was documented, and, since this sequence cannot take place at constant pressure with increasing temperature, the initial metastable formation of andalusite is inferred. The fact that metastable andalusite can be documented in one area may mean that andalusite occurring in other contact metamorphic areas is also metastable.

APPENDIX

Mineral Abbreviations Used in the Text

<u>Mineral</u>	<u>Abbreviation</u>
Chlorite	chl
Garnet (almandite)	gar
Staurolite	stl
Aluminum silicate	Al-silicate (or Al)
Andalusite	and
Sillimanite	silli
Kyanite	ky
Muscovite	musc
Actinolite	act
Amphibole	amph
Hornblende	hbl
Epidote	ep
Clinozoisite	cz
Calcite	calc
Biotite	bio
Plagioclase feldspar	plag
Ilmenite	ilm
Quartz	qtz
Graphite	graph
Cordierite	cord

Assemblages of Metamorphic Samples Discussed in Text

Sample no.	Musc	Chl	Bio	Gar	Stl	Al-silicate	Ilm	Graph	Ep
10	x	x	x	x	-	-	x	x	-
40	-	-	x	x	x	ky	x	x	-
154A	x	x	x	x	-	-	x	x	-
154B	x	x	x	x	-	-	x	-	-
165A	-	x	x	x	x	-	x	x	-
165G	-	-	x	x	x	-	x	x	-
173	-	x	x	x	x	and	x	x	-
175	-	x	x	x	x	and	x	x	-
188A	-	x	x	x	-	-	x	x	-
188B	(x)	-	x	x	x	and-silli	x	x	-
188C	-	x	x	x	-	-	x	-	x
222	x	x	x	x	-	-	x	x	-
272	x	x	x	x	-	-	x	x	x
314	(x)	-	x	x	x	silli	x	x	-
320B	(x)	-	x	x	x	ky-silli-and	x	x	-
350A	-	x	x	x	x	-	x	x	-
350B	-	x	x	x	x	-	x	x	-
350C	-	x	x	x	x	ky	x	x	-
350D	-	x	x	x	x	-	x	x	-
350F	-	x	x	x	x	-	x	x	-
362B	(x)	x	x	x	x	-	x	x	-
370A	-	-	x	x	x	ky-silli	x	x	-
370B	-	x	x	x	x	-	x	x	-
371C	-	x	x	x	x	ky	x	x	-
372	(x)	-	x	x	x	ky	x	x	-
374	x	-	x	x	x	-	x	x	-
375	(x)	x	x	x	x	-	x	x	-
377C	(x)	-	x	x	x	silli	x	x	-
382	-	x	x	x	x	-	x	x	-
384	-	x	x	x	x	-	x	x	-
410	-	x	x	x	(x)	silli	x	x	-

Quartz and plagioclase in all samples. Pyrrhotite, pyrite, tourmaline, apatite, and zircon can be present.

x: mineral present in assemblage
 -: mineral absent from assemblage
 (x): mineral present but not part of
 stable assemblage

Analytical Technique

The microprobe and accessories.

The analyses were made on a three-channel Applied Research Laboratory microprobe (model EMX) equipped with a pulse height amplifier on each channel. LiF crystals were used on two channels for analyzing Mn and Fe; KAP was used on the third channel for the analysis of Mg. Ca, Ti, and Zn were analyzed with LiF crystals, and Si and Al were analyzed on ADP and KAP crystals, respectively. Data was printed out on an I.B.M. electric typeprinter. Prior to September 15, 1965, all three channels had sealed-proportional gas-counter detectors. After that date, a continuous-flow gas-counter detector was installed on the channel with the KAP crystal. However, most of the data for this thesis was collected before September 15, 1965. The continuous-flow detector has the advantage of giving considerably higher counting rates for Mg than the proportional counter.

Polishing technique.

Mineral grains were mounted in epoxy resin in one-quarter inch brass tubes. These tubes were given a rough polish on grit papers down to 600 grit emery paper. Final polish was accomplished in 24 hours on a Fisher vibratory polisher using one-quarter micron alumina as an abrasive.

Polished thin sections were made by Mr. Rudolf Von Huene of Caltech. From the polished section, a one-inch disk was cut using

a diamond drill press. The polish was seldom entirely satisfactory over the whole thin section but was satisfactory over a sufficient area to measure reliable data.

Carbon coating.

To make the sample conducting, a thin coating of graphite was sputtered on the sample in an evacuated bell-jar. Precise control on carbon thickness was not possible, but it was found that counting rates were unchanged for any thickness greater than that which gives a purple color to a brass surface.

Experimental conditions.

Because the counting rates for Mg are lower than for Fe and Mn, conditions were chosen which gave the maximum counting rate for Mg without destruction of the sample. Mg counts increase with increasing voltage for a given sample current reading until a maximum of 25 KV, after which the counting rate decreases with higher voltage. Although 25 KV was chosen as the operating voltage, this decreased filament life so markedly that it is suggested that 15 or 20 KV's might be a more convenient voltage, especially since higher counting rates for Mg are now possible with the continuous-flow gas-counter detector.

Different minerals burn up at different sample currents for a given spot size. With the 2 micron spot size used in this work, the micas, which are the most susceptible to destruction, are not destroyed in runs of several minutes at a sample current of $.06 \mu\text{a}$. Sample currents greater than $.06 \mu\text{a}$ produce increasingly more rapid burnoffs

of the micas. Garnet and staurolite can tolerate sample currents between .1 and .2 μ a with small spot sizes; however, for comparative purposes it is useful to use a constant sample current reading for all minerals.

The current readings of .06 μ a were made on each sample and not on some reference mineral. Single analyses of 10 seconds each were made on individual points in a profile. When analyzing grain mounts or individual spots on a grain in a thin section, two repeats of 10 seconds each were made on a spot. The analysis of analyzed standards for the calibration curves consisted of 2 10-second repeats on each of at least 20 grains or spots within grains when less than 20 grains were available.

Standards

Although it is theoretically possible to calculate the weight percent of the oxides from the raw data alone, using synthetic materials of precisely known composition (Smith, 1965), it is less tedious to use working curves for each of the mineral groups based on chemically analyzed samples of minerals. In order to use working curves, only two corrections on the raw data are needed: background and interday normalization.

Figures 52-58 are calibration curves for the elements studied for five metamorphic minerals found in the Kwoiek Area plus one other, chloritoid. Table 14 gives the localities and the references to analyses for each mineral. All the Mn, Fe, and Mg data were collected over two days, Oct. 12-13, 1965. The Ti data were collected Jan. 20, 1966, the Al and Si data Jan. 28-29, 1966, and the Ca data April 24, 1965. Comparisons can be made directly to these charts by subtracting background, correcting for interday variations, and by normalizing to any of the specific minerals analyzed. The necessary correction factors are given in Table 15. Chl 10q was used as the interday reference for Mn, Fe, and Mg because (1) it has enough Mn, Fe, and Mg to give satisfactory counting rates, and (2) it is relatively homogeneous, although not ideally so. Because of the small inhomogeneities in chl 10q ten grains were analyzed before each run and the same 10 grains after each run. These same 10 grains were analyzed for interday reference on each run throughout the course of this study. The 10

Figs. 52 - 58. Calibration curves for translating background-corrected, normalized counting rates to weight percent of Mn, Fe, Mg, Ca, Ti, Si, and Al for staurolite (S), garnet (G), biotite (B), chlorite (C), chloritoid (CT), and cordierite (Cd). Where two or more calibration curves are on the same figure, the mineral symbols are used to distinguish them.

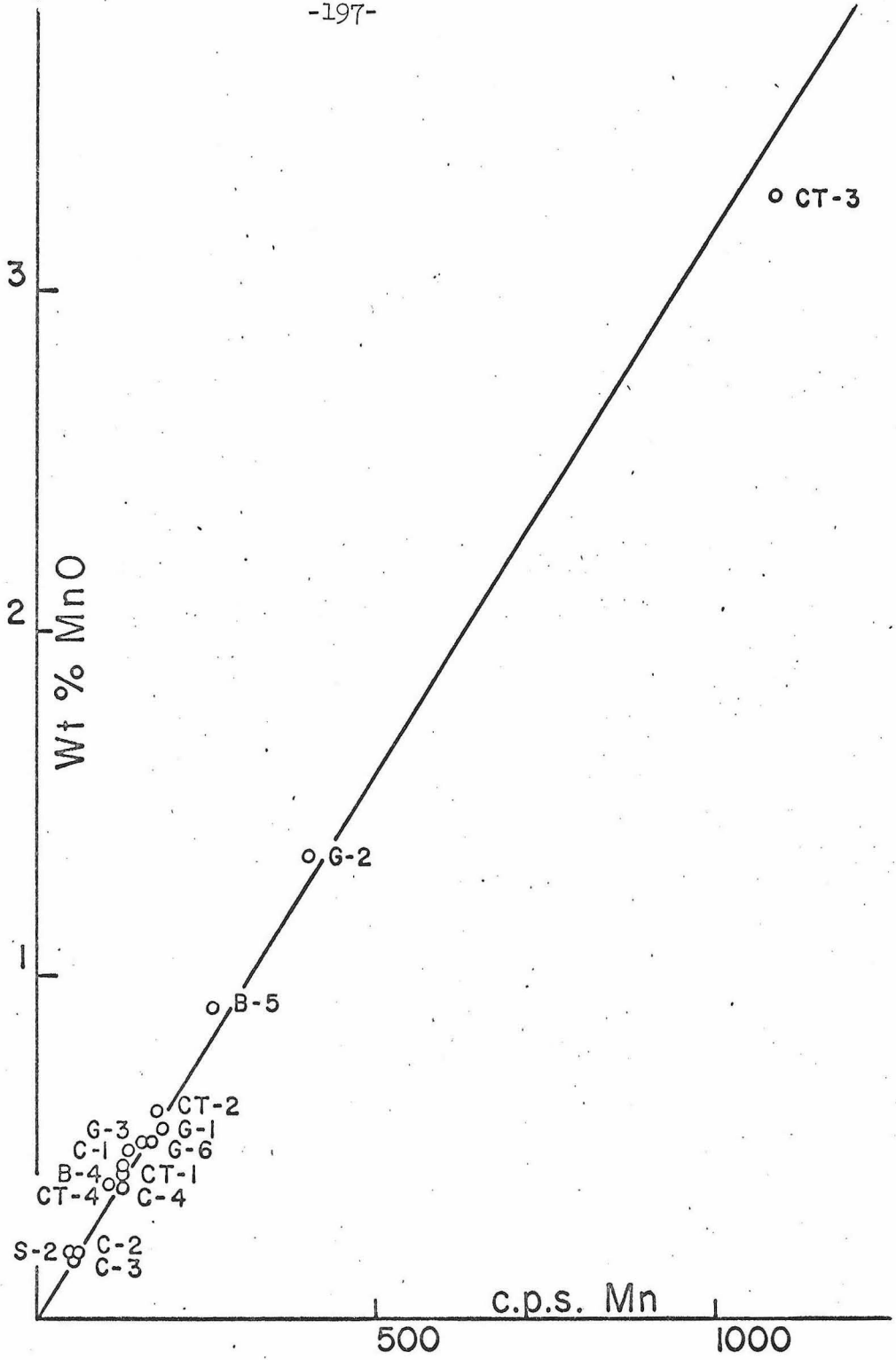


Fig. 52.

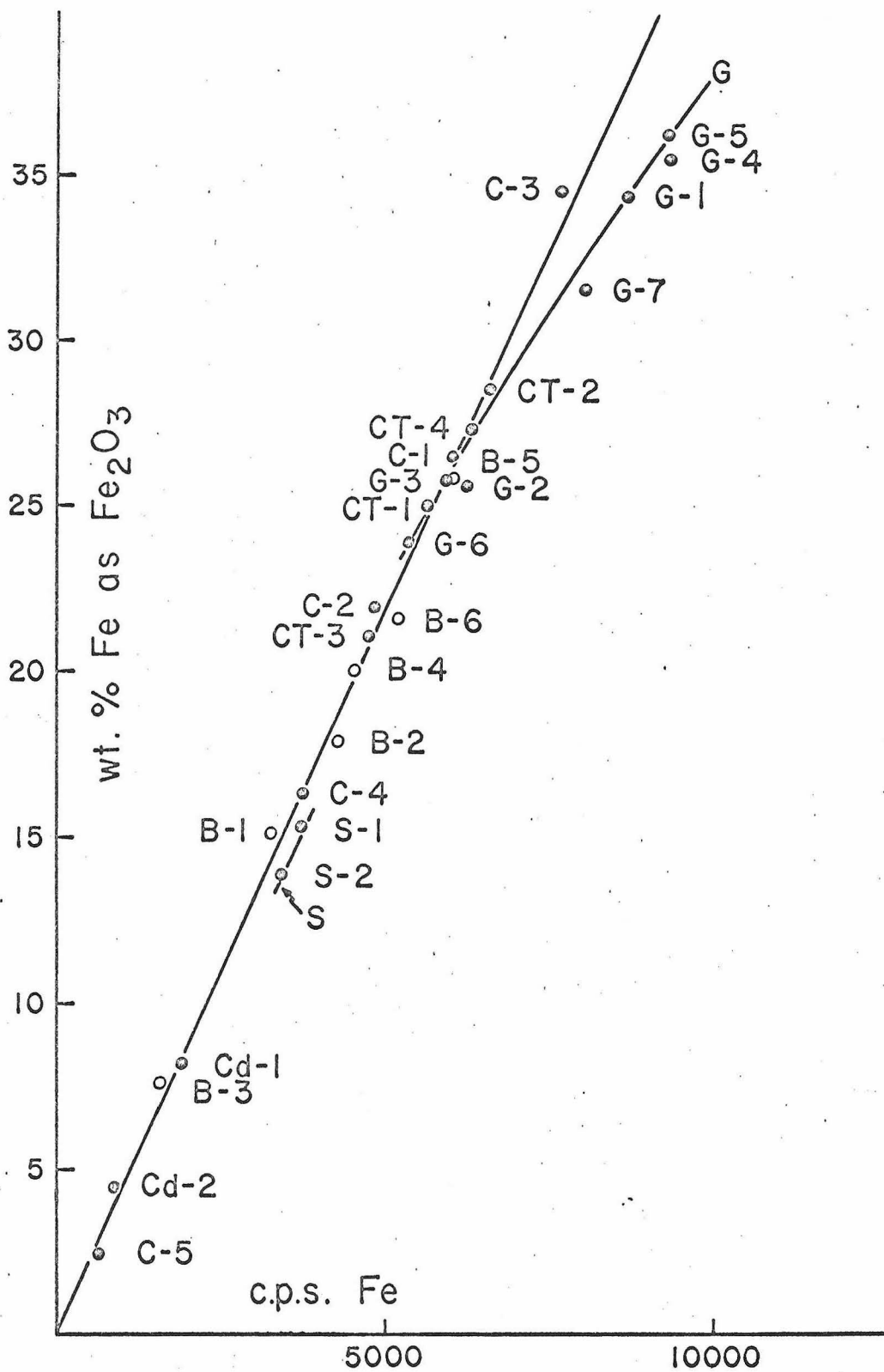


Fig. 53.

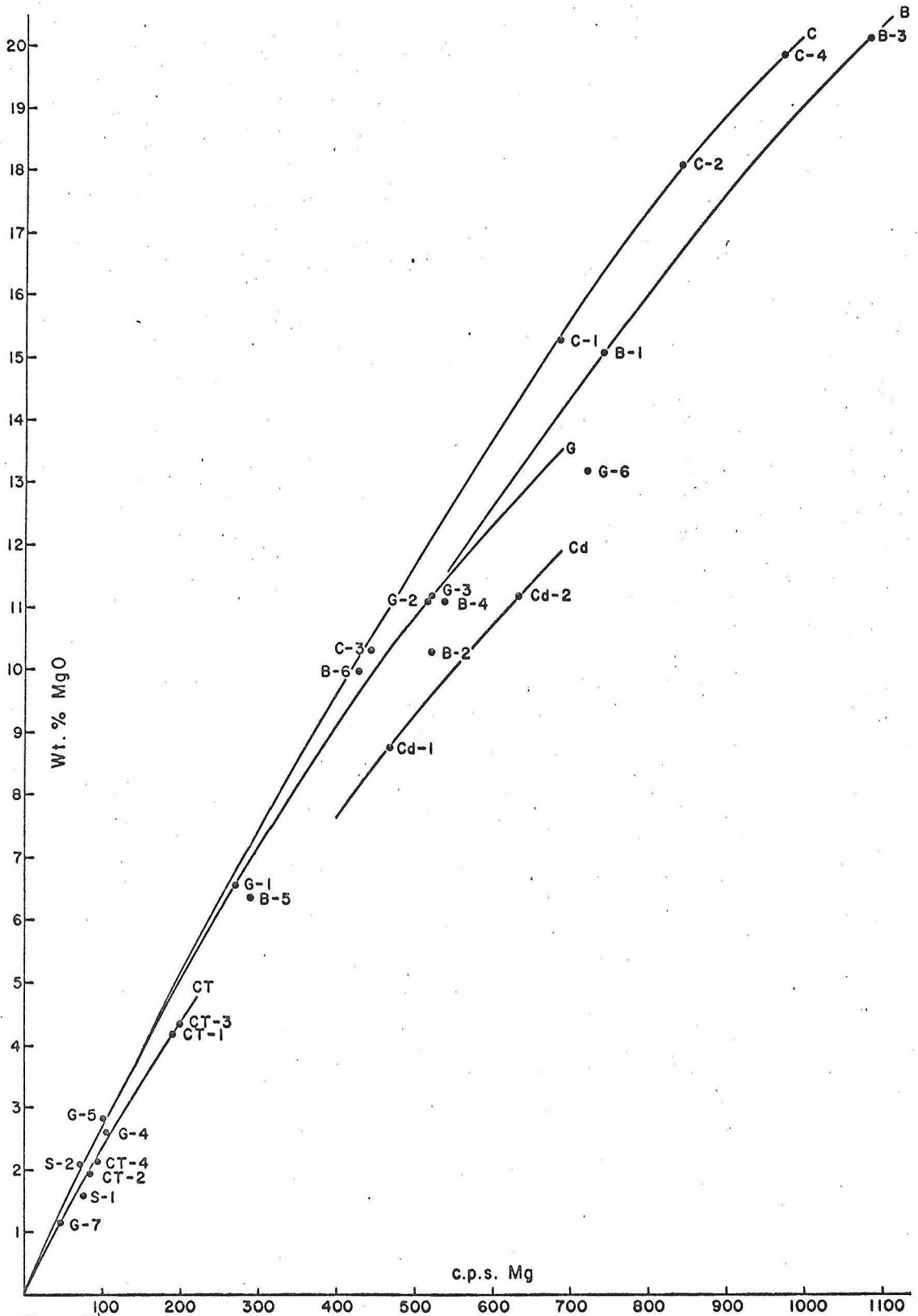


Fig. 54.

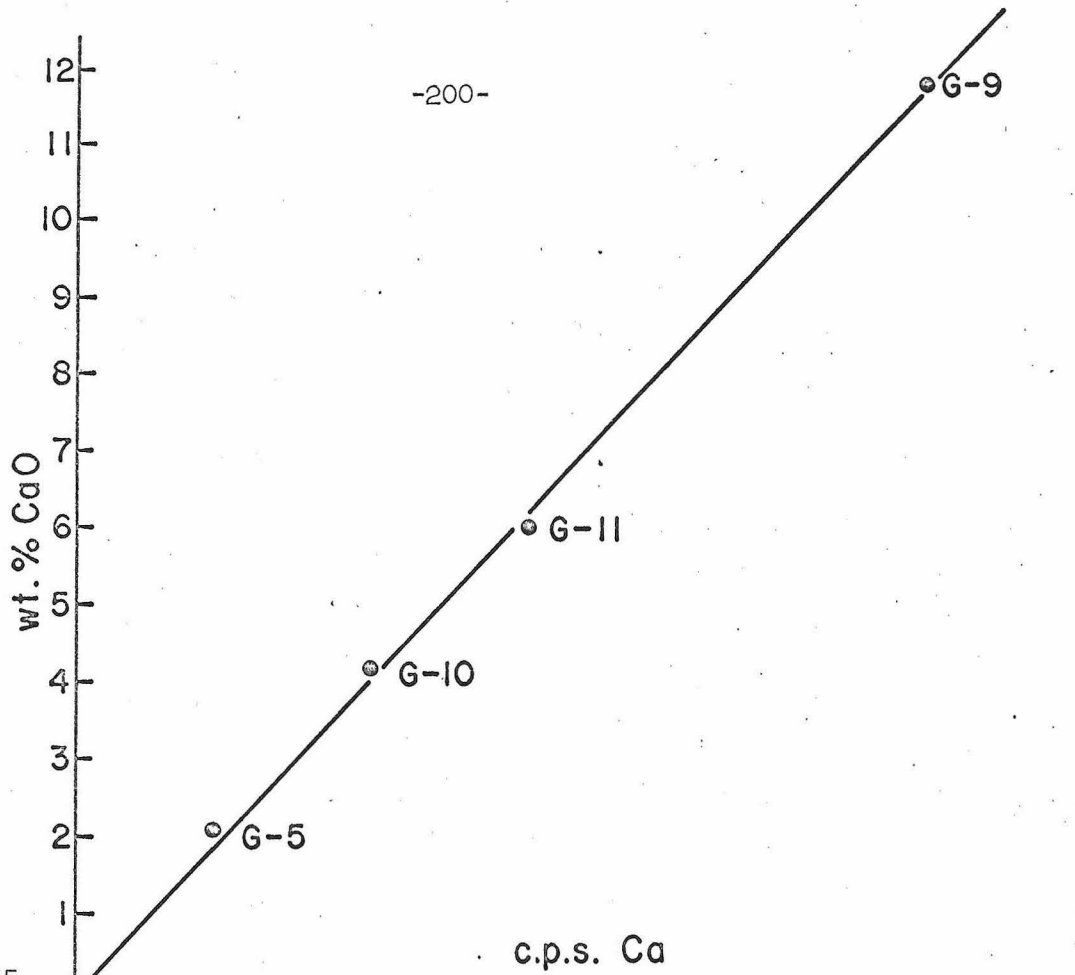


Fig. 55.

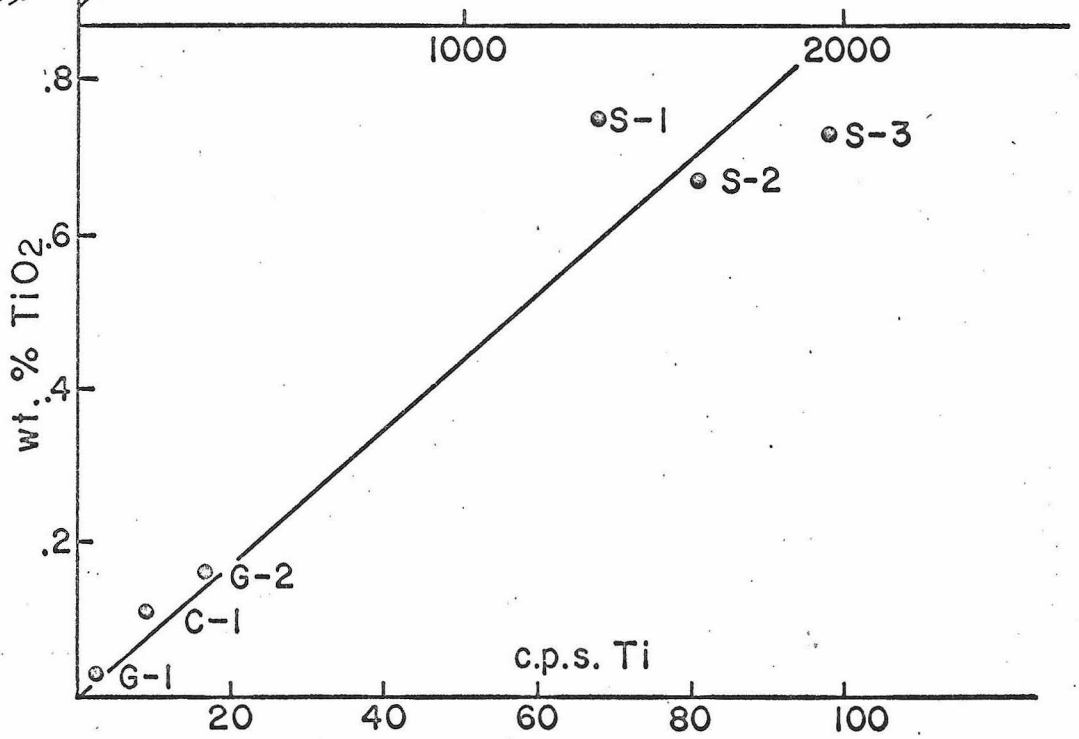


Fig. 56.

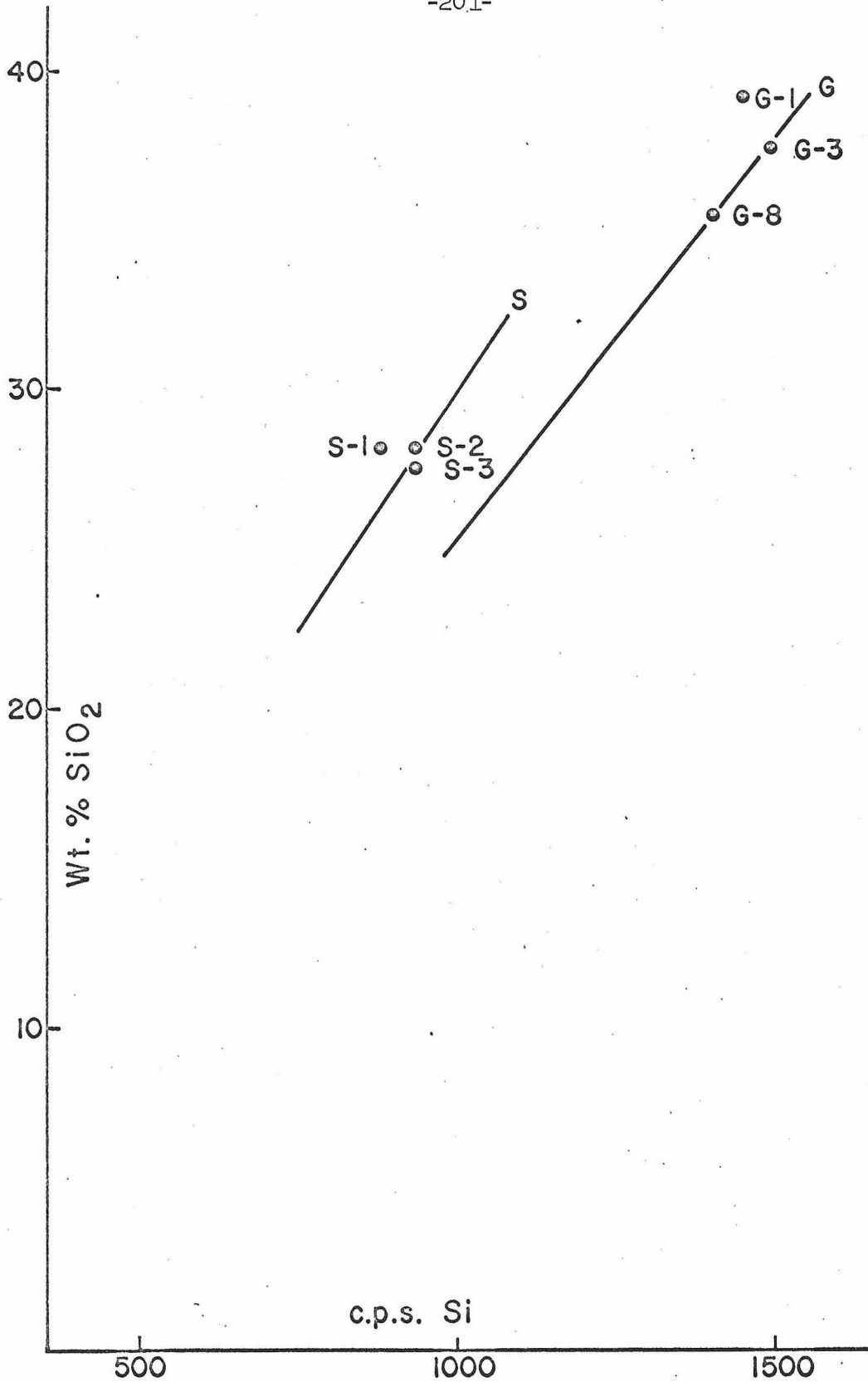


Fig. 57.

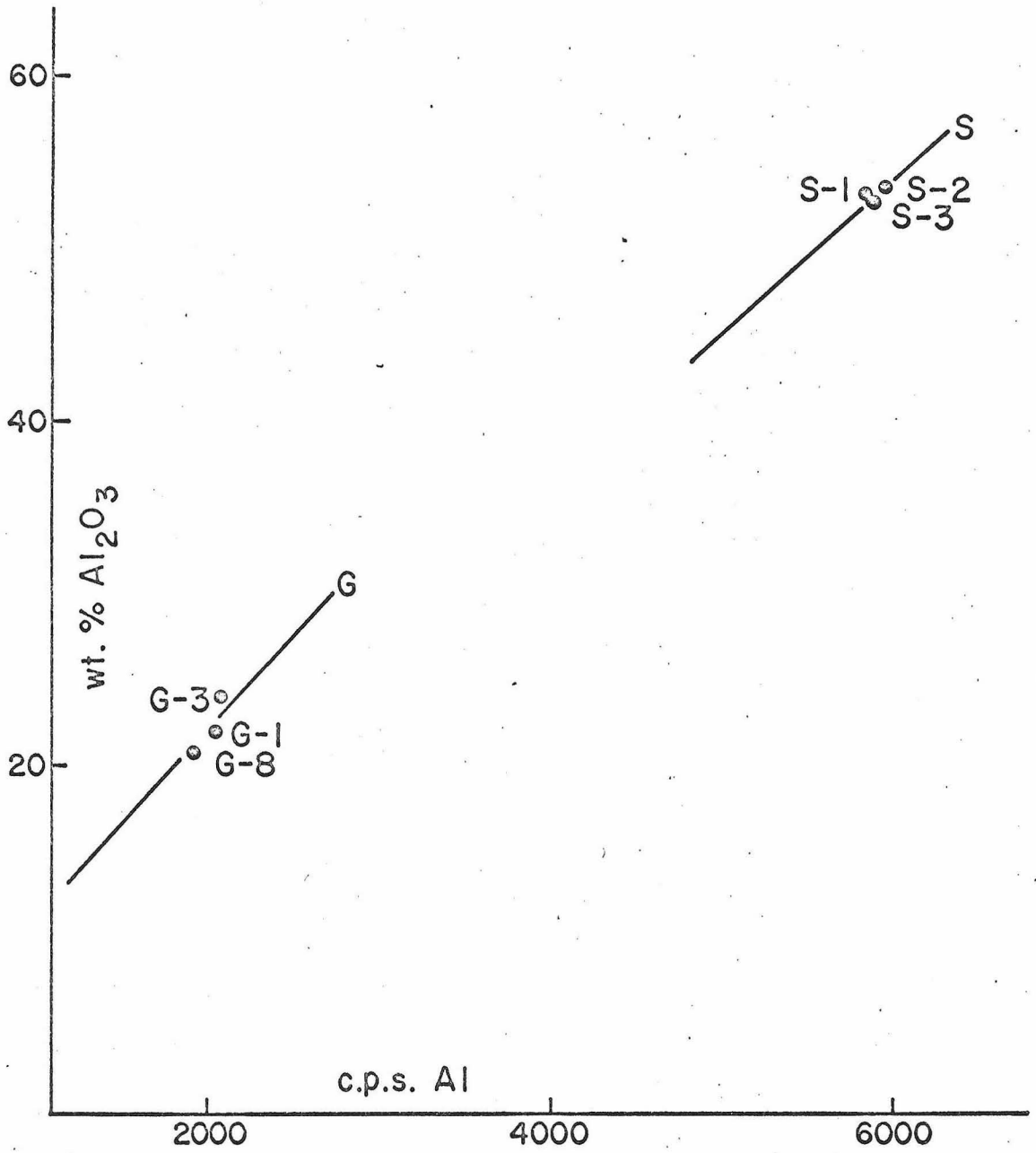


Fig. 58.

Samples Used for Microprobe Standards

<u>Garnet</u>	<u>Locality</u>	<u>Reference</u>
G-1	Sturbridge, Mass.	Barker (1962)
G-2	Cortlandt, N.Y.	Barker (unpublished)
G-3	Gore Mt., Vt.	Chodos (unpublished)
G-4	Errol quad, N.H.	Green (1963) ER-101 (zoned)
G-5	Errol quad, N.H.	Green (1963) D-2 (zoned)
G-6	Valle Codera, Italy	Barker (unpublished)
G-7	Lincoln Mt., Vt.	Albee (1965) LA-23a (zoned)
G-8	Nuevo Laredo, Mexico	Chodos (unpublished)
G-9	Ward Creek, Calif.	Lee, et al. (1963) 50-cz-59 (zoned)
G-10	Lincoln Mt., Vt.	Albee (1965) LA-34a (zoned)
G-11	Lincoln Mt., Vt.	Albee (1965) LA-10p (zoned)
 <u>Biotite</u>		
B-1	Cortlandt, N.Y.	Barker (unpublished)
B-2	Sturbridge, Mass.	Barker (1962)
B-3	Mason Mt., N.C.	Barker (1961)
B-4	Lincoln Mt., Vt.	Albee (1965) LA-168
B-5	Lithonia, Ga.	Silver (unpublished)
B-6	Errol quad, N.H.	Green (1963) ER-101
 <u>Chlorite</u>		
C-1	Lincoln Mt., Vt.	Albee (1965) LA-10q
C-2	Lincoln Mt., Vt.	Albee (1965) LA-10k
C-3	Lincoln Mt., Vt.	Albee (1965) LA-10p
C-4	Lincoln Mt., Vt.	Albee (1965) LA-25c
C-5	Belvidere Mt., Vt.	Albee (unpublished)
 <u>Staurolite</u>		
S-1	Errol quad, N.H.	Green (1963) D-2 (zoned)
S-2	Errol quad, N.H.	Green (1963) ER-101 (zoned)
S-3	Co. Galway, Eire	Leake (1958)
 <u>Chloritoid</u>		
CT-1	Lincoln Mt., Vt.	Albee (1965) LA-10k
CT-2	Lincoln Mt., Vt.	Albee (1965) LA-23a
CT-3	Lincoln Mt., Vt.	Albee (1965) LA-25c
CT-4	Lincoln Mt., Vt.	Albee (1965) LA-10p
 <u>Cordierite</u>		
Cd-1	Sturbridge, Mass.	Barker (1962)
Cd-2	Cortlandt, N.Y.	Barker (unpublished)

Table 15
Interday Factors

Date	Mn	Fe	Mg	Ti	Si	Al	Ca
Apr. 24, 1965	-	-	-	-	-	-	1.000
May 12	.970	.988	.983	-	-	-	-
May 31	1.000	1.000	1.000	-	-	-	.476
June 19	.774	1.023	.971	-	-	-	-
June 20	.785	1.015	.954	-	-	-	-
July 4	.782	1.009	.992	-	-	-	-
July 25	.791	1.007	.994	-	-	-	-
July 26	.774	1.004	1.004	-	-	-	-
Aug 2	.776	1.008	.986	-	-	-	-
Aug 3	.752	.999	.965	-	-	-	-
Aug 5	.777	1.001	.973	-	-	-	-
Aug 20	.764	.998	.982	-	-	-	-
Aug 21	.766	.997	.973	-	-	-	-
Aug 22	.748	.989	.981	-	-	-	-
Aug 27	.773	.991	.964	-	-	-	-
Aug 28	.773	.991	.970	-	-	-	-
Sept. 6	-	-	-	-	-	-	.524
Oct. 12	.889	.856	.732	-	-	-	-
Oct. 13	.893	.851	.742	-	-	-	-
Jan. 20, 1966	-	.885	.455	1.000	-	-	-
Jan. 21	-	-	-	.989	1.03	1.023	-
Jan. 28	-	-	-	.975	1.000	1.000	-
Jan. 29	-	-	-	.988	1.00	1.00	-

Approximate Backgrounds (c.p.s.)

Garnet	38	40	5	12	7	16	10 [#]
Staurolite	28	20	5	8	4	10	-
Biotite	32	30*	6**	11	6	16	-
Chlorite	29	30*	7 ^{##}	9	4	13	-

* 40 after Jan. 20, 1966

** 7 after Jan. 20, 1966

9 after Jan. 20, 1966

23 on Sept. 6, 1965

grains were normalized to the average counting rates of 25 random grains.

It can be seen in Figs. 52-58 that the best-fit curves for each mineral do not coincide exactly. This is because the positions of the curves are dependent on the absorbent qualities of each mineral for the radiation of each element and also on the mean atomic number. The curves are expected to be curved and not straight because the absorbent properties and mean atomic number of each mineral changes systematically with substitution of Fe and Mn for Mg.

For some of the curves there is considerable scatter. Some of this scatter is probably due to errors in the chemical analyses (most probable in the case of staurolite), some due to the aliquot of mineral analyzed with the microprobe not the same as that which was chemically analyzed (possibly true for S-1 and S-2), and some due to inhomogeneity of the mineral. This last source of error may apply to the garnets, some of which are strongly zoned, so that 20 points may not be a good statistical average; in Figs. 52-58 only the most homogeneous garnets are shown. Another source of error for the garnets is that they are not binary solutions but rather are solid solutions of at least four end members, each with its own absorbent, fluorescent, and mean atomic number characteristics.

No further attempt was made to refine the calibration curves for this study because the mineral compositional variations and petrologic problems can be understood without knowing the precise weight percent

of the elements. Only nine total analyses were made, five on garnet and four on a single zoned staurolite grain. The analyses gave reasonable totals but it is emphasized that the iron content of the garnet and the aluminum and silicon contents of the garnet and staurolite are the most likely to be the source of large error.

REFERENCES

- Albee, A.L., 1965a, Phase equilibria in three assemblages of kyanite-zone pelitic schists, Lincoln Mountain quadrangle, central Vermont: Jour. Petrol., v. 6, p. 246-301.
- _____, 1965b, Distribution of Fe, Mg, and Mn between garnet and biotite in natural mineral assemblages: Jour. Geol., v. 73, p. 155-164.
- _____, A.A. Chodos, and L.S. Hollister, 1966, Equilibrium volumes for different species in three assemblages of kyanite-zone pelitic schists, Lincoln Mountain quadrangle, central Vermont: Trans. Amer. Geoph. Union, v. 47, p. 213 (abs.).
- Banno, S., 1965, Notes on rock-forming minerals (34) : zonal structure of pyralspite garnet in Sanbagawa schists in the Bessi area, Sikoku: Jour. Geol. Soc. Japan, v. 71, p. 185-188.
- Barker, F., 1961, Anthophyllite - biotite - hypersthene - rhodolite assemblage, Mason Mountain, North Carolina: U.S. Geol. Surv. Prof. Paper 424C, p. 336-338.
- _____, 1962, Cordierite-garnet gneiss and associated microcline-rich pegmatite at Sturbridge, Massachusetts and Union, Connecticut: Amer. Min., v. 47, p. 907-918.
- Bell, P.M., 1963, Aluminum silicate system: experimental determination of the triple point: Science, v. 139, p. 1055-1056.
- Cairnes, C.E., 1942: Geol. Surv., Canada, Map 737A, Hope.
- Clark, S.P., 1961, A redetermination of equilibrium relations between kyanite and sillimanite: Amer. Jour. Sci., v. 259, p. 641-650.
- Corlett, M., and J.V. Smith, 1964, Significance of minor-element analysis by the microprobe x-ray emission analyses: Abs., Geol. Soc. Amer. Annual Meeting, Miami.
- Dike, P.A., 1951, Kyanite pseudomorphs after andalusite from Delaware Co., Penna.: Amer. Jour. Sci., v. 249, p. 457-458.
- Duffell, S., and K.C. McTaggart, 1952, Ashcroft map-area, British Columbia: Geol. Surv. Can. Mem. 262.
- Eskola, P., 1920, The mineral facies of rocks: Norsk. Geol. Tidsskr., v. 6, p. 143-194.
- Evans, B.W., 1965, Microprobe study of zoning in eclogite garnets: Abs., Geol. Soc. Amer. Annual Meeting, Kansas City.

- French, B.M., 1965, Some geological implications of equilibrium between graphite and a C - H - O gas phase at high temperatures and pressures: Goddard Space Flight Center, Greenbelt, Maryland.
- Frost, M.J., 1962, Metamorphic grade and iron-magnesium distribution between co-existing garnet-biotite and garnet-hornblende: Geol. Mag., v. 99, p. 427-438.
- Green, J.C., 1963, High-level metamorphism of pelitic rocks in northern New Hampshire: Amer. Min., v. 48, p. 991-1023.
- Hietanen, A., 1956, Kyanite, andalusite, and sillimanite in the schist in Boehls Butte quadrangle, Idaho: Amer. Min., v. 41, p. 1-27.
- _____, 1961, Metamorphic facies and style of folding in the Belt series northwest of the Idaho batholith: Bull. de la Commission geologique de Finlande, v. 33, p. 73-103.
- Kretz, R., 1959, Chemical study of garnet, biotite, and hornblende from gneisses of southwestern Quebec, with emphasis on distribution of elements in coexisting minerals: Jour. Geol., v. 67, p. 371-402.
- Kummel, B., 1961, History of the Earth: W.H. Freeman and Company, San Francisco.
- Leake, B.E., 1958, Composition of pelites from Connemara, Co. Galway, Ireland: Geol. Mag., v. 95, p. 281-296.
- Lee, D.E., R.G. Coleman, and R.C. Erd, 1963, Garnet types from the Cazadero area, California: Jour. Petrol., v. 4, p. 460-492.
- Mazor, E., and G.J. Wasserburg, 1965, Helium, neon, argon, krypton, and xenon in gas emanations from Yellowstone and Lassen volcanic National Parks: Geochim. Cosmochim. Acta, v. 29, p. 443-454.
- McIntire, W.L., 1963, Trace element partition coefficients--a review of theory and application to geology: Geochim. Cosmochim. Acta, v. 27, p. 1209-1265.
- Miyashiro, A., 1964, Oxidation and reduction in the earth's crust with special reference to the role of graphite: Geochim. Cosmochim. Acta, v. 28, p. 717-729.
- Neumann, H., J. Mead, and C.J. Vitaliano, 1954, Trace element variation during fractional crystallization as calculated from the distribution law: Geochim. Cosmochim. Acta, v. 6, p. 90-99.
- Newton, R.C., 1966, Kyanite-sillimanite equilibrium at 750° C: Science, v. 151, p. 1222-1225.

- Pearson, G.R., and S.M. Shaw, 1960, Trace elements in kyanite, sillimanite, and andalusite: *Amer. Min.*, v. 45, p. 808-817.
- Phinney, W.C., 1963, Phase equilibria in the metamorphic rocks of St. Paul Island and Cape North, Nova Scotia: *Jour. Petrol.*, v. 4, p. 90-130.
- Pitcher, W.S., and H.H. Read, 1963, Contact metamorphism in relation to manner of emplacement of the granite of Donegal, Ireland: *Jour. Geol.*, v. 71, p. 261-296.
- Rayleigh, Lord, 1902, On the distillation of binary mixtures: *Phil. Mag.*, sixth series, v. 4, p. 521-537.
- Rosenfeld, J.L., and A.B. Chase, 1961, Pressure and temperature of crystallization from elastic effects around solid inclusions in minerals?: *Amer. Jour. Sci.*, v. 259, p. 519-541.
- Seki, Y., and G.C. Kennedy, 1965, Muscovite and its melting relations in the system $KAlSi_3O_8 - H_2O$: *Geochim. Cosmochim. Acta*, v. 29, p. 1077-1083.
- Shams, F.A., 1965, An occurrence of kyanite pseudomorphs after andalusite from Amb. state, West Pakistan: *Min. Mag.*, v. 35, p. 669-671.
- Shaw, D.M., 1956, Geochemistry of pelitic rocks. Part III: major elements and general geochemistry: *Bull. Geol. Soc. Amer.*, v. 67, p. 919-934.
- Smith, J.V., 1965, X-ray-emission microanalysis of rock-forming minerals. I. experimental techniques: *Jour. Geol.*, v. 73, p. 830-864.
- Taylor, H.P., Jr., and S. Epstein, 1962, Relationship between O^{18}/O^{16} ratios in coexisting minerals of igneous and metamorphic rocks: *Bull. Geol. Soc. Amer.*, v. 73, p. 675-694.
- Thompson, J.B., 1957, Graphical analysis of mineral assemblages in pelitic schists: *Amer. Min.*, v. 42, p. 842-858.
- Tilley, C.E., 1935, The role of kyanite in the "hornfels zone" of the Carn Chuinneag granite (Ross-shire): *Min. Mag.*, v. 24, p. 92.
- Turner, F.J., and J. Verhoogen, 1960, *Igneous and Metamorphic Petrology*: McGraw-Hill Book Co., New York.

Weill, D.F., 1966, Stability relations in the Al_2O_3 - SiO_2 system calculated from solubilities in the Al_2O_3 - SiO_2 - Na_3AlF_6 system: Geochim. Cosmochim. Acta, v. 30, p. 223-237.

Wones, D.R., and H.P. Eugster, 1965, Stability of biotite: experiment, theory and application: Amer. Min., v. 50, p. 1228-1272.

Woodland, B.G., 1963, Petrographic study of thermally metamorphosed pelitic rocks in the Burke area, north-eastern Vermont: Amer. Jour. Sci., v. 261, p. 354-375.

Workman, D.R., and I.A. Cowperthwaite, 1963, An occurrence of kyanite pseudomorphing andalusite from So. Rhodesia: Geol. Mag., v. 100, p. 456-466.

Zen, E., 1963, Components, phases and criteria of chemical equilibrium in rocks: Amer. Jour. Sci., v. 261, p. 929-942.